University College London

Division of Medicine

Characterisation and utilisation of complementary murine and human models of inflammation to investigate pro-resolution/anti-inflammatory pathways in rheumatoid arthritis

James Robert William Glanville

A thesis submitted in fulfilment of the requirements for the Degree of Doctor of Philosophy

2024

Declaration

"I, James Robert William Glanville, confirm that the work presented in this thesis is my own. Where information has been derived from other sources, I confirm that this has been indicated in the thesis."

"Virtus tentamine gaudet."

Some of the content of this thesis has been published:

Glanville, J. R. W., Jalali, P., Flint, J. D., Patel, A. A., Maini, A. A., Wallace, J. L., Hosin, A., Gilroy, D. W**. Potent anti-inflammatory effects of an H_2S-releasing naproxen (ATB-346) in a human model of inflammation.** *The FASEB Journal*. 2021: 35(10): 1-15.

Abstract

Rheumatoid arthritis (RA) is the most common primary autoimmune inflammatory arthropathy worldwide. Inflammation is a combination of inflammatory 'go' signals counteracted and regulated by internal 'off' signals, leading to the clearance of the inflammatory stimulus and the initiation of resolution. Despite an increasing appreciation of the role of inflammation and its resolution in the development of autoimmune disease, this remains a relatively understudied field of research. This thesis describes novel murine models of both non-resolving and resolving inflammation with a complementary human model in both health and in RA patients using the same inflammatory stimulus; UV-killed *Escherichia coli* (UV-KEc). Collectively, these can be used to investigate potential pro-resolution/anti-inflammatory signals in RA. The intradermal injection of UV-KEc in both mouse and humans resulted in a significant inflammatory response, characterised by the influx of neutrophils. In mouse, at a dose of 1.5×10^8, this process was non-resolving at the end of the time-course (72h), defined by the absence of neutrophil clearance. At a dose of 1.5×10^7, inflammation had resolved with neutrophil numbers returning to baseline levels. At both doses, significant changes were identified in bone marrow neutrophil subsets, with an emergency release of developmentally immature neutrophils. A significant expansion of $Ly6C^{int}$ monocytes was also seen using both doses of UV-KEc. Furthermore, key endocannabinoids were detectable in both inflamed murine skin and plasma, with marked differences seen compared to un-injected controls; notably 2-arachidonoylglycerol (2-AG), *N*-palmitoylethanolamine (PEA) and *N*-arachidonoylethanolamine (AEA). I have also shown that the use of a traditional anti-inflammatory medication used in RA (naproxen) and a novel investigational hydrogen sulfide-releasing (H_2S) non-steroidal anti-inflammatory drug (NSAID), ATB-346, can be safely used in this system to investigate inflammatory pathways following the injection of UV-KEc into the skin of healthy volunteers. ATB-346 and naproxen were shown to be potently anti-inflammatory, as evidenced by a significant reduction in neutrophils at the inflamed site at 4h compared to healthy controls. ATB-346 also significantly increased the expression of cluster of differentiation 14 (CD14) on both classical and intermediate monocyte subsets at 48h, suggesting a switch towards an anti-inflammatory phenotype. ATB-346 and naproxen also suppressed cyclo

oxygenase (COX) equally, as measured by a significant reduction in prostaglandin E_2 (PGE_2) at 4h. Finally, the effect of UV-KEc-triggered dermal inflammation in RA patients who were in disease remission was investigated. RA patients demonstrated significantly increased levels of plasmacytoid dendritic cells at the site of inflammation at 48h. Using Uniform Manifold Approximation and Projection (UMAP) analysis, a unique population of interleukin-7 (IL-7) receptor $(CD127)^+$ macrophages was found in RA patients in disease remission at the site of inflammation, which was absent in all healthy controls. Two RA patients who did not have this population flared soon after the completion of the study, suggesting that these cells may be important for the maintenance of remission in RA. Counterintuitively, RA patients also reported significantly reduced pain and tenderness throughout the inflammatory time-course. The concept of harnessing mediators involved in the resolution of inflammation to treat patients with autoimmune disease is an attractive strategy, potentially negating the use of immunosuppressive therapies, which increase the risk of infection and malignancy. The work presented here aimed to identify anti-inflammatory/pro-resolution targets and the modulation of CD127/IL-7 signalling may represent one such novel pathway.

Impact Statement

The data presented in this thesis reveals several novel findings which will have impact on both academic research and clinical practice. The work presented here focuses on many facets of the human and murine immune systems, giving widespread applicability, with an emphasis on identifying pro-resolution/anti-inflammatory pathways which may be important in the maintenance of disease remission in RA. **Chapter 3** describes an accessible and reproducible novel murine model of dermal non-resolving inflammation, which can used as a tool by researchers to investigate the effect of differing inflammatory stimuli and the role of novel drugs both in health and in a range of diseases. **Chapter 4** describes a complementary resolving model of dermal inflammation in mouse, which can be used as a model to investigate pro-resolution/anti-inflammatory pathways which may be important for the maintenance of remission of autoimmune disease. Both mouse models also resulted in the expansion of Ly6C^{int} monocytes, which may also be important in the development of autoimmune disease and provide a platform to understand the significance of this understudied cell-type *in vivo*. Following publication of this technique, this will be freely available to any academic researcher or industry partner to better understand the biological significance of new pharmacological agents in pre- and post-clinical trials, with the advantage over human studies that knock-out animals may be used to gain valuable mechanistic insight. Data from **Chapter 5** has shown that this model of inflammation can be safely used to investigate the effects of investigational drugs and those treatments, which are used as standard of care in autoimmune disease. Importantly, I have demonstrated that this system is also responsive to such interventions. It also describes the use of one such novel therapeutic anti-inflammatory medication, ATB-346, and that this is as efficacious as conventional naproxen in its ability to reduce neutrophil infiltration during the acute phase of inflammation. This drug is now in Phase 2b trials and the pharmaceutical company are currently seeking FDA approval in the USA. Adding a new treatment option to the armoury for patients suffering from inflammation will prove invaluable and will be of immediate benefit to the general population as well as those suffering from inflammatory diseases, including RA. In **Chapter 6** a novel immune signature has been identified in RA patients, which may be key to the maintenance of remission of the disease and could

represent a druggable target for the treatment of RA. Furthermore, it may represent a novel biomarker which could be used to predict disease flare or response to treatment. This will not only open doors within the scientific community for new areas of research, moving the focus from the adaptive immune response to the innate, but with further investigation may in the longer-term allow the development of new treatments for RA patients. Given that RA affects 1% of the UK population, with one of the most disabling symptoms being pain, the finding of significantly reduced pain and tenderness levels at the site of inflammation will also build a platform for further research in this field. The findings resulting from this thesis require dissemination to the wider scientific and medical communities. As such, data from this thesis has already been presented at both local, national and international conferences. **Chapter 5** has been published in a peer-reviewed academic journal and work is currently in progress preparing several manuscripts for publication of the remaining data.

Acknowledgments

Firstly, I would like to acknowledge my supervisor and friend, Professor Derek Gilroy. I am eternally grateful that you provided me with the opportunity to work with you, firstly as an Academic Clinical Fellow all those years ago and later securing funding to keep me on as a PhD student. You have created a lab which perfectly blends incredibly passionate, bright and hardworking people, with laughter, friendship and a robust support network and I wouldn't have wanted to complete my PhD in any other group.

Another huge thank you must go to members of the Gilroy group, both past and present. In particular, Karen, Liv and PJ, you have been my collective rock, not just supporting me in my scientific endeavours, but also ensuring we had an absolute blast along the way and forging friendships that will last a lifetime. Thanks also to George, Michelle, Hannah, Amit, Roel, Maddy, Julia, Marc and of course the wonderful Justine, who paved the way for so much of our animal work. A big thank you must also go to Professor Arne Akbar and all members, past and present, from his group.

Finally, I dedicate this thesis to my family, friends, Tim and Herbie, whose love and support have allowed me to finish my PhD, at times under very challenging circumstances. My parents have provided me with unwavering support over the *many* years of university life and without them this PhD would not have been possible.

Contents

Table of contents

List of Figures

List of Tables

Non-standard abbreviations

AA – Arachidonic acid

ABHD6 – α/β-hydrolase domain-6

ACPA – Anti-citrullinated peptide antibodies

ACT1 – Nuclear factor activator 1

AD – Atopic dermatitis

AEA - *N*-arachidonoylethanolamine

AlA – Alopecia areata

ANOVA – Analysis of variance

Apaf-1 – Apoptotic protease activating factor

ASC – Adapter protein apoptosis associated Speck-like protein containing a CARD

ATP – Adenosine triphosphate

AxSpA – Axial spondyloarthritis

cAMP – Cyclic adenosine monophosphate

CAT – Cysteine aminotransferase

CB2 – Cannabinoid receptor type 2

CCP – Cyclic citrullinated peptide

CCR – C-C chemokine receptor

CD – Cluster of differentiation

CF – Cystic fibrosis

CBR – Cannabinoid receptor

CBS – Cystathionine β-synthase

C/EBP – CCAAT-enhancer-binding protein

cGMP – Cyclic guanosine monophosphate

c-Myc – c-Myelocytomatosis

CO – Carbon monoxide

COX - cyclooxygenase

CRP – C-reactive protein

CSE – Cystathionine γ-lyase

CYP – Cytochrome P450

DAGL – Diacylglycerol lipase

DAMP – Damage-associated molecular pattern

DCSSc – Diffuse cutaneous systemic sclerosis

DHET - Dihydroxyeicosatrienoic acid

DiHETE – Dihydroxyicosatetraenoic acid

DiHOME - Dihydroxy-octadecenoic acid

DM – Dermatomyositis

DNA – Deoxyribonucleic acid

DMARD – Disease modifying anti-rheumatic drug

EBV – Ebstein-Barr virus

EDTA – Ethylenediaminetetraacetic acid

ELISA – Enzyme-linked immunosorbent assay

EpDPE – Epoxy-docosapentanoic acid

EpETE – Epoxy-eicosatetraenoic acid

EPOME – Epoxy-octadacamonoenoic acid

ERA – Enthesitis-related arthritis

FAAH – Fatty acid amidase

FBC – Full blood count

FCS – Fetal calf serum

Gas – Growth arrest specific

Gfi-1 – Growth factor independent-1

GM-CSF – Granulocyte macrophage colony-stimulating factor

GMP – Granulocyte-monocyte progenitor cell

GPCR – G-protein-coupled receptor

GRE – Glucocorticoid response element

GI – Gastrointestinal

HETES – Hydroxyeicosatetraenoic acid

HLA – Human leucocyte antigen

HO – Heme oxygenase

HS – Hidradenitis suppurativa

H_2S – Hydrogen sulfide

ICAM – Intercellular adhesion molecule

ICOS – Inducible co-stimulator

IL – Interleukin

IMEM – Iscove's Modified Eagle Medium

inHg – Inches of mercury

IFN – Interferon

IRAK – Interleukin-1 receptor associated kinase

JAK – Janus kinase

JBT-101 – Lenabasum

JIA – Juvenile idiopathic arthritis

LFT – Liver function tests

LOX – Lipoxygenase

LPS – Lipopolysaccharide

LRRC33 – Leucine-rich repeat containing 33

LT – Leukotriene

MAGL – Monoacylglycerol lipase

MCP-1 – Monocyte chemoattractant-1

MD2 – Myeloid differentiation factor 2

MerTK – Mer tyrosine kinase

MFG-E – Milk fat globule epidermal growth factor

MFI – Mean fluorescence intensity

MHC II – Major histocompatibility complex class II

MIP - Macrophage inflammatory protein

MKP-1 – Mitogen-activated protein kinase

MMP – Metalloproteinase

MP – Mononuclear phagocyte

MS – Multiple sclerosis

MST – 3-mercaptopyruvate

MyD88 – Myeloid differentiation factor 88

NAAA – *N*-acylethanolamine-hydrolysing acid amidase

NADPH – Nicotinamide adenine dinucleotide phosphate

NAE – *N*-acylethanolamine

NAPE – *N*-acylphosphatidylethanolamine

NeO – Neuromyelitis optica

NETS – Neutrophil extracellular traps

NF-κB – Nuclear Factor kappa-light-chain-enhancer of activated B cells

NLRC4 – Nacht, LRR family caspase activation and Recruitment domain-Containing 4

NLRP3 – Nacht, LRR family pyrin domain containing protein-3

NO – Nitric oxide

NSAID – Non-steroidal anti-inflammatory

OD – Optical density

OEA – *N*-oleoylethanolamine

OLFM – Olfactomedin

P – Psoriasis

PAMP – Pathogen-associated molecular patterns

PBS – Phosphate-buffered saline

PEA – *N*-palmitoylethanolamine

PECAM - Platelet endothelial cell adhesion molecule

PG - Prostaglandin

PGI_2 – Prostacyclin

PI3K – Phosphatidylinositol-3 kinase

PL – Phospholipase

PMN – Polymorphonuclear cell

PDL-1 – Programmed death ligand-1

PRR - Pattern recognition receptor

PsA – Psoriatic arthritis

PtdSer – Phosphatidylserine

PUFA – Polyunsaturated fatty acid

p38 MAPK – Protein 38 Mitogen-Activated Protein Kinase

RA – Rheumatoid arthritis

Rac – Ras-related C3 botulinium toxin substrate

RANTES – Regulated upon Activation, Normal T cell Expressed and presumably Secreted

RF – Rheumatoid factor

ROS – Reactive oxygen species

RvE1 – Resolvin E1

SD – Standard deviation

Siglec-8 – Sialic acid-binding immunoglobulin n-like lectin

SLE – Systemic lupus erythematosus

SHC-1 – Src homology domain-containing transforming protein 1

SHP-2 – Src homology region 2 domain-containing phosphatase 2

SOCS – Suppressor of cytokine signalling

SPM – Specialised pro-resolving mediator

STAT – Signal transducer and activator of transcription

TGF – Transforming growth factor beta

THC – Tetrahydrocannabinol

TIM – T cell/transmembrane, immunoglobulin and mucin

TLR – Toll-like receptor

TNF – Tumour necrosis factor alpha

TRAF6 – Tumour necrosis factor receptor-associated factor 6

TRPV – Transient receptor potential vanilloid

TXA_2 – Thromboxane A_2

TYK – Tyrosine kinase

U+E – Urea and electrolytes

UC – Ulcerative colitis

UMAP – Uniform manifold approximation and projection

UV-KEc – Ultraviolet-killed *Escherichia coli*

VCAM – Vascular cell adhesion molecule

WOMAC – Western Ontario and McMaster Universities Arthritis Index

2-AG – 2-arachidonoylglycerol

1 Introduction

1.1 Inflammation

Inflammation is our body's programmed sequence of events in response to an inflammatory stimulus; be this an injury or an infection. The aim of this process is to protect the body, bringing about a return to homeostasis. Classically, this stimulus-response system is characterised by Celsus' cardinal tetrad of inflammation: calor (heat), rubor (redness or erythema), dolor (pain) and tumour (swelling) (1–4). Whilst ultimately aiming to fight infection or trauma, sometimes this inflammatory response is prolonged, such that it can begin to damage the tissues of the body rather than repair them (3). Virchow later introduced the fifth cardinal sign of inflammation as loss of function, highlighting the impact of prolonged inflammation in damaging tissue (5). Inflammation ensues in a highly coordinated fashion, the timeline of which is shown in **Figure 1.1**. Longer term, the aim of this process is to establish immune memory, thus enabling the host to mount a more rapid and specific response to the inciting stimulus should this be encountered again in the future (6). Importantly, dysregulation of inflammatory resolution pathways leads to chronic inflammation, promoting breach of tolerance and the development of autoimmune disease (7).

The primary focus of this thesis is to develop tools with which to investigate immune dysregulation using murine and human models of inflammation, both in health and disease. The aim is to develop an experimental, translational model of inflammation that can be safely used in patients with autoimmune disease, focusing on RA, to investigate inflammatory signals involved in maintaining disease remission. To appreciate the cellular responses and signalling involved in switching off inflammation, it is first important to understand how inflammation begins.

1.2 Onset of inflammation

The main role of the acute phase of the inflammatory response is to enable immune cells to enter the site of inflammation and destroy invading pathogens/other antigenic targets recognised as foreign (8). Key to this process is the ability of the immune system to recognise invading pathogens as 'non-self'. Cells can do this by a number of means, including highly conserved pattern recognition receptors (PRRs), which bind to pathogen-associated molecular patterns (PAMPs) and damage-associated molecular patterns (DAMPs) (9). Examples of PRRs include Toll-like receptors (TLRs) and scavenger receptors. TLR-4, for example, recognises lipopolysaccharide (LPS), a major constituent of the outer membrane of Gram-negative bacteria, such as *E. coli* (8).

Typically, the first leucocytes to arrive at the site of inflammation are the polymorphonuclear cells (PMNs), either by innate sensing of foreign antigenic material or in response to pro-inflammatory cytokines and/or chemokines released by other cells resident at the site of inflammation (10–12). To enable extravasation and infiltration of these PMNs (in the most part neutrophils), endothelial cells upregulate adhesion molecules such as endothelial (E)-selectin and intracellular adhesion molecule (ICAM)-1 (2, 10). The main function of these cells is to phagocytose and thus destroy invading pathogens by a range of intracellular (including the generation of reactive oxygen species [ROS] or myeloperoxidase) or extracellular mechanisms (the formation of neutrophil extracellular traps [NETs]) (3). The transition from the acute phase to the resolution phase is characterised by the replacement of these neutrophils by mononuclear phagocytes (namely monocytes, macrophages and to a lesser extent dendritic cells) as shown in **Figure 1.1** (13).

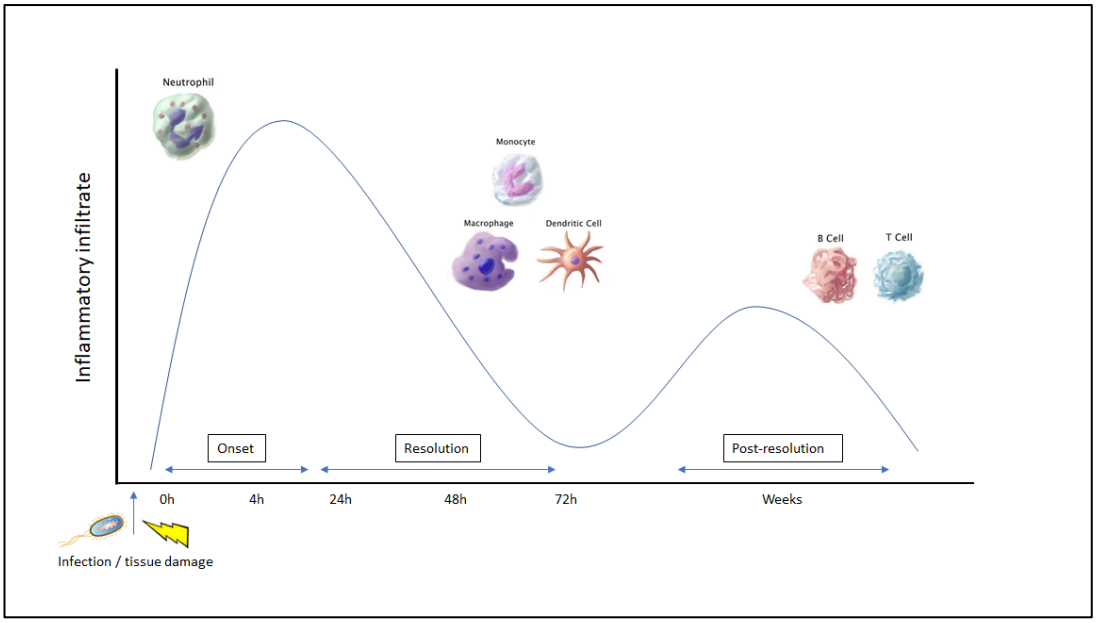

Figure 1.1. Timeline of the acute inflammatory response in humans. Inflammation onset begins in response to tissue injury or an invading pathogen. The acute phase is characterised by the infiltration of PMNs and secretion of pro-inflammatory cytokines by resident macrophages. Following elimination of the stimulus by phagocytosis, the resolution phase begins, characterised by the infiltration of mononuclear phagocytes to the site of inflammation who are then able to efferocytose apoptosing PMNs thus clearing the site of inflammatory debris. Soluble mediators are broken down and the post-resolution phase commences, which may continue for several weeks, enabling effective establishment of a memory adaptive response and bringing about a state of adapted homeostasis.

1.3 Resolution of inflammation

Historically thought to be a passive process with the flames of inflammation gradually dying out of their own accord and bringing an end to inflammation, the resolution phase is now known to be a complex and immunologically active process (10, 11, 14). This involves the intricate signalling between a myriad of immune cells, cytokines, chemokines and lipid mediators to enable clearance of pathogens and immune debris from the acute phase of inflammation, thus maintaining tolerance (3, 13). The resolution phase occurs between the peak influx of inflammatory cells and restoration of homeostasis, at the transition point of replacement of neutrophils with mononuclear cells, a process mediated by numerous signalling pathways, including IL-6 produced

locally by fibroblasts, endothelial cells and keratinocytes, in response to tumour necrosis factor-α (TNF- α) and IL-1β. In doing do, IL-6 switches to trans-signalling, promoting the release of chemokine (C-C motif) ligand-2 (CCL2), a potent chemoattractant for monocytes (15).

1.3.1 Efferocytosis

As adhesion molecule expression declines and remaining pro-inflammatory soluble mediators are catabolised, fewer neutrophils and monocytes are recruited to the site of inflammation (8). Primarily, neutrophils then undergo programmed apoptosis or necrosis and are efferocytosed by mononuclear phagocytes (3, 10), although a small proportion undergo reverse migration to the lymphatic system and ultimately the lymph nodes (16, 17). The specific recognition of an apoptotic cell is dependent on changes in the expression of cell surface molecules. During apoptosis, the dying cell upregulates the expression of various ‘eat me’ signals triggering phagocytic uptake, including nucleotides, phospholipids and phosphatidylserine (PtdSer) (18). PtdSer is transported from the outer to the inner leaflet of the phospholipid bilayer through the activation of caspases, such as caspase-9, which is activated by the cytochrome c/apoptotic protease activating factor (Apaf-1) apoptosome, leading to further activation of effector caspases 3 and 7 (18).

Receptors on the surface of macrophages can bind to PtdSer, including the T cell/transmembrane, immunoglobulin and mucin (TIM) family with TIM-4 binding PtdSer avidly and mediating the phagocytic phase of the apoptotic cell (19). Once bound, other soluble proteins, including protein S/growth arrest specific (Gas)-6 and milk fat globule epidermal growth factor (MFG-E)-8, which activate their respective receptors (mer tyrosine kinase [MerTK] and integrin-αE), leads to ras-related C3 botulinium toxin substrate (Rac)-1 activation and actin polymerisation. This allows the phagocytosis of the apoptotic cell by macrophages (20). In turn, this leads to a complex and highly regulated cascade of cellular signalling in response to anti-inflammatory and pro-resolving cytokines and lipid mediators, triggering the

conversion of the pro-inflammatory and efferocytosing macrophage to an anti-inflammatory/pro-resolution phenotype; the so-called ‘M2’ macrophage. This is characterised by the upregulation of co-inhibitory molecules, including programmed death ligand-1 (PDL1) and inducible costimulator (ICOS) ligand and the release of numerous soluble mediators including IL-10, transforming growth factor (TGF)-β, PGE_2 and cyclic adenosine monophosphate (cAMP) (14, 21). Surviving cells (in the most part mononuclear phagocytes) can then leave the site of inflammation using the local draining lymphatic system. Though controversial, further specialised pro-resolving mediators (SPMs), including resolvin E1 (RvE1), protectin D1 and maresin are also released by macrophages following ingestion of apoptotic cells, further hastening the termination of inflammation. From a clinical perspective, failure of efferocytosis has been suggested to be involved in the pathogenesis of various autoimmune disease, including RA and systemic lupus erythematosus (SLE), due to the failure to clear apoptotic cellular debris and the subsequent development of anti-nuclear antibodies directed against cellular immunogens (22–24).

1.3.2 Switching off pro-inflammatory signals

To further facilitate the resolution of inflammation, several regulatory mechanisms exist to dampen pro-inflammatory signalling. TLR signalling can lead to the activation of nuclear factor kappa-light-chain-enhancer of activated B cells (NF-κB) and the subsequent production of pro-inflammatory TNF-α following PAMP recognition (25). Leucine-rich repeat containing 33 (LRRC33) is a TLR homologue lacking the Toll-IL-1 (TIR) domain, losing its ability to interact with downstream adaptors and signalling proteins and can interact with TLRs, thus dampening pro-inflammatory responses leading to reduced NF-κB activation and subsequent pro-inflammatory cytokine production (26). Similarly, macrophages expressing Girdin, an actin-binding protein, can recognise LPS, leading to suppression of pro-inflammatory cytokines production *via* the NF-κB pathway (27). This is mediated through its C-terminally located TIR-like BB-loop (TILL) motif, which binds the cytoplasmic TIR modules of TLR4 in a manner that precludes receptor dimerisation, which is a prerequisite for pro-inflammatory signalling. Thus, a myriad of endogenous signalling pathways exist

which counteract the highly programmed sequence of events leading to the acute inflammatory immune response.

1.3.3 Soluble lipid mediators in inflammation and resolution

In addition to cytokines and chemokines, numerous soluble lipid mediators contribute to the complex, coordinated inflammatory response (28). Eicosanoid lipids mediators are oxidised derivatives of polyunsaturated fatty acids (PUFAs) synthesised by the action of COX, lipoxygenase (LOX) and cytochrome P450 pathways. The predominant substrate for eicosanoid synthesis is arachidonic acid (AA) (29).

1.3.3.1 Prostanoids

Prostanoids, consisting of PGs and thromboxane, are a group of soluble lipid mediators derived from the PUFA, AA, found in the plasma membrane of cells (30). AA is released from the phospholipids resident in the bilayer by the action of phospholipase A_2 (PLA_2) during inflammation (31). Under the influence of PGG and H or COX, PGH_2 is generated, which is rapidly converted to PGD_2, PGE_2, $PGF_{2\alpha}$, prostacyclin (PGI_2) and thromboxane A_2 (TXA_2) by tissue-specific synthases, as shown in **Figure 1.2** (30). The diversity of terminal synthases and receptors gives rise to a wide range of biological functions. PGE_2 is one of the most abundant PGs and is involved in regulating immune responses, blood pressure, gastrointestinal integrity and fertility (32). Dysregulation in the synthesis of PGE_2 can lead to a range of pathological conditions including autoimmune disease, atherosclerosis (33), Alzheimer's disease and cancer (32, 34). PGE_2 is traditionally thought of as pro-inflammatory due to enhanced vasodilatation and vascular leak (35), but following resolution of inflammation also has multiple anti-inflammatory roles, including suppression of bacterial phagocytosis and nicotinamide adenide dinucleotide phosphate (NADPH)-mediated killing (36), inhibition of T cell proliferation (37) and

reduction in pro-inflammatory mediators (21). Indeed, Trivedi *et al.* (2006) showed using $hPGD_2$ synthase ($hPGD_2S$) knock-out and transgenic mice that $PGD_2S^{-/-}$ animals displayed a more severe inflammatory response histologically compared to transgenic animals (38). Additionally, lymph node lymphocytes from knock-out animals showed hyperproliferation and increased IL-2 synthesis, effects that were rescued by 15d-PGJ_2 (through inhibition of NF-κB activation and not peroxisome proliferator-activated receptor [PPAR] signalling), but not PGD_2. Therefore, $hPGD_2S$ may act as an internal braking signal essential for bringing about the resolution of T helper (Th)-1-driven delayed type hypersensitivity reactions and $hPGD_2S$-derived cyclopentenone PGs may protect against inflammatory diseases (including RA), where T lymphocytes play a pathogenic role. Overall, rapidly following the onset of acute inflammation by the inciting stimulus, circulating concentration of prostanoids significantly increase in line with upregulation of PG synthases (PGSs) and play integral roles during acute inflammation and pro-resolution pathways (14).

1.3.3.2 Leukotrienes and lipoxins

LOX enzymes (5-, 12- and 15-LOX) metabolise AA to leukotrienes (LT) and lipoxins (LX) (39). These classes of lipids also show great variation in biological function with both pro-inflammatory and anti-inflammatory functions. Leukotrienes, including LTB_4, are biosynthesised intracellularly and are potent pro-inflammatory mediators, acting as a chemoattract to neutrophils and eosinophils (40). Lipoxins are generated transcellularly and include LXA_4 and LXB_4 as shown in **Figure 1.2** (41). They are generally thought of as anti-inflammatory/pro-resolution and have been shown to inhibit neutrophil infiltration into inflamed tissue (41–43), increase levels of the TGF-β (44), enhance mononuclear cell infiltration and stimulate efferocytosis (41, 45). It has been postulated that LXB_4 may play a role in the development of RA, with knock-out mice showing resistance to the development of collagen-induced arthritis and thus suggesting a role in the pathophysiology of the disease (46, 47).

1.3.3.3 Cytochrome P450 lipids

The cytochrome P450 (CYP) epoxygenase enzymes make up a family of membrane-bound proteins and are involved in around 90-95% of enzyme reactions in the human body (48). They are also responsible for the metabolism of around 95% of pharmaceuticals on today's market and play a key role in steroid and fatty acid hydroxylation, PUFA metabolism and cholesterol biosynthesis (49). In particular, they produce epoxy-oxylipins from phospholipid bilayer AA by phospholipase A_2, predominantly by the action of CYP2C8, CYP2C9 and CYP2J2 (50). Multiple P450 epoxygenase enzymes are involved in PUFA metabolism, as summarised in **Figure 1.2**. AA can generate allelic oxidised hydroxyeicosatetraenoic acids (HETEs) 5-, 8-, 9-, 11-, 12- and 15-HETE, as well as terminal ω-hydrolysed 16-, 17-, 18-, 19- and 20-HETE (48). Epoxygenases also catalyse the formation of epoxy-eicosatetraenoic acids (EETs) 5,6-, 8,9-, 11,12- and 14,15-EET, subsequently metabolised by soluble epoxide hydrolase (sEH) to dihydroxyeicosatrienoic acids (DHETs), 5,6-, 8,9-, 11,12-, and 14,15-DHET. Epoxygenases are also able to metabolise PUFAs other than AA into further eicosanoids. Linoleic acid can be converted to epoxy-octadacamonoenoic acids (EpOMEs), 9,10- and 12,13-EpOME and further metabolised by sEH to dihydroxy-octadecenoic acids (DiHOMEs), 9,10-DiHOME and 12,13-DiHOME. In the presence of epoxygenase, docosahexaenoic acid (DHA) is converted to 19,20-epoxy-docosapentanoic acid (EpDPE) and then 13,14-, 16,17- and 19,20-dihydroxydocosapentaenoic0 acid (DiHDPA) by sEH. Finally, eicosapentaenoic acid (EPA) is converted to epoxy-eicosatetraenoic acids (EpETEs) 17,18-EpETE and subsequently metabolised by sEH to dihydroxyicosatetraenoic acids (DiHETEs), 17,18-DiHETE and 14,15-DiHETE (51). Cytochrome P450 lipids play important roles in inflammation as both pro-inflammatory or anti-inflammatory mediators, having been shown to stimulate smooth muscle cell contractility and endothelial cell activation in cardiovascular disease (52), improve airway resistance and vascular tone in obstructive airway disease (53) and inhibit sodium and potassium exchange in renal disease (54). More recently, these lipids have been shown to have anti-inflammatory effects in RA, likely attributed to PPAR-γ activation, leading to reduced bone resorption and osteoclastogenesis, thus making them an exciting area for future research and potential novel therapeutic strategies in inflammatory arthritides (55).

The synthesis of the numerous AA-derived lipid mediators is complex and they are generated *via* several different metabolic pathways. These have been summarised in **Figure 1.2**.

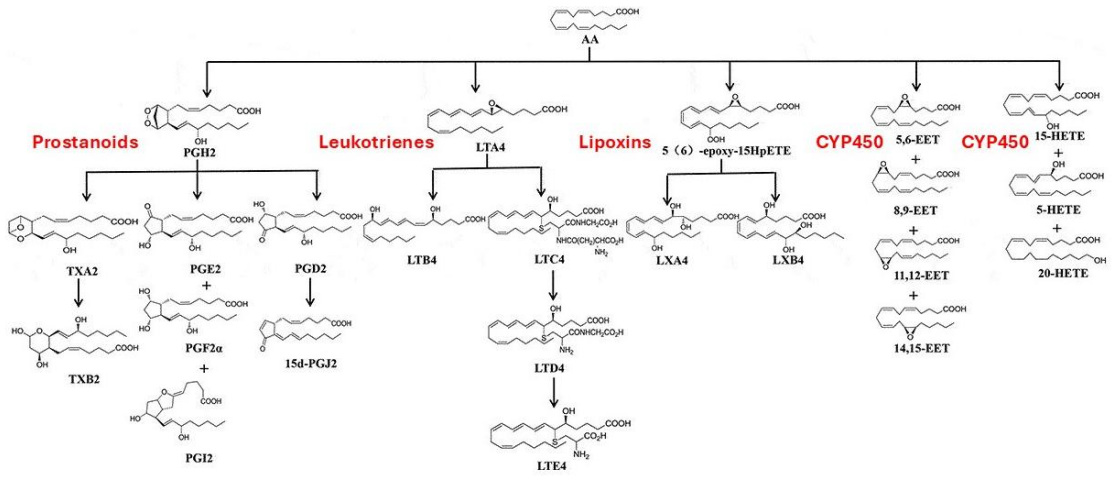

Figure 1.2. Schematic showing the biosynthesis of lipid mediators from AA. AA is metabolised *via* three main metabolic pathways: COXs, LOXs and CYP450 pathways. Depicted are prostanoids (PGs and TXAs), leukotrienes, lipoxins and CYP450-derived lipid mediators. Adapted from Cheng and Rong (2018) (56).

1.3.3.4 Specialised pro-resolution mediators

SPMs represent a subset of lipid signalling molecules able to dampen inflammation mediated through several pro-resolution pathways (57). They are generated from the omega-3 fatty acids DHA and EPA and fall into three families of molecules: resolvins, protectins and maresins. RvE1, derived from EPA, exerts a pro-resolution effect by interaction *via* G-protein-coupled receptor (GPCR) and LTB_4, a potent neutrophil chemoattractant important in the initiation of acute inflammation (40). In doing so, RvE1 attenuates this signal leading to a reduction in neutrophil infiltration and degranulation (58). RvD1 has also been shown to stimulate monocytic phagocytosis and enhance efferocytosis of apoptotic cells (59). However, SPMs remain controversial in the literature in view of original published data being acquired without using accepted scientific standards for quantification and quoted levels, which may not have been detectable (60, 61). Nevertheless, the identification of bioactive lipid

mediators regulating onset and resolution phases of inflammation and their interactions with other soluble lipids makes them and their pro-resolution action an interesting area for further research, particularly in autoimmunity.

1.3.3.5 Endocannabinoids

Endocannabinoids are soluble lipid mediators with the most studied including AEA (anandamide), PEA, *N*-acylethanolamine (NAE) and *N*-oleoylethanolamine (OEA) (62). NAE, AEA and PEA are synthesised from membrane *N*-acylphosphatidylethanolamine (NAPE) precursors either directly through a NAPE-selective phospholipase D or through the serial action of phospholipase C, followed by phosphatase or phospholipase A_2 and then lysophospholipase D (63). Additionally, 2-AG is primarily produced from phospholipid-derived diacylglycerols by the actions of diacylglycerol lipase (DAGL) A and B (62, 64).

Endocannabinoids exert their biological function by binding and activating several membrane-bound proteins (65). NAE and AEA are both derived from AA and can bind and activate two GPCRs; cannabinoid receptor 1 ($CB\text{-}_1$) and 2 ($CB\text{-}_2$) (66). An overview of endocannabinoid activation pathways is shown in **Figure 1.3**. Their production from cell membrane lipid precursors is activity-dependent and their action terminated by hydrolysis *via* various lipases (62). AEA signalling is terminated by two amidases, fatty acid amide hydrolase (FAAH) and *N*-acylethanolamine-hydrolysing acid amidase (NAAA), whereas monoacylglycerol lipase (MAGL) and α/β-hydrolase domain 6 (ABHD6) are two esterases involved in regulating 2-AG signalling (67).

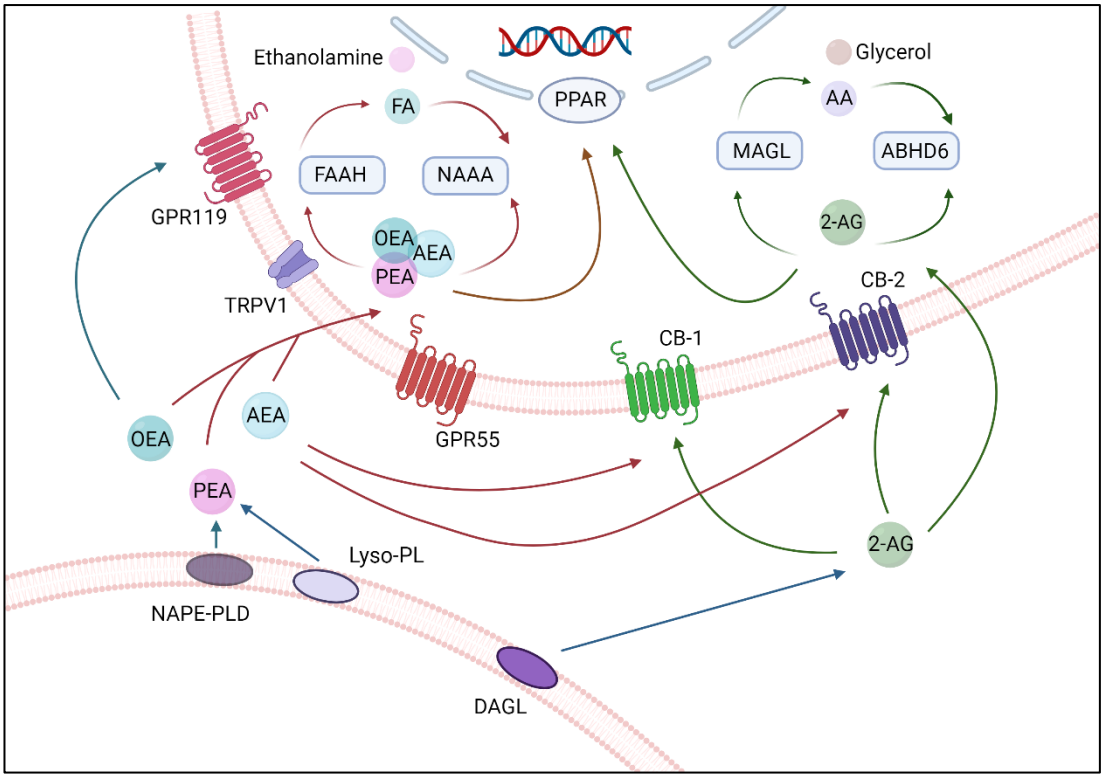

Figure 1.3. Schematic showing the endocannabinoid system at a glance. Bioactive lipids can activate the following: (i) G protein-coupled receptors such as the CB-$_1$ and CB-$_2$ cannabinoid receptors (AEA, 2-AG), GPR119 (OEA), or GPR55 (putatively by PEA); (ii) the channel receptor TRPV1 (AEA); and (iii) the PPARs (AEA, OEA, PEA, 2-AG). These lipids are hydrolysed inside the cell by several lipases. The two prime enzymes hydrolysing NAEs are the serine amidase FAAH and the cysteine amidase NAAA. 2-AG is hydrolysed by two serine hydrolases, MAGL and ABHD6.

In addition to generating AEA and 2-AG, the enzymes responsible for their biosynthesis also produce other bioactive lipids (62). These lipids do not always bind to cannabinoid receptors, but they do share their metabolic pathways and some molecular targets with endocannabinoids. For instance, PEA and OEA, differing from AEA by the presence of an acyl chain, do not bind to cannabinoid receptors but to nuclear PPARs and GPCRs, including GPR119 (68). 2-oleoylglycerol, a 2-AG analogue, also lacks significant affinity for the cannabinoid receptors but binds and activates GPR119 (69). Furthermore, GPR55 and the transient receptor potential vanilloid (TRPV)-1 channel (activated by AEA) are additional targets related to the endocannabinoid system for the development of novel therapeutics (68). Increasing

evidence suggests that the endocannabinoid system plays an important role in the pathogenesis of RA, by inhibiting pro-inflammatory cytokines and matrix metalloproteinases, reducing T cell activation, fibroblast-like synoviocyte proliferation and the formation of auto-antibodies (70). In doing so, they have been postulated to be important in anti-inflammatory/pro-resolution pathways (71). A number of pharmacological agents, including lenabasum, a selective CB-$_2$ analogue, have been developed to target this complex biological system, with varying degrees of success (72, 73). The endocannabinoid system is gaining interest as a drug target given its potential application in the treatment of autoimmune disease, cancer, cardiovascular disease and neurodegenerative disease, although remains a relatively understudied field (74, 75).

Overall, changes in gene expression in immune cells are frequently associated with production and secretion of inflammatory mediators in response to a particular stimulus. Secretion of these mediators into the extracellular milieu results in further amplification and/or modification of the original signal. Examples of intracellular signalling pathways include the mitogen-activated protein kinase (MAPK) pathway, the Janus kinases (JAK) pathway, the signal transducers and activators of transcription (STAT) pathway, spleen tyrosine kinase (Syk) signalling and the NF-κB pathway (76).

1.3.4 Gaseous signalling mediators

The three main gaseous signalling molecules which have been studied include nitric oxide (NO), H_2S and carbon monoxide (CO) (77). They have been termed the 'gasotransmitters', forming a family of gaseous signalling mediators with important physiological functions. These molecules have a both pro- and anti-inflammatory effects and have been suggested to hasten the resolution of inflammation, as well as accelerating wound healing (78, 79). They are of very low molecular weight, have short half-lives and can freely diffuse across membranes with wide ranging biological effects mediated through their interaction with several proteins and genes (80).

1.3.4.1 Nitric oxide

NO is a vasoactive substance secreted by the vascular endothelium, synthesised by endothelial NO synthases (eNOSs) as shown in **Figure 1.4** (81). NO plays several diverse roles in the immune system and has been implicated in the pathogenesis of several autoimmune diseases using rodent models, including autoimmune arthritis, uveitis, and nephritis (82). Broadly speaking, it is the product of macrophages, following activation by cytokines or innate microbial antigens or both (83). Its wide-ranging effects, from an immunoregulatory point of view, ranges from the inhibition of T and B cell proliferation *via* increased apoptosis, downregulating major-histocompatibility-complex class II (MHC II), costimulatory molecules or cytokines and the inhibition of leucocyte recruitment by downregulating adhesion molecules (84). Additionally, it impacts upon numerous signalling cascades leading to the up- or downregulation of multiple cytokines, chemokines and growth factors (e.g. IL-1, IL-6, IL-10, interferon gamma [IFN-γ], monocyte chemoattractant-1 [MCP-1] and TGF-β) (85). It has become apparent that the previous notion that NO was protective during infection and damaging to tissues during autoimmunity is likely an oversimplification.

The vasodilatory effects of NO have been investigated for more than three decades in the context of human disease, with its therapeutic benefit shown to be efficacious to varying degrees in cardiovascular disease (86, 87), sexual dysfunction/male infertility (88, 89) and neuronal plasticity, amongst others (90). Despite this, NO has numerous reaction partners (including DNA, proteins, thiols and ROS) and this in combination with the fact that the regulation and expression of the eNOS isoforms are so complex and multifactorial, means that NO-based therapies in autoimmune disease are not easy to investigate nor develop as novel drugs.

1.3.4.2 Carbon monoxide

In vivo formation of CO was first demonstrated in the 1950s by Sjöstrand, who observed that the degeneration of haemoglobin led to CO production (91). In the

following decade, heme oxygenase enzymes were found to be the enzymatic source of CO (92–94) and in the mid-1980s the two human isoforms were discovered: heme oxygenase-1 (HO-$_1$) and heme oxygenase-2 (HO-$_2$) (95, 96). These are both distinct gene products, the former being a stress-inducible isoform, with the latter being constitutively expressed. Both HO enzymes catalyse the oxidation of heme to further biologically active compounds: biliverdin (antioxidant), CO (a ligand of heme) and chelated iron (a regulator of a number of genes, including eNOSs) as shown in **Figure 1.4** (97). Stressors that upregulate HO-1 are diverse and include heat, tissue ischaemia, hyper-/hypoxia and radiation (98). Other than in the presence of adrenal corticosteroids, HO-$_2$ is not inducible, with this phenomenon due to the glucocorticoid response element (GRE) in the gene promotor region (99). It is thought that the CO liberated during the enzymatic breakdown of heme is most likely a signalling molecule for the generation of cyclic 3',5'-guanosine monophosphate (cGMP) in biological systems (96).

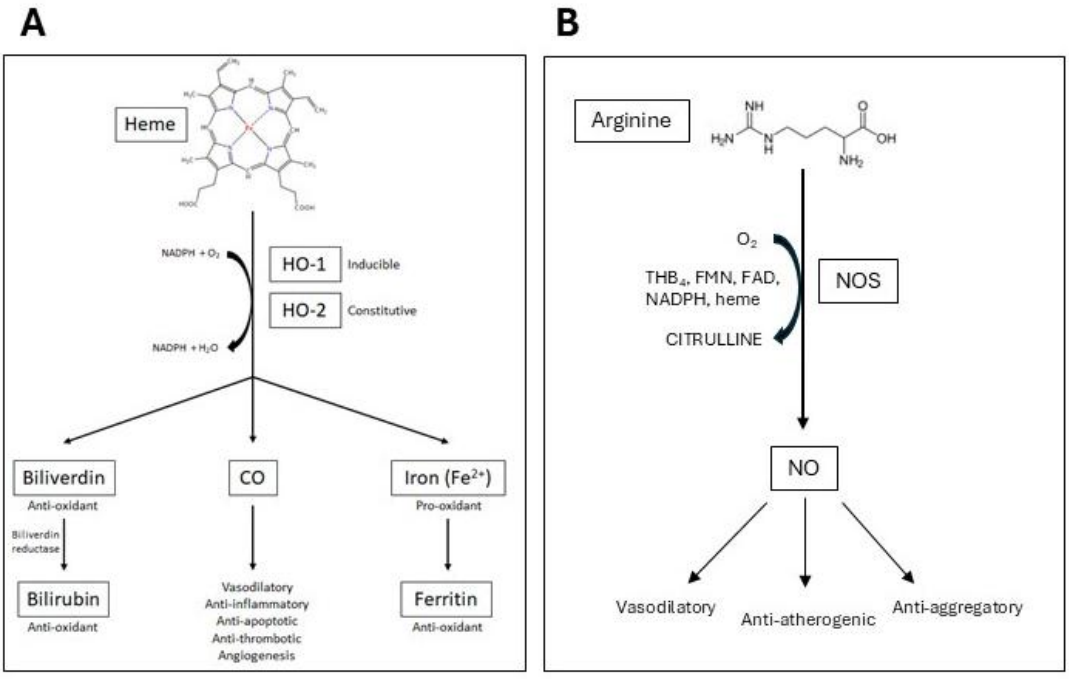

Figure 1.4. Simplified diagrams showing the metabolism of heme by HO enzymes and synthesis of NO from arginine by NOS. A) Briefly, HO cleaves the substrate protoporphyrin IX (PPIX)-Fe (III) forming biliverdin IXa, water and CO. In doing do, it releases the heme iron. This process requires NADPH-cytochrome p450 reductase in order to reduce the ferric heme-iron within the HO-heme complex. Three further oxygenation cycles ensue allowing the dissociation of ferrous iron from biliverdin. Biliverdin reductase is then able to reduce water-soluble biliverdin to the hydrophobic bilirubin. B) NO is synthesised by NOS from the amino acid L-arginine. This process involves a two-step oxidation where L-arginine is converted to L-citrulline and NO. NOS exists in three main isoforms: neuronal NOS (nNOS), inducible NOS (iNOS) and endothelial NOS (eNOS).

Willis *et al.* (1996) showed increasing activity of HO during an acute carrageenin-driven, complement-dependent inflammatory response in the rat pleural cavity was characterised by the early influx of PMNs (maximal at 6-12 hours) and later the influx of mononuclear phagocytes (maximal at the latest time-point of 48 hours) (100). This effect was reversed on inhibition of the HO system, suggesting an anti-inflammatory and pro-resolution role for HO, although the exact mechanism for this remains unknown. Furthermore, in an infected mouse model, Wegiel *et al.* (2014) showed HO-$_1$ deficiency resulted in impaired microbial clearance, worsening tissue damage and increased death (101, 102). They demonstrated that macrophage-generated HO-$_1$-derived CO promotes adenosine triphosphate (ATP) production and release by the bacteria, which in turn activates the Nacht, LRR family pyrin domain containing protein-3 (NLRP3) inflammasome, thus detecting products of damaged cells and optimising bacterial elimination. These defects in HO-$_1$–deficient macrophages were restored by administration of CO, suggesting that macrophage-derived CO enables the coordinated regulation of host immune response (101).

Other possible reasons for an altered inflammatory response in the context of increased HO activity may relate to cGMP signally, the antioxidant capacity of bilirubin and its metabolite biliverdin, or even depletion of heme itself; a molecule necessary for the generation of inflammatory AA lipid mediators, including PGs and thromboxane (96). Heme is also known to enhance bacterial virulence, binding to specific receptors on the bacterial surface thus increasing HO activity may suppress this binding and hence reduce virulence of the invading bacteria (103).

From a clinical perspective, patients with lower respiratory tract infections have been observed to have higher levels of CO in their exhaled breath, with levels reduced in those treated with antibiotics and recovering from illness (104). CO has also been shown to be elevated in the plasma of septic neonates (105). In a further group of septic patients, both arterial blood CO and HO-$_1$ expression on $CD14^+$ monocytes were elevated, correlating with increased survival compared to control (106). This, in combination with the observation that regulation of HO activity and CO production has serious ramifications for host physiology, and modulating this system, could make it an attractive target for developing further therapeutics.

1.3.4.3 Hydrogen sulfide

Whilst NO and CO are well established as vaso-modulators, H_2S may also be considered as a third classical gasotransmitter (107). Endogenous H_2S is produced in mammalian cells by the enzymic catalysis of L-cysteine and/or homocysteine depending on physiological conditions (108). These enzymes (cystathionine γ-lyase [CSE] and cystathionine β-synthase [CBS]) are present in both the cytosol and/or the mitochondria. This process is summarised in **Figure 1.5**. The release of H_2S from vascular smooth muscle cells at a physiologically relevant concentration relaxes the smooth muscle, thus leading to a vasodilatory effect mediated by the activation of ATP-sensitive potassium (K^+) channels and is likely regulated by NO (109). Latterly, H_2S can be scavenged by methaemoglobin or by metallo- or disulfide-containing compounds as well as oxidation and methylation metabolic pathways.

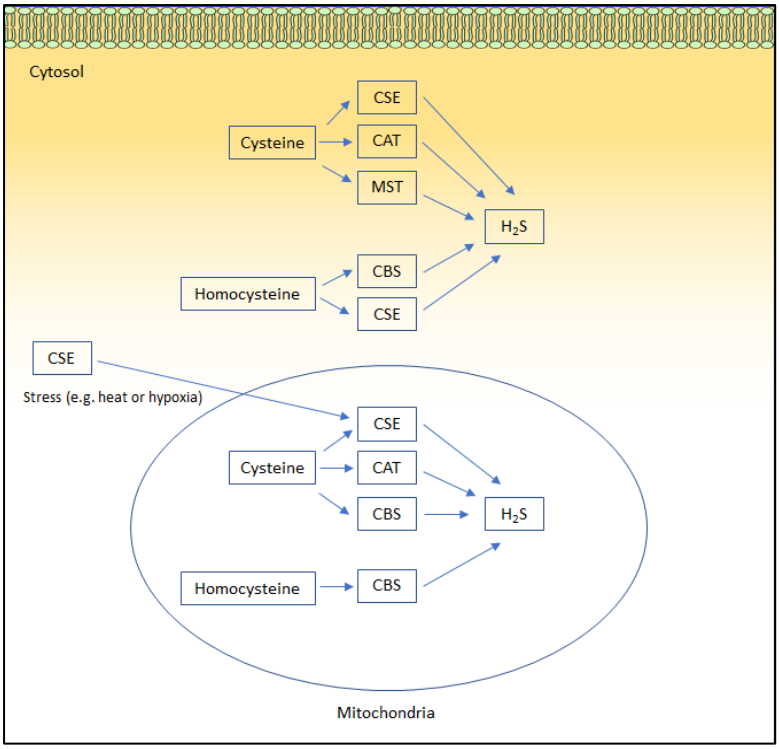

Figure 1.5. Simplified diagram showing the pathway for generating endogenous H_2S. Depending on cell-type and conditions of stress, endogenous generation may take place either in the cytosol or the mitochondria (or both). Briefly, CSE-facilitated H_2S production occurs in the cytosol, but as shown can translocate into the mitochondria under certain stressors to generate H_2S from cysteine. Cysteine aminotransferase (CAT) and 3-mercaptopyruvate (MST) are available in the cytosol allowing generation of H_2S. Cystathionine β-synthase is generally located in the cytosol but again can translocate under certain circumstances and certain cell-types.

H_2S influences numerous physiological and pathophysiological process and has been implicated in protection against hypertension and vascular remodelling, angiogenesis, atherosclerosis, liver disease, diabetes and neurodegenerative disorders (110). The anti-inflammatory role of H_2S is believed to act through several pathways to reduce inflammation and protect tissue from damage. Notably, H_2S can suppress PMN adhesion, rolling and extravasation thus reducing the associated oedema, as well as ameliorating damage from oxidative stress, promoting neutrophil apoptosis, driving macrophage differentiation to a more anti-inflammatory phenotype and reducing the production of inflammatory cytokines (111). The exact mechanism is unknown, however, some of the potential mechanisms by which these processes occur are

summarised in **Table 1.1**. Thus, the H_2S field has recently received significant scientific interest with the effects of its therapeutic utilisation being investigated in a range of human diseases, including ischaemic disease (112), blood pressure regulation and hypertension (113, 114).

Table 1.1. List of the potential mechanisms of action of H_2S in the context of immune responses and inflammation. Adapted from Wallace *et al*. (2007) (115).

Mechanism	Author(s)
Activation of K^+_{ATP} channel	(116, 117)
Inhibition of activation of NF-κB	(118, 119)
Inhibition of activation of p38 MAP kinase	(120, 121)
Inhibition of caspase-3 cleavage	(121)
Inhibition of heme oxygenase-1 expression	(119)
Inhibition of hypochlorous acid activity	(122)
Scavenging of peroxynitrite	(122)
Modulation of intracellular redox state	(123)
Elevation of intracellular cyclic AMP‡	(109)

1.4 Post-resolution phase

The exact time at which resolution occurs has been quantified using resolution indices and can be described as the point at which the PMN infiltration equals that of the infiltrating mononuclear cells (124). It is now known that following resolution of the initial acute, inflammatory response, there is a further phase in which the local environment remains immunologically active for several weeks (4, 125, 126). It has been shown in the Gilroy group, that in a murine model of acute zymosan-driven inflammation, numerous leucocytes repopulated the original site of inflammation, thus representing a second wave of immune cells (4, 125, 127). These included monocyte-derived macrophages, dendritic cells, myeloid-derived suppressor cells, along with the tissue-resident macrophages that had initially left the site of inflammation during the resolution phase. Additionally, an increase in T and B cell numbers was observed in both the blood and tissue. Of note, no further PMNs were recruited during this time

(125, 128). Thus, this altered local microenvironment may represent a bridging of the innate and adaptive immune responses. Furthermore, this ongoing subclinical immunological activity is now known to alter the biochemical makeup of the inflamed tissue longer term, meaning homeostasis is not restored and a period of 'adapted homeostasis' persists (129).

Newson *et al*. (2014) showed in a murine model of peritonitis induced by the intraperitoneal injection of zymosan A, that a second wave of mononuclear cells infiltrates into the inflamed site that persists for months (125). Polychromatic flow cytometric analysis of these cells revealed them to be myeloid-derived suppressor cells and macrophages as well as $CD4^+$, $CD8^+$ and natural killer (NK) lymphocytes. Expansion of the lymph nodes was also observed, with populations of monocyte-derived dendritic cells, memory T and B lymphocytes originating from the inflamed peritoneum identified. They described this period of ongoing immune activity as a third 'post-resolution' phase. Other groups have seen similar post-resolution changes, including prolonged defects in the integrity of draining lymphatics up to 10 months following resolution of infection with *Yersinia pseudotuberculosis* (130) and others have shown similar changes seen in animals infected with herpes simplex virus (HSV) (131).

Motwani *et al.* (2017) showed that neutrophil clearance and pro-inflammatory cytokine clearance, following UV-KEc-triggered dermal inflammation in humans, occurred by 72h (60). Despite this, following a lag phase of around four days there was an increase in numbers of memory T cells and $CD163^+$ macrophages at the inflamed site up to day 17, as well as increased biosynthesis of COX-derived prostanoids and DHA-derived D series resolvins (60). More recently, Feehan *et al.* (2024) showed that within days following resolution of *Streptococcus pneumoniae*-triggered murine lung inflammation, there was an influx of antigen-specific memory T lymphocytes, alveolar and interstitial macrophages into the tissue (129). The latter were enriched with genes that drive T cell chemotaxis and differentiation and PG synthesis suggesting these cells play a role in T cell development and limiting tissue injury at the site of inflammation. Taken together, it seems that whilst differences are seen in the tissues studied and inciting inflammatory stimulus used in studies in both

mouse and human, that resolution is not the end of innate-mediated immune responses and that there remains significant ongoing immunological activity. Furthermore, this process informs both memory response and preventing long-term tissue damage.

Inflammation is therefore a combination of inflammatory 'go' signals counteracted and regulated by internal 'off' signals, leading to the clearance of the inflammatory stimulus and the initiation of resolution followed by a period of ongoing immunological activity. In patients with chronic inflammatory diseases who are in remission, it is not known whether this period of disease inactivity is brought about by activation of internal anti-inflammatory signals, such as those that might suppress TNF-α, or whether there is activation of pro-resolution signals, or a combination of these processes.

This thesis will aim to investigate the pro-resolution and anti-inflammatory signals present in the resolution and post-resolution phase to better understand why some RA patients remain in remission off treatment and whether there are specific protective signals which remain active in the post-resolution phase following inflammation onset. To understand this, it is important to appreciate the immune dysregulation and underlying disease pathogenesis leading to autoimmune disease, exemplified by that seen in RA.

1.5 Inflammation resolution and autoimmune disease in humans

Autoimmune diseases are a group of complex and chronic disorders characterised by the immune system being misdirected toward the host and pose an increasing unmet clinical need (132). These conditions arise when the immune system, designed to protect the body against foreign substances, targets healthy cells, leading to damage and loss of function (132, 133). The clinical features of these diseases are a consequence of the inflammation and damage caused at the tissue level due to a systemic process resulting from the dysregulated immune response in these individuals and an inability to switch off inflammation (134). Autoimmune disease remains one of the biggest challenges facing healthcare today, affecting approximately

one in 10 individuals in the developed world, thus representing a major global socioeconomic burden (135). The exact cause of autoimmune disease remains unknown, although it is thought to be the culmination of genetic predisposition and environmental factors (133). Therapies for autoimmune disease are generally broad-acting and treat in a non-disease-specific manner, often associated with numerous and significant adverse effects, including infection and malignancy (136). Over 80 autoimmune diseases have now been described and this thesis will focus on RA, the most common autoimmune rheumatological disease worldwide (135).

1.5.1 Pathophysiology of rheumatoid arthritis

RA is one of the most common autoimmune diseases worldwide, affecting approximately 1% of the population (137). RA is characterised by synovitis, swelling and joint damage the latter being the end result of complex autoimmune and inflammatory processes involving both the innate and adaptive immune systems (138). Whilst numerous molecular, cellular, immunological, genetic and clinical studies have increased our understanding of the mechanisms underpinning this disease, the underlying pathophysiology and dysregulated immune response remains poorly understood.

1.5.1.1 Genetics factors

The initial stage in the pathobiology of RA involves the presentation of a driving antigen to an immunogenetically and environmentally susceptible host (139). Antigen-presenting cells, including synovial membrane-resident macrophages, infiltrating monocytes and dendritic cells ingest, process and present these foreign antigens to complementary Th receptors, following the differentiation of naïve $CD4^+$ T cells into distinct Th cell subsets, each with specific effector functions characterised by the cytokines produced (140). This process is mediated through MHC II glycoproteins to which the antigens are bound, to allow their presentation, thus initiating a cellular

immune response and resulting in the differentiation of B cells into antibody-secreting plasma cells (141). The human leucocyte antigen (HLA) locus (MHC locus), encoded on chromosome 6, is associated with increased risk of disease susceptibility with RA patients bearing *HLA-DRB1* alleles (*HLA-DRB1*1001*, *HLA-DRB1*0101*, *HLA-DRB1*0102*, *HLA-DRB1*1402* and *HLA-DRB1*04* members [for example **0401*, **0404*, **0405*, **0408*]), or *HLA-DR4* alleles or both; implicating a genetic component to disease susceptibility (142). The so-called 'shared epitope' is a five amino acid sequence motif in positions 70-74 of HLA-DRβ chains encoded by *HLA-DRB1* alleles present in different class II molecules and appears to determine susceptibility to the disease (139). Furthermore, null alleles for this gene have been shown to have a protective effect in RA (143). Studies of the prevalence of RA in monozygotic twins where one twin has RA, have shown a predisposition to developing the disease, but not all genetically identical sibs developed RA, suggesting that genetics are not solely responsible for the development of the disease (144).

1.5.1.2 Infective and endogenous triggers

Numerous infectious and non-infectious agents have been proposed as arthritogenic stimuli in the development of RA (145). Epstein-Barr virus (EBV) was initially suggested as one such pathogen in the 1980s, with around 80% of patients with RA having circulating antibodies directed against EBV-specific antigens (146). The virus is known as a polyclonal activator of B cells, leading to the production of immunoglobulins, including rheumatoid factor (RF) and causes a diminished cytotoxic T cell response (147). Parvovirus B19, a small DNA virus, can cause a self-limiting inflammatory arthropathy and despite a transiently detectable RF titre, this resolves spontaneously and the pattern of joint involvement does not resemble that of RA (148). Other pathogens have drawn attention in this regard, including rubella, mycoplasma, cytomegalovirus and herpesvirus, but have not received ongoing scientific support (149).

Endogenous collagen can induce arthritis in rodents and is used as an animal model for RA (150). Möttönen *et al.* (1988) found that despite elevated titres of anti-collagen

antibodies in the serum of patients with RA, increased levels did not precede the clinical onset of disease (151). Thus, Rowley *et al.* (1986) suggested that anti-collagen antibodies were more involved in the propagation of synovitis and tissue damage, likely initiated RF production and the more recently described citrullinated proteins (152). Together, RF-IgG and collagen-antibody complexes precipitate into the cartilage serving as a chemoattractant for immune cells to the tissue (152).

1.5.1.3 Epigenetics

Epigenetics are also important in the pathogenesis of RA. Glossop *et al.* (2015; 2016) showed that treatment-naïve RA patients display novel, disease-specific DNA methylation aberrations in a genome-wide study (153, 154). Citrullination describes the post-translational modification of the amino acid arginine into citrulline, leading to altered peptides and has been shown to be key to the pathogenesis of RA (155). James *et al.* (2010) showed this conversion generates 'altered-self' peptides; proteins that can be bound and presented by *HLA-DRB*1001* leading to altered binding affinity and suggested this as an important factor in the initiation and progression of RA (156). Evidence has emerged linking the development of RA with anti-citrullinated peptide antibodies (ACPAs), commonly measured in hospital reference laboratories as anti-cyclic citrullinated peptide (anti-CCP) auto-antibodies and these are present in the sera of up to two thirds of RA patients (157). Other citrullinated peptides are also likely to be important, such as the intracellular protein vimentin. Recently, ACPAs isolated from RA sera were shown to enhance NF-κB activity and TNF-α production in monocytes and tissue-resident macrophages by binding to citrullinated Grp78, a surface protein, further highlighting the potential role of altered peptides in the pathogenesis of RA (158). Interestingly, the initial appearance of RF and ACPA precedes the development of the clinical features of RA involving the synovium by a median of 4.5 years (138). Thus, it seems that citrullinated, but not always native peptides, stimulate specific T cell responses and lead to loss of immune tolerance, notably to self-proteins that contain a citrulline residue.

1.5.1.4 Environmental triggers

Tobacco smoke is the only environmental factor that has a clear association with the development of RA and has been shown to upregulate pro-inflammatory cytokines, including IL-1α, IL-1β, IL-6 and IL-8 (159). In addition to the increase in cytokine production, smoking also upregulates the expression of heat shock proteins in synovial fibroblasts leading to chronic inflammation (160). Furthermore, smoking has been shown to increase the likelihood of increased levels of ACPAs which is associated with an increased risk of developing RA (161). Diet, body mass index, alcohol intake and caffeine have also been implicated as environmental triggers for RA (162). In particular, a diet rich in omega-3 fatty acids, is thought to be protective against RA (163). Given that that these PUFAs are also metabolised by COX enzymes responsible for the generation of PGs, a high concentration of fatty acids is thought to saturate the enzymatic capacity of COX, leading to a reduction in pro-inflammatory PGs (164).

1.5.1.5 Immune cell infiltration

Synovitis occurs as a consequence of leucocyte infiltration into the synovium in response to adhesion molecules and chemokines described in **Section 1.2**. This leads to hypoxia due to a mismatch in cellular burden and vascular supply (165), stimulating angiogenesis in response to local secretion of vascular endothelial growth factor (166). Cells of the innate immune system, including macrophages, mast cells and NK cells are located in the synovial membrane, whereas neutrophils are typically found in the synovial fluid (167). Macrophages are important effectors of synovitis acting through phagocytosis, antigen presentation and the release of pro-inflammatory cytokines, ROS, prostanoids, and matrix-degrading enzymes (168). Cytokines play a key role in the propagation of the immune response in RA both within the synovium and systemically and these have been summarised in **Table 1.2**.

TLRs also play a role in RA pathogenesis. TLRs expressed on monocytes, tissue-resident macrophages, and dendritic cells initiate the inflammatory response upon exposure to an immunogenic stimulus in RA, as would be expected with a pathogen,

resulting in the rapid expression of pro-inflammatory cytokines that mediate an immune response, recruiting circulating neutrophils, monocytes and lymphocytes (169). Macrophages and dendritic cells accumulate processed antigen and migrate to peripheral lymphoid tissue where antigen is presented to cells of the adaptive immune system with resultant activation of cellular immunity and production of antibodies, including autoantibodies, such as RF and ACPA (170). Unlike with the clearance of an invading pathogen, in RA, the inflammatory response remains chronically activated resulting in tissue damage characteristic of the disease (171).

1.5.1.6 Autoantibodies in RA

Along with immune cell infiltration into the inflamed joint characteristic of RA, immune complexes are critical to the pathogenesis of the disease (168). Self-aggregating complexes of RF are thought to be largely responsible for tissue damage in RA with their effects mediated by a complex cascade involving complement activation and stimulation of phagocytes *via* complement (in the most part the anaphylatoxin C5a) and Fc receptors (172). RF-containing immunoglobulin complexes consist of antigens and antibodies to putatively identified microbial epitopes which activate complement and phagocytes inducing signalling pathways and result in the production of pro-inflammatory cytokines (including TNF-α and IL-1β), PGs, mononuclear cell factor and other tissue-damaging molecules (including metalloproteinases such as collagenase) by macrophages (173). Neutrophils, which comprise more than 90% of total cell population in synovial fluid, take up immune complexes through Fc receptors, triggering the release of hydrolytic enzymes, the generation of ROS and products of AA metabolism, thus promoting an inflammatory response and tissue damage (174). ACPA recognise citrullinated protein residues, which result from the conversion of arginine to citrulline by peptidyl arginine deiminase (172). ACPA-containing immune complexes induce TNF-α secretion by macrophages *via* engagement of FcγRIIa at the surface of these cells, leading to increased numbers of infiltrating lymphocytes and activate the complement system *via* the classical and alternative pathways (175). Indeed, both RF- and ACPA-positive

(seropositivity) status are associated with the development of more erosive disease in RA (176).

Table 1.2. The role of cytokines in RA. Major representative cytokines, respective cytokine receptors, signal transduction pathways and pathological effects during inflammation and the progression of RA. Adapted from Kondo *et al.* (2021) (177).

Cytokine (receptor)	**Major signalling pathways**	**Roles in rheumatoid arthritis**
TNF-α (TNFR 1/2)	NF-kB, MAPKs, PI3K	Osteoclastogenesis, TNFR1; T_{reg} inhibition, Proinflammatory cytokine production TNFR2; T_{reg} activation Epigenomic modification (acetylation/methylation) memTNF; protective against arthritis
IL-6 (IL-6R)	gp130, JAK1/ 2, Tyk2, STAT1/3, PI3K, SHP-2, ERK	Osteoclastogenesis Proinflammatory cytokine production Autoantibody production Th-17 differentiation, T_{reg} inhibition
IL-33 (ST2-IL-1)	RacP, MyD88, IRAKs, TRAF6, NF-kB, MAPKs, AP1	Pro-inflammatory cytokine production Activation of mast cells, T_{regs}, Th-2, and ILC2
IL-1β (IL-1R)	MyD88, IRAKs, TRAF6, NF-kB MAPKs, AP1	Inflammation Th-17 differentiation, T_{reg} inhibition
IL-18 (IL-18Rα/18Rβ)	MyD88, IRAKs, NF-kB	Inflammation Neutralisation
IL-23 (IL-12Rβ1/IL-23R)	Tyk2, JAK2, STAT3/4	Activation of Th-17, NKT, and ILC3 cells Cytokine production (IL-17, TNF-α, GM-CSF)
IL-17 (IL-17R)	ACT1, TRAF6, NF-kB, MAPKs	Proinflammatory cytokine production Osteoclastogenesis Activation of synovial fibroblasts, macrophages
IL-7 (IL-7R)	JAK1/3, STAT3/5, PI3K, AKT	Differentiation, expansion of Th-17 cells T_{reg} differentiation Osteoclastogenesis
IL-21	JAK1/3, STAT1/3/5	Autocrine amplification of Th-17 cells Th17 differentiation, Treg inhibition
GM-CSF (GM-CSFR)	JAK2, STAT3/5	Macrophage activation Proinflammatory cytokine production

Cytokine (receptor)	Major signalling pathways	Roles in rheumatoid arthritis
IL-2 (IL-2R)	JAK1/2/3, STAT3/5, SHC-1, ERK	Late phase: arthritogenic Activation of ILC2, NK cells, Th-17 cells, IL-33 production Early phase: Anti-arthritogenic *via* IFN-γ Low dose IL-2 T_{reg} activation

TNF-α = tumour necrosis factor-α; TNFR = tumour necrosis factor receptor; memTNF = membrane TNF; JAK = Janus kinase; Tyk2 = tyrosine kinase 2; STAT = signal transducer and activator of transcription; PI3K = phosphatidylinositol-3 kinase; SHP-2 = Src homology region 2 domain-containing phosphatase 2; ERK = extracellular signal regulated kinase; Th = T helper; T_{reg} = T regulatory; IL = interleukin; IL-1-RacP = IL-1 receptor accessory protein; MyD88 = myeloid differentiation factor *88*; IRAKs = interleukin-1 receptor associated kinases; TRAF6 = tumour necrosis factor receptor-associated factor 6; MAPK = mitogen-activated protein kinase; NF-κB = nuclear factor-kappa B; AP1 = activator protein 1; ILC2 = group 2 innate lymphoid cells; NKT = natural killer T cell; ACT1 = nuclear factor activator 1; GM-CSF = granulocyte macrophage colony-stimulating factor; SHC-1 = Src homology domain-containing transforming protein 1; IFN-γ = interferon-gamma.

1.5.1.7 Adaptive immune response

Mononuclear cells, predominantly dendritic cells, present antigens to T cells that are present in the synovium as the first signal for T cell activation (178). The second signal, the costimulatory signal, requires the interaction of CD80/86 on the antigen-presenting cell with the CD28 on the T cell (179). Following T cell activation, naïve Th cells differentiate into three major subpopulations (Th-1, Th-2, and Th-17) each with distinct cytokine production profiles and functions (180). Dendritic cells and macrophages both secrete TGF-β, IL-1β, IL-6, IL-21 and IL-23, cytokines that support Th-17 differentiation and the secretion of IL-17A, IL17F, IL-22, IL-26, IFN-γ, whilst suppressing production of regulatory T cells (T_{regs}), culminating in a pro-inflammatory environment (168). In turn, IL-17A stimulates fibroblast-like synoviocytes to produce IL-26, leading to the production of the pro-inflammatory cytokines IL-1β, IL-6 and TNF-α (181). Humoral immune responses are also integral to the pathogenesis of RA, not only in their ability to differentiate in antibody producing cells, but also owing to defective B cell tolerance checkpoints, which can result in autoreactive B cells that can present antigen and activate T cells, as well as producing both pro- and anti-inflammatory cytokines (182).

1.5.2 Treating inflammation in autoimmune disease

1.5.2.1 Non-steroidal anti-inflammatory drugs

A key strategy for treating the symptoms of inflammation in RA is based largely upon inhibiting factors that drive this process, thus reducing pain, temperature, swelling, redness and ultimately regaining function. Such treatments include NSAIDs, including naproxen, ibuprofen and diclofenac, which work by blocking the production of PGs synthesised by COX enzymes 1 and 2 (183). COX-1 expression does not change significantly with inflammation but is thought to be important in the resolution of inflammation and COX-2 is the most responsive enzyme to pro-inflammatory mediators (184).

One such NSAID, naproxen, is used to treat the pain and inflammation associated with inflammatory rheumatic and non-rheumatic conditions, including RA. Its effects are generally thought to be related to the inhibition of both COX-1 and COX-2 enzymes and the consequent decrease in PG concentrations found in inflamed tissues, including synovial fluid and blood (185). Peak plasma concentrations are achieved within two hours and it is completely absorbed following oral administration, with naproxen demonstrating similar analgesic and anti-inflammatory efficacy to other commonly used NSAIDs (e.g. aspirin, diclofenac, ibuprofen, indomethacin, ketoprofen and piroxicam) (186). Naproxen binds extensively, in a concentration-dependent manner, to plasma albumin and is eliminated following biotransformation to glucuroconjugated and sulphate metabolites which are excreted in urine (187).

Importantly, adverse effects can hamper endogenous homeostatic systems, thus further predisposing to serious infection (188–190). Of note, NSAIDs increase cardiovascular risk (191–194) as well as causing unacceptably high levels of gastrointestinal (GI) upset, with mucosal irritation and even ulcer formation, often leading to cessation of drug use from a safety and tolerability point of view (194). Such GI effects may, to some extent, be limited by the co-administration of gastroprotective drugs, such as proton pump inhibitors (195), but given the growing problem of polypharmacy and the propensity for untoward drug interactions, clearly single agents are preferable where at all possible.

More recently, attention has turned to an emerging class of compounds with significant anti-inflammatory effects, the H_2S-releasing NSAIDs (H_2S-NSAIDs) (78). These consist of a conventional NSAID to which an H_2S-reasing moiety is covalently attached. One such H_2S-NSAID, ATB-346, has shown a markedly reduced GI adverse effect profile (in terms of ulceration and bleeding) in animal studies, making it an attractive alternative to its native naproxen for long-term use, whose use is limited by both GI and cardiovascular adverse effect (196). Furthermore, it was shown that after oral administration of ATB-346, plasma levels of naproxen derived from the compound were much lower than equimolar doses of naproxen but maintained COX inhibition and analgesic effects equally (197).

1.5.2.2 Corticosteroids

Corticosteroids, such as prednisolone, are used in acute flares of RA, acting through the glucocorticoid receptor (GR) and inhibiting the transcription of a number of pro-inflammatory cytokines, bradykinin and PGs (198). Whilst effective at rapidly reducing the level of inflammation and improving symptoms in RA patients, corticosteroids have numerous adverse effects relating to their long-term use, including hypertension, reduced bone mineral density, hyperglycaemia, insomnia and psychiatric symptoms (199) . Furthermore, there is a significant increase in the risk of serious infection, up to two-fold (200), which is particularly dangerous in patients who may also be taking concomitant immunosuppressive therapy and who already have a dysregulated underlying immune system.

Collectively, whilst these treatments ameliorate disease symptoms to varying degrees, they do not bring a ‘cure’ and are ineffective in a significant subset of patients. Furthermore, these adverse effects can also lead to patients turning to opioids for the debilitating symptom of uncontrolled pain, which whilst often effective at reducing this pain, can lead to increasing drug tolerance and dependence (201, 202).

1.5.2.3 Disease modifying anti-rheumatic drugs and targeted therapy

Over the last two decades, the treatment of autoimmune disease has evolved dramatically, with the advent and increasing clinical utilisation of synthetic, conventional (c), biologic (b) and targeted synthetic (ts) DMARDs across a range of autoimmune diseases. These target specific pathogenic cytokine(s) or upstream inflammatory signalling pathways, but not all RA patients respond to treatment suggesting other possible drivers of the pathogenesis of RA, which could be targeted for the development of novel therapeutics (203). Examples include cDMARDs such as methotrexate and sulfasalazine and the bDMARDs such as infliximab (anti- TNF-α), anakinra (anti-IL-1) and tocilizumab (anti-IL-6) (204).

1.5.2.3.1 Conventional disease-modifying anti-rheumatic drugs

Methotrexate has been used in the treatment of RA since the 1980s and to this day is still often the first line treatment (205). Methotrexate inhibits dihydrofolate reductase, and at high doses, as used in haematological malignancies, reduces the level of purine and pyridine pools in T cells whilst reducing T cell proliferation, with the net effect of arresting the S phase of the cell cycle and increasing apoptosis (206). At lower dose, as in the treatment of RA, its effect is thought to be exerted through the upregulation of adenosine signalling pathway, suppressing early T and B cell expansion and inducing an anti-inflammatory state (207). Methotrexate, whilst effective for most patients, is limited in its long-term use by adverse effects including GI upset, often with profound nausea and vomiting, as well as significant general malaise, hair thinning/loss, oral ulcer formation and multiple blood dyscrasias (anaemia, thrombocytopenia, neutropenia and lymphopenia) (208). Other cDMARDs in routine clinical use for the treatment of RA includes sulfasalazine which can lead to increased T cell apoptosis and reduced T cells activation and proliferation (209, 210). Hydroxychloroquine, another cDMARD, may interfere with lysosomal activity and autophagy and alter signalling pathways and transcriptional activity resulting in pro-inflammatory cytokine inhibition, although its exact mechanism of action is unknown (211). Finally, leflunomide, a selective inhibitor of pyrimidine synthesis, can suppress

IL-1β and interrupt T and B cell signalling, thus reducing their accumulation in inflamed tissue (212).

1.5.2.3.2 Biologic disease-modifying anti-rheumatic drugs

Following the activation of B and T cells, a myriad of cytokines are involved in the amplification and perpetuation of inflammation found in the joints of patients with RA (177). As early as 1988, Firestone *et al.* showed that in the synovium of RA patients, IL-6 followed by IL-1β and TNF-α were in the highest concentration and that these could be targeted therapeutically, with the first clinical trial of infliximab (the first commercial anti-TNF-α monoclonal antibody) taking place in 1992 (213, 214). These small proteins are produced by several immune cells, as well as fibroblasts, affecting the gene expression in circulating cells as well as those found in the RA synovium (215). Whilst these cytokines would seem an obvious target for treating RA, their activities and interactions are complex, often having opposing effects on cell proliferation or growth under different conditions, with either synergistic, additive or inhibitory effects, depending on the environment (216). Nevertheless, numerous cytokines and immune signalling pathway regulatory proteins have been exploited specifically for the development of new therapeutics and have become commonplace in the treatment of RA in a more targeted way as compared to NSAIDs, corticosteroids and cDMARDs (203). The use of TNF-α inhibitors, along with numerous other bDMARDs, has revolutionised the treatment of RA and other autoimmune diseases, however, only around a third of RA patients who received initial treatment with a TNF-α inhibitor show a clinical response (217).

1.5.2.3.3 Targeted synthetic disease modifying anti-rheumatic drugs

The development of tsDMARDs, also known as small molecule inhibitors, signalled a further breakthrough in the treatment of RA. This large family of small molecules target mostly the several types of kinases essential for downstream signalling of pro-

inflammatory cytokines (218). These include both the JAK and signal transducer and activator of transcription (STAT) signalling pathways (219). In humans, the JAK family comprises JAK1, JAK2, JAK3 and tyrosine kinase (TYK)-2 (220). Activation and transphosphorylation of JAKs induces STAT recruitment, dimerisation and nuclear translocation, resulting in transcriptional responses. The JAK-STAT signalling pathway plays a pivotal role in orchestrating a range of immune responses, notably T-cell polarisation, haematopoiesis and inflammation (221). Moreover, dysregulated JAK-STAT signalling contributes to autoimmune and chronic inflammatory phenotypes and tsDMARDs are now routinely used in the treatment of RA. However, JAK-STAT pathway inhibition does not come without risk, with increased incidence of thromboembolic events, cytopenias (particularly lymphopenia), transaminitis, renal impairment, reactivation of herpes zoster, hypercholesterolaemia and malignancy (222). Nevertheless, they are an evolving cornerstone in the treatment of autoimmune disease, but safer and more tolerable alternatives are needed. Current bDMARDs and tsDMARDs in current use in the UK are summarised in **Table 1.3**.

Overall, the treatment of RA is multifaceted, targeting multiple aspects of the inflammatory response as summarised in **Figure 1.6**.

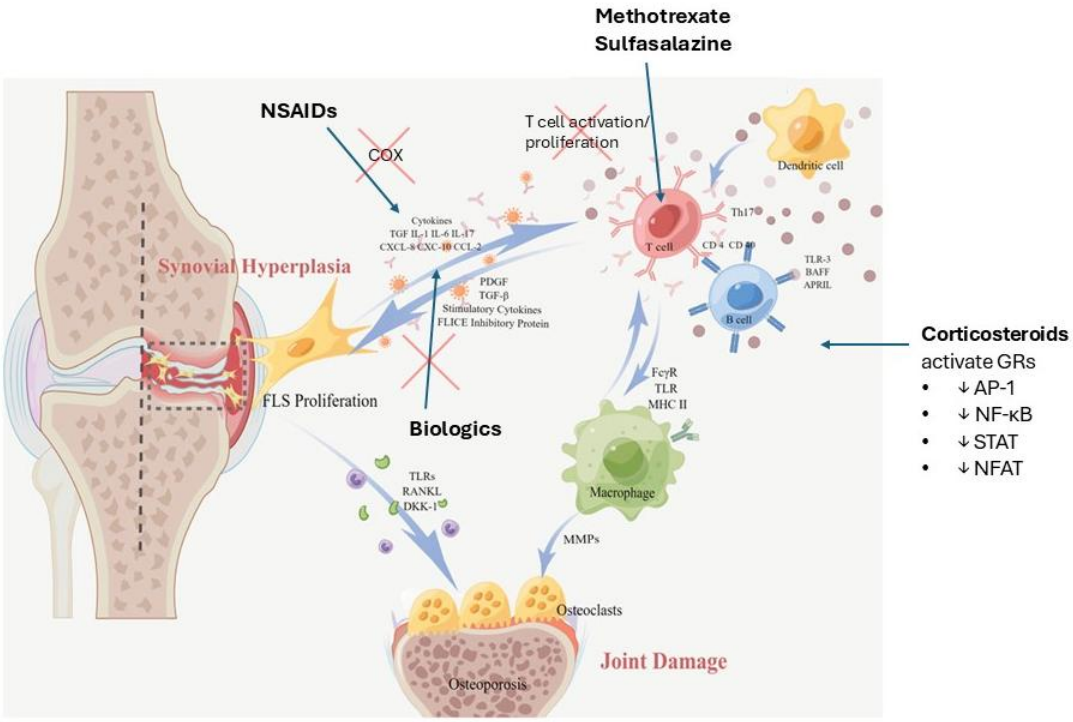

Figure 1.6. Key therapeutic strategies in RA. Treatment targets for RA are shown in this schematic. Red crosses indicate the pathways which specific drugs block to reduce inflammation and joint damage in RA patients. Adapted from Tong *et al.* (2023) (223).

Table 1.3. Examples of biologic and small molecule DMARDs used to treat autoimmune diseases. Adapted from Fugger *et al.* (2020) (224).

Target	Drug	Mechanism	Clinical use
JAK	Tofacitinib	Inhibits JAK1, JAK2, JAK3	RA, JIA, PsA, AxSpA, UC
	Baricitinib	Inhibits JAK1, JAK2	RA, AlA, AD
	Filotinib	Inhibits JAK1	RA, UC
	Upadacitinib	Inhibits JAK1, JAK2, JAK3, TYK2	RA, AxSpA, PsA, UC, CD, AD
TNF-α	Infliximab, etanercept, adalimumab, golimumab, certolizumab	Inhibits TNF-α	RA, JIA, PsA, AxSpA, P, UC, CD
IL-17a	Secukinumab/ixekizumab	Inhibits IL-17a	JIA (ERA), AxSpa, PsA, P, HS/PsA, P, AxSpA
IL-12/23p40	Ustekinumab	Inhibits IL-12 and IL-23	PsA, AxSpA, UC, CD
IL-23p19/IL-23a	Guselkumab/risankizumab	Inhibits IL-23	PsA, P, CD
IL-6R	Tocilizumab, sarilumab	Inhibits IL-6R	RA, JIA, NeO
CD20	Rituxumab/ocrelizumab	Depletes $CD20^+$ B cells	RA/MS
CTLA-4	Abatacept	Blocks CD80 and CD86 co-stimulation	RA, JIA, PsA

JAK = Janus kinase; TYK = Tyrosine kinase; RA = Rheumatoid arthritis; JIA = Juvenile idiopathic arthritis; PsA = Psoriatic arthritis; AxSpA = Axial spondyloarthritis; UC = Ulcerative colitis, AlA = Alopecia areata; AD = Atopic dermatitis; P = Psoriasis; ERA = Enthesitis-related arthritis; HS = Hidradenitis suppurativa; NeO = Neuromyelitis optica; MS = Multiple sclerosis.

1.6 Murine models of inflammation

Before studying inflammation resolution in RA patients, it is important to appreciate whether analogous experiments can be employed in animal models. This can provide

complementary data and allow the use of non-clinical grade pharmacological agents and genetically modified animals to gain mechanistic and functional understanding. Transgenic mice permit the pharmacodynamic analysis of targeted therapies *in vivo*, allowing researchers to gain insight into a discrete gene or protein that may contribute to a disease and thus serve as a viable therapeutic target. Animal models have proven to be valuable research tools in the study of pathogenic mechanisms of disease, but each comes with their own advantages and disadvantages. Numerous animal models have been developed over the years to investigate inflammation, mostly in mouse (225).

Inflammation can be triggered by a range of stimuli, including trauma, thermal insult, live or dead microbials and pharmacological agents. Models have been developed focusing on the immune response in a range of tissue types, including the skin, lung, joints, gastrointestinal system, central nervous system, heart, liver and kidneys (226, 227). Many have focused on modelling specific human disease using a myriad of inflammatory stimuli, including sepsis (228), peritonitis (125), pneumonia (229), colitis (230), hepatitis (231), psoriasis (232) and inflammatory arthritis (233). Notable examples include the collagen-induced arthritis and imiquimod-induced psoriasis models. The collagen-induced arthritis model is the most commonly studied autoimmune model of RA, utilising the application of complete Freund's adjuvant and type II collagen, leading to the development of inflammatory arthritis at around day 21-28 (234, 235). Murine models of RA utilise either induced arthritis (such as the collagen-induced model) or genetically modified animal. The most commonly used examples are shown in **Figure 1.7**. The most frequently used psoriasis model involves the application of imiquimod, a ligand of TLR7 and 8, inducing a psoriasiform dermatitis and has been successfully used for investigating both *ex vivo* and *in vivo* topical therapies for psoriasis (232).

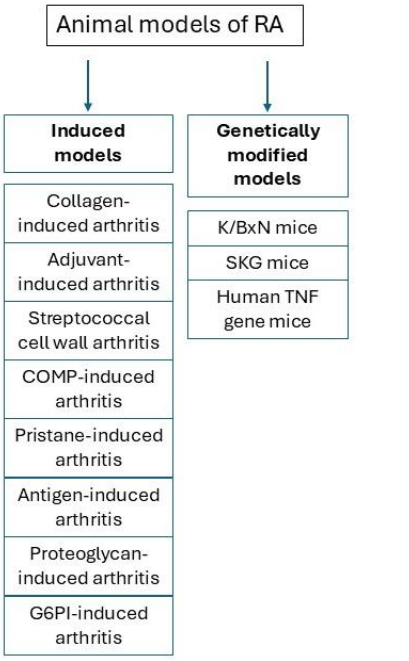

Figure 1.7. Examples of the most utilised murine models of RA. Joint inflammation is triggered by the use of an inducible agent, including collagen, adjuvant, Streptococcal cell wall, cartilage oligomeric matrix protein, pristane, antigen, proteoglycan or glucose-6-phosphate isomerase or using genetically modified animals prone to joint inflammation.

Yu *et al.* (2016) reported a protocol using flow cytometric analysis of non-lymphoid tissues to allow the accurate identification and quantification of murine immune cells (236, 237). Their approach, however, was limited in that they provided only a limited overview of immune cell repertoires and did not explore dynamic changes temporally following an inflammatory insult. Whilst using LPS and influenza as stimuli for inflammation in the mouse lung, the protocol detailed for skin involved removing and digesting the ear without any inflammatory stimulus and with only a rudimentary antibody panel. Sakamoto *et al.* (2021) have more recently described a similar strategy for acquiring a single-cell suspension for flow cytometric analysis, again limited by the lack of time-course data and absence of inflammatory insult (238). Furthermore, no data exists on dermal inflammation over time using these models in either a resolving or non-resolving manner.

Other groups have used live bacteria in mouse skin but did not utilise flow cytometry tools, rather focusing on histopathological and microbiological analyses. Kugelberg *et al.* (2005) applied mouse skin with the pathogens *Staphylococcus aureus* and *S. pyogenes*, although this was a topical application only as opposed to either subcutaneous or intradermal routes (239). The skin suture-model or burnt skin model have also been used, where the infection is introduced into the deeper layers of the skin. For the skin suture-model, a bacteria-impregnated nylon suture is implanted in an artificial wound (scalpel incision) (240), whereas the burnt skin model involves the application of bacteria to thermal damaged skin (241). These models are limited in that they involve trauma to the animal, increasing the severity of the protocol as well as confounding effects of the trauma on the inflammation caused by the bacteria alone.

1.7 Human models of experimental inflammation

There remains a paucity of human translational, experimental models of inflammation *in vivo.* This is largely due to ethical concerns surrounding inducing inflammation in healthy volunteers and patients with pre-existing inflammatory diseases; the latter being those in which elucidation of immune dysregulation is needed. Murine models have been used extensively for decades forming a cornerstone of modern biomedical research to investigate basic pathophysiological mechanisms, identify potential novel therapeutic targets and allow the pre-clinical evaluation of drugs before carrying forward into human clinical trials (242). Importantly, whilst in humans, acute inflammation due to different stimuli results in highly similar genomic responses, the corresponding responses in mouse models correlate poorly with human disease (243).

The most studied models of experimental inflammation in humans include systemic endotoxaemia models (244–250). Kiers *et al*. (2017) have characterised a model of systemic inflammation triggered by the intravenous infusion of endotoxin in healthy volunteers. This resulted in a controlled, transient and reproducible systemic inflammatory response but also resulted in headache, nausea, shivering, muscle aches and fever in participants (251). Additionally, studies of systemic inflammation must

be conducted in a clinical research facility attended by clinicians with monitoring of vital signs including temperature, blood pressure, oxygen saturations and heart and respiratory rates, which is both time consuming and costly. The Gilroy group has extensive experience in utilising stimulated local inflammation in healthy volunteers including the intradermal injection of UV-KEc (60, 252–254) and varicella zoster virus (255) and the topical application of cantharidin, a substance derived from the blister beetle *Cantharis vesicatoria* (253). The intradermal administration of other inflammatory stimuli to investigate immune responses has also been reported, including tuberculin purified protein derivative (256) and *S. pneumoniae* (257). Local administration of antigens triggering both local and systemic inflammation in this way has strength in that the inflamed tissue is easily accessible for acquisition and is not hampered by significant adverse effects experienced by participants, as seen with systemic endotoxaemia. In addition, others have used heat-killed *E. coli* in the disease setting, in patients with inflammatory bowel disease (258). However, two of the patients injected with *E. coli*, both known to have ulcerative colitis, subsequently developed an exuberant and protracted inflammatory response, resembling that seen in the neutrophilic dermatosis, pyoderma gangrenosum (259). Whilst giving insight into the possible mechanisms underlying the inflammatory process seen in ulcerative colitis, this highlights the risk of inducing inflammation in patients with pre-existing inflammatory disease.

Thus, there remains a need for translational, experimental human models of inflammation to study human inflammatory diseases that resemble the inflammatory response seen clinically in disease but also utilising a uniform dose of inflammatory stimulus to avoid heterogeneity. Such models should also facilitate minimally invasive sampling of inflamed tissue and be acceptable to both healthy volunteers and patients with inflammatory disease. Given limitations in both human and murine models of inflammation, to investigate inflammatory pathways it is therefore important to combine complementary *in vivo, ex vivo* and *in vitro* human studies with animal studies and clinical trials in patients.

1.8 Concluding remarks

Over the past 50 years, research has focused on understanding the mediators that cause chronic inflammatory responses to treat these diseases, predominantly aiming to inhibit the synthesis or action of mediators that drive inflammation, however, more recently there has been increased interest in the resolution process, a critical requirement for the inflammatory response to switch off. Given that recent studies of immune responses during acute inflammation suggest that resolution is not the end of innate-mediated immune responses and that there is further immunological activity occurring after the resolution cascade is complete, it may be possible to harness endogenous resolution pathways for the development of novel treatments for RA. It is feasible that these patients upregulate pro-resolution and/or anti-inflammatory pathways to maintain disease remission and this could prove a tractable and novel target for the development of therapeutics for the treatment of RA.

As such, I aim to develop complementary murine and human models of inflammation to safely investigate these signals in RA patients who are in remission. Whilst it may seem counterintuitive to investigate immune responses in RA patients using a murine dermal model of inflammation rather than an induced arthritis model in mouse, this has significant advantages. Importantly, the methodology is easily reproducible both in mouse and humans, with high cell yield for analysis, as well as good tolerability of the inflammatory stimulus to the animals. The aim will be to create a window into the immune system of both species following the onset of inflammation using the same inflammatory stimulus, to gain insight into the pro-resolution/anti-inflammatory pathways that may be upregulated following acute inflammation to maintain disease remission in RA patients.

1.9 Hypothesis and aims

Recent studies from the Gilroy group and others have shown that there is a long-lasting period of post-resolution immune activity following the resolution of acute inflammation, inducing adaptive lymphocyte responses, maintaining tolerance and invoking local tissue immunity (255, 260, 261).

Hypothesis: RA patients in remission maintain low levels of clinically active disease by the upregulation of protective, pro-resolution/anti-inflammatory pathways.

Specifically, I aim to develop and characterise murine and human models of inflammation, unified by the same inflammatory stimulus (UV-KEc), spanning the onset, resolution and post-resolution phases. The ultimate aim is to characterise an experimental model in which to safely investigate the pathways leading to and maintaining remission in patients with inactive RA, aiming to identify potential targets for novel treatments.

The main aims of the chapters presented here are:

1. Develop a murine model of dermal inflammation to characterise the local and systemic immune response.

2. Develop a murine model of resolving dermal inflammation to characterise the local and systemic immune response during the post-resolution phase and identify potential pro-resolution/anti-inflammatory pathways.

3. Establish that an analogous human model of resolving dermal can be safely used to investigate pro-resolution pathways and that the system responds to conventional RA therapies.

4. Develop a human model of resolving dermal inflammation to characterise the local and systemic immune response in RA patients in remission and identify potential pro-resolution/anti-inflammatory pathways.

2 Materials and Methods

2.1 Human studies

2.1.1 Ethics statement

The healthy volunteer study detailed here was approved by University College London (UCL) Institutional Ethics Committee (**Project Number: 10527/001**). Following consultation with both scientific and clinical colleagues, a detailed protocol was drawn up, along with Patient Information Sheets (PIS), screening and informed consent forms (**Appendix 4-6**). Written, informed consent was taken from all volunteers prior to voluntary participation in the study.

Study procedures for patients with autoimmune disease (RA) required National Health Service (NHS) ethical approval. Thus, a complete application was submitted using the Integrated Research Application System (IRAS). To ensure this was acceptable to the patient cohort, study documents were discussed and approved by patient representatives from the Patient Research Partnership, established by the University of Birmingham Rheumatology Research Group. All relevant documentation were reviewed by independent colleagues prior to submission to IRAS. Contracts were established with the Sponsor (UCL) and participating NHS sites through the Joint Research Office (University College London Hospital [UCLH] and UCL) along with The Doctors' Laboratory (TDL) for the processing of peripheral blood samples. The study was approved by the West Midlands Solihull NHS Research Ethics Committee (**Ref: 15/WM/0368, IRAS ID: 177924**). An application was also submitted and approved for the study to be incorporated into the Clinical Research Network Portfolio (**ID: 20234**). The study was then submitted for approval to Research and Development teams at each participating NHS site. Research study sites included UCLH and University Hospitals Birmingham NHS Foundation Trust. In addition, I gained honorary clinical contracts at the study sites, to enable me to recruit patients. The latest version of the PIS, screening and informed consent forms are included in **Appendix 1-3**.

All data were used and stored in line with the General Data Protection Regulation (2018). All procedures were carried out in line with the Helsinki Declaration, adopted by the 18th World Medical Assembly, as amended in 1983. An online, secure data collection platform was designed using REDCap®, with the secure storage of participant information using the UCL Data Safe Haven, requiring a two-factor authentication process.

2.1.2 Healthy volunteer study

2.1.2.1 Volunteer recruitment

For the healthy volunteer study, 23 healthy, male volunteers aged 18– 50 were recruited using university mailing lists and study advertisements displayed on staff and student noticeboards across UCL campuses. Exclusion criteria included chronic inflammatory illness, allergy to NSAIDs, recent illness (within the preceding seven days), use of regularly prescribed medication or over-the-counter medication (within the last seven days), vaccination within the last three months, current smokers, use of recreational drugs and those enrolled in another study. During the study, participants were asked to refrain from caffeinated products, alcohol, and heavy exercise.

Volunteers were randomly allocated to one of three treatment arms in this single-blind study, with the experimental subjects unaware of which arm they had been allocated to. Seven volunteers were assigned to the naproxen arm and took 500 mg twice daily for three days prior to UV-KEc injection. Seven volunteers were assigned to the ATB-346 arm and took 250 mg once daily (the equi-effective dose to naproxen) for three days prior to injection. Seven volunteers took no drug during the study and served as the untreated control group. One volunteer from each of the naproxen and untreated control groups dropped out before completion of the study; one giving no reason and the other because they were already enrolled in another study.

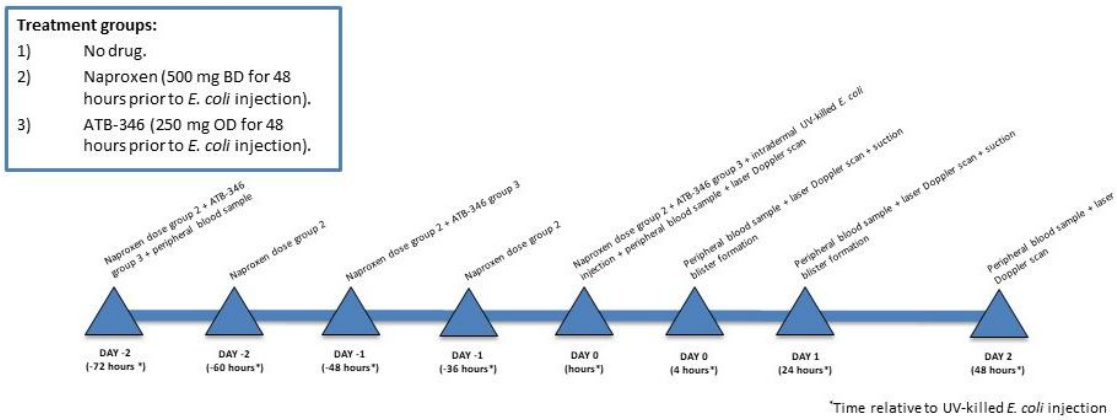

Figure 2.1. Healthy volunteer study design. To investigate the feasibility and safety of using conventional RA treatments in the UV-KEc-triggered model of inflammation, 21 volunteers were recruited and allocated to three treatment arms. Seven participants took no drug, serving as the untreated control group. Seven participants took 500 mg naproxen twice daily for 48 hours prior to UV-KEc injection and seven took 250 mg ATB-346 once daily for 48 hours prior to UV-KEc injection. Clinical measurements, including laser Doppler imaging and peripheral blood were taken at baseline (0h), 4h, 24h and 48h. Blisters were formed using a negative pressure suction cup at 4h and 48h.

2.1.3 RA study

2.1.3.1 Volunteer recruitment

For the RA study, healthy volunteers and patients with RA were recruited as above (**Section 2.1.2.1**), with the addition of those referred to the study by consultant rheumatologist colleagues across the research study sites and with study advertisements displayed on staff and student noticeboards at the research study sites. Inclusion criteria included any patient meeting diagnostic criteria for RA who was not taking any DMARD, either conventional or biologic, or systemic corticosteroids and must have had a disease activity score (DAS)-28-CRP (262) of less than 3.2, indicating no significant disease activity. They also underwent screening bloods tests including a full blood count (FBC [haemoglobin, platelet count, total white cell count and differential]), urea and electrolytes (U+E [urea, creatinine, potassium, sodium,

chloride]) and liver function tests (LFT [total protein, albumin, bilirubin, alkaline phosphatase, alanine aminotransferase]), all of which had to be normal for that patient.

Exclusion criteria included pregnancy or breastfeeding, current smokers (including all nicotine-containing products), use of recreational drugs, concurrent human immunodeficiency virus (HIV) infection or other immunodeficiency, leucopenia or neutropenia, current infection or antibiotic treatment, lack of ability to provide informed consent, inability to stop NSAIDs for one week prior to the study and until after their final sample collection, personal or family history of pyoderma gangrenosum, participants who were unable to communicate effectively with the research team in English and finally patients who were involved in current research or had recently been involved in research. This was because the involvement of multiple studies could pose increased risk to the participant, or confound results of either study.

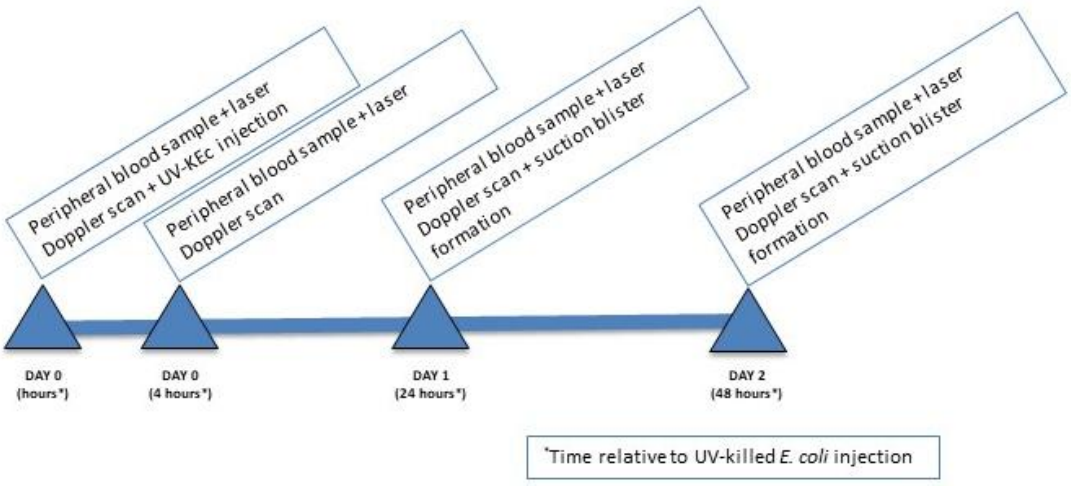

Figure 2.2. RA study design. To investigate the immune response in RA patients not currently on any anti-inflammatory or immunosuppression/immunomodulation therapy, 12 volunteers were recruited. Five of these were healthy controls and five were RA patients with an additional naïve healthy control and naïve RA patient. UV-KEc was injected intradermally on day zero. Clinical measurements, including laser Doppler imaging and peripheral blood was taken at baseline, 4h, 24h and 48h. Blisters were formed using a negative pressure suction cup at 24h and 48h.

2.1.4 UV-KEc preparation

E. coli (Strain: The National Collection of Type Cultures 10418, Source: Public Health England, UK) were reconstituted in 0.5 mL Luria Broth (LB, Sigma-Aldrich, Missouri, USA) and 150 µL streaked onto an agar plate with an LB alone plate as a control. These were incubated overnight in a shaking incubator at 250 *g* at 37 °C. Three colony forming units were stabbed using a sterile tip, each added to a 15 mL Falcon tube containing 10 mL LB and incubated for 4 hours at 37 °C. In a 2 L sterile conical flask, 750 µL was added to 750 mL LB, covered loosely with foil and transferred to a shaking incubator overnight at 37 °C. The contents of this was split between two centrifuge bottles and centrifuged at 4000 *g* for 10 minutes at 4 °C. The pellets were resuspended in 20 mL sterile phosphate-buffered saline (PBS) (Gibco, Paisley, UK) and combined in a 50 mL Falcon tube. The resulting tube was then centrifuged at 4000 *g* for 10 minutes at 4 °C.

The following day they were washed twice in PBS (2500 *g* for 20 minutes at 4 °C). To kill the bacteria, 10 mL was transferred to four sterile Petri dishes and exposed to UV light for 60 minutes (302 nm, ChemiDoc, Bio-Rad laboratories, California, USA). Counts were determined by optical density (OD) measurement, where OD600 = 0.365 equated to 10^8 *E. coli*/mL. The UV-KEc were resuspended in 0.9% sodium chloride and aliquoted into sterile Eppendorf tubes, obtaining a final count of 1.5×10^7/100 µL or 1.5×10^8/100 µL. Samples were confirmed be to non-viable by the Environmental Research Laboratory, UCLH NHS Foundation Trust, following 24 hours incubation on both blood and MacConkey agar plates and stored at −80 °C. Aliquots were thawed immediately prior to intradermal injection.

2.1.5 Intradermal injection of UV-KEc for human studies

All procedures were carried out under aseptic, non-touch technique. For all volunteers, the volar aspect of both forearms of each volunteer was cleaned using 70% isopropyl alcohol and 1.5×10^7 UV-KEc in 100 µL of 0.9% sodium chloride were injected using a sterile 30 G hypodermic needle *via* the intradermal route, into the marked site 7 cm from the antecubital fossa. This dose is known to elicit a consistent, safe and localised reaction, leading to redness (measuring 5-10 cm at maximum in diameter), mild tenderness, and warmth at the site of the UV-KEc injection. Inflammation was allowed to ensue and subsequently resolve for the duration of the study. In both the healthy volunteer and RA study, clinical measurements, laser Doppler imaging, and peripheral venous blood taken at pre-defined time-points representing baseline (0h), onset of inflammation (4h), and resolution phases (24h and 48h).

2.1.6 Peripheral blood analysis

For the healthy volunteer study, an FBC, U+E, LFT and C-reactive protein (CRP) were taken for each volunteer during the screening process. At each of the time-points, an FBC and CRP were collected using ethylenediaminetetraacetic acid (EDTA)-anticoagulated and spray-coated silica and polymer gel-containing Vacutainers® (Becton Dickinson, New Jersey, USA), respectively. All peripheral blood samples were processed at TDL (The Halo Building, London, UK). At each time-point, heparin-anticoagulated blood was centrifuged at 2000 *g* for 10 minutes at room temperature to separate the plasma, which was split into 500 µL aliquots using Protein LoBind® Eppendorfs and stored at −80 °C for subsequent soluble mediator analysis.

For the RA study, leucocytes were isolated from whole, peripheral blood. Venepuncture was performed on volunteers as described in the paragraph above using EDTA-anticoagulated Vacutainers®. From this, 1 mL was added to 9 mL ammonium-chloride-potassium lysis buffer (ACK, Lonza Group AG, Basel, Switzerland) and left on a rocker for 7 minutes, or until the solution was clear, indicating that the

erythrocytes had lysed. The cells were then pelleted by centrifugation at 500 *g* for 5 minutes at 4 °C. The supernatant was discarded and the cells washed using 10 mL PBS again at 500 *g* for 5 minutes at 4 °C. Cells were resuspended in 1 mL staining buffer, counted and stored at 4 °C until required.

2.1.7 Laser Doppler imaging

A laser Doppler imager (moor LDI- HIR, Moor Instruments Ltd., Devon, UK) was used to acquire data quantifying microvascular hyper-reactivity. At the pre-defined time-points described, the forearm was placed under the scanner at a set distance of 58 cm. The scanner emits a laser which is scattered by erythrocytes. The resulting Doppler shift is dependent on the velocity and concentration of cells at the site and therefore represents blood flow and thus leucocyte trafficking. The obtained data are displayed as colour-coded flux images, which are then analysed using the moorLDI software (Version 6.1), representing arbitrary perfusion units (blood flow), a hitherto unappreciated marker of resolution at the site of inflammation. Total flux (blood flow) was calculated by multiplying the number of "valid" pixels (those demonstrating blood flow above the background level of 300 perfusion units) and the mean blood flow of these valid pixels. The mean was taken from both forearms for each volunteer. Representative flux images and accompanying photographs are shown in **Figure 2.3**.

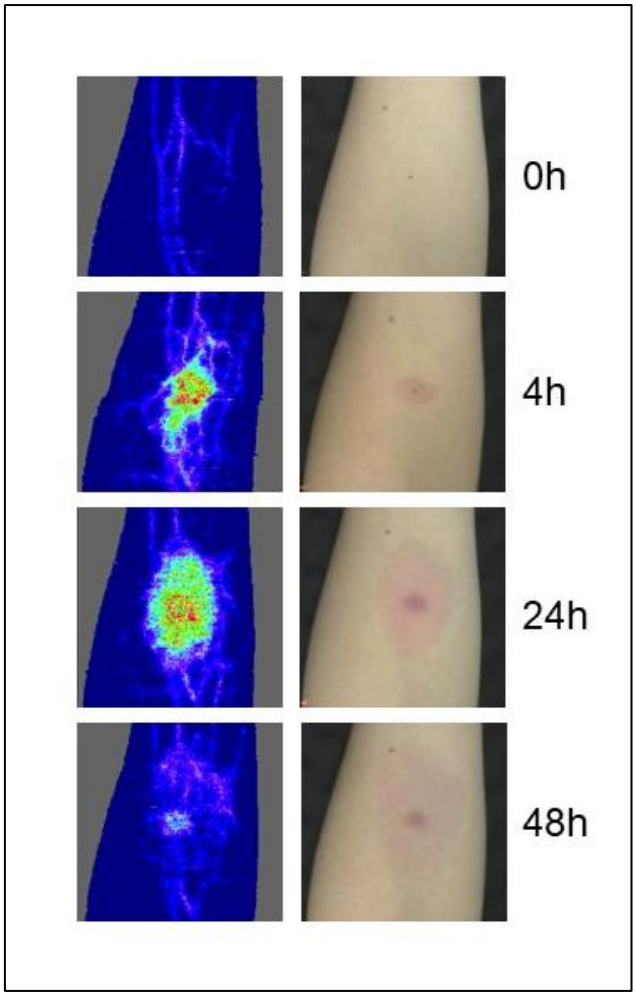

Figure 2.3. Assessment of vascular hyper-reactivity at the site of UV-KEc-triggered resolving acute resolution. In all studies, acute inflammation was triggered by the intradermal injection of 1.5 x 10^7 UV-KEc suspended in 100 µL 0.9% sodium chloride. Vascular response and blood flow was assessed using a laser Doppler imager (moorLDI-HIR, Moor Instruments Ltd., Devon, UK). Representative flux images and photographs are shown here from baseline (0h), 4h, 24h and 48h.

2.1.8 Clinical measurements

As a further parameter of inflammation (and resolution thereof), a visual analogue score (0-10) was used to quantify the pain experienced at the site of inflammation (where 0 = no pain; 10 = worst pain imaginable). This was repeated for elicited tenderness with the application of a 100 g weight. Temperature was measured using an electronic, infrared thermometer (Thermofocus® 01500A3, Tecnimed Srl, Varese, Italy) both centrally (forehead) and at the site of injection. The clinical procedures room, where all measurements were taken, was kept at a constant, ambient temperature of 21 °C using an air conditioning unit and the ambient temperature of the room was taken using the same technique at each time-point.

2.1.9 Skin blister formation and inflammatory exudate collection

Inflammatory exudate was obtained from the site of the UV-KEc injection by the formation of a blister at two time-points. For the healthy volunteer study, this was at 4h and 48h, whereas in the RA study, this was at 24h and 48h. This process involved placing a suction blister chamber centred over the site of UV-KEc injection, connected to a negative pressure instrument (NP- 4, Electronic Diversities Ltd., Maryland, USA). The suction chamber at the base has an orifice plate with a 10 mm aperture, through which the blister is formed by a standardised, gradually incrementing negative pressure, starting at 2 inches of mercury (inHg) until a uniloculated blister begins to form. The maximum pressure used was 9 inHg and after the blister had fully formed, the pressure was gradually reduced back to baseline following a standardised protocol, with the whole process taking approximately 1.5h to 2h.

The chamber was then removed and the blister pierced using a sterile 20 G hypodermic needle along the lateral border. The exudate was rolled out using a sterile 1 mL syringe and the contents aspirated using a 200 µL filter pipette tip. The fluid was immediately transferred into a V-bottom 96-well plate containing 50 µL of 3% sodium citrate (Sigma Aldrich, Missouri, USA) in PBS on ice to prevent coagulation. Extra holes

were created in the overlying skin to prevent re-accumulation of blister fluid and it was cleaned once more and covered with a sterile dressing (9 × 10 cm dressing, Mepore, Mölnlycke Health Care, Gothenburg, Sweden). The plate was then centrifuged at 1000 *g* for 5 minutes at 4 °C. An empty sterile Protein LoBind® tube (Eppendorf, Hamburg, Germany) was weighed, and the supernatant was added to this tube which was re-weighed. The difference in mass gave the blister volume. The fluid was split into 30 µL aliquots and stored at −80 °C for subsequent soluble mediator analysis. The pellet was resuspended immediately in 100 µL polychromatic flow cytometric staining buffer (5% fetal calf serum [FCS] [Gibco, Paisley, UK] in PBS with 2 mM EDTA [Sigma Aldrich, Missouri, USA]) containing antibodies specific to surface antigens as described below in **Section 2.1.10**.

2.1.10 Polychromatic flow cytometric analysis

Blister cells suspended in staining buffer made up as above (**Section 2.1.9**), were incubated with a cocktail of appropriate antibodies specific to cell surface markers along with 50 µL Brillian Stain Buffer (BD, New Jersey, USA) to prevent fluorescent dye interactions, for 30 minutes (4 °C, in the dark), along with corresponding fluorescence minus one (FMO) controls. **Table 2.1** shows the antibody cocktail and consequent panel used for all volunteers in the healthy volunteer study. Stained cells were then washed using staining buffer at 500 *g* for 3 minutes at 4 °C. Cell profiles were acquired immediately using a flow cytometer (either LSR Fortessa™, or LSRForetessa™ X-20) (BD, New Jersey, USA) using BD FACSDiva™ software (BD, New Jersey, USA). Polychromatic flow cytometric data, including compensation, were performed using FlowJo software (BD, New Jersey, USA).

Table 2.1. Fluorochrome-conjugated antibodies used in the healthy volunteer study. List of antibodies against surface antigens, the fluorophore conjugated to, the clone, dilution and manufacturer used for flow cytometric analysis of immune cells in the healthy volunteer.

Surface marker	Fluorochrome	Clone	Dilution	Manufacturer
CD45	BV785	HI30	1:100	BioLegend
CD19	FITC	HIB19	1:100	BioLegend
CD20	FITC	2H7	1:100	BioLegend
CD3	FITC	HIT3a	1:100	BioLegend
CD56	FITC	HCD56	1:100	BioLegend
HLA-DR	BV510	L243	1:100	BioLegend
CD14	BV605	63D3	1:100	BioLegend
CD16	APC	3G8	1:100	BioLegend
CD62L	PE-Cy7	DREG-56	1:100	BioLegend
Siglec-8	PE	7C9	1:100	BioLegend
CD197/CCR7	BV711	GO43H7	1:100	BioLegend
CD163	BV421	GHI/61	1:100	BioLegend
CD86	PerCP-Cy5.5	BU63	1:100	BioLegend

Prior to each acquisition on the flow cytometer, single-stain compensation controls were run for each fluorophore being used, as well as an unstained sample, to account for the spectral overlap. Compensation beads (UltraComp eBeads, Invitrogen, Massachussets, USA) were used, which bind and set a baseline fluorescence. To achieve this, 1 µL of each fluorophore was added to 20 µL of compensastion beads, incubated for 30 minutes at 4 ºC in the dark and washed in the same way as the samples.

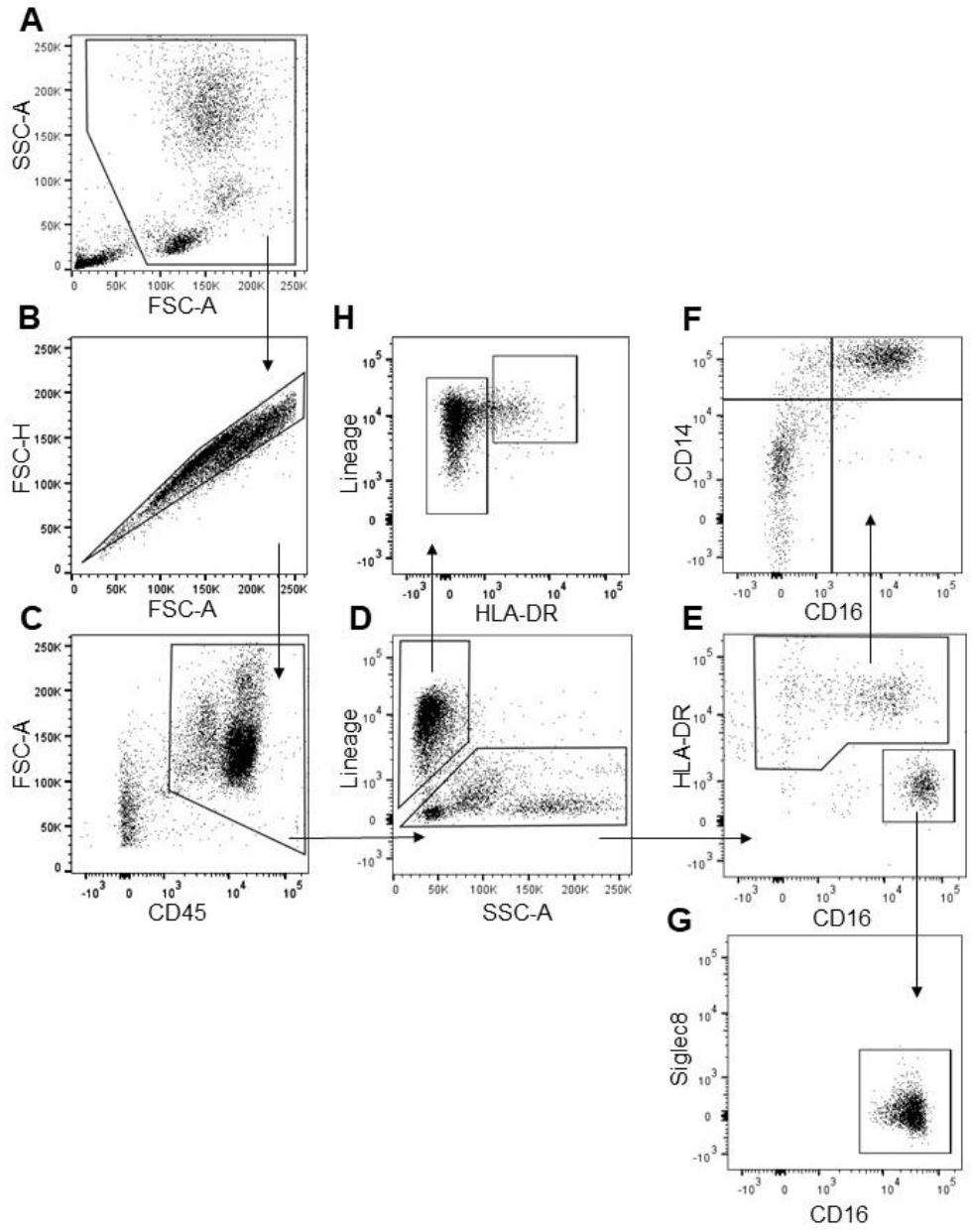

Figure 2.4. Characterisation of inflammatory cell infiltrate into skin blisters following in the intradermal injection of UV-KEc. Inflammatory exudate was obtained using a negative pressure suction cup at the site of UV-KEc-triggered resolving acute inflammation, with cells separated by centrifugation. Cells were incubated with a fluorophore-tagged antibody cocktail. Stained cells were acquired using BD LSR Fortessa^{TM} and analysed using FlowJo software (BD, New Jersey, USA). Representative dot plots for polychromatic flow cytometric gating strategy are shown. Following (A) exclusion of debris, the gating strategy employed allowed identification of (B) single cells, (C) CD45^{+} haematopoietic immune cells, (D) total lymphocytes (top left box), (E) neutrophils (bottom right box) and total mononuclear phagocytes (top box), (F) mononuclear phagocyte subsets (classical [top left box], intermediate [top right box], non-classical monocytes [bottom right box] and dendritic cells [bottom left box]), (H) B cells (left box) and T/NK cells (right box). Arrows indicate gating strategy.

2.1.10.1 Identification of immune cells in healthy volunteer study

To identify leucocyte subsets during the different phases of inflammation, blister exudate was obtained following suction using a negative pressure cup. Cells were separated by centrifugation and characterised using polychromatic flow cytometry and a gating strategy focusing on cells of the myeloid lineage (**Figure 2.4**). After exclusion of debris (**Figure 2.4A**) and doublets (**Figure 2.4B**), cells of haematopoietic origin ($CD45^+$) were identified (**Figure 2.4C**). Neutrophils (**Figure 2.4E**) were identified as $Lineage^-$ (Lin^-: CD3, CD19, CD20 and CD56), $HLA\text{-}DR^-$, $CD16^+$ and confirmed as $Siglec8^-$. Total mononuclear phagocytes (MPs) were identified as Lin^- and $HLA\text{-}DR^+$. Further classification into MP subtypes was obtained based on the expression of CD14 and CD16: classical monocytes ($CD14^+$, $CD16^-$), intermediate monocytes ($CD14^+$, $CD16^+$), non-classical monocytes ($CD14^-$, $CD16^+$) and dendritic cells ($CD14^-$, $CD16^-$) (**Figure 2.4F**). Lin^+ cells were further divided into B cells ($HLA\text{-}DR^+$) and T/NK cells ($HLA\text{-}DR^-$) based on expression of HLA-DR (**Figure 2.4H**).

2.1.11 Fluorescence minus one controls

To ensure appropriate gating was employed to identify populations of cells, FMO controls were used in all flow cytometric analyses (both human and animal studies), ensuring gating identified truly negative or truly positive cell populations. A representative example of this is shown in **Figure 2.5**.

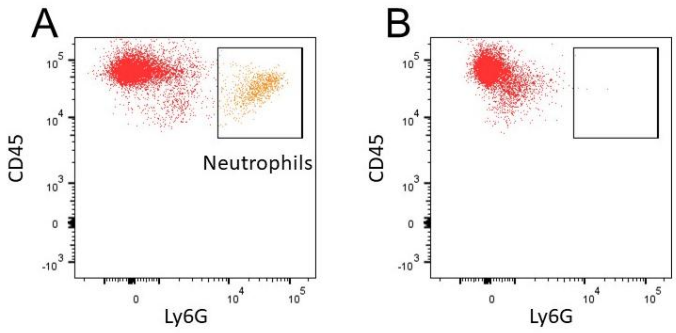

Figure 2.5. Example of fluorescence minus one (FMO) control. In all flow cytometric analyses, FMO controls were used to ensure appropriate gating of true positive and negative cell populations. Here, a murine skin single cell suspension was either (A) fully stained or (B) fully stained minus the Ly6G antibody conjugated to BUV395, allowing the true population of murine dermal neutrophils to be identified.

2.1.12 Cell number quantification

Cell number quantification from single cell suspensions throughout were performed using either (i) the Countess™ automated cell counter, (ii) manual haemocytometer, (iii) counting beads (CountBright™ absolute counting beads, [Invitrogen, Massachusetts, USA]) or (iv) for some flow cytometry experiments, the whole sample was run dry to give an absolute cell count per sample.

The Countess™ automated cell counter (Invitrogen, Massachusetts, USA) is a benchtop automated cell counter that performs both cell count and viability measurements using 0.4% trypan blue stain (Invitrogen, Massachusetts, USA). To count the cells, 10 µL of sample was taken from a single cell suspension and diluted 1:2 in trypan blue. Subsequently 10 µL was transferred into the channel of a Countess™ Cell Counting Chamber Slide (Invitrogen, Massachusetts, USA). The counter draws in 0.4 µL, equivalent to the counting of four 1 mm x 1 mm squares in a Neubauer haemocytometer.

To perform a manual cell count, 10 µL of a single cell suspension was diluted 1:2 with trypan blue as above and transferred onto the grid of a Neubauer haemocytometer. Using a Primovert light microscope (Zeiss, Jena, Germany), the number of cells present per mL was calculated using the following formula:

Cells/mL = (Average number of cells counted per square x 10^4 x dilution factor)

Following staining for polychromatic flow cytometric acquisition, 20 µL of CountBright™ absolute counting beads of a known concentration were added to each sample. The counting beads could then be visualised on the dot plots owing to their characteristic high forward scatter (FSC) and low side scatter (SSC) profile and could be distinguished from debris due to a broad range of excitation wavelength. These were used to calculate the absolute total number of cells in the sample as a ratio of bead events to cell events using the following formula:

Cells/sample = (Number of cell events/number of bead events) x (number of beads added to sample/volume of sample)

2.1.13 Mass cytometric analysis

For the RA study, time of flight mass cytometry (CyTOF) was employed to allow the investigation of the immune system of these patients at a more granular level. The Maxpar® Direct Immune Profiling Assay (MDIPA) kit (Standard Biotools, California, USA) was utilised and samples acquired on the Helios XT SAE 20W-50 system (Standard Biotools, California, USA). As each tube can stain up to three million cells, blood and blister samples were combined by employing a barcoding strategy as described below. In addition, the system was optimised by the addition of further drop-in extra- and intra-cellular antibodies, to allow the identification of all major immune cells involved in the innate immune response and the resolution of acute inflammation, as well as investigating the adaptive immune response.

To barcode blood and blister cells, CD45 antibodies bound to different heavy metal isotopes allowed the downstream separation of these two blister and blood populations and the ability to maximise the use of each tube. As there was no ‘Maxpar-ready’ antibody against CD141, a secondary Maxpar anti-FITC antibody was added to bind to a drop-in conventional FITC anti-CD141 antibody, allowing detection of CD141. The antibodies included in the MDIPA tube, along with the drop-in surface and

intracellular antibodies are shown in **Table 2.2**. Data acquired was analysed using the Maxpar® Pathsetter software (Standard Biotools, California, USA).

Table 2.2. Antibody panel used in mass cytometry. Antibody targets and cell markers are shown for mass cytometric analysis. MDIPA tube (right column) shows the 30 antibody targets in the pre-filled MDIPA tube, extracellular add-on (middle column) shows the drop-in extracellular antibodies and the intracellular add-on (right column) shows the drop in intracellular antibodies incorporated into the antibody panel.

MDIPA tube				**Extracellular add-on**	**Intracellular add-on**
CD3	CD25	CD56	CCR6	CD45 (106Cd)	sEH
CD4	CD27	CD57	CCR7	FITC CD141	TGF-β
CD8	CD28	CD66b	CXCR3	CD62L	HO-1
CD11c	CD38	CD123	CXCR5	CBD2	IFN-γ
CD14	CD45	CD127	HLA-DR	CD1c	FOXP3
CD16	CD45RA	CD161	IgD		
CD19	CD25	CD294	TCRγδ		
CD20	CD45RO	CCR4			

In brief, whole venous blood was collected using (EDTA)-anticoagulated Vacutainers® (Becton Dickinson, New Jersey, USA) at baseline (0h), 4h, 24h and 48h post-UV-KEc injection. On day one, 1 mL of the 0h and 4h blood was added to 9 mL of ACK lysing buffer each in a 15 mL Falcon tube and gently inverted. This was placed on rocker for 7 minutes or until clear to ensure erythrocyte lysis. Tubes were centrifuged at 400 *g* for 5 minutes, at room temperature. The resulting pellet was resuspended in 10 mL PBS, taking 10 µL to count using the manual haemocytometer as described in **Section 2.1.12**. The tubes were then centrifuged at 400 *g* for 5 minutes, at room temperature and resuspended in 1 mL cell staining buffer (CSB) (Standard Biotools, California, USA). From this, 1.5 x 10^6 were taken from the 0h sample and

added to a 96-well V-bottom plate and centrifuged at 400 *g* for 5 minutes, at room temperature, whilst the 4h samples remained on ice in the 1 mL CSB. The 0h pellet was resuspended in the barcoding CD45 antibody cocktail (2 µL CD45 106Cd in 98 µL CSB) and incubated for 60 minutes, in the dark, at room temperature, gently vortexing every 15 minutes.

The CD45 barcode was washed off using 200 µL CSB, twice. The 4h sample was also centrifuged with the second wash. The 0h sample was resuspended in 45 µL CSB and combined with the 4h pellet. To this 5 µL TruStain FcX™ block (Biolegend, London, UK) was added and incubated for 10 minutes, in the dark at room temperature. The extracellular antibody cocktail (**Table 2.2**) was added to the well and the entirety transferred to the MDIPA tube containing the standard tube extracellular antibody cocktail. This was incubated for 60 minutes, in the dark, at room temperature, gently vortexing every 15 minutes. The samples (now in one MDIPA tube) were washed using 1 mL CSB and centrifuged at 400 *g* for 5 minutes, at room temperature, twice. After the second wash the supernatant was carefully aspirated using a pipette leaving a residual of around 50 µL so as not to disturb the pellet. This was resuspended in 100 µL anti-FITC antibody cocktail and incubated for 30 minutes in the dark at room temperature, gently vortexing after 15 minutes. The samples were washed using 1 mL CSB and centrifuged at 400 *g* for 5 minutes at room temperature, twice. After the second wash the supernatant was carefully aspirated using a pipette leaving a residual of around 50 µL so as not to disturb the pellet.

For the intracellular staining, the eBioscience™ FOXP3/transcription staining buffer set was used (Invitrogen, Massachusetts, USA). The resulting pellet was resuspended in 200 µL 'Fix/Perm' working solution for 45 minutes in the dark at room temperature. This was washed in 2 mL Perm Buffer from the kit at 400 *g* for 5 minutes at room temperature again leaving a 50 µL residual. This was resuspended in the intracellular antibody cocktail (**Table 2.2**) and incubated for 60 minutes in the dark at room temperature. This was washed in 2 mL Perm Buffer twice as before. To 1 mL Maxpar 'Fix and Perm', 1 µL intercalator-Ir (iridium, 125 µL stock thawed immediately before use) was added and the pellet resuspended in this cocktail. The samples were incubated

at 4 °C overnight, washed twice in 1 mL CSB and left pelleted in CSB overnight, or for up to 48 hours, before running the samples on the Helios XT SAE 20W-50 system. For the 24h and 48h blister and blood samples, the same process was used however the blister samples were barcoded using the CD45 antibody cocktail as described above.

Blisters were formed as described in **Section 2.1.9**. and immediately centrifuged at 1000 *g* for 5 minutes, at 4 °C. The pellet was resuspended in 200 µL ACK lysing buffer for 2 minutes, on ice and centrifuged at 1000 *g* for 5 minutes, at 4 °C. The blister fluid supernatant was aliquoted and stored at -80 °C for subsequent analysis and the pellet resuspended in 1 mL CSB. Again, 10 µL was taken for counting using the manual haemocytometer and the blister cells stained using the CD45 barcode antibody cocktail as above. Because cell yield is much lower for blisters (typically between 20,000 and 100,000), 3 x 10^6 blood cells were used to maximise the capacity of the tube and reduce blister cell loss by mass effect.

Data acquired was processed using the Helios XT SAE 20W-50 system software and analysed using FlowJo software. Representative quality control and manual gating strategy for separating out the blood and blister samples based on CD45 barcoding from the same MDIPA tube is shown in **Figure 2.6**. Sequential gating through residual, centre, offset, width, length, selection of live/dead, and DNA positive events allowed the identification of single events. Using CD45 bound to two separate metals, blood cells and blister cells from the same tube were debarcoded to reveal two population of cells, representing the blood and blister cells, respectively. Data was cleaned using Cytobank Premium software (Beckman Coulter, California, USA) to remove aggregates, debris, normalisation beads, doublets and dead cells. This method uses Gaussian parameters (centre, width, offset and residual) for each event, prior to determination of immune cell-types.

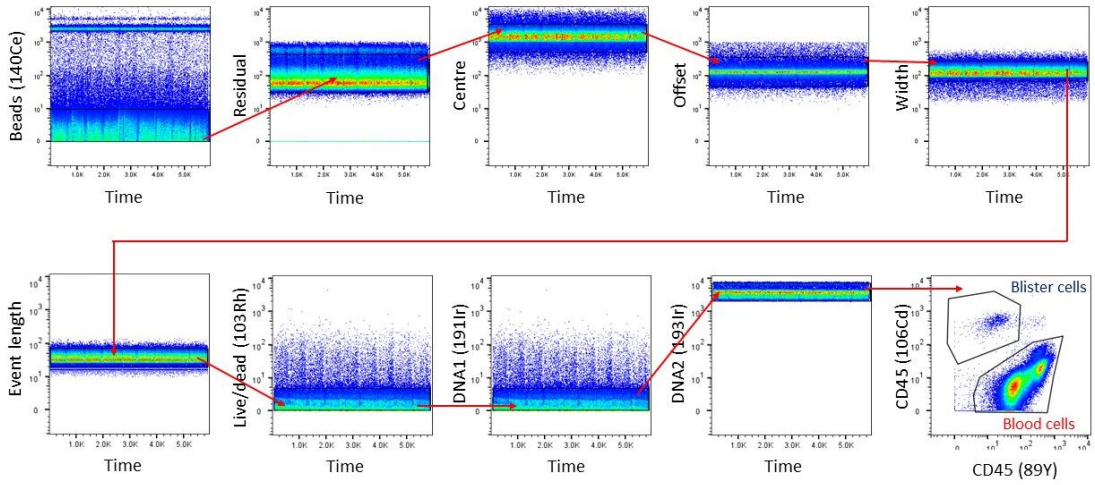

Figure 2.6. Quality control and gating strategy for mass cytometry data. Representative mass cytometry gating strategy showing steps taken to clean the data and identify the blood (blue) and blister (red) cell populations from one MDIPA tube (bottom right panel).

2.1.14 Identification of immune cells in the RA study

To identify leucocyte subsets during the different phases of inflammation, blister exudate was obtained following suction using a negative pressure cup. Cells were separated by centrifugation and characterised using polychromatic flow cytometry and a gating strategy focusing on cells of the myeloid lineage. Data was cleaned using Cytobank Premium software (Beckman Coulter, California, USA) to remove aggregates, debris, normalisation beads, doublets and dead cells (**Figure 2.6**). Cells of haematopoietic origin ($CD45^+$) were identified and blood and blister cells differentiated based on separate $CD45^+$ heavy metal isotope antibody binding. This strategy allowed the identification of granulocytes, including neutrophils ($CD45^+$, $CD66b^+$, $CD16^+$, $CD294^+$), eosinophils ($CD45^+$, $CD66b^+$, $CD294^+$, $CD16^-$) and basophils $CD45^+$, $HLA\text{-}DR^-$, $CD11c^-$, $CD123^+$, $CD294^+$. B cells were defined as $CD45^+$, $CD19^+$, $CD20^+$ as well as B cell subsets: naïve B cells ($CD45^+$, $CD19^+$, $CD20^+$, $CD27^-$), memory B cells ($CD45^+$, $CD19^+$, $CD20^+$, $CD27^+$) and plasmablasts ($CD45^+$, $CD19^+$, $CD20^-$, $CD38^+$). Total monocytes were defined as ($CD45^+$, $CD11c^+$, $HLA\text{-}DR^+$) and the monocyte subsets: classical ($CD45^+$, $CD11c^+$, $HLA\text{-}DR^+$, $CD14^+$, $CD16^-$), intermediate ($CD45^+$, $CD11c^+$, $HLA\text{-}DR^+$, $CD14^+$, $CD16^+$) and non-classical

monocytes ($CD45^+$, $CD11c^+$, $HLA\text{-}DR^+$, $CD14^-$, $CD16^+$). NK cells were defined as ($CD45^+$, $CD3^-$, $CD45RA^+$, $CD123^-$, $CD56^+$) with early NK cells ($CD45^+$, $CD3^-$, $CD45RA^+$, $CD123^-$, $CD56^+$, $CD57^-$) and late NK cells ($CD45^+$, $CD3^-$, $CD45RA^+$, $CD123^-$, $CD56^+$, $CD57^+$). Total dendritic cells ($CD45^+$, $CD14^-$, $HLA\text{-}DR^+$, $CD16^-$) were identified as well as dendritic cell subtypes: plasmacytoid ($CD45^+$, $CD14^-$, $HLA\text{-}DR^+$, $CD16^-$, $CD123^+$, $CD11c^-$), conventional ($CD45^+$, $CD14^-$, $HLA\text{-}DR^+$, $CD16^-$, $CD123^-$, $CD11c^+$, $CD38^-$), myeloid ($CD45^+$, $CD14^-$, $HLA\text{-}DR^+$, $CD16^-$, $CD123^-$, $CD11c^+$, $CD38^+$) and $CD141^+$ dendritic cells ($CD45^+$, $CD14^-$, $HLA\text{-}DR^+$, $CD16^-$, $CD123^+$, $CD11c^+$, $CD141^+$). Total T cells were $CD45^+$, $CD3^+$, with αβ T cells $CD45^+$, $CD3^+$, $TCR\gamma\delta^-$ and γδ T cells $CD45^+$, $CD3^+$, $CD4^-$, $CD8^-$, $TCR\gamma\delta^+$. More granular phenotyping was possible for both CD8 αβ T cells ($CD45^+$, $CD3^+$, $TCR\gamma\delta^-$, $CD8^+$, $CD4^-$) and CD4 αβ T cells ($CD45^+$, $CD3^+$, $TCR\gamma\delta^-$, $CD4^+$, $CD8^-$). Naïve CD8 αβ T cells ($CD45^+$, $CD3^+$, $TCR\gamma\delta^-$, $CD8^+$, $CD4^-$, $CCR7^+$, $C45RA^+$, $CD45RO^-$), central memory CD8 αβ T cells ($CD45^+$, $CD3^+$, $TCR\gamma\delta^-$, $CD8^+$, $CD4^-$, $CCR7^+$, $C45RA^-$, $CD45RO^+$), effector memory CD8 αβ T cells ($CD45^+$, $CD3^+$, $TCR\gamma\delta^-$, $CD8^+$, $CD4^-$, $CCR7^-$, $C45RA^-$, $CD45RO^+$, $CD27^+$) and terminal effector CD8 αβ T cells $CD45^+$, $CD3^+$, $TCR\gamma\delta^-$, $CD8^+$, $CD4^-$, $CCR7^-$, $C45RA^-$, $CD45RO^+$, $CD27^-$) were identified. Similarly, naïve CD4 αβ T cells ($CD45^+$, $CD3^+$, $TCR\gamma\delta^-$, CD^{4+}, $CD8^-$, $CCR7^+$, $C45RA^+$, $CD45RO^-$), central memory CD4 αβ T cells ($CD45^+$, $CD3^+$, $TCR\gamma\delta^-$, $CD4^+$, $CD8^-$, $CCR7^+$, $C45RA^-$, $CD45RO^+$), effector memory CD4 αβ T cells ($CD45^+$, $CD3^+$, $TCR\gamma\delta^-$, $CD4^+$, $CD8^-$, $CCR7^-$, $C45RA^-$, $CD45RO^+$, $CD27^+$) and terminal effector CD4 αβ T cells ($CD45^+$, $CD3^+$, $TCR\gamma\delta^-$, $CD4^+$, $CD8^-$, $CCR7^-$, $C45RA^-$, $CD45RO^+$, $CD27^-$) were defined. T regulatory cells were identified as ($CD45^+$, $CD3^+$, $TCR\gamma\delta^-$, $CD4^+$, $CD8^-$, $CCR4^+$, $CD45RA^-$, $CD45RO^+$, $CD25^+$, $CD127^-$, $Foxp3^+$). Th-1 cells were ($CD45^+$, $CD3^+$, $TCR\gamma\delta^-$, $CD4^+$, $CD8^-$, $CCR4^-$, $CD45RA^-$, $CD45RO^+$, $CXCR5^-$, $CXCR3^+$, $CCR6^-$), Th-2 cells ($CD45^+$, $CD3^+$, $TCR\gamma\delta^-$, $CD4^+$, $CD8^-$, $CCR4^+$, $CD45RA^-$, $CD45RO^+$, $CXCR5^-$, $CXCR3^-$, $CCR6^-$) and Th-17 cells ($CD45^+$, $CD3^+$, $TCR\gamma\delta^-$, $CD4^+$, $CD8^-$, $CCR4^+$, $CD45RA^-$, $CD45RO^+$, $CXCR5^-$, $CXCR3^-$, $CCR6^+$). Finally, CD4-mucosal-associated variant T/(MAVT) also known as natural killer T (NKT) cells were defined as ($CD45^+$, $CD3^+$, $TCR\gamma\delta^-$, $CD4^-$, $CD28^+$, $CD161^+$).

2.1.14.1 Multidimensional representation

Using the Cytobank Premium software (Beckman Coulter, California, USA) and R software programming language, multidimensional UMAP plots were generated, enabling visualisation of high-dimensional single-cell data. UMAP is an algorithm that takes a high-dimensional dataset and reduces it to a low-dimensional plot that retains much of the original information. Individual events are represented in a visual manner similar to a dot or scatter plot, while using all pairwise distances in high dimension to determine each cell's location in the plot. Using the Cytometry dATa analysis Tools package (CATALYST, Bioconductor, USA), this generates clusters to allow easy visualisation of different cell-types in RA patients and healthy controls. A cluster number of 30 was chosen to minimise the within-cluster sum of squares (a measure of how tight each cluster is) and maximising the between-cluster sum of squares (a measure of how separated each cluster is from the others). Convention dictates a range of 20-50 clusters for appropriate resolution of clusters and 30 gave the clearest output, whilst still permitting the identification of important immune cell-types.

2.1.15 Blister fluid soluble mediator analysis

The supernatant from the inflammatory blister exudate was diluted in the appropriate assay diluent and all assays were performed as per manufacturer's instructions.

2.1.15.1 Cytokine analysis

For IL-10 and TNF-α quantification, a customised two-plex Magnetic Luminex® assay was used as per manufacturer's instructions (R&D Systems Inc, Bio-techne, Minnesota, USA). Briefly, samples were diluted 1:1 with the kit Calibrator Diluent RD6-52 (55 µL of each) allowing for 50 µL of samples and standards to be added to the customised 96-well plate in duplicate. 50 µL of the Microparticle Cocktail was

added to each well, sealed with a foil plate sealer and incubated at room temperature for 2h on a horizontal orbital microplate shaker at 800 rpm. Using the custom magnet, Wash Buffer was applied by exposing the bottom of the plate to the magnet for 1 minute before removing the reagent. Each well was then washed with 100 µL of Wash Buffer. Next, 50 µL Biotin-Antibody Cocktail was added to each well and covered with a foil plate sealer. Using the magnetic device, the wells were washed three times with 100 µL Wash Buffer as before. Next, 50 µL Streptavidin-PE was added to each well, covered with a foil plate sealer and incubated at room temperature for 30 minutes on a horizontal orbital microplate shaker at 800 rpm. The wells were washed with Wash Buffer three times as before, with a final 100 µL Wash Buffer added to each well. This was incubated for two minutes on a horizontal orbital microplate shaker at 800 rpm and the plate read immediately. Values for each sample were assigned in relation to the standard curve using R&D Systems Quantist Analysis Software (R&D Systems Inc, Bio-techne, Minnesota, USA).

2.1.15.2 Prostaglandin E_2 quantification

For PGE_2 quantification, an enzyme-linked immunosorbent assay (ELISA) was used (GE Healthcare, Chicago, USA) as per manufacturer's recommendation. Using the reagents provided, Lysis Reagent 1 either hydrolyses cell membranes to release intracellular PGE_2, or dissociates PGE_2 from soluble receptors and interfering binding proteins present. Lysis reagent 2 sequesters the dodecyltrimethylammonium bromide in Lysis Reagent 1 and ensures PGE_2 is free for subsequent analysis. The antisera and PGE_2 'Peroxidase Conjugate' were reconstituted using Lysis Reagent 2. The assay is based on competition between unlabelled PGE_2 and a fixed quantity of peroxidase-labelled PGE_2 for a limited number of binding sites on a PGE_2-specific antibody. Lipids were not extracted prior to running the assay.

Briefly, plasma and blister fluid were diluted at 1:10 using Buffer A. The standard was serially diluted using Lysis Reagent 1 starting at 1:40 (2.5-320 pg/ µL). 50 µL of samples and standards were added in duplicate to a 96-well microtiter plate with the

addition of 50 µL of 3% sodium citrate to each well. 50 µL of both Lysis Reagent 1 and the antibody containing 'Lysis Reagent 2' were added to the non-specific binding (NSB) wells and 50 µL of Lysis Reagent 1 into the blank wells. To this, 50 µL of the Peroxidase Conjugate was added to all wells except blank and NSB. The plate was covered and incubated at room temperature for one hour on a microplate shaker. All wells were washed four times using the Wash Buffer and 150 µL of 3,3′,5,5′-tetramethylbenzidine (TMB) substrate was added to all wells and left again to incubate covered, at room temperature for a further 30 minutes. Finally, 100 µL of 0.1 M sulfuric acid was added into each well to stop the reaction and the plate was read for OD using a spectrophotometer at 450 nm within 30 minutes. Values for each sample were assigned in relation to the standard curve (**Figure 2.7**).

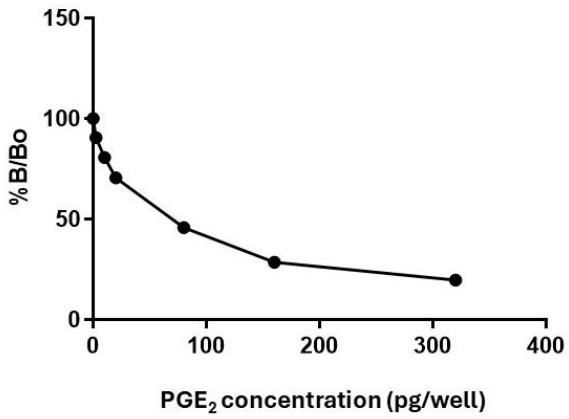

Figure 2.7. Endotoxin assay standard curve. Healthy, male volunteers were randomised to receive either ATB-346 (250 mg daily), naproxen (500 mg twice daily) or no drug (untreated control) prior to UV-KEc injection. Following the intradermal injection of 1.5 x 10^7 UV-KEc into the volar aspect of each forearm for all participants, blisters were formed using a negative pressure suction cup at two time-points (4h and 48h), one per forearm for each volunteer. Human PGE_2 solid-phase sandwich ELISA was used. Samples were diluted in PBS (1:10) and run in duplicate with standards and controls where %B/Bo represents percentage standard binding. Values for each sample were assigned in relation to the standard curve shown.

2.1.15.3 Endotoxin quantification

To detect and quantify Gram-negative bacterial endotoxin levels in the blister exudate, chromogenic Limulus Amoebocyte Lysate (LAL) assays were used. LAL is an aqueous extract from the amoebocytes of the Atlantic horseshoe crab (*Limulus polyphemus*), containing various serine proteases, including proenzymes and coagulase. These enzymes interact with bacterial endotoxin allowing its detection in two ways using two kits.

The PYROGENT®-5000 kit (Lonza, Basel, Switzerland) is a quantitative, kinetic assay. Samples were mixed with the reconstituted LAL Reagent and monitored over time for the appearance of turbidity (increasing OD) using a spectrophotometer. This is due to the reaction between endotoxin and a proenzyme thus activating coagulase. This in turn hydrolyses specific bonds within coagulogen also present in LAL, leading to the generation of coagulin, which self-associates forming a gelatinous clot. The LAL assay measures the increase in OD preceding this clot and the time required before the appearance of turbidity is inversely proportional to the amount of bacterial endotoxin present using a standard curve derived from known concentrations of endotoxin.

Briefly, blister fluid was diluted at 1:20, using endotoxin-free water provided in sterile, endotoxin-free Eppendorf tubes (Eppendorf, Hamburg, Germany). Subsequently 100 µL of endotoxin standards and samples were dispensed into a 96-well round-bottomed plate and pre-incubated for 10 minutes at 37 °C before adding 100 µL of LAL reagent before reading the plate at 340 nm over 100 reads with a ‘delta T’ of 60 seconds.

To confirm the initial findings, a portable endotoxin testing unit (EndoSafe nexgen-PTS; Charles River, UK) was also used to measure levels of bacterial endotoxin. Serine proteases also present in LAL are activated by endotoxin which subsequently cleave chromophore p-nitroaniline (pNA) from synthetic substrates. Again, using a spectrophotometer, pNA levels are indicative of the amount of endotoxin present in a

given sample and can be quantified following excitation at 350 nm within the blister fluid. Briefly, blister fluid was diluted at 1:80, using the manufacturer's endotoxin-free water provided in sterile, endotoxin-free Eppendorf tubes (Eppendorf, Hamburg, Germany). From this, 25 µL was added to the four channels of a LAL EndoSafe-PTS cartridge. By capillary action, the samples were drawn through the channels, each coated with the LAL working reagent and a chromogenic synthetic substrate with two of these channels spiked with endotoxin acting as a positive control. Once at the optical cell within the unit, pNA levels were then quantified and displayed as the mean concentration of endotoxin per millilitre of sample.

2.2 Animal studies

2.2.1 Animals

Wild type, inbred, eight-week-old male C57BL6/J mice were maintained in accordance with UK Home Office regulations (Project Licence: P69E3D849) and housed in individual ventilated cages (IVCs). All procedures were carried out under the UK Home Office Animals (Scientific Procedures) Act 1986.

2.2.2 Bacteria

UV-KEc bacterial stocks were prepared as described in in **Section 2.1.4**. In addition to UV-KEc being resuspended in 0.9% sodium chloride and aliquoted into sterile Eppendorf tubes obtaining a final count of 1.5×10^7/100 μL, a selection of further concentrations were prepared ranging from 1.5×10^7/100 μL to 1.5×10^8/100 μL. Samples were again confirmed be to non-viable by the Environmental Research Laboratory, UCLH NHS Foundation Trust following 24h incubation on both blood and MacConkey agar plates and stored at −80 °C. Aliquots were thawed immediately prior to intradermal injection.

2.2.3 Procedures

A summary of all UV-KEc intradermal injection and tissues retrieved from the sacrificed animals is shown in **Figure 2.8**. In all animal studies, each mouse was weighed at each time-point.

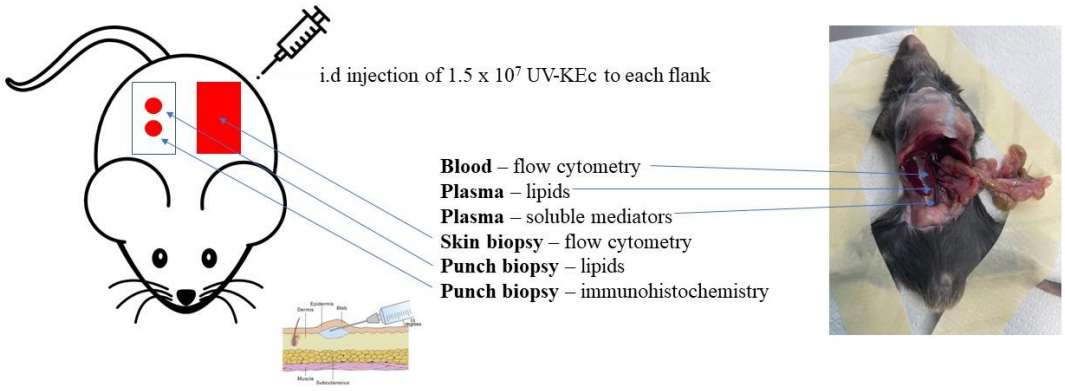

Figure 2.8. Summary graphic of animal procedures used in the UV-KEc-triggered murine dermal inflammation mode. Timeline showing UV-KEc administration and tissues acquired for processing and subsequent analysis, including blood (PBMCs and plasma) and skin (punch biopsies and skin patches for enzymatic and mechanical digestion).

2.2.3.1 UV-KEC

Prior to UV-KEc injection, C57BL6/J mice were anaesthetised and shaved over the flanks. Mice were injected intradermally with either two 1 x 10^7 (on each flank, mimicking the human dosing regimen) or 1 x 10^8 (on the right flank) UV-KEc in 100 µL saline using a using a sterile 30 G hypodermic needle and the animals were allowed to recover from anaesthesia.

2.2.3.2 Blood leucocytes and plasma

C57BL6/J mice were sacrificed by rising concentration of CO_2. Before coagulation occurred, the animals were secured in a supine position within a laminar flow biosafety cabinet. The abdominal wall was dissected and internal organs moved to the side to reveal the inferior vena cava. Using a sterile 28 G hypodermic needle and 1 mL syringe containing 100 µL 0.5 M EDTA, the vena cava was punctured and whole venous blood aspirated to dryness and stored immediately on ice.

Back in the laboratory, either 100 µL, 200 µL or 300 µL of blood was added to 5 mL ACK lysing buffer in a 15 mL Falcon tube. This was left on the rocker for 3 minutes at room temperature. Meanwhile, the remaining blood was centrifuged at 500 *g* for 10 minutes at 4 °C, with the plasma being aliquoted and stored at -80 °C for subsequent analysis. The now lysed blood was topped up to 15 mL with PBS and centrifuged at 500 *g* at 4 °C. The resulting pellets were resuspended in 100 µL antibody cocktail in a 96-well V-bottom plate and incubated for 30 minutes in the dark at 4 °C. The wells were topped up with 150 µL FACS buffer using a multichannel pipette and centrifuged at 500 *g* for 5 minutes at 4 °C. Pellets were then resuspended in 150 µL FACS buffer and 150 µL 4% PFA and either 10 or 20 µL of counting beads, ready for acquisition on the flow cytometer.

2.2.3.3 Skin biopsy patch for flow cytometric analysis

As above, following rising concentration of CO_2 as the initial method of sacrifice, and subsequent exsanguination as the method of confirmation of death, skin tissue was acquired. A skin patch approximately 30 mm by 20 mm was excised by dissection and added to 3 mL HBSS in a 7 mL Bijou tube (Thermo Fisher Scientific, Massachusetts, USA) then placed immediately on ice. The skin was floated in a Petri dish containing 1 mL HBSS and excess fat and hair was removed. The skin tissue was then weighed before being minced with scissors and added to a C-tube (Miltenyi, Bisley, UK) containing 5 mL HBSS, 20 µL (800 units) DNase I and 20 mg (2 mg/mL) collagenase IV and incubated for 60 minutes in an orbital incubator at 37 °C. The C-tubes were then placed in the gentleMACS™ dissociator (Miltenyi, Bisley, UK), using the 'Spleen' setting and then passed through a 40 µm cell strainer into a 50 mL Falcon tube to yield a single-cell suspension. This was topped up to 25 mL with HBSS and centrifuged at 800 *g* for 5 minutes at 4 °C.

The supernatant was gently aspirated and the pellet resuspended in 30 mL PBS and the samples centrifuged at 500 *g* for 5 minutes at 4 °C. The resulting pellets were resuspended in 100 µL antibody cocktail in a 96-well V-bottom plate and incubated

for 30 minutes in the dark at 4 °C. The wells were topped up with 150 µL FACS buffer using a multichannel pipette and centrifuged at 500 *g* for 5 minutes at 4 °C. Pellets were then resuspended in 150 µL FACS buffer and 150 µL 4% PFA and either 10 or 20 µL of counting beads, ready for acquisition on the flow cytometer.

2.2.3.4 Skin punch biopsy and optimum cutting temperature medium embedding

Skin punch biopsies were acquired using 3 mm single-use punch biopsies (Stiefel, North Carolina, USA). The tissue was taken from the inflamed area of the skin biopsy patch, dissected and processed as described in **Section 2.2.3.3**. Tissue-Tek optimum cutting temperature (OCT) medium (Sakura Finetek, Newbury, UK) was added to moulds and the punch biopsies were added to these. The moulds were topped up with OCT and floated in liquid nitrogen before storing immediately at -80 °C for subsequent histopathological analysis. Additionally, a second punch biopsy was taken per animal in the same way but placed in an empty Cryovial rather than an OCT-filled mould and immediately submerged in liquid nitrogen to snap freeze the samples. After 5 minutes, these were transferred to storage at -80 °C for subsequent lipid extraction.

2.2.3.5 Bone marrow neutrophil isolation

Following exsanguination and skin biopsy removal, the animals were then processed for bone marrow sampling. To access the tissue, the right femur was dissected from each animal. The head and tail of the femur was cut using scissors and a 5 mL syringe containing 5 mL HBSS with a 28 G hypodermic needles attached, was placed in the superior end of the medullary cavity and gently instilled through the length of the bone. The cell-containing fluid exiting the distal end of the femur was collected in a 15 mL Falcon tube and topped up to 15 mL with HBSS. This was centrifuged at 400 *g* for 5 minutes at 4 °C. The pellets were resuspended in 1 mL ACK lysing buffer and incubated for 30 seconds before topping up with 10 mL HBSS and centrifuging at 400

g for 5 minutes at 4 °C. The pellets were resuspended in 10 mL PBS and centrifuged as before. The resulting pellets were resuspended in 100 µL antibody cocktail in a 96-well V-bottom plate and incubated for 30 minutes in the dark at 4 °C. The wells were topped up with 150 µL FACS buffer using a multichannel pipette and centrifuged at 500 *g* for 5 minutes at 4 °C. Pellets were then resuspended in 150 µL FACS buffer and 150 µL 4% PFA and either 10 or 20 µL of counting beads, ready for acquisition on the flow cytometer.

2.2.3.6 Polychromatic flow cytometry analysis

Single cell suspensions were generated from murine blood, skin and bone marrow leucocytes as detailed in **Section 2.2.3.2, 2.2.3.3-2.2.3.4** and **2.2.2.5**, respectively, were suspended in staining buffer and were incubated with a cocktail of antibodies specific to cell surface markers for 30 minutes in the dark at 4 °C, along with appropriate FMO controls (see previous example in **Figure 2.1.11**). The antibodies used for murine studies are shown in **Table 2.3**.

For the skin and blood leucocyte flow cytometric analysis leucocyte, true events were identified following the exclusion of debris, doublets and non-live cells. Subsequently, cells of haematopoietic origin ($CD45^+$) were identified. The following cell-types were then defined: neutrophils ($SSC\text{-}A^+$, $Ly6G^+$), T cells ($CD3^+$), NK cells ($NK1.1^+$), eosinophils ($Siglec\text{-}F^+$), B cells ($CD19^+$), conventional dendritic cells ($CD11b^+$, MHC II^+, $F4/80^-$, $Langerin^-$), plasmacytoid dendritic cells ($CD11b^-$, $CD11c^+$), macrophages ($CD11b^+$, MHC II^+, $F4/80^+$, $Langerin^-$), Langerhans cells ($CD11b^+$, MHC II^+, $F4/80^-$, $Langerin^+$) and monocytes ($CD11b^+$, MHC II^-).

For the bone marrow flow cytometric analysis of neutrophils, neutrophil subsets were defined as granulocyte myeloid precursors cells (GMPs; $CD45^+$, Lin^- [CD3, CD19, NK1.1, F4/80, Siglec-F], $CD117^+$, $CD16/32^+$), pre-neutrophils ($CD45^+$, Lin^-, $CD117^{int}$, $CD11b^+$, $CXCR4^-$), immature neutrophils ($CD45^+$, Lin^-, $CD117^-$, $Ly6C^+$, $CXCR4^+$, $CD101^-$) and mature neutrophils ($CD45^+$, Lin^-, $CD117^-$, $Ly6C^+$, $CXCR4^+$, $CD101^+$).

Table 2.3. Antibodies used for flow cytometric analysis of murine immune cells. The antibody panel used for investigation of murine bone marrow is highlighted in green, for skin and blood leucocytes is shown in blue. Live dead viability stain used in all panels is shown in orange.

Surface marker	Fluorochrome	Clone	Dilution	Manufacturer
CD45	AF700	30-F11	1:100	BioLegend
CD19	PE	1D3/CD19	1:100	BioLegend
NK1.1	PE	S17016D	1:100	BioLegend
CD3	PE	17A2	1:100	BioLegend
Siglec-F	PE	S17007L	1:100	BioLegend
F4/80	PE	QA17A29	1:100	BioLegend
Ly6G	BUV395	1A8	1:100	BD
CXCR2 (CD182)	FITC	SA044G4	1:100	BioLegend
CD66a	BV421	Mab-CC1	1:100	BioLegend
CD62L	BV605	MEL-14	1:100	BioLegend
CD34	APC-Cy7	HM34	1:100	BioLegend
CD11b	PerCP-Cy5.5	M1/70	1:100	BioLegend
CD16/32	BV711	93	1:100	BioLegend
CD117	BV785	2B8	1:100	BioLegend
CXCR4	PE-Dazzle	L276F12	1:100	BioLegend
CD101	PE-Cy7	REA301	1:100	Miltenyi
Ly6C	BV510	HK1.4	1:100	BioLegend
CD54	APC	YN1/1.7.4	1:100	BioLegend
CD45	BV711	30-F11	1:100	BioLegend
CD19	FITC	1D3/CD19	1:100	BioLegend
CD3	PE	17A2	1:100	BioLegend
NK1.1	BV785	PK136	1:100	BioLegend
Siglec-F	BV421	S17007L	1:100	BioLegend
Ly6G	BUV395	1A8	1:100	BioLegend
Ly6C	BV510	HK1.4	1:100	BioLegend
F4/80	APC	QA17A29	1:100	BioLegend
Langerin (CD207)	PE-Cy7	4C7	1:100	BioLegend
MHC-II	AF700	M5/114.15.2	1:100	BioLegend
CD11b	PerCP-Cy5.5	M1/70	1:100	BioLegend
CD11c	BV605	N418	1:100	BioLegend
Live/dead	Zombie UV™	N/A	1:100	BioLegend

Stained cells were washed using staining buffer at 500 g for 5 minutes at 4 °C. Cell profiles were then acquired immediately using a flow cytometer (LSR Fortessa™ X-20, BD, New Jersey, USA) using BD FACSDiva™ software. Polychromatic flow cytometric data, including compensation, were performed using FlowJo software. Representative gating strategies for murine blood leucocytes, skin, and bone marrow and peritoneal washouts are shown in **Figure 2.9, 2.10** and **2.11**, respectively.

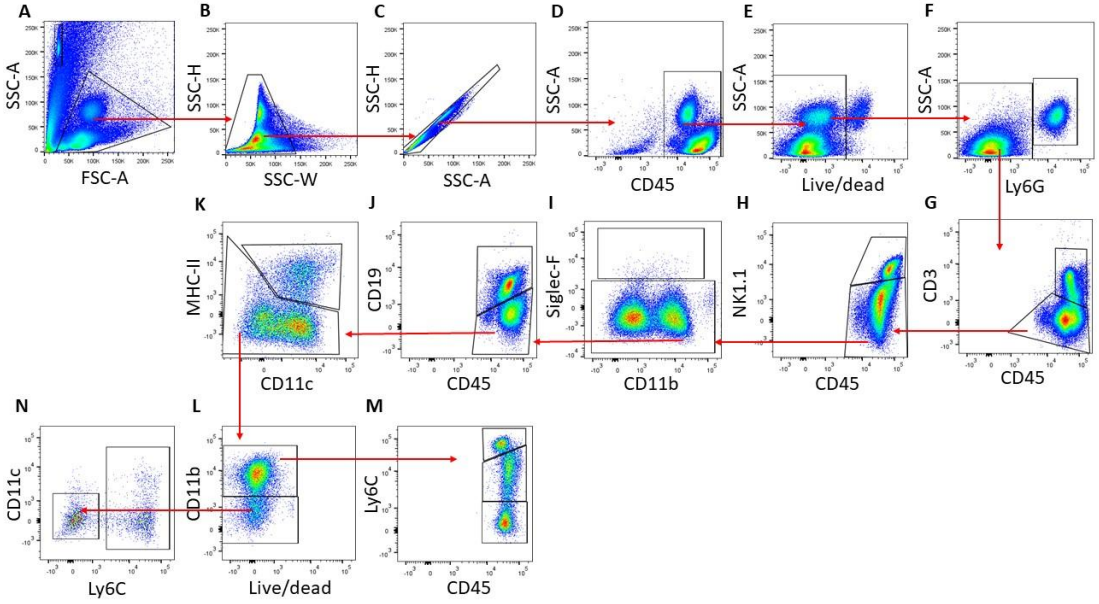

Figure 2.9. Gating strategy for circulating immune leucocyte profiles in a dermal model of inflammation following intradermal injection of UV-KEc. Male C57BL/6J mice were anaesthetised and inoculated with 100 µL sterile saline containing 1.5 x 10^7 UV-KEc or 1.5 x 10^8 UV-KEc, 100 µL. Whole venous blood was taken from the inferior vena cava and immune leucocytes isolated using ACK lysing buffer. Cells were incubated with a fluorophore-tagged antibody cocktail. Stained cells were acquired using BD LSR Fortessa™ X-20 and analysed using FlowJo software (BD, New Jersey, USA). Representative dot plots for polychromatic flow cytometric gating strategy are shown. Following exclusion of debris (A), the gating strategy employed allowed identification of (B-C) single cells, (D) $CD45^+$ haematopoietic immune cells, (E) live cells, (F) neutrophils (right box), (G) T cells (top box), (H) NK cells (top box), (I) eosinophils (top box), (J) B cells (top box), (K) dendritic cells (top box), (L) total monocytes (top box), (M) monocyte subsets ($Ly6C^{hi}$ [top box], $Ly6C^{int}$ [middle box] and $Ly6^{lo}$ monocytes [bottom box]). Counting beads can also be seen in panel (A), top left box. Arrows indicate gating strategy.

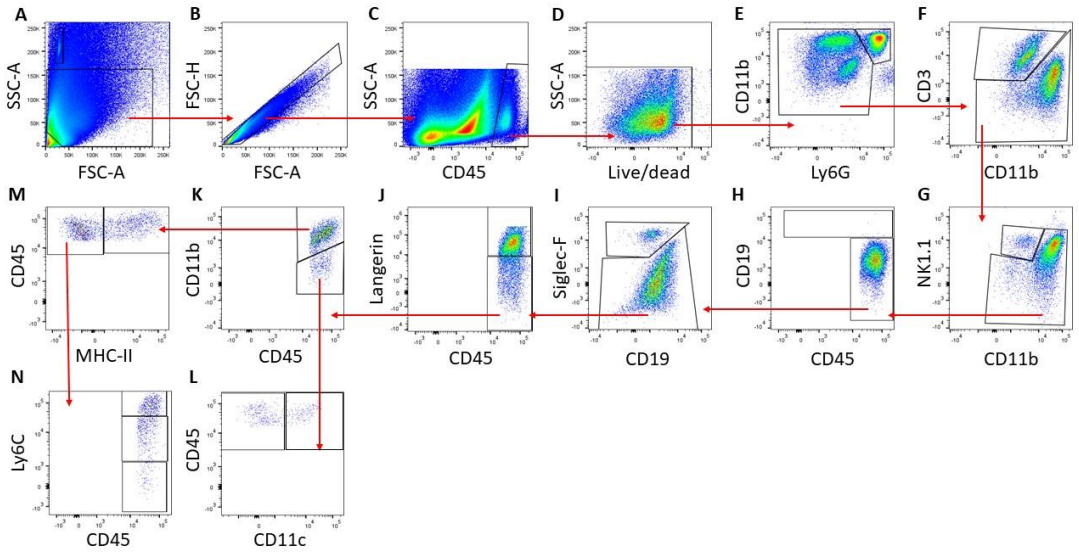

Figure 2.10. Gating strategy for murine skin immune leucocyte profiles in a dermal model of inflammation following intradermal injection of UV-KEc. Male C57BL/6J mice were anaesthetised and inoculated with 100 µL sterile saline containing 1.5 x 10^7 UV-KEc or 1.5 x 10^8 UV-KEc, 100 µL. Skin was excised, minced and enzymatically digested yielding a single-cell suspension. Cells were incubated with a fluorophore-tagged antibody cocktail. Stained cells were acquired using BD LSR Fortessa^{TM} X-20 and analysed using FlowJo software (BD, New Jersey, USA). Representative dot plots for polychromatic flow cytometric gating strategy are shown. Following exclusion of debris (A), the gating strategy employed allowed identification of (B) single cells, (C) CD45$^+$ haematopoietic immune cells, (D) live cells, (E) neutrophils (top right box), (F) T cells (top left box), (G) NK cells (top left box), (H) B cells (top box), (I) eosinophils (top box), (J) Langerhans cells (top box), (L) dendritic cells (right box), (M) total monocyte monocytes (left box), (N) monocyte subsets (Ly6C^{hi} [top box], Ly6C^{int} [middle box] and Ly6^{lo} monocytes [bottom box]). Counting beads can also be seen in panel (A), top left box. Arrows indicate gating strategy.

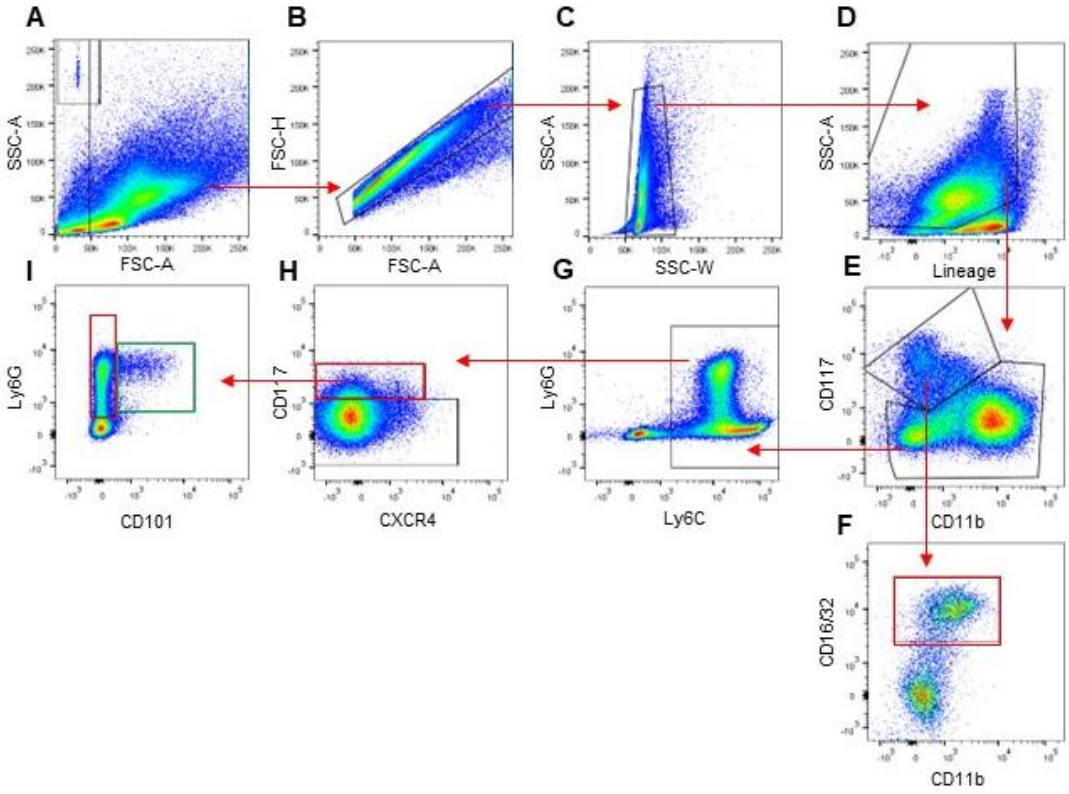

Figure 2.11. Gating strategy for bone marrow neutrophil subsets in a dermal model of inflammation following intradermal injection of UV-KEc. Male C57BL/6J mice were anaesthetised and inoculated with 100 µL sterile saline containing 1.5 x 10^7 UV-KEc or 1.5 x 10^8 UV-KEc, 100 µL. the right femur was dissected and flushed with HBSS yielding a single-cell suspension. Cells were incubated with a fluorophore-tagged antibody cocktail. Stained cells were acquired using BD LSR Fortessa^{TM} X-20 and analysed using FlowJo software (BD, New Jersey, USA). Representative dot plots for polychromatic flow cytometric gating strategy are shown. Following exclusion of debris (A), the gating strategy employed allowed identification of (B-C) single cells, (D) lineage ($CD3^+$, $CD19^+$, $NK1.1^+$ and $Siglec\text{-}F^+$) negative cells, (E) $CD117^+$ cells, (F) GMPs (red box), (G) $Ly6C^+$ cells, (H) pre-neutrophils (red box), (I) immature (red box) and mature (green box) neutrophils (top box). Counting beads can also be seen in panel (A), top left box. Arrows indicate gating strategy.

2.2.4 Lipid extraction and measurement of endocannabinoids

Endocannabinoid levels were quantified in collaboration with Dr Mireille Al Houayek (Université Catholique de Louvain, Belgium). AEA, 2-AG, PEA and OEA concentrations were determined using high-performance liquid chromatography and mass spectroscopy (HPLC-MS). Briefly, tissues were homogenised in 10 mL chloroform ($CHCl_3$) and appropriate respective deuterated internal standards (200 pM) were added to each sample prior to lipid extraction. 5 mL methanol (CH_3OH) and 2.5 mL distilled water were then added and lipids extracted by vigorous mixing. The resulting organic layer was recovered and dried under nitrogen.

The lipid fraction was then purified by solid-phase extraction over silica and the endocannabinoids eluted using 1:1 ethyl acetate. The resulting lipid fraction was analysed by HPLC-MS using a LTQ Orbitrap mass spectrometer (Thermo Fisher Scientific, Massachusetts, USA). Analyte separation was achieved using specific C-18 and LC-18 Supelguard pre-columns (3 µm, 4 x 150 mm) (Sigma-Aldrich, Missouri, USA). Mass spectrometry analysis in the positive mode was performed with an atmospheric pressure chemical ionisation (APCI) source. Capillary and APCI vaporiser temperatures were set at 250 and 400 °C, respectively. Endocannabinoids were quantified by isotopedilution using their respective deuterated standard. The calibration curves were generated and the data were normalised by tissue sample mass/volume.

2.3 Indices of resolution

Historically, inflammatory resolution has been defined by the visual inspection using light microscopy to assess the histological appearance of inflamed tissue. More recently, Bannenberg *et al.* (2005) proposed a set of resolution indices that may better quantify inflammatory resolution (124). These indices include Ψ_{max}, the maximal number of neutrophils present in inflamed tissue; T_{max}, the time at which Ψ_{max} occurs; T_{50}, the time at which neutrophils reach 50% of those seen at Ψ_{max} and the resolution

interval (R_i), the time interval from T_{max} to T_{50} and $I_{PMN=mono}$, the intersection where the increase in neutrophils equals that of the mononuclear cells. These indices provide operative and unbiassed assessments of resolution, which can be utilised to investigate the impact of endogenous signals as well as synthetic anti-inflammatory agents.

2.4 Statistical analysis

Prism GraphPad software (Version 8.2.1, GraphPad Software Inc., California, USA) was used for generating figures and for statistical analysis for all mouse data and both the healthy volunteer human and RA studies. Additionally, R software programming language and the cytometry data analysis package CATALYST were used for generating figures and statistical analysis for the RA study. Data are expressed as individual values with the mean and standard deviation (SD). Data were tested for normal distribution using the D'Agostino's K^2 and Shapiro-Wilk normality tests. For normally distributed data, differences between multiple groups were probed using ordinary one-way or two-way analysis of variance (ANOVA) and Tukey's multiple comparisons test. To compare the mean between two groups, a student's *t*-test was used. For non-normally distributed data, differences were probed for using Kruskal–Wallis test and Dunn's multiple comparisons test. A p value of < 0.05 was taken as the threshold of significance with graphical representation of $*p < 0.05$; $**p < 0.01$, $***p < 0.001$ and $****p < 0.0001$.

3 Characterisation of a novel murine model of non-resolving dermal inflammation

3.1 Introduction

To investigate the inflammatory response in RA patients and identify pro-resolution/anti-inflammatory signals, I set out to develop an analogous murine model of dermal inflammation to an existing *in vivo* model in human. One such model previously developed in the Gilroy group, is a novel model of self-resolving acute inflammation triggered by the intradermal injection of UV-KEc into the forearms of healthy volunteers (252). This is an easily accessible site, making it ideal for sample collection for the study of inflammation. The human model utilises a negative pressure suction cup to generate a blister by gently separating the dermal and epidermal layers. This blister contains an inflammatory exudate consisting of infiltrating immune cells into the site of inflammation and can be sampled in a temporal manner and analysed by polychromatic flow cytometry. Whilst able to model real-life disease and drug effect, it is limited in that only clinical grade pharmacological agents can be used and transgenic experiments are not possible in humans. A small number of papers have attempted to develop models of murine dermal inflammation with mixed success and low cell yield, as described in **Section 1.6** (238, 263). However, none have described a time-course to allow the sampling of murine immune cells in a temporal manner to represent the onset, resolution and post-resolution phases of inflammation.

I set out to use the same inflammatory stimulus, UV-KEc, to trigger murine dermal inflammation, aiming to characterise the cellular profiles of infiltrating and resident immune cells in inflamed mouse skin, complemented with blood, bone marrow and lipid mediator analysis. Due to differences in the architecture of murine skin compared to human, it was not possible to use a negative pressure suction cup to generate an inflammatory exudate-containing blister. Therefore, I sought to biopsy and process inflamed dermal tissue, to yield a single-cell suspension for polychromatic cytometric analysis comparable to the human model described (252).

3.2 Hypothesis

Previous work in the Gilroy group using the UV-KEc-triggered human dermal model of inflammation, demonstrated that inflammation onset was characterised by the influx of neutrophils to the inflamed site, peaking at 4h, with resolution shown by a subsequent reduction in neutrophil numbers at the site (252). This gives rise to the hypothesis that: **intradermal injection of UV-KEc into murine skin elicits an acute inflammatory response, characterised by the influx of neutrophils to the inflamed site.**

To investigate the feasibility of this as a model of inflammation, I developed five main aims:

1. Demonstrate that intradermal injection of UV-KEc into mouse skin results in an inflammatory response.
2. Characterise the inflammatory infiltrate in mouse skin following the intradermal injection of UV-KEc.
3. Characterise the systemic immune response and changes in circulating blood leucocytes following intradermal injection of UV-KEc.
4. Investigate bone marrow neutrophil subsets following the intradermal injection of UV-KEc.
5. Extract and quantify key endocannabinoid concentrations from the inflamed skin.

3.3 Results

3.3.1 Naïve and sham mice are equivalent

To determine whether to use naïve or sham animals to control for inflammation triggered by UV-KEc, animals were anaesthetised and injected intradermally with 1.5 x 10^8 UV-KEc in 100 μL of 0.9% sodium chloride, 100 μL of 0.9% sodium chloride alone (sham) or no procedure (naïve). Neutrophil ($CD45^+$, $CD11b^+$, $Ly6G^+$) infiltration into the skin was used as a marker of inflammation onset and was determined by flow cytometry (**Figure 3.1**).

Baseline numbers of neutrophils in un-injected animals were similar across all groups. There was a slight rise in neutrophil numbers seen at 24h in the naïve and sham groups, falling back to baseline levels by 72h, although there were no significant differences between these two groups at any time-point. In animals injected with UV-KEc, neutrophil numbers began to rise at 24h, increasing progressively up to 72h compared to baseline ($p < 0.001$). Overall, resolution of inflammation did not occur during this time-course, as defined by absence of neutrophil clearance (264). Thus, injecting saline into the skin of mice does not cause acute inflammation and sham controls were chosen for this project.

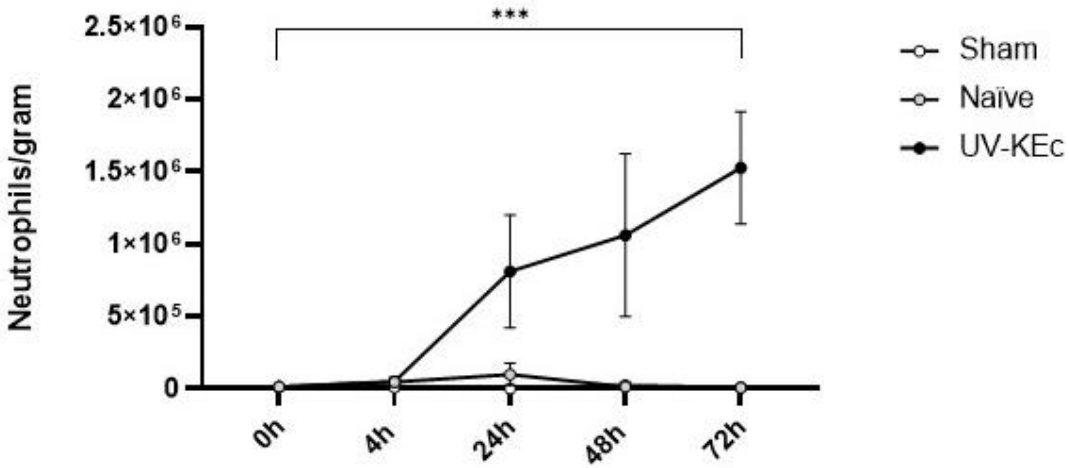

Figure 3.1. Neutrophil influx in UV-KEc injected, saline-injected and naïve mice. Male C57BL/6J mice were anaesthetised and inoculated with either UV-KEc, saline (sham) or not subjected to any injection (naïve). Skin was harvested and enzymatically digested with total number of neutrophils determined by flow cytometry at baseline (0h), 4h, 24h, 48h and 72h. Data are presented as mean with SD; $n = 5$. *$p < 0.05$, **$p < 0.01$, ***$p < 0.001$, ****$p < 0.0001$.

3.3.2 Intradermal injection of 1.5 x 10^8 UV-KEc results in the formation of granuloma-like tissue at the site of inoculation

Following the injection of 1.5 x 10^8 UV-KEc, it was observed that on the underside of the skin excised from the inflamed area, that there was the formation of localised, granuloma-like tissue (**Figure 3.2**). This tissue was seen in all animals, at all time-points from 24h onwards. This granuloma-like tissue was included in the enzymatic digestion of the skin and investigated using flow cytometry.

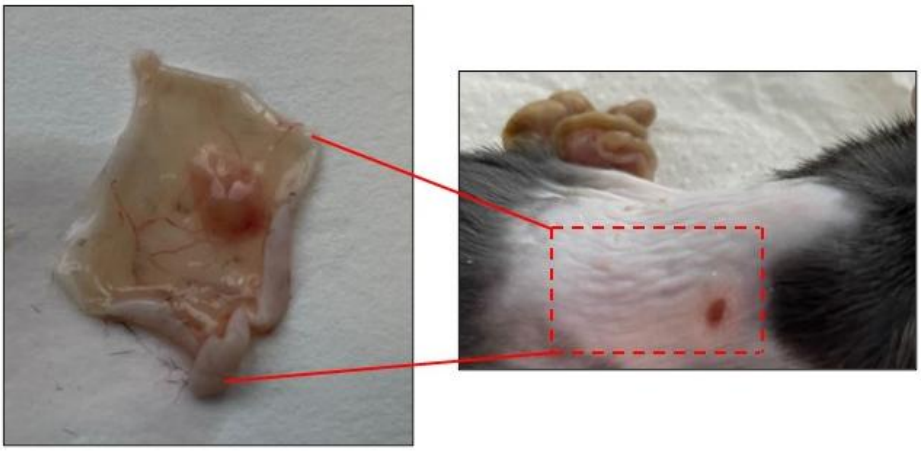

Figure 3.2. Granuloma-like tissue formation following the injection of 1.5 x 10^8 UV-KEc into mouse skin. Following intradermal injection of 1.5 x 10^8 UV-KEc, a visible granuloma formed at the site of the injection. Depicted is a representative photograph of the 48h time-point of one animal.

3.3.3 Intradermal injection with 1.5 x 10^8 UV-KEc is a non-resolving model of inflammation

To determine temporal profiles of resident and infiltrating cells in the inflamed skin following injection with UV-KEc, time-points were chosen to mirror the human model of inflammation previously developed in the Gilroy group at baseline (0h), 4h, 24h, 48h and 72h (252). Animals were weighed at each time-point to gauge the systemic impact of intradermal UV-KEc. Following intradermal injection of 1.5 x 10^8 UV-KEc, animals began to lose weight 4h post-injection and by 24h this had fallen significantly by a mean of 8.1% body mass compared to baseline (**Figure 3.3A**). At 48h, body weight began to recover and at 72h the mean mass returned to near pre-injection levels. Immune cell ($CD45^+$) influx was assessed at each time-point with levels beginning to increase at 4h (**Figure 3.3B**). Levels continued to rise and were significantly higher than baseline at 48h ($p < 0.05$) and peaking at 72h ($p < 0.0001$).

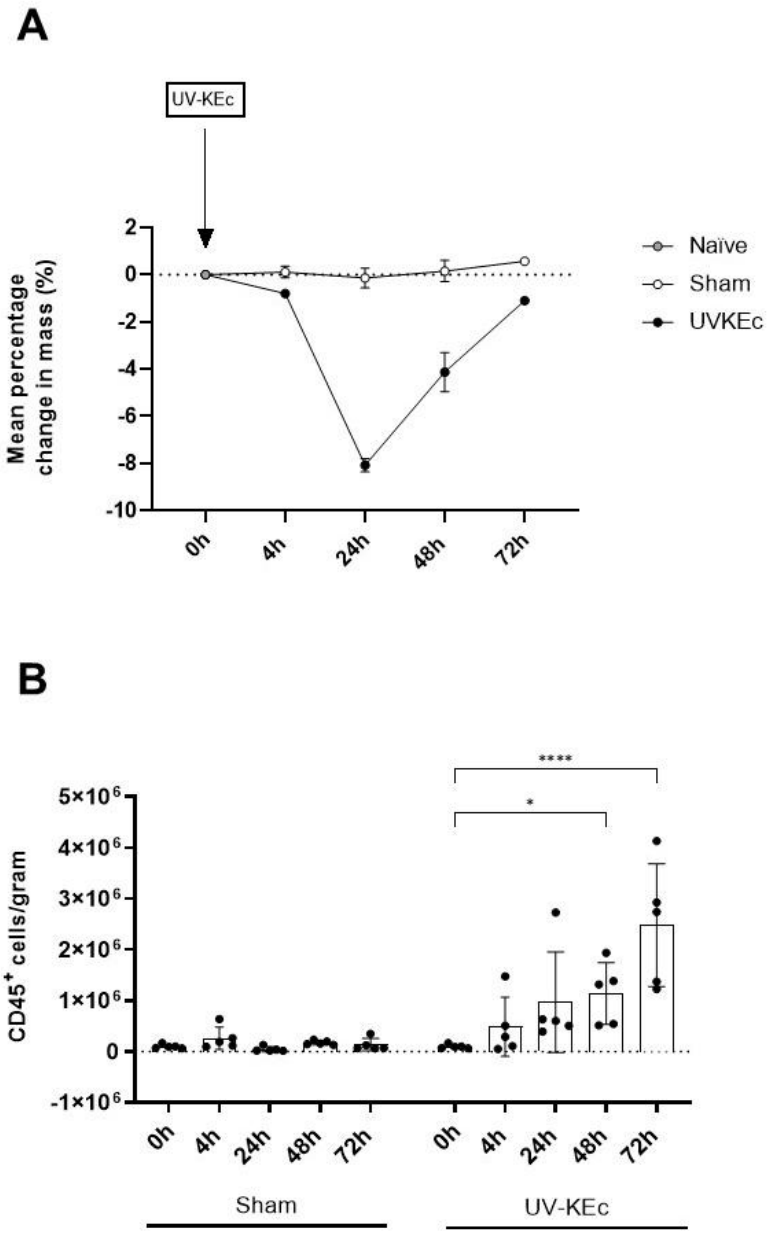

Figure 3.3. Intradermal injection of 1.5 x 10^8 UV-KEc is a model of non-resolving inflammation in murine skin. Male C57BL/6J mice were anaesthetised and inoculated with 100 µL sterile saline containing 1.5 x 10^8 UV-KEc, 100 µL of saline alone (sham) or not subjected to any procedure (naïve). Skin was harvested and enzymatically digested at baseline (0h), 4h, 24h, 48h and 72h. Animals were weighed at each time-point (A). The resulting single-cell suspension was stained for polychromatic flow cytometry and the total number $CD45^+$ immune cells infiltrating into the skin over 72h was determined by flow cytometry (B). Data are presented as individual data and mean with SD; $n = 5$. *$p < 0.05$, **$p < 0.01$, ***$p < 0.001$, ****$p < 0.0001$.

3.3.4 Temporal profiles of infiltrating cells in a murine dermal model of non-resolving inflammation

Following the intradermal injection of UV-KEc, populations of immune leucocytes in the inflamed skin were determined by flow cytometric analysis using a single-cell suspension from digested, inflamed skin. There were few immune cells present in the naïve skin (**Figure 3.4A-J**). Infiltrating total monocyte numbers began to increase significantly at 24h from baseline ($p < 0.05$), peaking at 72h ($p < 0.0001$) (**Figure 3.4B**). Conventional dendritic cell numbers increased significantly at 72h ($p < 0.0001$) (**Figure 3.4C**). Plasmacytoid dendritic cells rose significantly at 48h compared to baseline ($p < 0.05$) and peaked at 72h ($p < 0.0001$) (**Figure 3.4D**). Macrophage numbers began to rise significantly at 48h ($p < 0.05$), peaking at 72h ($p < 0.0001$) (**Figure 3.4E**). Langerhans cells began to increase in number at 48h ($p < 0.0001$), peaking at 72h ($p < 0.0001$) (**Figure 3.4F**). T cell numbers showed a biphasic response with an initial peak at 4h compared to baseline ($p < 0.01$), dropping significantly at 24h ($p < 0.01$), before a second peak at 72h ($p < 0.01$) (**Figure 3.4G**). No significant changes were identified in B cell numbers at any time-point (**Figure 3.4H**). NK cell numbers only began to increase significantly 72h ($p < 0.0001$) (**Figure 3.4I**). Eosinophils began to rise significantly at 48h ($p < 0.05$), peaking at 72h ($p < 0.0001$) (**Figure 3.4J**). There were no significant differences seen in any immune cell-type in sham animals at any time-point (**Figure 3.4A-I**). Thus, these data suggest that the onset of inflammation in the skin using this model is between 4h and 24h, with most cell-types (except B cells) peaking in number at the final time-point (72h). Therefore, inflammation in the mouse skin did not resolve during this time-course.

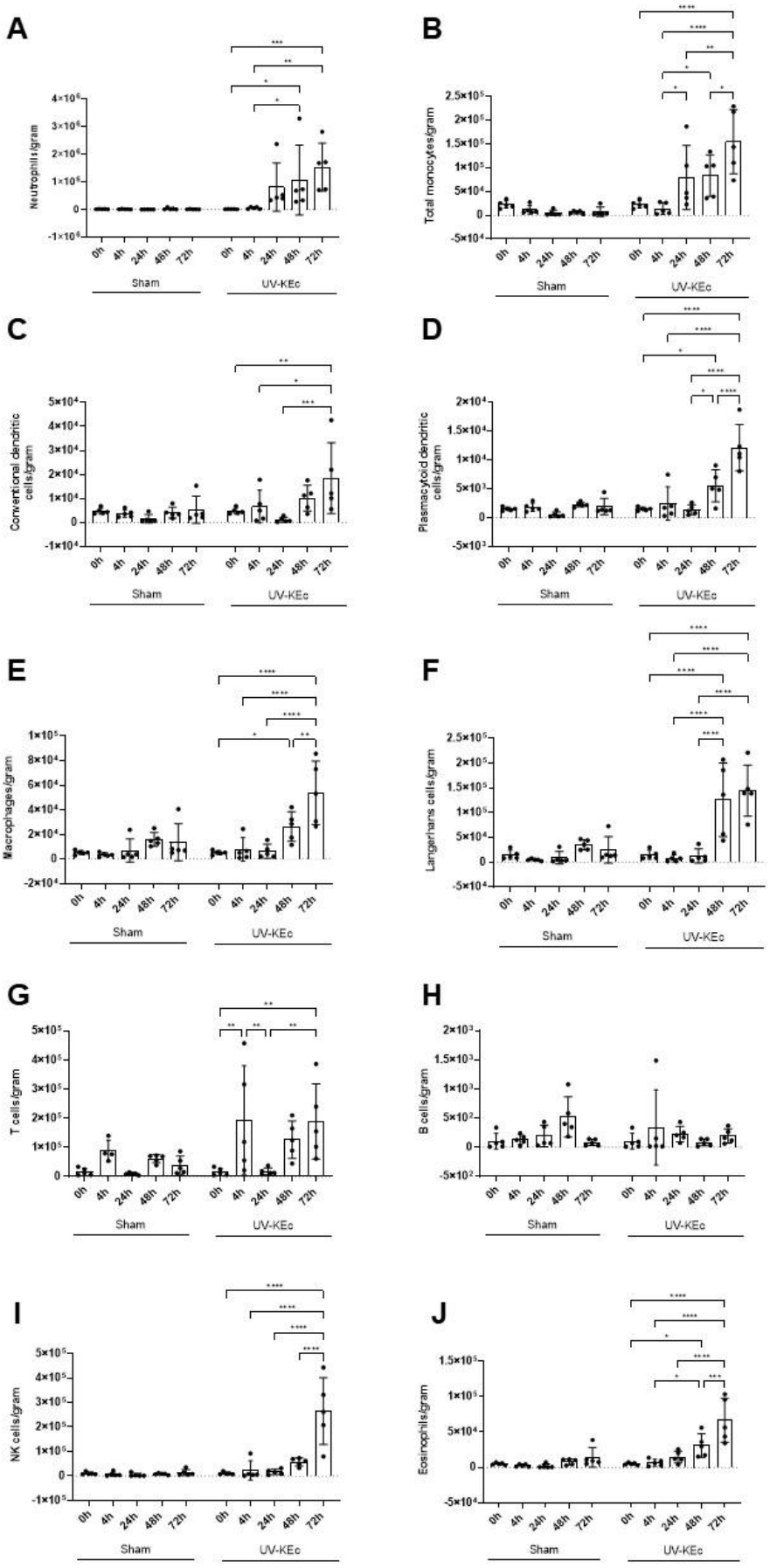
A
Neutrophils/gram
B
Total monocytes/gram
C
Conventional dendritic cells/gram
D
Plasmacytoid dendritic cells/gram
E
Macrophages/gram
F
Langerhans cells/gram
G
T cells/gram
H
B cells/gram
I
NK cells/gram
J
Eosinophils/gram
0h
4h
24h
48h
72h
Sham
UV-KEc

Figure 3.4. Temporal profiles of infiltrating immune cells into skin following UV-KEc-induced dermal inflammation in a non-resolving model of inflammation. Male C57BL/6J mice were anaesthetised and inoculated with 100 µL sterile saline containing 1.5 x 10^8 UV-KEc or 100 µL of saline alone (sham). Skin was harvested and enzymatically digested at baseline (0h), 4h, 24h, 48h and 72h. The resulting single-cell suspension was stained for polychromatic flow cytometry and the total number of infiltrating immune cells in the skin was determined. Depicted are (A) neutrophils, (B) total monocytes, (C) conventional dendritic cells, (D) plasmacytoid dendritic cells, (E) tissue macrophages, (F) Langerhans cells, (G) T cells, (H) B cells, (I) NK cells and (J) eosinophils. Data are presented as individual data points and mean with SD; $n = 5$. *$p < 0.05$, **$p < 0.01$, ***$p < 0.001$, ****$p < 0.0001$.

3.3.5 Temporal profiles and proportions of infiltrating monocyte subsets in a murine dermal model of non-resolving inflammation

To investigate infiltrating numbers and relative proportions of monocyte subsets, polychromatic flow cytometry was used to identify Ly6C^{hi} (CD45$^+$, CD11b$^+$, MHC II$^-$, Ly6C^{hi}), Ly6C^{int} (CD45$^+$, CD11b$^+$, MHC II$^-$, Ly6C^{int}) and Ly6C^{lo} (CD45$^+$, CD11b$^+$, MHC II$^-$, Ly6C^{lo}) monocyte subsets. In the skin, all monocyte subsets began to infiltrate at 24h, peaking at 72h compared to baseline (Ly6C^{hi}, $p < 0.01$; Ly6C^{int}, $p < 0.0001$ and Ly6C^{lo}, $p < 0.0001$). No significant differences were seen in any monocyte subset in the sham group at any time-point (**Figure 3.5A-C**). In the UV-KEc group, there was a significant expansion of Ly6C^{int} monocytes, accounting for just 7.0% of total monocytes at baseline, but increasing to 61.3% at 72h (**Figure 3.5D**).

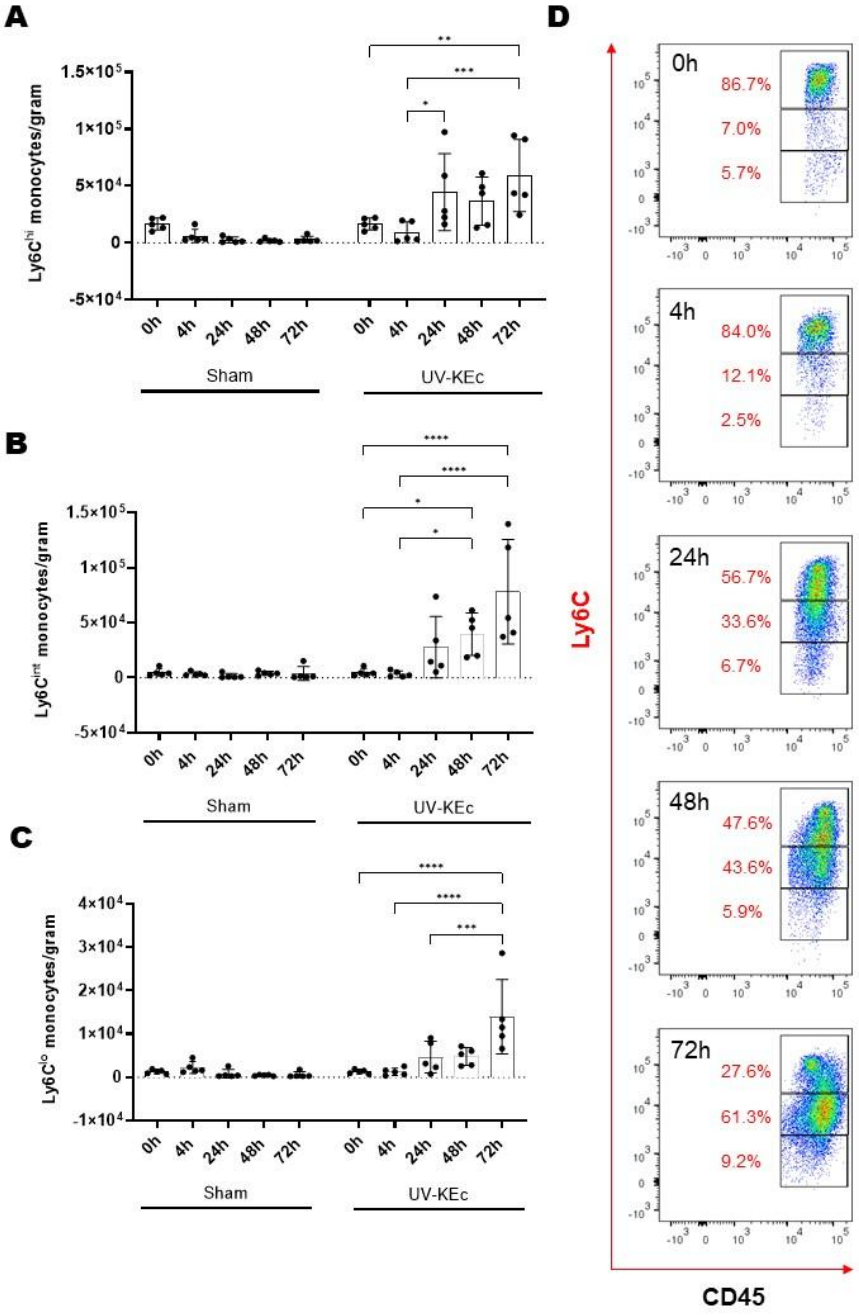

Figure 3.5. Temporal profiles of infiltrating monocyte subsets into skin following UV-KEc-induced dermal inflammation in a non-resolving model of inflammation. Male C57BL/6J mice were anaesthetised and inoculated with 100 µL sterile saline containing 1.5 x 10^8 UV-KEc or 100 µL of saline alone (sham). Skin was harvested and enzymatically digested at baseline (0h), 4h, 24h, 48h and 72h. The resulting single-cell suspension was stained for polychromatic flow cytometry and the monocyte subset numbers were determined. Depicted are (A) Ly6C^{hi} monocytes numbers, (B) Ly6C^{int} monocyte numbers and (C) Ly6C^{lo} monocyte numbers. Representative dot plots are also shown at all time-points depicting the relative proportions of Ly6C^{hi} (top box), Ly6C^{int} (middle box) and Ly6C^{lo} monocytes of total monocytes (D). Data are presented as individual data points and mean with SD; $n = 5$. *$p < 0.05$, **$p < 0.01$, ***$p < 0.001$, ****$p < 0.0001$.

3.3.6 Temporal profiles of circulating immune cells in a murine dermal model of non-resolving inflammation

To understand the systemic changes occurring during non-resolving UV-KEc-triggered dermal inflammation, peripheral venous blood was sampled from the inferior vena cava of anaesthetised C57BL/6J mice and immune cells isolated using ACK lysing buffer. Circulating $CD45^+$ cells increased throughout the time-course, although there were no significant differences in either group (**Figure 3.6A**). In animals injected with UV-KEc, neutrophils were the first myeloid cell-type to significantly peak in blood at 4h ($p < 0.01$) (**Figure 3.6B**). Neutrophil numbers then began to decrease significantly between 4h and 72h compared to baseline ($p < 0.05$), although did not return to pre-injection levels, suggesting ongoing inflammation. Total monocyte numbers also began to increase at 4h, decreasing again at 48h, with a further slight increase at 72h, although these changes were not significant (**Figure 3.6C**). Conventional dendritic cell numbers increased significantly at 72h ($p < 0.0001$) (**Figure 3.6D**). Plasmacytoid dendritic cell numbers initially dipped at 4h and peaked between 24h and 48h ($p < 0.01$), before a second dip at 72h ($p < 0.05$) (**Figure 3.6E**). Macrophage numbers increased significantly between baseline and 48h ($p < 0.01$), with levels maintained at 72h (**Figure 3.6F**). Langerhans cells, sharply increased in blood at 24h ($p < 0.0001$) before declining between 24h and 48h ($p < 0.0001$) (**Figure 3.6G**). T cell numbers initially dipped in the UV-KEc group at 4h before increasing significantly at 48h ($p < 0.01$), with levels maintained at 72h (**Figure 3.6H**). B cell numbers dropped at 4h, although this was not significant, before increasing significantly at 48h ($p < 0.05$) and further still at 72h ($p < 0.001$) (**Figure 3.6I**). NK cell numbers increased significantly between baseline and 48h ($p < 0.0001$) with a slight dip at 72h (**Figure 3.6J**). No significant differences were seen in either group in terms of eosinophil numbers (**Figure 3.6K**). No significant differences were detected in the sham group for any cell-type at any time-point (**Figure 3.6A-K**).

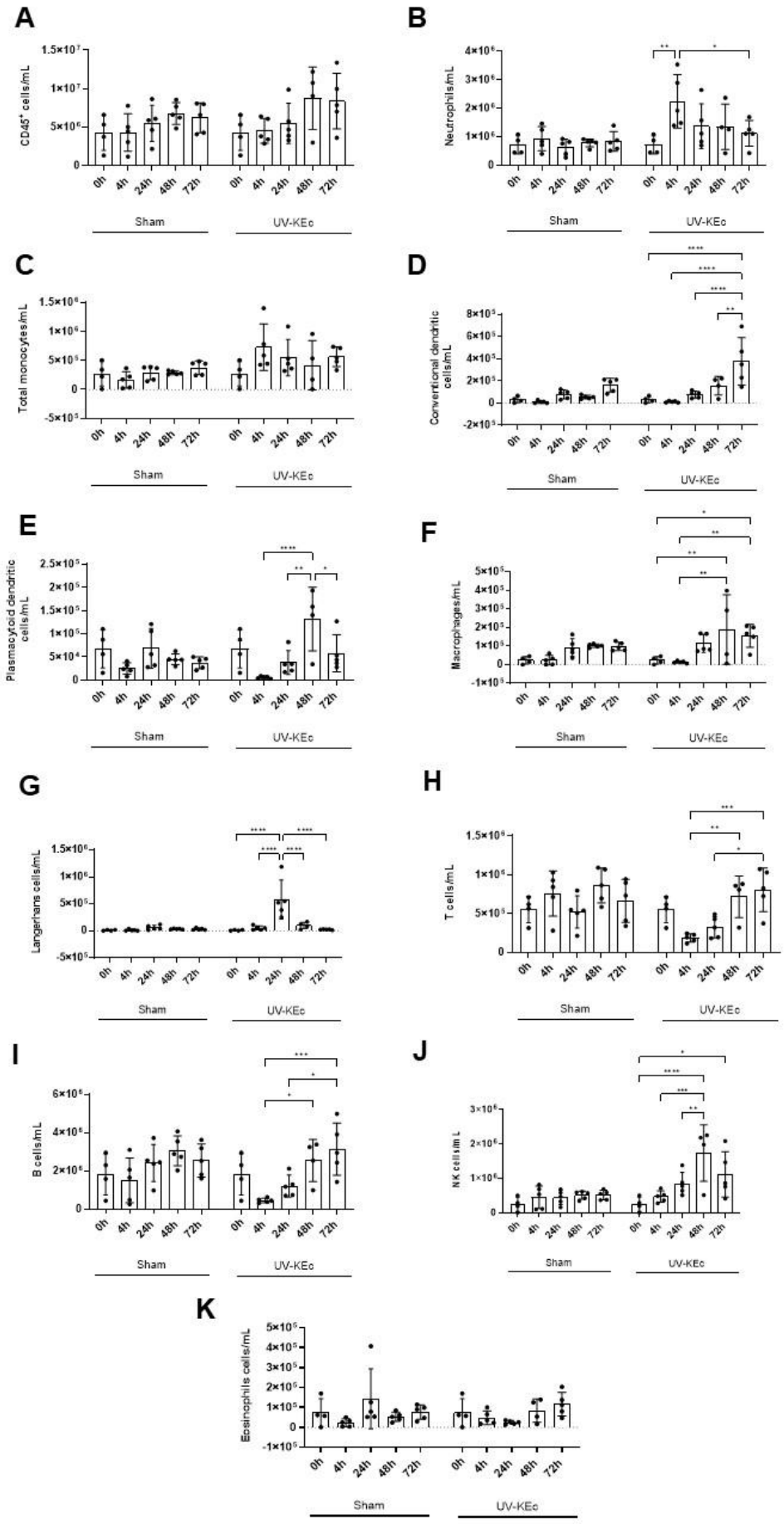
A
CD45+ cells/mL
1.5×10⁷
1×10⁷
5×10⁶
0
0h 4h 24h 48h 72h 0h 4h 24h 48h 72h
Sham
UV-KEc
B
Neutrophils/mL
4×10⁶
3×10⁶
2×10⁶
1×10⁶
0
**
*
0h 4h 24h 48h 72h 0h 4h 24h 48h 72h
Sham
UV-KEc
C
Total monocytes/mL
1.5×10⁶
1×10⁶
5×10⁵
0
-5×10⁵
0h 4h 24h 48h 72h 0h 4h 24h 48h 72h
Sham
UV-KEc
D
Conventional dendritic cells/mL
8×10⁵
6×10⁵
4×10⁵
2×10⁵
0
-2×10⁵
****
****
****
**
0h 4h 24h 48h 72h 0h 4h 24h 48h 72h
Sham
UV-KEc
E
Plasmacytoid dendritic cells/mL
2.5×10⁵
2×10⁵
1.5×10⁵
1×10⁵
5×10⁴
0
****
**
*
0h 4h 24h 48h 72h 0h 4h 24h 48h 72h
Sham
UV-KEc
F
Macrophages/mL
5×10⁵
4×10⁵
3×10⁵
2×10⁵
1×10⁵
0
-1×10⁵
*
**
**
**
0h 4h 24h 48h 72h 0h 4h 24h 48h 72h
Sham
UV-KEc
G
Langerhans cells/mL
1.5×10⁶
1×10⁶
5×10⁵
0
-5×10⁵
****
****
****
****
0h 4h 24h 48h 72h 0h 4h 24h 48h 72h
Sham
UV-KEc
H
T cells/mL
1.5×10⁶
1×10⁶
5×10⁵
0
***
**
*
0h 4h 24h 48h 72h 0h 4h 24h 48h 72h
Sham
UV-KEc
I
B cells/mL
6×10⁶
4×10⁶
2×10⁶
0
***
*
*
0h 4h 24h 48h 72h 0h 4h 24h 48h 72h
Sham
UV-KEc
J
NK cells/mL
3×10⁶
2×10⁶
1×10⁶
0
*
****
***
**
0h 4h 24h 48h 72h 0h 4h 24h 48h 72h
Sham
UV-KEc
K
Eosinophils cells/mL
5×10⁵
4×10⁵
3×10⁵
2×10⁵
1×10⁵
0
-1×10⁵
0h 4h 24h 48h 72h 0h 4h 24h 48h 72h
Sham
UV-KEc

Figure 3.6. Temporal profiles of circulating immune cells following UV-KEc-induced dermal inflammation in a non-resolving model of inflammation. Male C57BL/6J mice were anaesthetised and inoculated with 100 µL sterile saline containing 1.5 x 10^8 UV-KEc or 100 µL of saline alone (sham). Immune cells were isolated using ACK lysing buffer and the resulting single-cell suspension was stained for polychromatic flow cytometry and the total number of circulating immune cells was determined. Depicted are (A) $CD45^+$ immune leucocytes, (B) neutrophils, (C) total monocytes, (D) conventional dendritic cells, (E) plasmacytoid dendritic cells, (F) macrophages, (G) Langerhans cells, (H) T cells, (I) B cells, (J) NK cells and (K) eosinophils. Data are presented as individual data points and mean with SD; $n = 5$. *$p < 0.05$, **$p < 0.01$, ***$p < 0.001$, ****$p < 0.0001$.

3.3.7 Temporal profiles and proportions of circulating monocyte subsets in a murine dermal model of non-resolving inflammation

To investigate circulating numbers and relative proportions of monocyte subsets, polychromatic flow cytometry was again used to identify $Ly6C^{hi}$, $Ly6C^{int}$ and $Ly6C^{lo}$ monocytes subsets. In blood, circulating $Ly6C^{hi}$ monocyte numbers rapidly peaked at 4h in the UV-KEc group ($p < 0.001$), before progressively decreasing back to levels similar to baseline at 72h ($p < 0.01$) (**Figure 3.7A**). Circulating $Ly6C^{int}$ monocyte numbers in UV-KEc-injected animals rose significantly at 24h ($p < 0.01$) before falling back to baseline levels by 72h ($p < 0.001$) (**Figure 3.7B**). $Ly6C^{lo}$ monocyte numbers increased significantly by 48h ($p < 0.01$) and were maintained at 72h in UV-KEc-injected animals (**Figure 3.7C**). No significant differences were seen in any monocyte subset numbers in sham controls (**Figure 3.7A-C**). In terms of proportions, at baseline the predominant monocyte subtype was the $Ly6C^{hi}$ cell-type in the UV-KEc group (64.1%), and this decreased throughout the time-course (29.5% at 72h) (**Figure 3.7D**). $Ly6C^{int}$ monocytes were at very low levels at baseline in the UV-KEc group, with a significant expansion seen at 24h, correlating with an increase in circulating numbers. The proportion of $Ly6C^{int}$ monocytes subsequently decreased between 24h and 72h, back to near baseline proportions (**Figure 3.7B,D**).

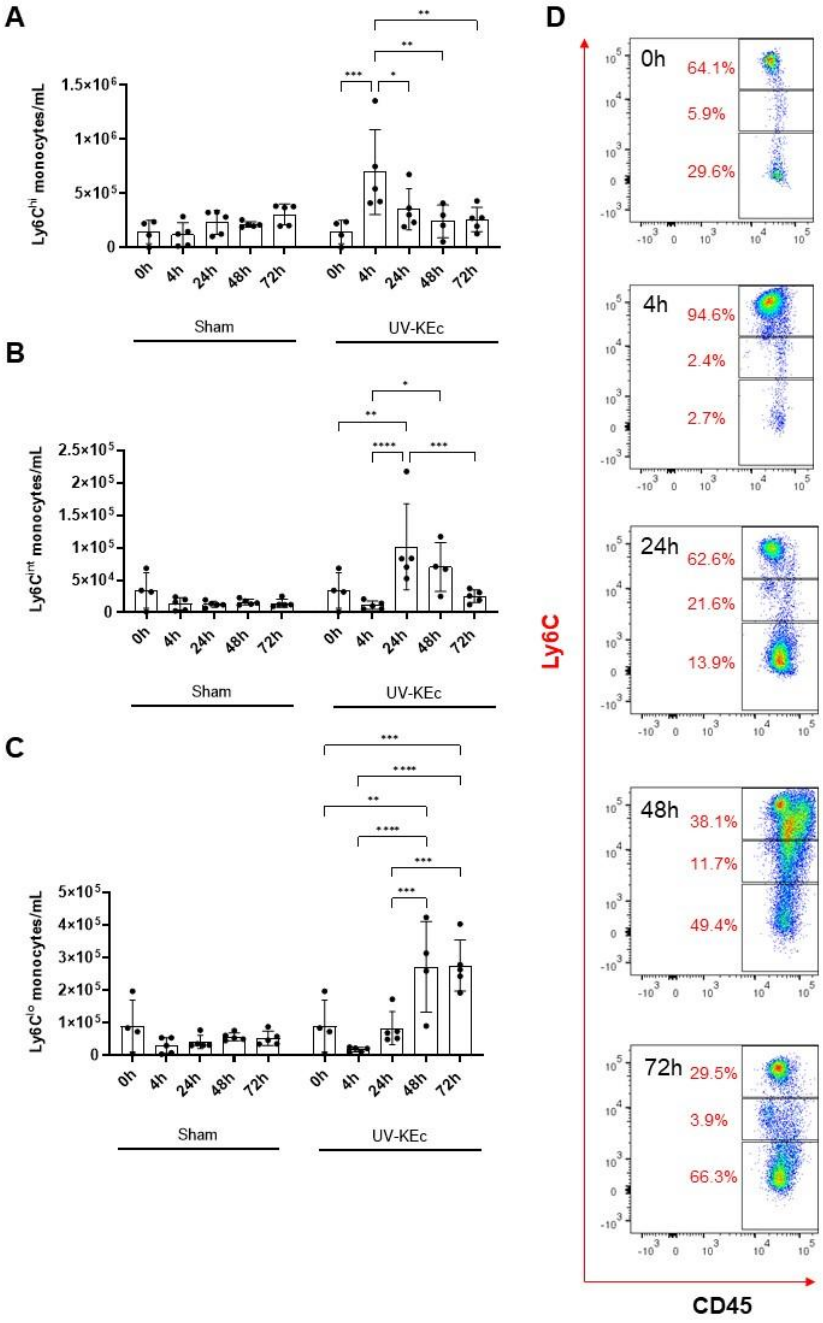

Figure 3.7. Temporal profiles of circulating monocyte subsets following UV-KEc-induced dermal inflammation in a non-resolving model of inflammation. Male C57BL/6J mice were anaesthetised and inoculated with 100 µL sterile saline containing 1.5 x 10^8 UV-KEc or 100 µL of saline alone (sham). Immune cells were isolated using ACK lysing buffer and the resulting single-cell suspension was stained for polychromatic flow cytometry and the monocyte subset numbers were determined. Depicted are (A) Ly6C^{hi} monocyte numbers, (B) Ly6C^{int} monocyte numbers and (C) Ly6C^{lo} monocyte numbers. Representative dot plots are also shown at all time-points depicting the relative proportions of Ly6C^{hi} (top box), Ly6C^{int} (middle box) and Ly6C^{lo} monocytes of total monocytes (D)Data are presented as individual data points and mean with SD; $n = 5$. *$p < 0.05$, **$p < 0.01$, ***$p < 0.001$, ****$p < 0.0001$.

3.3.8 Temporal profiles of bone marrow neutrophil subsets in a murine dermal model of non-resolving inflammation

Having identified significant changes in both circulating and infiltrating neutrophil numbers, I wanted to further investigate bone marrow neutrophil subsets to understand whether there was an emergency release from the marrow of neutrophils in response to the inflammatory insult, so assessed neutrophil subsets at their different stages of development: GMPs ($CD45^+$, Lin^- [CD3, CD19, NK1.1, F4/80, Siglec-F], $CD117^+$, $CD16/32^+$), pre-neutrophils ($CD45^+$, Lin^-, $CD117^{int}$, $CD11b^+$, $CXCR4^-$), immature neutrophils ($CD45^+$, Lin^-, $CD117^-$, $Ly6C^+$, $CXCR4^+$, $CD101^-$) and mature neutrophils ($CD45^+$, Lin^-, $CD117^-$, $Ly6C^+$, $CXCR4^+$, $CD101^+$). Following the intradermal injection of 1.5 x 10^8 UV-KEc, bone marrow GMP numbers dipped at 2h then significantly increased between 2h and 48h ($p < 0.01$), with levels maintained above baseline at 72h ($p < 0.05$) (**Figure 3.8A**). Pre-neutrophils showed a biphasic response with numbers starting to fall at 2h with a significant decrease between baseline and 4h ($p < 0.05$), reaching a trough at 24h ($p < 0.05$) before increasing significantly back to baseline levels at 48h ($p < 0.05$) and further still at 72h ($p < 0.01$) (**Figure 3.8A**). Immature neutrophil numbers dropped significantly at 2h ($p < 0.05$) and remained low at 4h and 24h, before rising again at 48h, with numbers maintained at this level at 72h ($p < 0.05$) (**Figure 3.8A**). Mature neutrophil numbers fell significantly at 2h ($p < 0.05$) and remained low at both 4h and 24h ($p < 0.05$). Between 24h and 48h, mature neutrophil numbers increased significantly ($p < 0.05$) and were maintained at 72h ($p < 0.001$), but not back to levels seen at baseline (**Figure 3.8A**). Proportions of immature to mature neutrophils increased from baseline (78.1%) at 2h (96.4%), with levels maintained at 4h (99.4%) and 24h (99.1%), before falling back to baseline levels at 48h (77.0%) (**Figure 3.8B**). Taken together, these data suggest that all neutrophil subsets are released from the bone marrow as early as 2h in response to UV-KEc, with the most marked decreases seen for immature and mature neutrophils. All subsets were able to repopulate in the bone marrow above baseline except mature neutrophils.

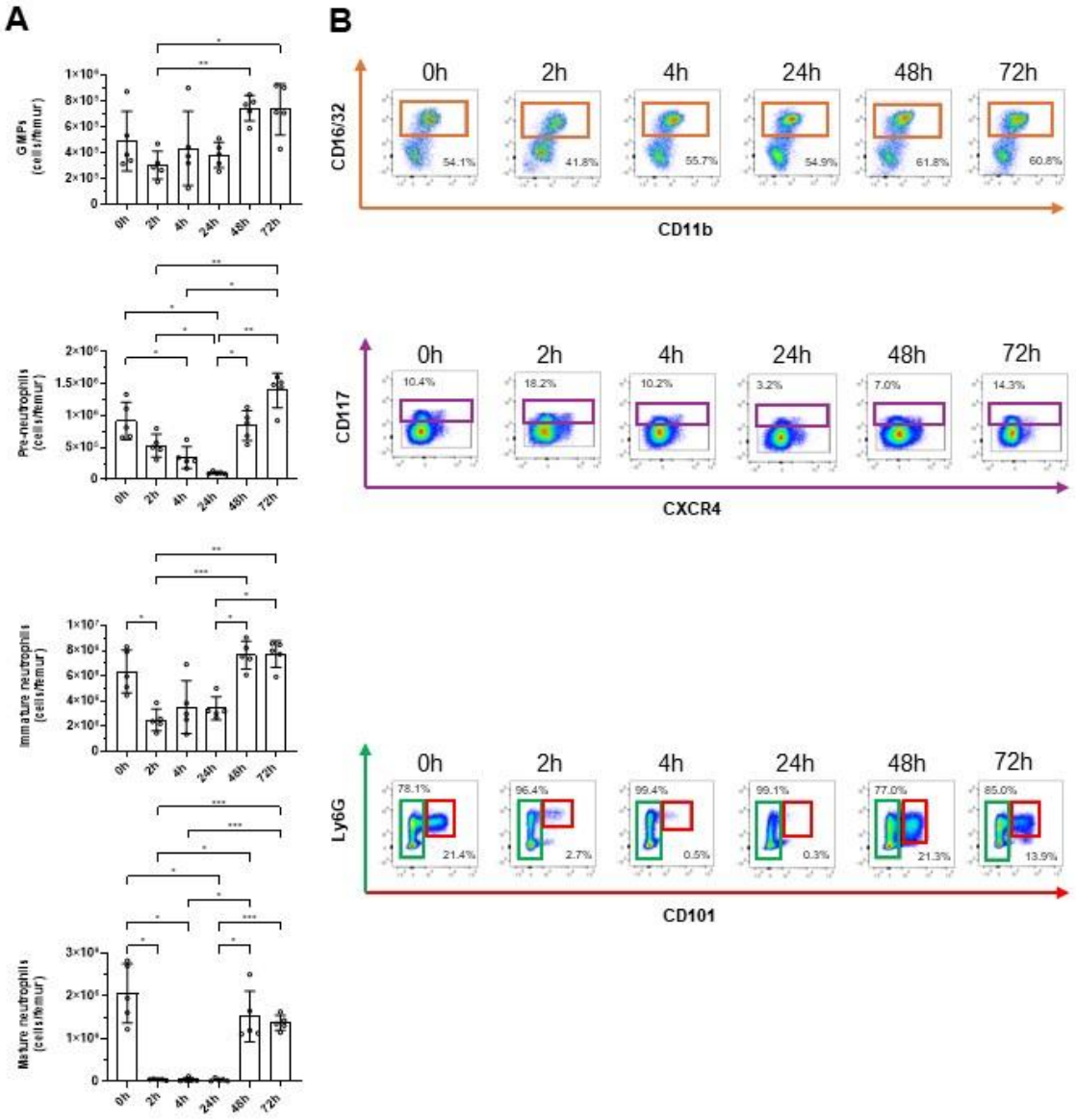

Figure 3.8. Temporal profiles of bone marrow neutrophils following UV-KEc-induced dermal inflammation in a non-resolving model of inflammation. Male C57BL/6J mice were anaesthetised and inoculated with 100 µL sterile saline containing 1.5 x 10^8 UV-KEc or no injection (naïve). The right femur was dissected and flushed with HBSS yielding a single-cell suspension at baseline (0h), 4h, 24h, 48h and 72h. The resulting single-cell suspension was stained for polychromatic flow cytometry and the number of bone marrow neutrophil subsets determined. Depicted are GMPs, pre-neutrophils, immature neutrophils and mature neutrophils at all time-points (A). Representative dot plots are also shown for each neutrophil subset (GMPs [orange], pre-neutrophils [purple], immature neutrophils [green] and mature neutrophils [red]) with relative percentages at each time-point (B). Data are presented as individual data points and mean with SD; $n = 5$. *$p < 0.05$, **$p < 0.01$, ***$p < 0.001$, ****$p < 0.0001$.

3.3.9 Bone marrow neutrophil subsets surface expression in a murine dermal model of non-resolving inflammation

Following the intradermal injection of UV-KEc, the phenotype of bone marrow neutrophil subsets was investigated, quantifying surface antigen expression by MFI. GMPs showed significantly reduced CD62L expression at 4h ($p < 0.001$) and steadily regained this to levels higher than baseline by 72h ($p < 0.001$) (**Figure 3.9A**). GMP CD16 expression fluctuated over time after an initial dip at 2h, before peaking at 4h ($p < 0.01$) and falling back to levels below baseline by 72h (**Figure 3.9B**). There was a marked peak in GMP CD11b expression at 2h ($p < 0.001$) before falling back to near baseline levels by 4h ($p < 0.01$) and increasing up to 72h ($p < 0.01$), above baseline levels (**Figure 3.9C**). Changes in pre-neutrophil CD62L expression were less marked with a slight decrease between 2h, 4h and 24h ($p < 0.05$) and a steady increase until 72h ($p < 0.05$) (**Figure 3.9D**). No significant changes were seen in pre-neutrophil CD16 expression until 24h, with expression highest at 48h and a significant decrease at 72h ($p < 0.01$), back to baseline levels (**Figure 3.9E**). Pre-neutrophil CD11b expression increased significantly at 2h ($p < 0.001$), decreasing back to near baseline levels at 4h ($p < 0.05$) with similar expression seen across the remaining time-points (**Figure 3.9F**). Immature neutrophil CD62L expression initially reduced between 0h and 24h, albeit not significantly, peaking at 48h before a significant drop at 72h ($p < 0.01$) (**Figure 3.9G**). CD16 expression on immature neutrophils dipped slightly at 2h ($p < 0.05$), rising steadily and peaking at 48h compared to baseline ($p < 0.001$) with a decline at 72h ($p < 0.01$), but not returning to baseline levels (**Figure 3.9H**). Immature neutrophil CD11b expression increased significantly at 2h ($p < 0.001$), decreasing at 4h ($p < 0.01$) with similar expression seen across the remaining time-points but not returning to baseline levels (**Figure 3.9I**). Mature neutrophil CD62L expression decreased at 2h, although not significant, and remained low until 48h where it increased significantly ($p < 0.05$) and remained at this level at 48h (**Figure 3.9J**). Overall, mature neutrophils had higher expression of CD62L at baseline compared to all other neutrophil subsets. Mature neutrophil CD16 expression decreased from 0h to 2h ($p < 0.01$), increasing significantly by 24h ($p < 0.01$) with levels maintained throughout the remaining time-points (**Figure 3.9K**). There was a significant increase in mature neutrophil CD11b expression at 2h ($p < 0.001$), gradually decreasing back

to near baseline levels by 48h and 72h. Overall, there was a marked increase in CD11b across all neutrophil subsets in response to UV-KEc with significantly higher CD11b expression in mature neutrophils at all time-points.

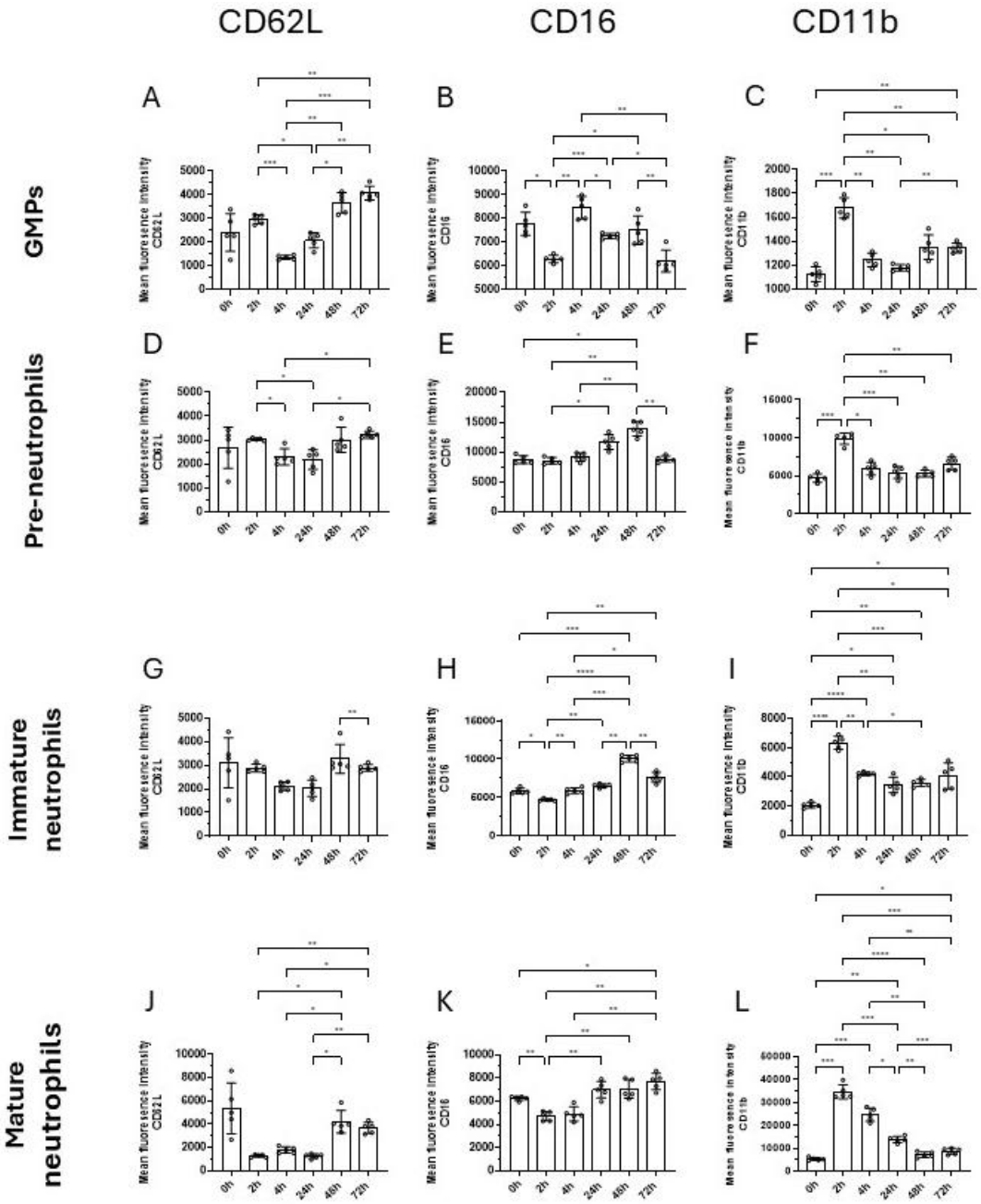

Figure 3.9. Bone marrow neutrophil subsets antigen expression following UV-KEc-induced dermal inflammation in a non-resolving model of inflammation. Male C57BL/6J mice were anaesthetised and inoculated with 100 µL sterile saline containing 1.5 x 10^8 UV-KEc or no injection (naïve). The right femur was dissected and flushed with HBSS yielding a single-cell suspension at baseline (0h), 4h, 24h, 48h and 72h. The resulting single-cell suspension was stained for polychromatic flow cytometry and surface antigen expression shown as MFI for CD62L, CD16 and CD11b. Depicted are GMPs (A-C), pre-neutrophils (D-F), immature neutrophils (G-I) and mature neutrophils (J-L) at all time-points. Data are presented as individual data points and mean with SD; $n = 5$. *$p < 0.05$, **$p < 0.01$, ***$p < 0.001$, ****$p < 0.0001$.

3.3.10 Temporal profiles of endocannabinoids extracted from UV-KEc-inflamed skin in a murine dermal model of non-resolving inflammation

At the time of developing the UV-KEc-triggered dermal inflammation model in mouse, I met with Dr Mireille Al Houayek (Université Catholique de Louvain, Belgium), who has a specialist interest in endocannabinoid lipid mediators. In addition to cellular trafficking, I wanted to investigate other possible mediators which may play a role in the resolution of inflammation which could give clues to the signalling pathways involved in maintaining remission in RA. Unfortunately, I did not have enough tissue from the punch biopsies acquired from the inflamed skin to perform standard lipidomic analysis alongside, although these techniques are well described in murine skin (265, 266). Endocannabinoids have wide-ranging biological activity and have been implicated in both the pathogenesis of RA and resolution of inflammation (70, 71). As such, in collaboration with Dr Al Houayek, I had the opportunity to determine whether endocannabinoids could be extracted from inflamed mouse skin using this model of inflammation and whether concentrations of these soluble lipid mediators change over time. Concentrations of key endocannabinoids, namely 2-AG, PEA, AEA and OEA, were determined from inflamed mouse skin and quantified by HPLC-MS.

Levels of 2-AG, PEA, AEA and OEA, were detectable by HPLC-MS. There were no significant differences between the UV-KEc and sham groups at baseline or 4h for any endocannabinoid assessed. Levels of 2-AG were significantly higher at 24h in animals

injected with UV-KEc ($p < 0.05$) (**Figure 3.10A**). There was a significantly lower concentration of PEA in the skin of animals injected with UV-KEc at 48h ($p < 0.01$) (**Figure 3.10B**). There were no significant differences in AEA or OEA concentration at any time-point (**Figure 3.10C-D**). Collectively, these data suggest a role for both 2-AG and PEA in the onset and/or resolution of murine dermal inflammation.

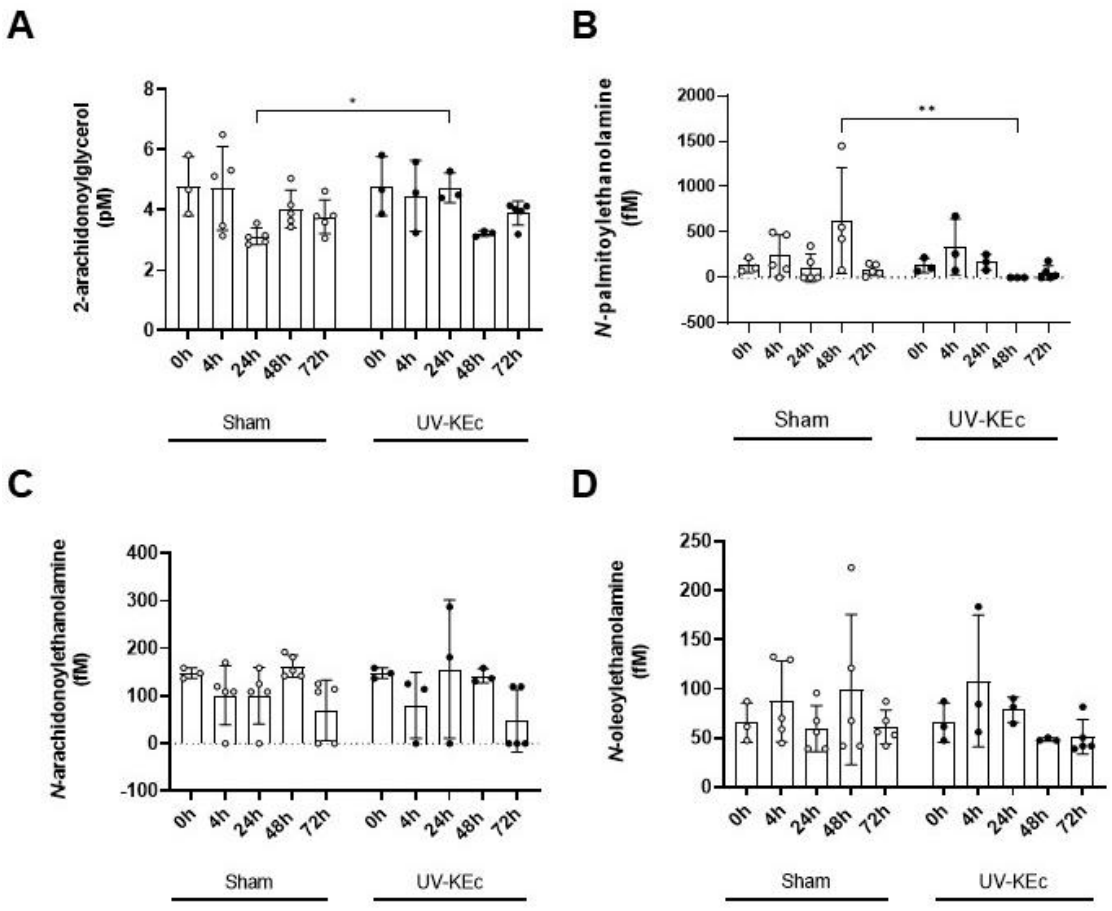

Figure 3.10. Temporal profiles of endocannabinoids extracted from UV-KEc-inflamed skin following UV-KEc-induced dermal inflammation in a non-resolving model of inflammation. Male C57BL/6J mice were anaesthetised and inoculated with 100 µL sterile saline containing 1.5 x 10^8 UV-KEc or 100 µL saline alone (sham). Endocannabinoids were extracted from skin biopsies and levels determined by HPLC-MS at baseline (0h), 4h, 24h, 48h and 72h. Depicted are (A) 2-arachidonoylglycerol (2-AG), (B) *N*-palmitoylethanolamine (PEA), (C) *N*-arachidonoylethanolamine (anandamide [AEA]) and (D) *N*-oleoylethanolamine (OEA). Data are presented as individual data points and mean with SD; $n = 5$. *$p < 0.05$, **$p < 0.01$, ***$p < 0.001$, ****$p < 0.0001$.

3.4 Summary of findings

The aim of this chapter was to determine the feasibility of UV-KEc-induced dermal inflammation as means to investigate the murine immune response.

To main conclusions of this chapter are:

- Injection of 1.5 x 10^8 UV-KEc into mouse skin causes a significant inflammatory response characterised by the influx of neutrophils, which is non-resolving at 72h.
- Following UV-KEc injection into the skin of mice there is a systemic inflammatory response detectable in circulating leucocytes.
- Marked changes are seen in bone marrow neutrophil subsets numbers and phenotype following intradermal injection of UV-KEc, with the emergency release of mature neutrophils in response to dermal inflammation as early as 2h, along with GMPs, pre-neutrophils and immature neutrophils, but to a lesser extent.
- Key endocannabinoids, namely 2-AG, PEA, AEA and OEA, are detectable in mouse skin and the concentrations of 2-AG and PEA are significantly affected by UV-KEc.

3.5 Discussion

In this chapter, I aimed to develop a murine model of dermal inflammation analogous to the human UV-KEc-triggered model previously described by the Gilroy group (252). I developed a novel model of non-resolving dermal inflammation using UV-KEc, characterised by the influx of neutrophils into the inflamed tissue that failed to clear by 72h, a time-point at which acute inflammation is expected to resolve (267). I was able to characterise immune cell profiles both at the site of inflammation and in circulation, focusing on monocyte subsets and bone marrow neutrophils, as well as determining key endocannabinoid concentrations in the skin.

3.5.1 High dose UV-KEc triggers a non-resolving model of murine dermal inflammation at 72h

Data from these experiments demonstrates that inflammation triggered by 1.5 x 10^8 UV-KEc peaks at 4h in blood and 72h in the inflamed skin, as evidenced by a significant increase in neutrophils at these times. In the blood, neutrophils numbers decreased by 72h, but not back to baseline, while in skin, inflammation was ongoing. There was also a corresponding increase in phagocytic mononuclear cells, also peaking at 72h in animals injected with UV-KEc. Whilst the inflammatory stimulus used here was the same as that used in human healthy volunteer study by Motwani *et al*. (2016), they described a resolving model as evidenced by the clearance of neutrophils by 72h (267). Thus, the murine model reported here may not have captured the pro-resolution and anti-inflammatory signals set out to investigate. As such, inflammation was ongoing and the 'off switch' signals may not have been activated. The paradigm for many years was that non-resolving inflammation was the result of excessive production of pro-inflammatory mediators such as IL-1β, IL-6, TNF-α, IL-8, IL-17, LTB_4, PGE_2, PGI_2 and complement C5a and C3b, but it is now clear that defective resolution can also contribute to this process, with insufficient anti-inflammatory/pro-resolution mediators also playing a key role (268). Therefore, it is likely that failed inflammatory resolution pathways may account for the data reported

here. This model of non-resolving inflammation in mouse skin provides a novel platform in which to investigate pro-resolution and anti-inflammatory signal which may be suppressed in the context of an overwhelming inflammatory stimulus.

3.5.2 UV-KEc dose selection

LPS is a surface component of Gram-negative bacteria, such as the UV-KEc used in this study, recognised by immune cells through TLR4 (269). LPS preferentially induces pro-inflammatory cytokines and IFN responses, causing a robust pro-inflammatory 'cytokine storm' and it now known that this is a dose-dependent phenomenon (270). This pro-inflammatory phase is later followed by a refractory period, with reduced cytokine expression likely due to the induction of a myriad of negative regulators, including IL-1 receptor-associated kinase (IRAK-M), phosphatidylinositol-3-kinase (PI3K), mitogen-activated protein kinase (MKP)-1 and suppressor of cytokine signalling (SOCS) (271). Additionally, it has been shown that innate leucocytes manifest dynamic and distinct inflammatory responses with rising doses of LPS and that they may utilise distinct intracellular signalling circuitries modulated by adaptor molecules such as Toll-interacting protein (Tollip), in both resolving and non-resolving inflammation (270). Tollip is known to regulate both the NF-κB and TLR-IL-1 pathways. At high-dose LPS, Tollip may serve as a negative regulator of the NF-κB pathway, facilitating the resolution of inflammation and clearance of cellular debris. Whilst TLR4 expression is significantly increased in patients with inflammatory bowel disease, Tollip expression is significantly decreased and *Tollip*$^{-/-}$ mice have been shown to be susceptible to colitis, suggesting a possible role in the pathogenesis of inflammatory diseases (272). Therefore, in the novel model of UV-KEc-triggered dermal inflammation reported here, UV-KEc surface LPS likely acts on immune cells through its interaction with TLR4, resulting in local inflammatory cytokine production and subsequent infiltration of neutrophils. However, it does not reach the refractory stage, likely due to the absence or insufficient levels of anti-inflammatory regulators such as IRAK-M, PI3K, MKP-1 and SOCS and low levels of Tollip with ongoing activation of the NF-κB pathway. The dose of LPS is therefore important in the balance between pro- and anti-inflammatory pathways

and the ongoing presence of neutrophils at the site of inflammation would suggest there had been failure of clearance of UV-KEc at 72h.

From a clinical perspective, TLRs and the NLRP3 inflammasome, needed for the release of pro-inflammatory IL-1β, have been implicated in the pathogenesis of RA using models of experimental arthritis, where the formation of arthritogenic immune complexes with ACPAs and citrullinated peptides have been shown to bind TLR4 (273). However, a recent trial using a humanised monoclonal antibody to block TLR4 in RA patients showed no significant differences for any efficacy endpoints in terms of composite disease activity scores (274). Thus, blocking the TLR4 pathway alone does not improve clinical disease parameters, and this process is more complex. Indeed, it is known that TLR4 alone is not sufficient for LPS recognition and that myeloid differentiation factor 2 (MD2) must have physical association to induce ligand activation (275). In addition, CD14 serves as a chaperone to recruit LPS to the TLR4-MD2 complex to facilitate micropinocytosis by mononuclear phagocytes (276) and CD11b may modulate LPS-induced signalling through both MyD88-dependent pathways (277). Therefore, it is likely that the ongoing presence of CD14 and CD11b-expressing mononuclear phagocytes seen at the site of inflammation at 72h may represent TLR4-independent signalling. Thus, this model and the modulation of UV-KEc dose (and therefore LPS) can be used to investigate the balance between pro-inflammatory and pro-resolution/anti-inflammatory signals and elucidate the role of LPS in the pathogenesis of RA.

3.5.3 Granuloma-like tissue formation following UV-KEc injection

The formation of granulomatous tissue was observed in all mice injected with high dose UV-KEc from 24h onwards at the site of the injection. Granulomas are organised aggregates of immune cells, predominantly comprised of mononuclear phagocytes, including infiltrating monocytes, dendritic cells and tissue-resident macrophages (278). Granulomas have evolved as a protective response to destroy or sequester particles but can also be pathological in the context of infection and inflammatory

disease (279). Granuloma formation is driven either by non-specific inflammation caused by trauma or foreign bodies or by reacting to a specific pathogen or antigen, such as LPS, although the underlying pathophysiology is poorly understood (280). Granulomas have previously been reported in murine models of inflammation using parasite egg antigen in immunosuppressed animals (both athymic and using immunosuppressive treatments such as cicosporin) (281, 282) and have therefore been felt to be a T cell-independent process, whilst NK cell activity has been proposed to suppress granuloma formation. Therefore, in this model of inflammation the granuloma likely formed as a consequence of high levels of UV-KEc and/or failed resolution of inflammation. This would suggest that the dose of 1.5 x 10^8 UV-KEc blocked resolution.

In this novel murine model of dermal inflammation, infiltrating T lymphocytes into the inflamed skin demonstrated a biphasic profile with an initial peak, peaking at 4h and 72h. NK cells were the only cell-type have low levels throughout the time-course, rising significantly at 72h. Granuloma-like tissue was first observed in the skin of animals injected with UV-KEc at 24h. Granulomatous colitis has been reported in both cats and dogs following exposure to *E. coli* (283, 284), although *E. coli*-induced granuloma formation has not been previously described in mouse skin. It has been suggested that IFN-γ-dependent activation of mononuclear cells steers their polarisation and promotes granuloma formation and that IFN-γ is involved in the initiation of cutaneous granuloma formation (278, 280). Given that IFN-γ is produced chiefly by NK cells, as well T cell subsets (278), the peak in NK cells and second peak in T cells at 72h in the inflamed skin may represent the source of IFN- γ, important for the maintenance of the granuloma and polarisation of infiltrating monocytes.

At the initial time of granuloma formation at 24h, neutrophil and monocyte ($Ly6C^{hi}$ and $Ly6C^{int}$, but not $Ly6C^{lo}$) numbers were significantly higher than sham control. Bettke *et al.* (2022) showed in a model of persistent *Salmonella typhi* infection that inflammatory $Ly6C^{hi}$ monocytes promote granuloma formation in a model of non-resolving salmonellosis, with depletion of these cells resulting in regression of established granulomas (285). Patients with the granulomatous disease, sarcoidosis,

have been shown to have increased numbers of inflammatory monocytes expressing high levels of TNF-α, IL-6 and upregulated TLR2 expression, with levels correlating with increased granuloma formation and progressive disease (286, 287). In a mouse model of *M. tuberculosis* infection, *TNF-α*$^{-/-}$ animals also showed markedly reduced granuloma formation (288). The major source of TNF-α is known to be mononuclear phagocytes, although T cells are also capable of producing substantial amounts of this cytokine. Furthermore, in a murine model of *Yersinia pseudotuberculosis* infection, mice lacking circulating inflammatory monocytes failed to form granulomas, demonstrated defective neutrophil activation and succumbed to *Y. pseudotuberculosis* infection (289). This process was also independent of dendritic cells. It has also been shown that in response to mycobacterial infection, monocyte progenitors and infiltrating monocytes give rise to multinucleated giant cells, a specialised macrophage found in granulomas (290). The neutrophil S100A9 protein has also been suggested to be important in the initial steps of granuloma formation and the ongoing recruitment of circulating neutrophils to the site of inflammation (291). Besides its function in facilitating transendothelial migration of neutrophils, S100A9 promotes the secretion of pro-inflammatory cytokines, establishing a niche for granuloma formation. S100A9 may also upregulate the production of mononuclear cell chemoattractants, activation of macrophages and assist their transformation into epithelial cells, resulting in the formation of an organised granuloma. Taken together, this would suggest the granuloma formation seen in this model involves a complicated interplay between different immune cell-types at different times, including neutrophils, monocytes, T cells and NK cells. It is possible that infiltrating T cells (and not NK cells) at 4h are a source of IFN-γ, activating infiltrating Ly6C^{hi} and Ly6C^{int} monocytes and neutrophils at 24h to initiate granuloma formation through production of pro-inflammatory cytokines including TNF-α. The peak of NK cells at 72h may represent either a secondary source of IFN-γ to maintain the granuloma or a compensatory mechanism to suppress it.

Overall, the granuloma formation seen in this model likely serves as a protective mechanism in response to failed/incomplete pathogen clearance, enabling the sequestration of UV-KEc, in attempt to facilitate the resolution of inflammation. From

a clinical point of view, the generation of granuloma-like tissue and profiling of immune cell trafficking described in this model, will allow its utilisation in the investigation of human granulomatous diseases, including rheumatoid nodules (seen in rheumatoid arthritis), granuloma annulare, necrobiosis lipoidica (seen in diabetic patients), interstitial granulomatous dermatitis, sarcoidosis, tuberculosis and leishmaniasis.

3.5.4 Neutrophils numbers and phenotypes following the intradermal injection of UV-KEc

Following the intradermal injection of 1.5 x 10^8 UV-KEc, all bone marrow neutrophil subsets reduced from 2h onwards. It is likely that given the substantial inflammatory insult from UV-KEc, that there was an emergency release of mature, immature and pre-neutrophil subsets. This suggests that in response to the significant ongoing inflammation, neutrophils still undergoing terminal maturation were released from the bone marrow to infiltrate into the site of inflammation. Therefore, the emergency release and granulopoiesis seen in response to the intradermal injection of 1.5 x 10^8 UV-KEc in this non-resolving model of inflammation, is a consequence of overwhelming numbers of bacteria and/or failed inflammatory resolution in the inflamed skin.

As neutrophils are the first circulating leucocyte to encounter pathogens, most studies have focused on investigating their role in innate immune responses, however, more recent studies have shown that these cells possess a greater functional diversity than previously thought. During steady state, most circulating neutrophils are mature neutrophils, also known as normal density neutrophils, owing to their density relative to the gradient medium Ficoll-Paque^{TM} used to isolate PBMCs (292–294). There is further diversity within neutrophils phenotypically, with circulating neutrophils expressing varying levels of CD177 for example, the neutrophil antigen that interacts with platelet endothelial cell adhesion molecule (PECAM)-1 (295). Around 25% of neutrophils express olfactomedin (OLFM)-4, which acts as an anti-apoptotic factor

and facilitates cell adhesion and is also found in NETs (296, 297). Others have described neutrophils as 'young' ($CXCR4^{lo}$, $CD62L^{hi}$) and 'aged' ($CXCR4^{hi}$, $CD62L^{lo}$) (297). 'Aged' neutrophils are functionally distinct from 'young' (naïve) neutrophils, with enhanced formation of NETs, ROS, vascular endothelial growth factors and metalloproteinases (MMP-9) (298). Additionally, they can be classified based on their expression of the T cell receptor αβ and hence their ability to interact with the adaptive immune response, as well as those which co-express $CXCR4^{+}$ and $CD49^{+}$ and those which express vascular endothelial growth factor receptor (VEGFR)-1, which are pro-angiogenic (299, 300). Given that I have shown a significant reduction in bone marrow $CXCR4^{+}$ neutrophils at 2h following UV-KEc injection, this represents the release of 'aged' or mature neutrophils, which correlates with a significant increase in circulating total neutrophils at 4h and subsequent infiltration into the inflamed skin by 24h. There was also a significant reduction in $CXCR4^{+}$ immature neutrophils in the bone marrow at 2h, who differ in phenotype from mature neutrophils by the absence of CD101 expression. In a murine model of lung inflammation, $CD101^{-}$ neutrophils have been shown to retain the ability to migrate to inflamed tissues and acquire a pro-inflammatory phenotype upon infiltration, whereas GMPs and pre-neutrophils do not (301). Overall, this would suggest that all neutrophil subsets contributed to the increase seen in total circulating neutrophils at 4h, whereas only immature and mature neutrophils contributed to the increasing total neutrophils seen in the inflamed skin at 24h.

It is known that under inflammatory conditions that immature neutrophils are released from the bone marrow following increasing levels of granulocyte-colony-stimulating factor (G-CSF) (302), which can carry out anti-microbial functions and suppress T cell proliferation through CD11b and ROS production (303). In a murine model of endotoxaemia, it was shown that there was a release of immature neutrophils from the bone marrow into the circulation with lower expression of CD16 compared to mature neutrophils (304). Functionally, these cells were less primed for ROS release and demonstrated fewer interactions with opsonised bacteria (304). Whilst I did not investigate the circulating neutrophil subsets in this model, there was a significant decrease in CD16 expression in bone marrow GMPs, immature and mature neutrophil

subsets at 2h, suggesting intrinsic low functionality and further exemplifying the emergency release of neutrophils in response to an overwhelming inflammatory insult. It is therefore possible that in characterising the phenotype of functionally deficient neutrophils using this model, that targets for treatment may be identified to modulate their expression and treat inflammation without the need for immunosuppression and the increased risk of infection associated.

When examining CD11b expression on bone marrow neutrophil subsets in this study by MFI, there was a marked increase in all subsets at 2h, remaining elevated throughout the time-course. Zhou *et al*. (2005) have shown that challenging neutrophils with LPS activates TLR4 and induces the *de novo* synthesis of CD11b on neutrophils *via* c-Jun NH_2-terminal kinase (JNK)/c-Jun/PU.1 and NF-κB pathways (305). This response did not occur in *TLR4*$^{-/-}$ neutrophils, suggesting that TLR4 may be capable of amplifying the response to LPS *via* upregulation of CD11b. Furthermore, they also showed that adhesion and transmigration of TLR4$^{-/-}$ neutrophils was markedly reduced. Thus, the significant increase in CD11b expression in bone marrow neutrophils at 2h represents a possible mechanism to enhance initial capture of neutrophils at the endothelium and subsequent transmigration into the inflamed site.

Neutrophils are a heterogenous cell-type, with each neutrophil subpopulation displaying unique phenotypic and functional properties (292). It has been shown that there is a strong correlation in neutrophil gene expression between mouse and human, suggesting transcriptional conservation in homeostasis and a shared core inflammation programme under inflammatory conditions (306). This includes genes encoding the IL-1 family members CD14, IL-4R, CD69 and PD-L1 with NF-κB and AP-1 complex being important drivers. It has also been shown that neutrophil activation by *E. coli*, type I or type III IFN and G-CSF results in upregulation of core inflammation genes (307). Given the significant homology between human and murine neutrophils, this novel model of inflammation can be used as an experimental tool to investigate neutrophil biology both in health and disease.

3.5.5 Intradermal injection of injection of 1.5 x 10^8 UV-KEc causes a significant expansion in Ly6C^{int} monocytes

In humans, intermediate and non-classical monocytes are known to arise from classical monocytes, with monocyte differentiation occurring exclusively in blood (244, 308). More recently, intermediate monocytes have also been characterised in mouse, and shown to possess many of the inflammatory characteristics of classical monocytes (309). Analogously, in mouse it has been shown that Ly6C^{lo} monocytes arise from Ly6C^{hi} monocytes both in bone marrow and the peripheral circulation using BrdU labelling (310). However, it is becoming increasingly clear that monocytes are more heterogenous than previously recognised. It is now understood that at least three distinct murine monocyte subpopulations exist (Ly6C^{hi}, Ly6C^{int} and Ly6C^{lo}) and the relative proportions of these subsets differ depending on host conditions (309). Following the intradermal injection of 1.5 x 10^8 UV-KEc, there was a significant expansion of the Ly6C^{int} monocyte subset population in both circulation and in the inflamed skin. However, it is not known whether the infiltrating Ly6C^{int} monocytes arise from the circulating Ly6C^{int} monocyte pool or whether they are due to conversion of infiltrating Ly6C^{hi} monocytes within the inflamed skin. This shift in monocyte differentiation towards Ly6C^{int} monocytes, analogous to that seen with neutrophils under inflammatory conditions, was observed from 24h onwards. These findings were similar to those reported following the experimental infection of mice with *Listeria monocytogenes* (311).

In humans, intermediate monocytes have high expression of HLA-DR and are capable of antigen presentation and subsequent T cell activation and proliferation (312, 313). They are also potent producers of TNF-α, IL-1β, IL-6 and ROS (314, 315). It has also been proposed that they have both pro- and anti-inflammatory properties as can also produce IL-10 and TGF-β (316). Importantly, intermediate monocytes are expanded in several diseases, including RA, and likely contribute to their pathogenesis (315). In RA, patients have higher circulating intermediate monocytes with increased numbers also found within synovial tissue (317). Intermediate monocytes have been shown to infiltrate into the synovium, differentiating into inflammatory macrophages, driving T cell activation, and into osteoclasts, leading to bone erosion and consequent joint

destruction characteristic of the RA (318). Activated intermediate monocytes upregulate CD14, CD16, HLA-DR, TLRs and integrin β1 and β2 expression and interact with myeloid and lymphoid cells in a positive loop manner, propagating the inflammatory process within the RA joint (315). Furthermore, higher proportions of intermediate monocytes to classical and non-classical monocytes in RA correlates with disease activity (319). In addition to RA, increased number of intermediate monocytes are seen in other autoimmune diseases including SLE (320), Crohn's disease (321), Graves' disease (322) and sarcoidosis (323) as well as in stroke (324) and atherosclerosis (325, 326). It is therefore likely that the significant expansion of intermediate monocytes seen in this non-resolving model of inflammation may be important to maintain ongoing inflammation likely due to the local production of TNF-α, IL-1β, IL-6 and ROS, as seen in diseases associated with increased levels of intermediate monocytes. Given that intermediate monocytes also have anti-inflammatory capacity, understanding the biological factors which control the switch from pro- to anti-inflammatory will be important in understanding the pathophysiology of these diseases. It has been previously suggested to classify murine monocyte subsets as either classical ($Ly6C^{hi}$) or non-classical ($Ly6C^{lo}$), as it is difficult to discriminate a true intermediate subset (327). However, the data reported here shows a clear phenotypically distinct population, which can be investigated using this model of non-resolving inflammation.

3.5.6 Effects of 1.5×10^8 UV-KEc on endocannabinoid concentrations

Following the intradermal injection of UV-KEc, levels of 2-AG in the inflamed skin were significantly higher compared to sham control at 24h. 2-AG is a signalling lipid that activates the cannabinoid CB_1 and CB_2 receptors, highly expressed on immune cells and is involved in a wide array of physiological functions and immune cell regulation (328). Navarini *et al.* (2022) have shown that plasma levels of 2-AG are increased in patients with SLE and correlates with disease activity and that 2-AG is able to modulate type 2 IFN production from $CD4^+$ T cells mediated through CB_2 activation (328). IFNs are known to underpin important immune responses against

viral infections and tumours, modulating adaptive immune pathways and thus playing a key role in the development of autoimmune disease (329). *In vitro* studies of the effect of synthetic cannabinoids CP55,940 and WIN55,212-2 on the synovial fibroblasts of RA patients showed a reduction in the production of pro-inflammatory cytokines and matrix metalloproteinases (330). Furthermore, both CB_1 and CB_2 have been shown to be present in the synovium of RA patients and 2-AG has been identified in the synovial fluid of these patients but not in healthy controls (331). In an experimental model of autoimmune encephalitis, animals treated with 2-AG demonstrated a polarisation in macrophages towards the anti-inflammatory 'M2' phenotype (332), suggesting a further possible role in the regulation of inflammation and a neuro-protective effect of 2-AG. Thus, having shown a significant increase in 2-AG at the inflamed site in this non-resolving model of inflammation, taken together with the anti-inflammatory role of 2-AG previously reported, elevated levels seen in SLE patients with high disease activity and in the synovium of RA patients, this suggests that 2-AG is involved in pro-resolution pathways. Given the overwhelming inflammatory stimulus with 1.5×10^8 UV-KEc, 2-AG was not able to overcome this to bring about inflammatory resolution.

In addition to the significant peak in 2-AG in UV-KEc-injected animals at 24h, there was a significant reduction in PEA levels in the UV-KEc group at 48h compared to sham, with almost undetectable levels seen at this time. PEA is a shorter, fully saturated analogue of AEA and is found in most mammalian tissues acting as an important analgesic, anti-inflammatory and neuroprotective mediator (333, 334). Impellizzeri *et al.* (2013) showed in a mouse model of collagen-induced arthritis that PEA was protective against the development of arthritis both in its anti-inflammatory capacity, inhibition of pro-inflammatory cytokines (IL-β, IL-6 and TNF-α) and chemokines (MCP-1, macrophage inflammatory protein [MIP]-Iα and MIP-2) but also protecting cartilage and bone damage, likely mediated through the reduced activation of mast cells (335). In other animal models, similar findings have been reported and have suggested that this process was mediated through decreased activation of the NF-κB system (336). Little research has been done investigating the role of PEA in human disease. One such study used PEA supplementation in non-hospitalised COVID-19-

infected patients and showed that this resulted in an anti-inflammatory effect, with reduced levels of P-selectin, IL-2 and IL-1β (337). However, they did not report clinical outcomes. Given P-selectins role in the initial attachment of platelets and endothelial cells to leucocytes and the rolling of immune cells towards inflamed tissue, this is clearly important in the propagation and amplification of the immune response. PEA has also been recently investigated in a double-blind randomised placebo-controlled study in patients with knee osteoarthritis and demonstrated significantly reduced pain and stiffness scores (338). Given the previously reported anti-inflammatory role of PEA and the significant decrease in PEA seen in the inflamed skin with levels almost undetectable at 48h and 72h, it is likely that the overwhelming inflammation triggered by the intradermal injection of 1.5 x 10^8 UV-KEc led to an exhaustion of the supply of PEA and that it too has a role in pro-resolution pathways, potentially acting by suppressing activation of the NF-κB pathway. However, the biological effect of PEA in this setting was not able to overcome the ongoing inflammation in this non-resolving model. Overall, these data suggest that both 2-AG and PEA play a role in the resolution of inflammation in this non-resolving model.

In this chapter, I have described a novel murine dermal model of non-resolving inflammation and shown it to be a viable tool to investigate inflammatory pathways. I have shown that the injection of 1.5 x 10^8 UV-KEc into mouse skin causes a significant inflammatory response characterised by the influx of neutrophils, which is non-resolving at 72h and led to the formation of granuloma-like tissue at the site of inflammation. This was accompanied by a systemic inflammatory response detectable in circulating leucocytes, including the expansion of a phenotypically distinct subset of intermediate monocytes and the emergency release of both mature and developmentally immature neutrophil subsets from the bone marrow. I have shown for the first time, that it is possible to extract and quantify key endocannabinoids from inflamed mouse skin and that both 2-AG and PEA may have a role in pro-resolution pathways. To further investigate anti-inflammatory/pro-resolution signals, I next aimed to develop a murine model of resolving dermal inflammation. The goal being to develop and characterise complementary, comparative models of non-resolving and

resolving inflammation to understand pro-resolution/anti-inflammatory signals which may be upregulated or suppressed during the different phases of inflammation.

4 Utilisation of a novel murine dermal model of inflammation to investigate the resolution of inflammation

4.1 Introduction

4.1.1 Utilising the dermal model of inflammation as a research tool

Having successfully developed a novel murine model of non-resolving inflammation, I wanted to develop a complementary model in which inflammation had resolved. The purpose of this being to understand cellular trafficking and signals involved in the resolution of inflammation and during the post-resolution phase, that might be important in maintaining disease remission in RA patients. To do so, a lower dose of UV-KEc (1.5×10^7/100 µL in 0.9% sodium chloride) was injected intradermally into the flanks of each animal, analogous to the forearm injections utilised in the resolving human blister model (252).

4.2 Hypothesis

By using a lower dose of UV-KEc as the inflammatory stimulus, I aimed to develop a model in which inflammation had entered the resolution phase, as previously described in humans (252). This gives rise to the hypothesis that: **intradermal injection of 1.5 x 10^7 UV-KEc in murine skin, results in a resolving inflammatory response, characterised by the influx of neutrophils and their clearance by 72h.**

To investigate the feasibility of this as a model of resolving inflammation, I developed five main aims:

1. Develop a resolving murine model of dermal inflammation triggered by the intradermal injection of 1.5 x 10^7 UV-KEc.
2. Characterise the inflammatory infiltrate in mouse skin using this model of inflammation.
3. Characterise the systemic immune response and changes in circulating blood leucocytes using this model.
4. Investigate circulating and bone marrow neutrophil subsets using this model to gain insight into the origins of infiltrating neutrophils at the site of UV-KEc-triggered inflammation.
5. Extract and quantify key endocannabinoid concentrations from inflamed skin and plasma during resolving inflammation.

4.3 Results

4.3.1 Intradermal injection with 1.5 x 10^7 UV-KEc is a resolving model of inflammation

Animals were weighed before UV-KEc injection and at each time-point after injection. Animals injected with UV-KEc began to lose weight at 4h post-injection and by 24h this had fallen significantly by a mean of 4.3% body mass ($p < 0.0001$) (**Figure 4.1A**). At 48h, mean mass began to recover and by 72h the mean mass was at near pre-injection levels. Intradermal injection of 1.5 x 10^7 UV-KEc resulted in acute inflammation in mouse skin, with total infiltrating $CD45^+$ immune cells beginning to rise at 4h and peaking at 24h ($p < 0.001$) (**Figure 4.1B**). Total $CD45^+$ cells then decreased at 48h, returning to baseline levels at 72h, suggesting resolution of inflammation. Macroscopically, there was no evidence of erythema or granuloma-like tissue formation using 1.5 x 10^7 UV-KEc, unlike that seen using the 1.5 x 10^8 UV-KEc dose in **Chapter 3**.

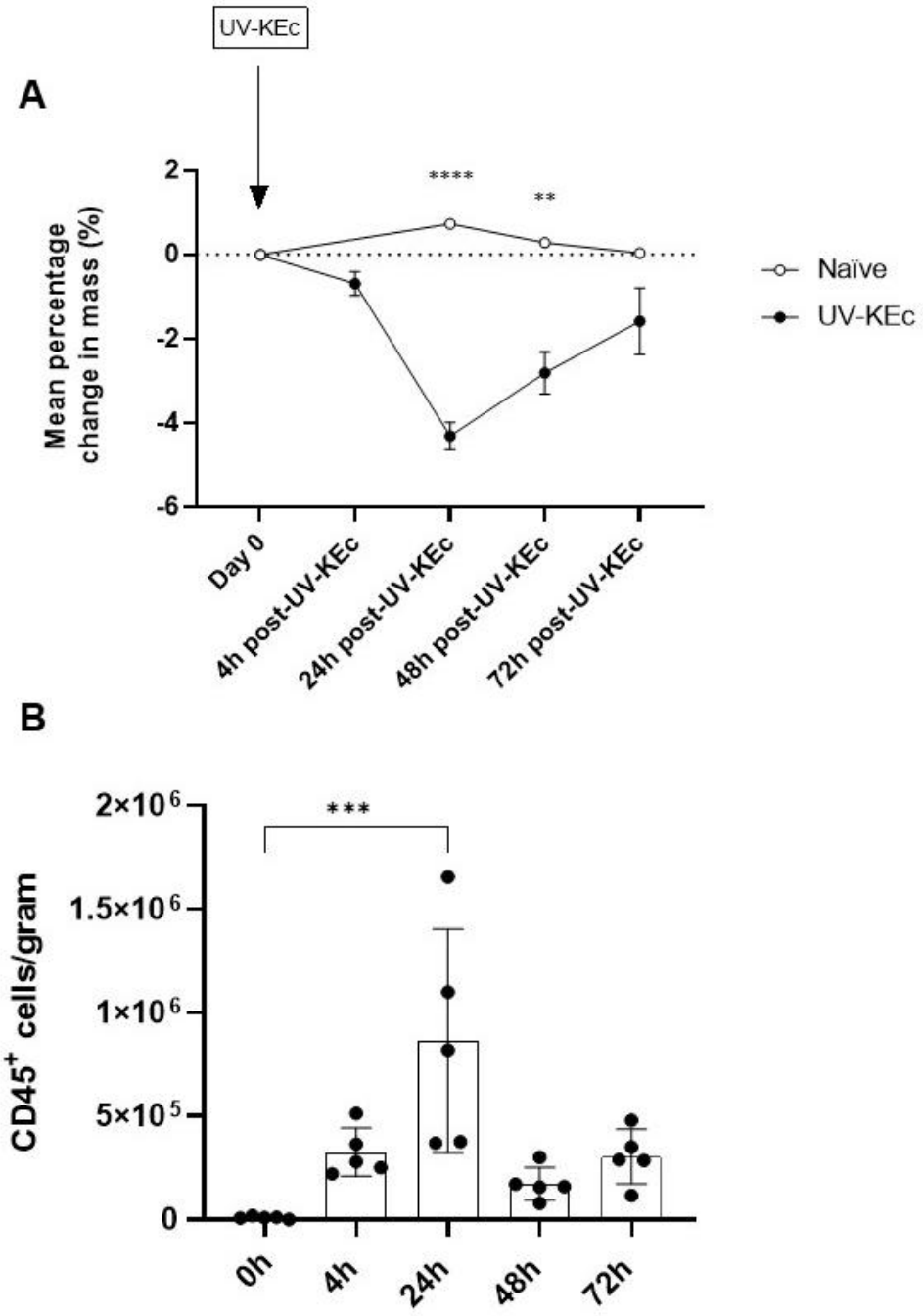

Figure 4.1. Intradermal injection with 1.5 x 10^7 UV-KEc is a model of resolving inflammation in murine skin. Male C57BL/6J mice were anaesthetised and injected with two intradermal injections of 100 µL sterile saline containing 1.5 x 10^7 UV-KEC or no injection. Animals were weighed (A) and skin was harvested and enzymatically digested at baseline (0h), 4h, 24h, 48h and 72h. The resulting single-cell suspension was stained for polychromatic flow cytometry and total number $CD45^+$ immune cells infiltrating into the skin over 72h was determined by flow cytometry (B). Data are individual data points and mean with SD; (A) $n = 5$. *$p < 0.05$, **$p < 0.01$, ***$p < 0.001$, ****$p < 0.0001$.

4.3.1 Temporal profiles of infiltrating cells in a murine dermal model of resolving inflammation

Following injection with UV-KEc, neutrophils were the first myeloid cell-type to rise significantly at 4h compared to naïve animals ($p < 0.01$) and peaked at 24h ($p < 0.001$) (**Figure 4.2A**). Neutrophil numbers then dropped at 48h, returning to baseline levels at 72h. Total monocyte numbers also began to increase at 4h in both groups, rising significantly at 24h ($p < 0.001$) before dropping at 48h, although not significant. Total monocytes returned to baseline levels by 72h ($p < 0.05$) (**Figure 4.2B**). Both conventional and plasmacytoid dendritic cells peaked at 24h in the inflamed skin ($p < 0.001$), then dropped at 48h and again at 72h, back to near baseline levels (**Figure 4.2C-D**). Macrophage numbers began to rise at 4h, peaking significantly at 24h ($p < 0.01$) decreasing steadily until 72h, although did not return to baseline numbers (**Figure 4.2E**). Langerhans cells peaked at 24h ($p < 0.001$), gradually declining until 72h, but not reaching baseline levels (**Figure 4.2F**). T cells showed a biphasic profile with numbers beginning to rise significantly at 24h ($p < 0.01$), with a slight dip at 48h before a further significant peak at 72h compared to baseline ($p < 0.001$) (**Figure 4.2G**). B cell numbers began to rise significantly at 48h ($p < 0.01$), with a further drop at 72h, although levels remained significantly higher compared to baseline at this time ($p < 0.05$) (**Figure 4.2H**). NK cells numbers increased significantly at 24h ($p < 0.001$), decreasing again at 48h and further still at 72h to levels like that at 4h (**Figure 4.2I**). Eosinophils began to increase at 4h with a significant peak at 24h, then dropping at 48h to levels like those at 4h and this was maintained at 72h. Collectively, these data suggest that the onset of inflammation in the skin using this model is at 4h, with most cell-types peaking in number at 24h and returning to basal levels by 72h. As infiltrating neutrophils had been cleared from the site of inflammation at 72h, this would suggest that inflammation had resolved in the mouse skin by the end of the time-course.

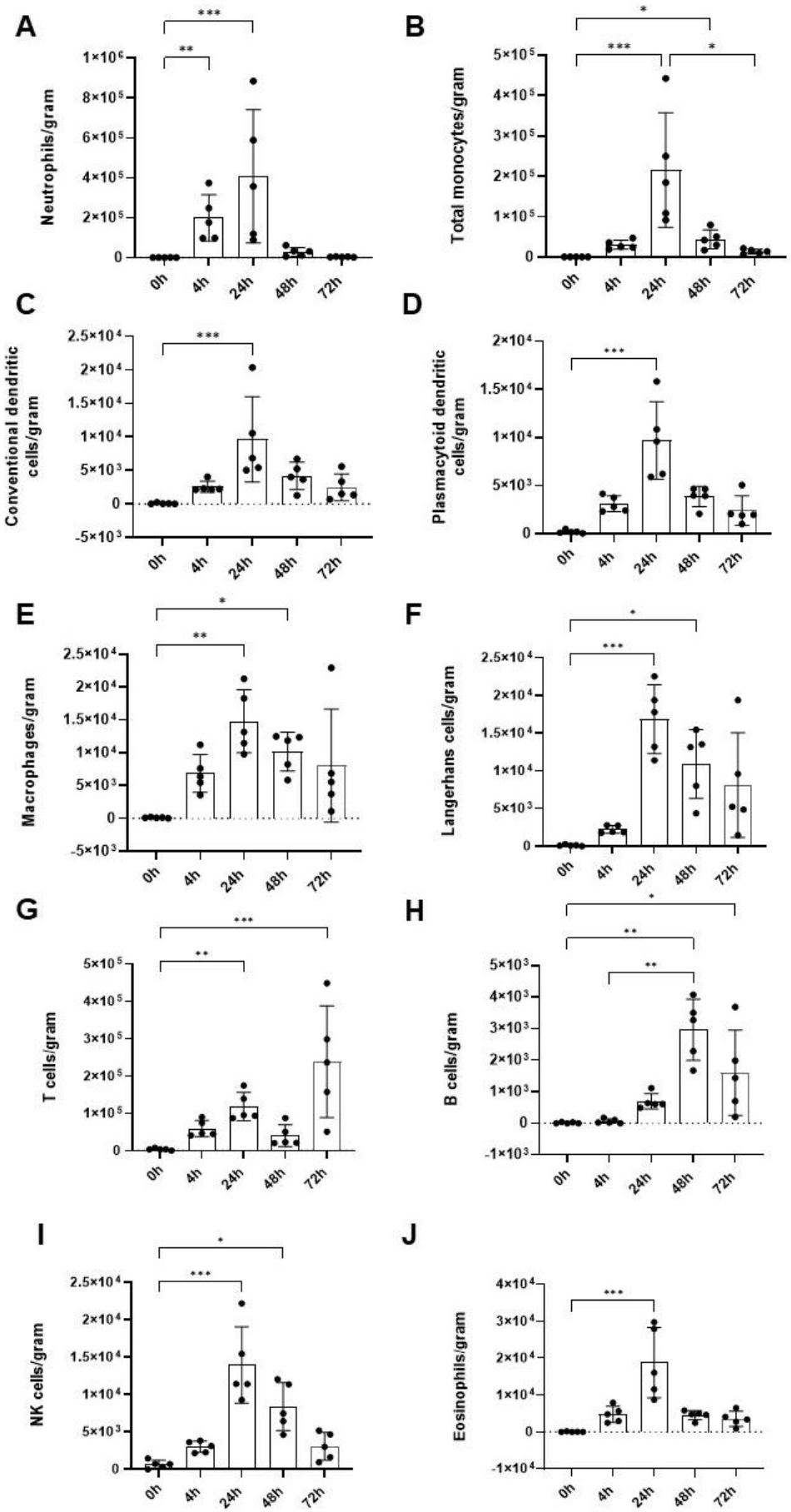
A
Neutrophils/gram
1×10⁶
8×10⁵
6×10⁵
4×10⁵
2×10⁵
0
***
**
0h
4h
24h
48h
72h
B
Total monocytes/gram
5×10⁵
4×10⁵
3×10⁵
2×10⁵
1×10⁵
0
*
***
*
C
Conventional dendritic cells/gram
2.5×10⁴
2×10⁴
1.5×10⁴
1×10⁴
5×10³
0
-5×10³
D
Plasmacytoid dendritic cells/gram
2×10⁴
1.5×10⁴
1×10⁴
5×10³
0
E
Macrophages/gram
F
Langerhans cells/gram
G
T cells/gram
5×10⁵
4×10⁵
3×10⁵
2×10⁵
1×10⁵
0
H
B cells/gram
5×10³
4×10³
3×10³
2×10³
1×10³
0
-1×10³
I
NK cells/gram
J
Eosinophils/gram
4×10⁴
3×10⁴
2×10⁴
1×10⁴
0
-1×10⁴

Figure 4.2. Temporal profile of infiltrating immune cells into the skin following UV-KEc-induced resolving dermal inflammation. Male C57BL/6J mice were anaesthetised and injected with two intradermal injections of 100 µL sterile saline containing 1.5 x 10^7 UV-KEc or no injection. Skin was harvested and enzymatically digested at baseline (0h), 4h, 24h, 48h and 72h. The resulting single-cell suspension was stained for polychromatic flow cytometry. Depicted are (A) neutrophils, (B) total monocytes, (C) conventional dendritic cells, (D) plasmacytoid dendritic cells, (E) macrophages, (F) Langerhans cells, (G) T cells, (H) B cells, (I) NK cells and (J) eosinophils. Data are presented as individual data points and mean with SD; $n = 5$. *$p < 0.05$, **$p < 0.01$, ***$p < 0.001$, ****$p < 0.0001$.

4.3.1 Temporal profiles and proportions of infiltrating monocyte subsets in a murine dermal model of resolving inflammation

To investigate how this model of inflammation affects the proportions of the different subsets of infiltrating monocytes, polychromatic flow cytometry was used to identify Ly6C^{hi}, Ly6C^{int} and Ly6C^{lo} monocytes (**Figure 4.3**). In the inflamed mouse skin, Ly6C^{hi} monocyte infiltration began to rise significantly at 4h ($p < 0.05$), peaking at 24h compared to baseline ($p < 0.001$) (**Figure 4.3A**). Ly6C^{hi} monocyte then dropped significantly at 48h, with a further significant reduction between 24h and 72h ($p < 0.05$). Ly6C^{int} monocyte numbers increased significantly at 24h ($p < 0.01$) with levels maintained at 48h before a reduction at 72h, although not significant (**Figure 4.3B**). Ly6C^{lo} monocyte infiltration began to rise at 24h ($p < 0.001$), falling at 48h, but still significantly higher than baseline ($p < 0.05$) and a further decrease at 72h, although not back to baseline levels (**Figure 4.3C**). **Figure 4.3D** shows the relative proportions of the three monocyte subsets defined by their expression of Ly6C. Ly6C^{hi} monocytes are the predominant cell-type in steady state and at both 4h and 24h following UV-KEc injection. At both 48h and 72h, Ly6C^{int} monocytes were the predominant subset in the inflamed skin. Ly6C^{lo} monocytes were the fewest cell-type at all time-points and whilst numbers were relatively low compared to the other subsets, the proportion of Ly6C^{lo} monocytes increased from 0.64% at baseline to 3.5% at 72h; an 18-fold increase (**Figure 4.3D**).

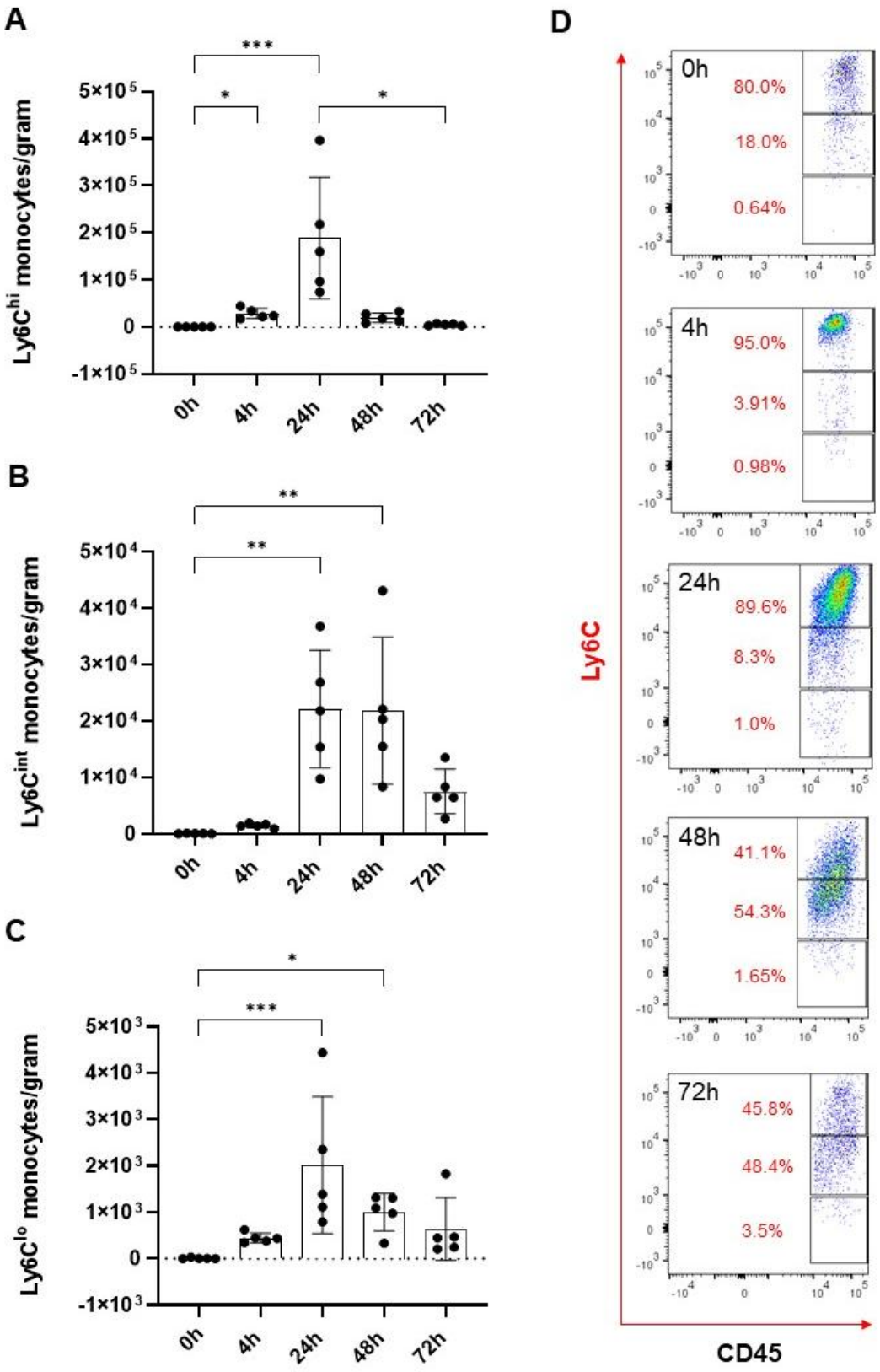
A
Ly6C^hi monocytes/gram
5×10^5
4×10^5
3×10^5
2×10^5
1×10^5
0
-1×10^5
***
*
*
0h
4h
24h
48h
72h
B
Ly6C^int monocytes/gram
5×10^4
4×10^4
3×10^4
2×10^4
1×10^4
0
**
**
0h
4h
24h
48h
72h
C
Ly6C^lo monocytes/gram
5×10^3
4×10^3
3×10^3
2×10^3
1×10^3
0
-1×10^3
*
***
0h
4h
24h
48h
72h
D
Ly6C
CD45
0h
80.0%
18.0%
0.64%
4h
95.0%
3.91%
0.98%
24h
89.6%
8.3%
1.0%
48h
41.1%
54.3%
1.65%
72h
45.8%
48.4%
3.5%

Figure 4.3. Temporal profile of infiltrating monocyte subsets into the skin following UV-KEc-induced resolving dermal inflammation. Male C57BL/6J mice were anaesthetised and inoculated with two intradermal injections of 100 µL sterile saline containing 1.5 x 10^7 UV-KEc. Skin was harvested and enzymatically digested at baseline (0h), 4h, 24h, 48h and 72h. The resulting single-cell suspension was stained for polychromatic flow cytometry. Depicted are (A) Ly6C^{hi} monocytes numbers, (B) Ly6C^{int} monocyte numbers and (C) Ly6C^{lo} monocyte numbers Representative dot plots are also shown at all time-points depicting the relative proportions of Ly6C^{hi} (top box), Ly6C^{int} (middle box) and Ly6C^{lo} (bottom box) monocytes of total monocytes (D). Data are presented as individual data points and mean with SD; $n = 5$. *$p < 0.05$, **$p < 0.01$, ***$p < 0.001$, ****$p < 0.0001$.

4.3.2 Defining resolution indices using a UV-KEc-triggered murine dermal model of acute, resolving inflammation

To define the resolution phase of inflammation and its components, I analysed the interplay between neutrophil and mononuclear cell infiltration and clearance at the site of UV-KEc-triggered inflammation. Neutrophil and mononuclear cell numbers are shown in **Figure 4.4A**. Neutrophils, the first effector leucocytes, peaked at 24h, followed by mononuclear cells. Combining the sum of all infiltrating mononuclear cells, namely circulating monocytes, dendritic cells, and macrophages, resolution can be defined in quantitative terms as the relative proportions of these two cell-types across the 72h time-course. Resolution indices have previously been described by Bannenberg *et al.* (2005) and have been applied to this model for quantitative asessment of inflammatory resolution following UV-KEc injection (44). Between 24h (T_{max}) and 36.9h (T_{50}), total neutrophil numbers decreased from 2.04 x 10^5 (Ψ_{max}) to 1.02 x 10^5 (R_{50}), representing a 50% reduction in neutrophil numbers. Mononuclear cells also peaked at 24h, but to a lesser extent. The R_i, or period of neutrophilic loss, is therefore 24-36.9h using this model of resolving inflammation. At 42.3h, the number of neutrophils equalled the infiltrating mononuclear cell numbers, representing the intersection point, or $I_{PMN=mono}$. Between 24h and 72h after the onset of inflammation (T_0), neutrophil numbers gradually decreased, followed by mononuclear cells, but at a slower rate and not returning to pre-UV-KEc injection levels. Thus, this model can be used in cojunction with these resolution indices, to provide operative and unbiased assessments of resolution and can be used to evaluate

the anti-inflamamtory/pro-resolving pathways in RA patients, which may be important in maintaining disease remission.

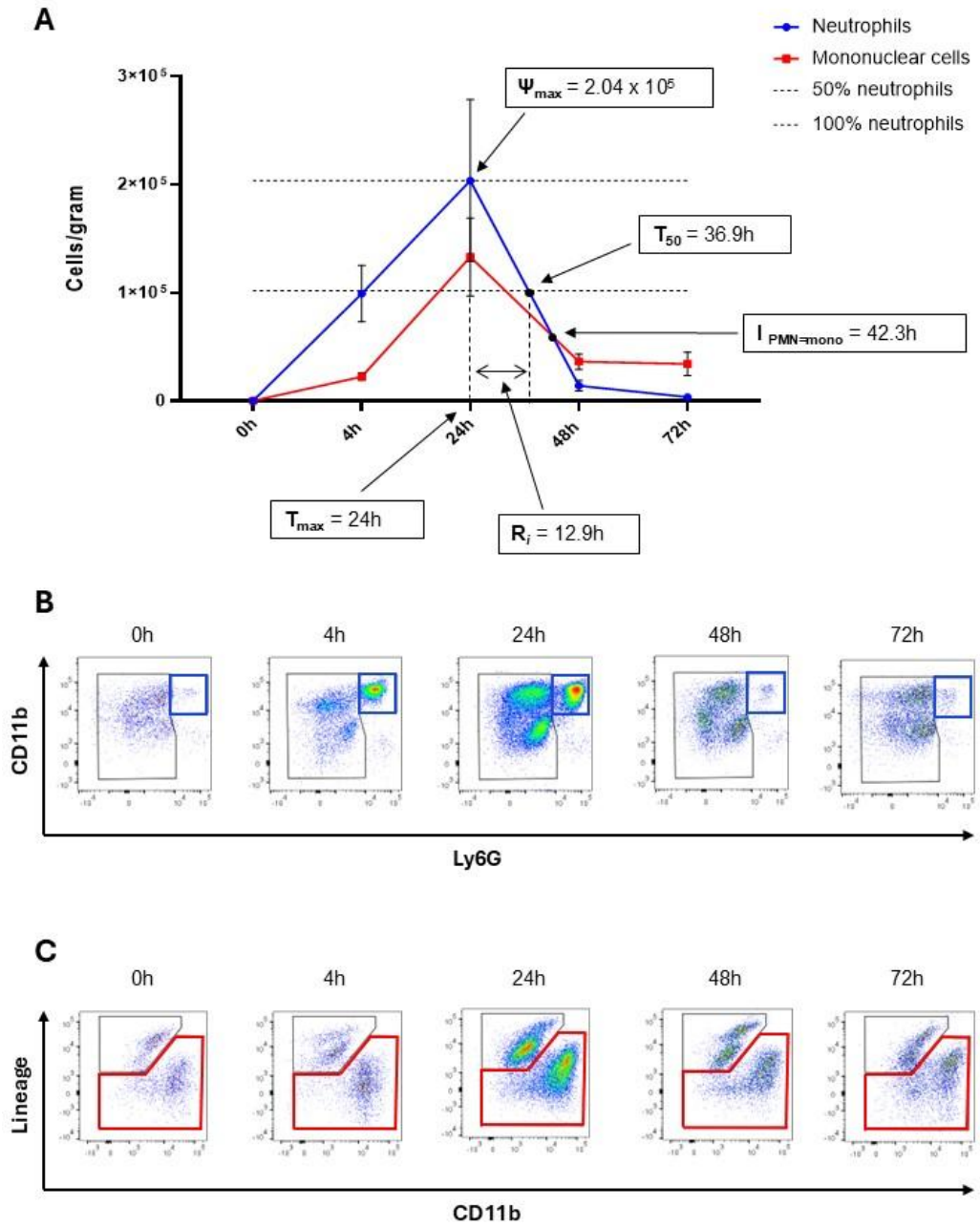

Figure 4.4. Dermal neutrophil and mononuclear cell composition following UV-KEc injection: Resolution indices. Male C57BL/6J mice were anaesthetised and inoculated with two intradermal injections of 100 µL sterile saline containing 1.5 x 10^7 UV-KEc. Skin was harvested and enzymatically digested at baseline (0h), 4h, 24h, 48h and 72h. The resulting single-cell suspension was stained for polychromatic flow cytometry. (A) Depicted is a time-line showing the resolution of acute inflammation and was defined in operative and quantitative terms using the following resolution indices: 1) magnitude (Ψ_{max}, T_{max}), the time-point (T_{max}) when neutrophil (PMN) numbers are maximum (Ψ_{max}); 2) duration (T_{50}), the time-point when neutrophil numbers reduce to 50% (R_{50}) of Ψ_{max}; 3) R*i*, the time interval from maximum neutrophil numbers (Ψ_{max}) to the 50% reduction point (T_{50}) (i.e., $T_{50} - T_{max}$) and 4) point of intersection ($I_{PMN=mono}$), the time-point when the increase in mononuclear cells intersects the decrease in neutrophils (i.e., neutrophil numbers = mononuclear cell numbers). (B) Representative dot plots of infiltrating neutrophils (B) ($Ly6G^{hi}$; blue box) and total mononuclear cell numbers (C) (Lin^-, $Ly6G^{lo}$, red box) are also shown throughout the time-course. Data are presented as individual data points and mean with SD; $n = 5$. *$p < 0.05$, **$p < 0.01$, ***$p < 0.001$, ****$p < 0.0001$.

4.3.1 Temporal profiles of circulating immune cells in a murine dermal model of resolving inflammation

In blood, neutrophils peaked at 4h before gradually decreasing up to 48h ($p < 0.05$), with numbers of neutrophils similar at 48h and 72h (**Figure 4.5A**). Total monocyte numbers followed a similar pattern but peaked significantly at 4h ($p < 0.05$), before decreasing at 24h and back to baseline levels by 48h ($p < 0.05$) (**Figure 4.5B**). Conventional dendritic cells increased in number at 4h and peaked at 24h, before significantly decreasing at 48h ($p < 0.001$) with levels maintained at 72h (**Figure 4.5C**). Plasmacytoid dendritic cell numbers initially dipped at 4h, before rising significantly at 24h ($p < 0.01$), then gradually decreasing back to baseline levels at 72h (**Figure 4.5D**). Unsurprisingly, both macrophages and Langerhans cells were relatively fewer in number in circulation compared to other cell-types and both peaked significantly at 24h ($p < 0.01$), before rapidly falling back to baseline levels at 48h (**Figure 4.5E-F**). T cell numbers dropped significantly at 4h, with no further significant differences seen during throughout the time-course (**Figure 4.5G**). There was a marked decrease in B cell numbers at 4h ($p < 0.001$) and numbers recovered by 48h ($p < 0.05$) before dipping again at 72h, although not significant (**Figure 4.5H**). NK cell numbers began to increase at 4h with similar levels seen at 48h, before

dropping significantly back to baseline levels at 72h ($p < 0.05$) (**Figure 4.5I**). Eosinophil numbers were relatively few in the blood, dropping initially at 4h ($p < 0.05$) with a marked increase between 4h and 72h; the only cell-type to do so ($p < 0.001$) (**Figure 4.5J**). Collectively, these data suggest that the onset of systemic inflammation in blood using this model is at 4h, as seen in the blood using the higher 1.5 x 10^8 UV-KEc dose. When investigating blood, inflammation has entered the resolution phase by 72h, with all cell-types except for eosinophils returning to baseline levels.

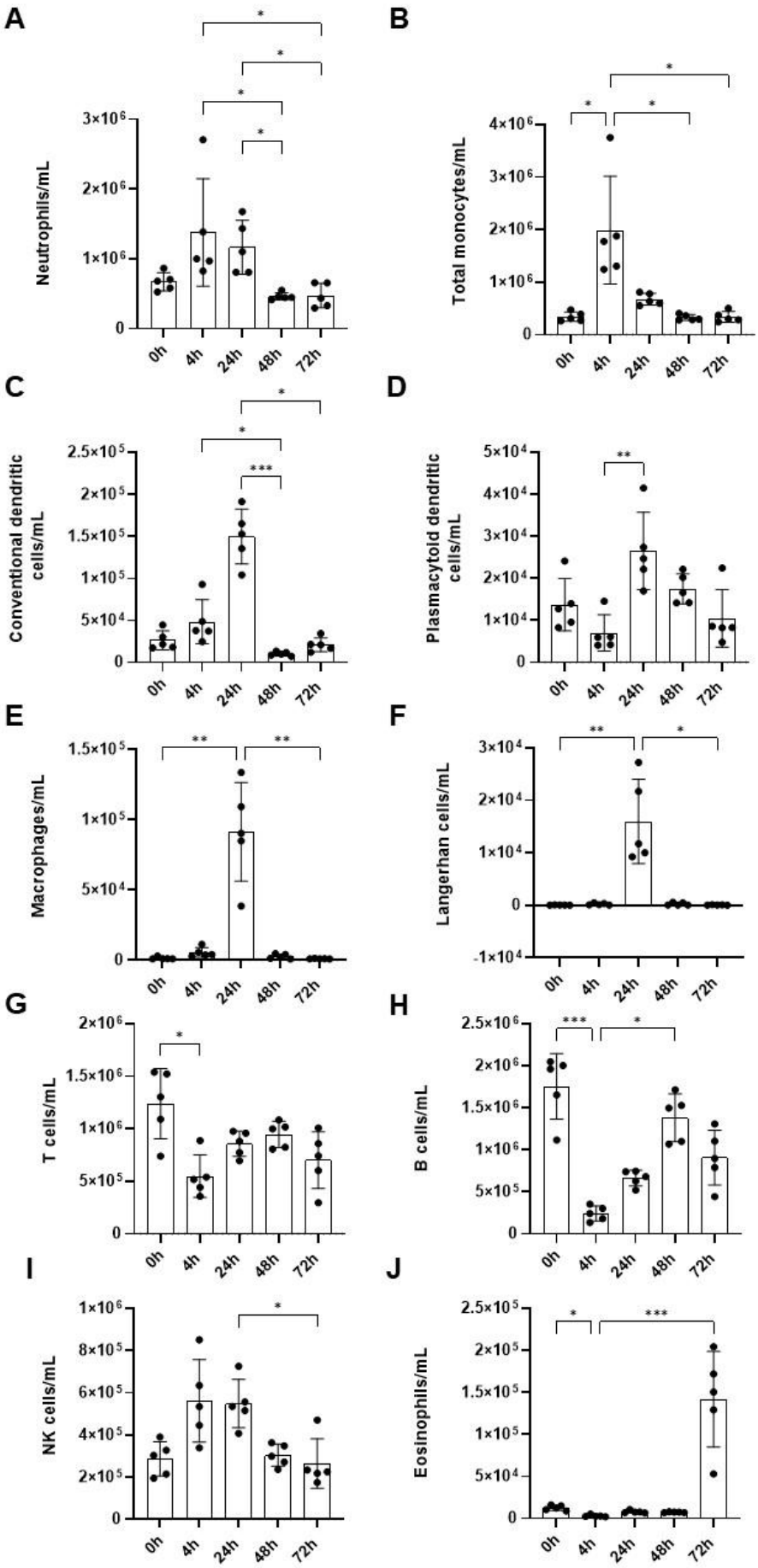
A
Neutrophils/mL
3×10^6
2×10^6
1×10^6
0
0h
4h
24h
48h
72h
B
Total monocytes/mL
4×10^6
3×10^6
2×10^6
1×10^6
0
C
Conventional dendritic cells/mL
2.5×10^5
2×10^5
1.5×10^5
1×10^5
5×10^4
0
D
Plasmacytoid dendritic cells/mL
5×10^4
4×10^4
3×10^4
2×10^4
1×10^4
0
E
Macrophages/mL
1.5×10^5
1×10^5
5×10^4
0
F
Langerhan cells/mL
3×10^4
2×10^4
1×10^4
0
-1×10^4
G
T cells/mL
2×10^6
1.5×10^6
1×10^6
5×10^5
0
H
B cells/mL
2.5×10^6
2×10^6
1.5×10^6
1×10^6
5×10^5
0
I
NK cells/mL
1×10^6
8×10^5
6×10^5
4×10^5
2×10^5
0
J
Eosinophils/mL
2.5×10^5
2×10^5
1.5×10^5
1×10^5
5×10^4
0

Figure 4.5. Temporal profile of circulating blood leucocytes following UV-KEc-induced resolving dermal inflammation. Male C57BL/6J mice were anaesthetised and inoculated with two intradermal injections of 100 µL sterile saline containing 1.5 x 10^7 UV-KEC. Immune leucocytes were isolated using ACK lysing buffer at baseline (0h), 4h, 24h, 48h and 72h with naïve controls. The resulting single-cell suspension was stained for polychromatic flow cytometry. Depicted are (A) neutrophils, (B) total monocytes, (C) conventional dendritic cells, (D) plasmacytoid dendritic cells, (E) macrophages, (F) Langerhans cells, (G) T cells, (H) B cells, (I) NK cells and (J) eosinophils. Data are presented as individual data points and mean with SD; $n = 5$. *$p < 0.05$, **$p < 0.01$, ***$p < 0.001$, ****$p < 0.0001$.

4.3.1 Temporal profiles and proportions of circulating monocyte subsets in a murine dermal model of resolving inflammation

To investigate how this model of inflammation affects the proportions of the different subsets of monocytes in systemic circulation, polychromatic flow cytometry was used to identify Ly6C^{hi}, Ly6C^{int} and Ly6C^{lo} monocytes. In blood, Ly6C^{hi} monocyte numbers peaked at 4h, decreasing significantly by 48h ($p < 0.001$) and returning to baseline levels by 72h (**Figure 4.6A**). Circulating Ly6C^{int} monocyte numbers rose significantly at 24h ($p < 0.05$), decreasing back to baseline levels by 72h ($p < 0.05$) (**Figure 4.6B**). Ly6C^{lo} monocyte numbers peaked at 24h and did not return to baseline levels by 72h, with no significant differences seen at any time-point (**Figure 4.6C**). The relative proportion of Ly6C^{hi} monocytes was greatest at 4h (87.6%) and there was a marked expansion seen in the Ly6C^{int} population at 24h and 48h and of Ly6C^{lo} monocytes at 24h, 24h and 72h (**Figure 4.6D**).

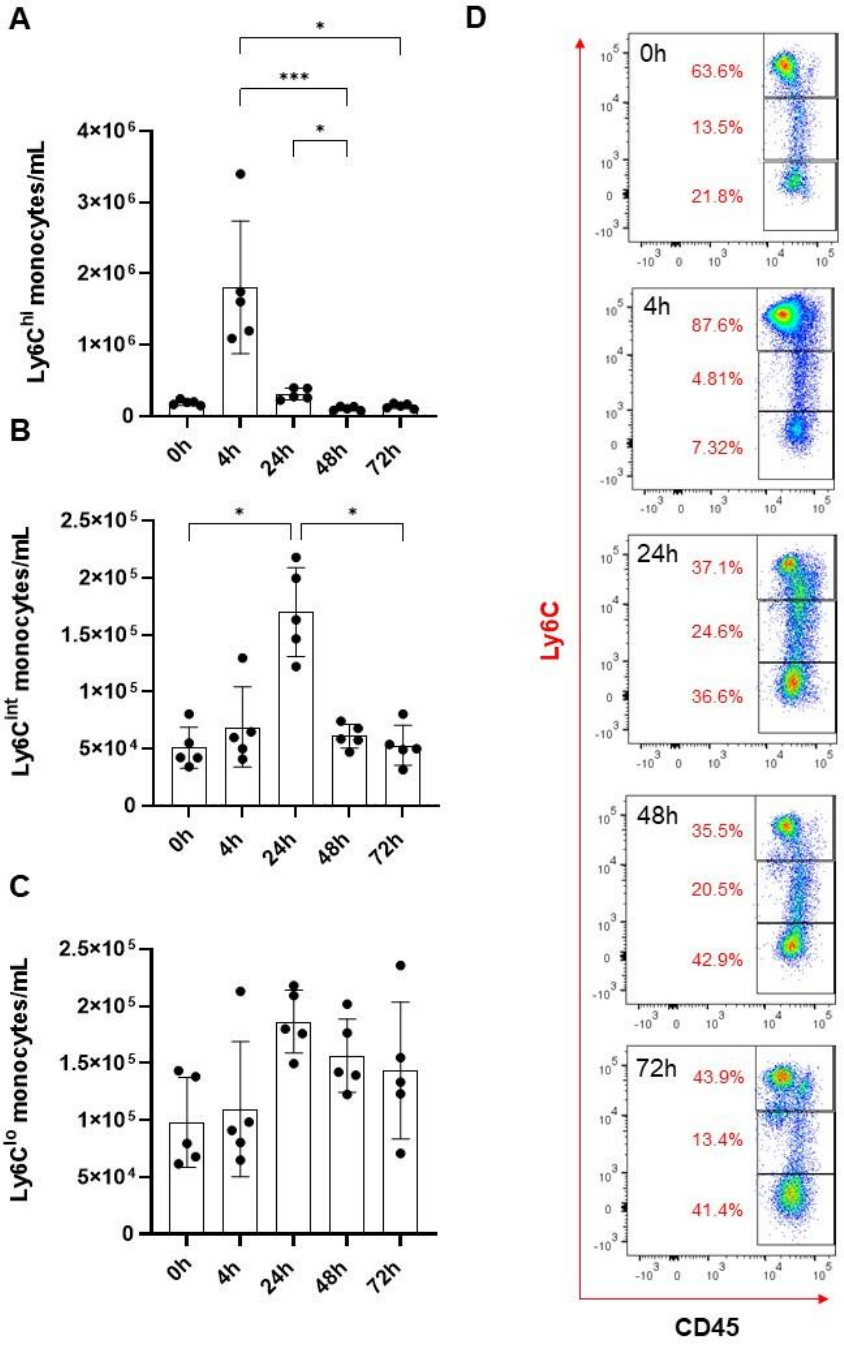

Figure 4.6. Temporal profile of circulating monocyte following UV-KEc-induced resolving dermal inflammation. Male C57BL/6J mice were anaesthetised and inoculated with two intradermal injections of 100 µL sterile saline containing 1.5 x 10^7 UV-KEc or no injection. Immune leucocytes were isolated using ACK lysing buffer at baseline (0h), 4h, 24h, 48h and 72h. The resulting single-cell suspension was stained for polychromatic flow cytometry. Depicted are (A) Ly6C^{hi} monocytes numbers, (B) Ly6C^{int} monocyte numbers and (C) Ly6C^{lo} monocyte numbers Representative dot plots are also shown at all time-points depicting the relative proportions of Ly6C^{hi} (top box), Ly6C^{int} (middle box) and Ly6C^{lo} monocytes of total monocytes (D). Data are presented as individual data points and mean with SD; $n = 5$. *$p < 0.05$, **$p < 0.01$, ***$p < 0.001$, ****$p < 0.0001$.

4.3.1 Temporal profiles and proportions of neutrophil subsets in a murine dermal model of resolving inflammation

4.3.1.1 Circulating neutrophil subsets

In addition to bone marrow neutrophil subsets, I wanted to investigate the circulating subsets so therefore analysed paired peripheral blood and bone marrow in this resolving model of inflammation to identify GMPs, pre-neutrophils, immature neutrophils and mature neutrophils. Following the intradermal injection of 1.5×10^7 UV-KEc, blood GMP numbers showed a biphasic profile, peaking at 2h with a second peak at 24h and decreasing below baseline levels at 48h ($p < 0.01$), although circulating GMP numbers were relatively fewer throughout the 72h time-course (**Figure 4.7A**). Pre-neutrophils numbers increased at 2h, peaking at 4h and decreased significantly between 4h and 24h ($p < 0.05$) (**Figure 4.7B**). Immature neutrophil numbers peaked at 4h, dropping significantly at 48h ($p < 0.05$), but did not return to baseline levels by 72h (**Figure 4.7C**). Mature neutrophil numbers peaked at 2h with a marked decrease seen at 24h ($p < 0.01$), coinciding with the maximal time of infiltration seen in the inflamed skin (**Figure 4.7D**). Mature neutrophil numbers recovered to near baseline levels at 48h, with a second decrease in numbers at 72h.

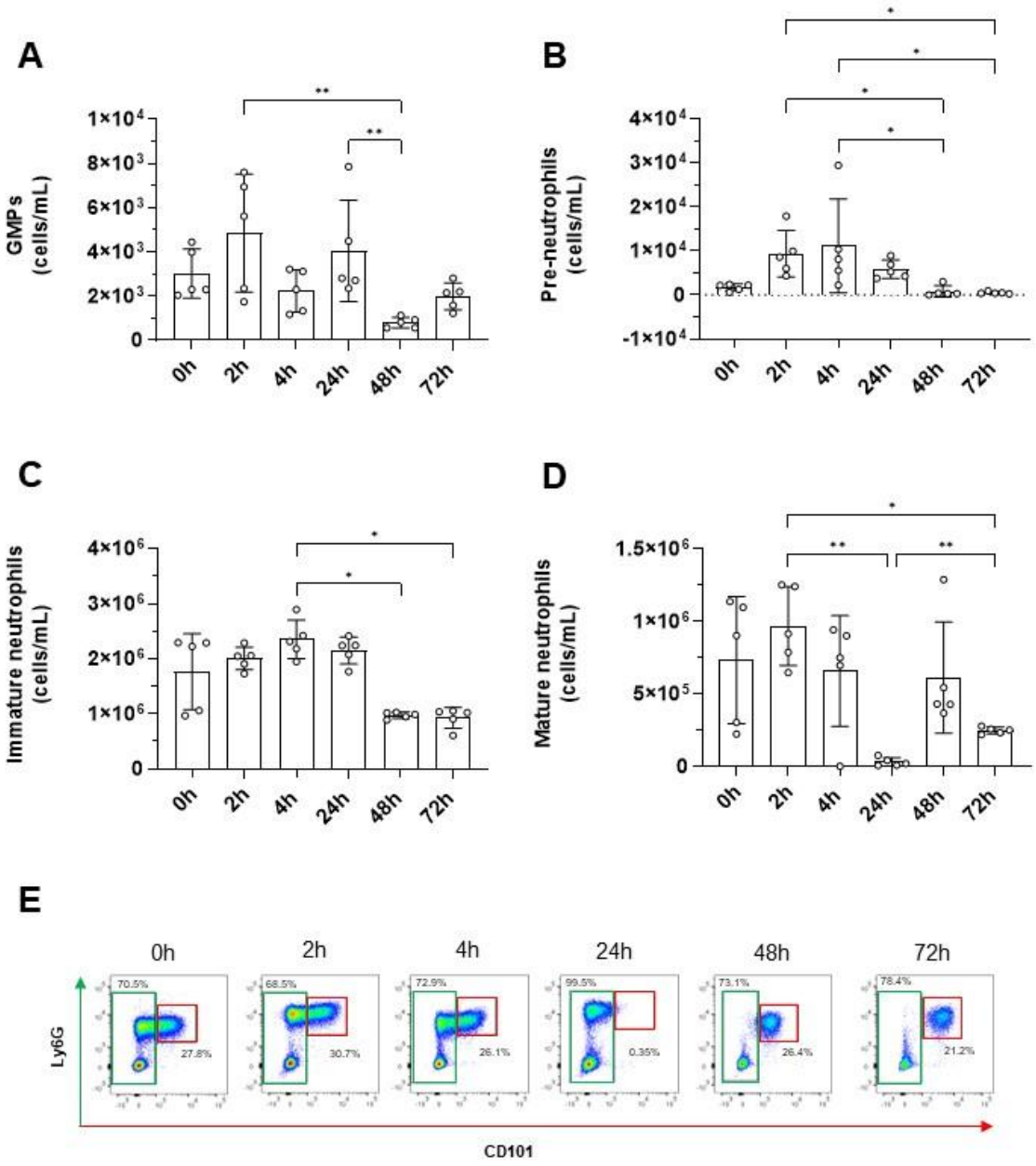

Figure 4.7. Temporal profile of blood neutrophil subsets following UV-KEc-induced resolving dermal inflammation. Male C57BL/6J mice were anaesthetised and inoculated with two intradermal injections of 100 µL sterile saline containing 1.5 x 10^7 UV-KEC or no injection. The right femur was dissected and flushed with HBSS yielding a single-cell suspension at baseline (0h), 4h, 24h, 48h and 72h. The resulting single-cell suspension was stained for polychromatic flow cytometry and the total number of bone marrow neutrophil subsets was determined. Depicted are (A) GMPs, (B) pre-neutrophils, (C) immature neutrophils and (D) mature neutrophils. Representative dot plots are also shown for immature (green) and mature (red) neutrophil subsets with relative percentages at each time-point (B). Data are presented as individual data points and mean with SD; $n = 5$. *$p < 0.05$, **$p < 0.01$, ***$p < 0.001$, ****$p < 0.0001$.

4.3.1.2 Bone marrow neutrophil subsets

Following the intradermal injection of 1.5 x 10^7 UV-KEc, bone marrow GMP numbers increased significantly at 24h compared to baseline ($p < 0.01$) and a further significant increase at 72h ($p < 0.01$) (**Figure 4.8A**). Pre-neutrophils showed a biphasic profile, peaking initially at 2h with a further peak at 72h ($p < 0.05$) (**Figure 4.8B**). Immature neutrophil numbers peaked significantly at 24h compared to baseline ($p < 0.05$) and declined thereafter (**Figure 4.8C**). Mature neutrophil numbers markedly decreased at 2h, suggesting a release from the bone marrow and remained significantly reduced at 4h (**Figure 4.8D**). Mature neutrophil numbers then began to rise again at 24h, before peaking significantly at 48h and staying elevated at 72h. This would suggest that the bone marrow was able to re-populate mature neutrophils numbers 48h after UV-KEc injection.

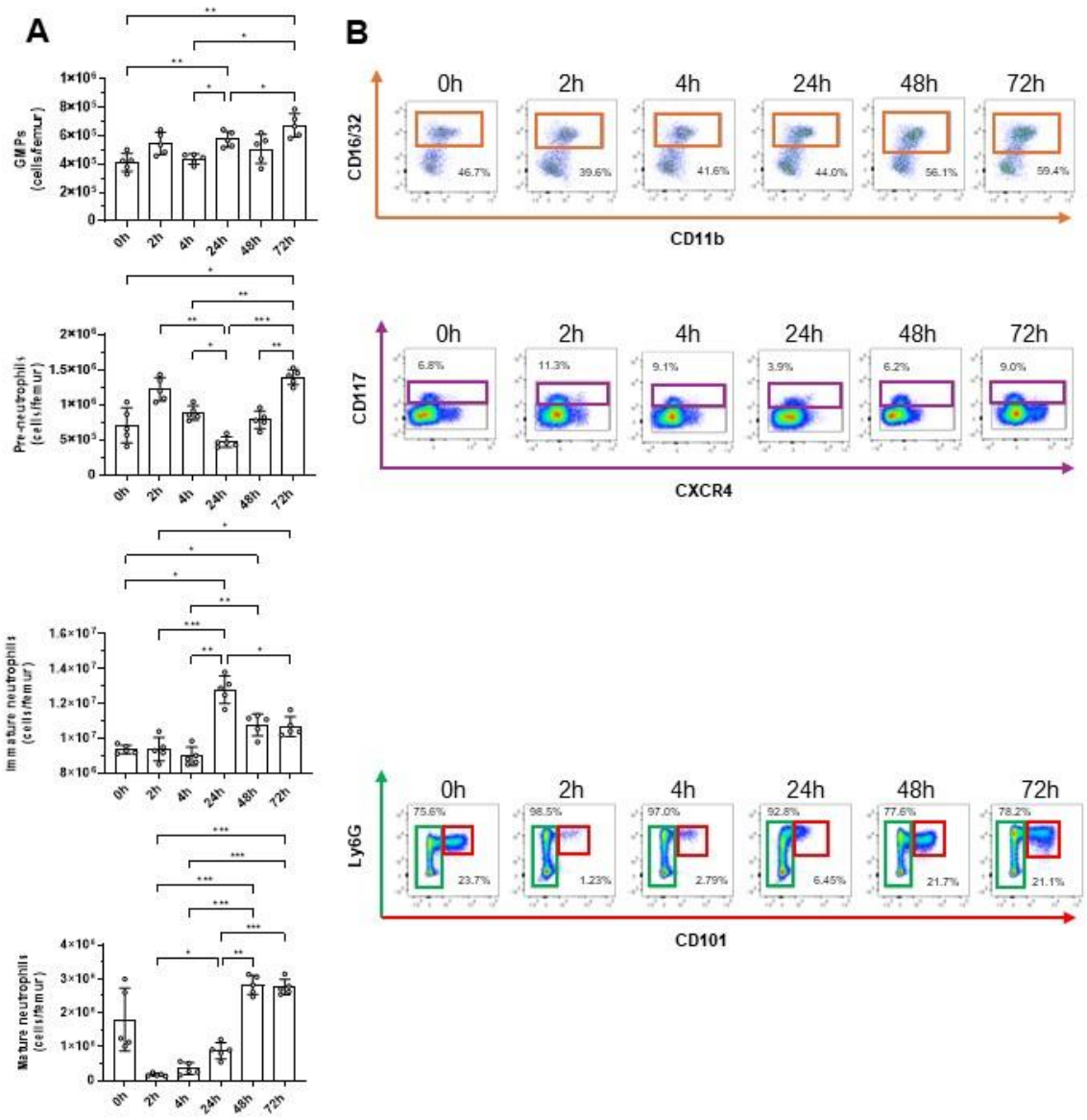

Figure 4.8. Temporal profile of bone marrow neutrophil subsets following UV-KEc-induced resolving dermal inflammation. Male C57BL/6J mice were anaesthetised and inoculated with two intradermal injections of 100 µL sterile saline containing 1.5 x 10^7 UV-KEc or no injection. The right femur was dissected and flushed with HBSS yielding a single-cell suspension at baseline (0h), 4h, 24h, 48h and 72h. The resulting single-cell suspension was stained for polychromatic flow cytometry and the total number of bone marrow neutrophil subsets was determined. Depicted are GMPs, pre-neutrophils, immature neutrophils and mature neutrophils at all time-points (A). Representative dot plots are also shown for each neutrophil subset with relative percentages at each time-point (B). Data are presented as individual data points and mean with SD; $n = 5$. *$p < 0.05$, **$p < 0.01$, ***$p < 0.001$, ****$p < 0.0001$.

4.3.1 Indices of resolution of circulating immune cells following UV-KEc-triggered murine dermal inflammation

As for the skin, resolution indices for circulating immune cells were calculated and are shown in **Figure 4.9**. Unlike in the skin, in blood T_{max} was at 4h following injection with UV-KEc (**Figure 4.9**). Between 4h (T_{max}) and 40.3h (T_{50}), total neutrophil numbers decreased from 1.37 x 10^6 (Ψ_{max}) to 0.69 x 10^6 (R_{50}), representing a 50% reduction in neutrophil numbers. Mononuclear cells also peaked at 4h, but to a greater extent than neutrophils. The R_i, was therefore 4-40.3h using this model of resolving inflammation. At 19.2h, the number of neutrophils equalled the infiltrating mononuclear cell numbers ($I_{PMN=mono}$). Time-point $I_{PMN=mono}$ in the skin was at 42.3h, meaning that resolution of inflammation occured 23.1h later than in the blood. Between 4h and 72h after the onset of inflammation (T_0), neutrophil numbers gradually decreased, but at a slower rate than mononuclear cells. Mononuclear cells returned to baseline levels by 72h, whilst neutrophils dropped below pre-UV-KEc injection levels.

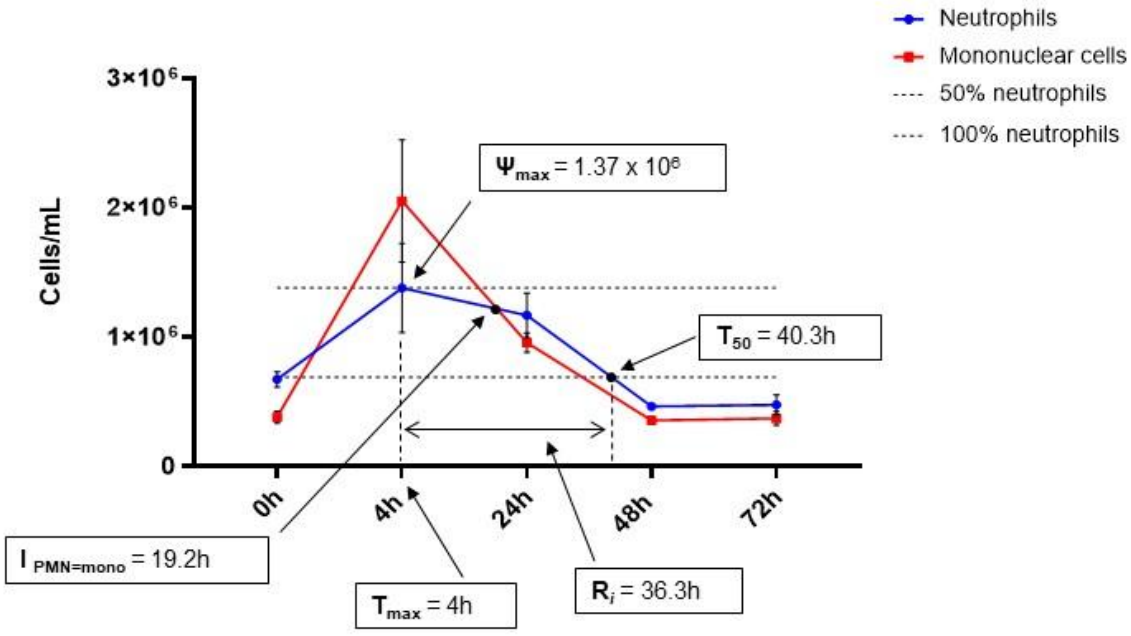

Figure 4.9. Circulating neutrophil and mononuclear cell composition following UV-KEc injection: Resolution indices. Male C57BL/6J mice were anaesthetised and inoculated with two intradermal injections of 100 µL sterile saline containing 1.5 x 10^7 UV-KEc or no injection. Immune cells were isolated using ACK lysing buffer at baseline (0h), 4h, 24h, 48h and 72h. The resulting single-cell suspension was stained for polychromatic flow cytometry. (A) Depicted is a time-line showing the resolution of acute inflammation and was defined in operative and quantitative terms using the following resolution indices: 1) magnitude (Ψ_{max}, T_{max}), the time-point (T_{max}) when neutrophil (PMN) numbers are maximum (Ψ_{max}); 2) duration (T_{50}), the time-point when neutrophil numbers reduce to 50% (R_{50}) of Ψ_{max}; 3) R*i*, the time interval from maximum neutrophil numbers (Ψ_{max}) to the 50% reduction point (T_{50}) (i.e., $T_{50} - T_{max}$) and 4) point of intersection ($I_{PMN=mono}$), the time-point when the increase in mononuclear cells intersects the decrease in neutrophils (i.e., neutrophil numbers = mononuclear cell numbers).

4.3.1 Infiltrating monocytes upregulate Langerin expression following the intradermal injection of UV-KEc contributing to the pool of Langerhans cells

Monocytes are rapidly recruited to inflamamtory sites and are known to give rise to a variety of cell-types, including macrophages, dendritic cells and Langerhans cells (339). **Figure 4.10A** shows the expression of Langerin (CD207) by MFI at each time-point for $Ly6C^{hi}$, $Ly6C^{int}$ and $Ly6C^{lo}$ monocyte subsets. $Ly6C^{hi}$ monocyte Langerin expression in steady state was neglible and began to increase at 4h, peaking significantly between 4h and 48h ($p < 0.05$), with a slight decrease between 48h and 72h. $Ly6C^{int}$ monocyte Langerin expression also began to rise at 4h, peaking significantly at 48h compared to baseline ($p < 0.01$). There were no significant differences in $Ly6C^{lo}$ monocyte Langerin expression at any time-point. $Ly6C^{hi}$ monocytes had the highest relative expression of Langerin by MFI at all time-points (**Figure 4.10B**). Taken together, these data suggest that infiltrating $Ly6C^{hi}$ and to a lesser extent $Ly6C^{int}$ monocytes into inflamed skin, but not $Ly6C^{lo}$ monocytes, contribute to the dermal pool of Langerhans cells. Furthermore, this would suggest the presence of two types of Langerhans cells that develop through different pathways during inflammation and steady state and that Ly6C may be important for the differentation of these monocytes.

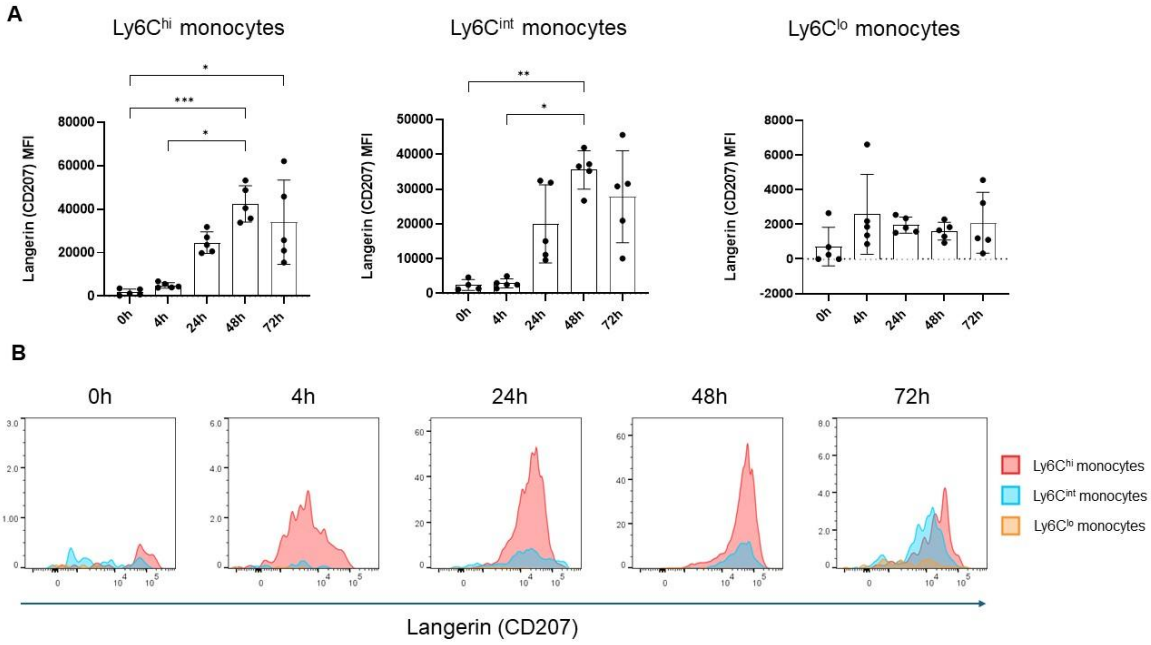

Figure 6.8. Differential expression of Langerin by infiltrating monocyte subsets following intradermal injection of UV-KEc in a resolving model of inflammation. Male C57BL/6J mice were anaesthetised and inoculated with two intradermal injections of 100 µL sterile saline containing 1.5 x 10^7 UV-KEc. Skin was harvested and enzymatically digested at baseline (0h), 4h, 24h, 48h and 72h. The resulting single-cell suspension was stained for polychromatic flow cytometry. (A) Depicted is the relative Langerin expression by MFI on Ly6C^{hi} monocytes (left), Ly6C^{int} monocytes (middle) and Ly6C^{lo} monocytes (right). (B) Also shown are combined histograms of the relative Langerin expression by MFI on all monocyte subsets at all time-points. Data are presented as individual data points and mean with SD; $n = 5$. *$p < 0.05$, **$p < 0.01$, ***$p < 0.001$, ****$p < 0.0001$.

4.3.1 Temporal profiles of endocannabinoids extracted from inflamed skin and plasma in a murine dermal model of resolving inflammation

As described in **Chapter 3**, concentrations of key endocannabinoids, namely AEA, 2-AG, PEA and OEA were determined by HPLC-MS in mouse skin following UV-KEc-triggered inflammation. In addition to mouse skin, matched plasma samples were also analysed by the same methodology to determine whether these lipids could also be extracted and levels determined from plasma.

As shown in **Chapter 3**, levels of 2-AG, PEA, AEA and OEA were detectable in the inflamed skin by HPLC-MS following the injection of UV-KEc at the lower dose of 1.5 x 10^7. These endocannabinoids were also detectable in the plasma of UV-KEc-injected animals. 2-AG was significantly lower in the skin of UV-KEc-injected animals at 4h ($p < 0.001$), 24h ($p < 0.001$), 48h ($p < 0.001$) and 72h ($p < 0.01$), compared to sham control (**Figure 4.11A**). Plasma 2-AG steadily increased following UV-KEc injection peaking at 48h, falling back to baseline levels at 72h, although this was not significant (**Figure 4.11B**). At 48h, there was a significant peak in the concentration of PEA in the skin in the UV-KEc group compared to sham control ($p < 0.01$) and this rapidly decreased at 72h but did not return to baseline levels (**Figure 4.11C**). Plasma PEA levels remained relatively constant throughout the time-course (**Figure 4.11D**). AEA levels peaked at 4h in the skin, significantly higher than that seen in the sham control group at this time ($p < 0.001$), and levels remained elevated compared to control at 24h, 48h ($p < 0.05$) and 72h ($p < 0.05$) (**Figure 4.11E**). Plasma PEA levels remained relatively constant throughout the time-course (**Figure 4.11F**). No significant differences were in identified in the concentration of OEA in the skin (**Figure 4.11G**) or plasma (**Figure 4.11H**) at any time-point.

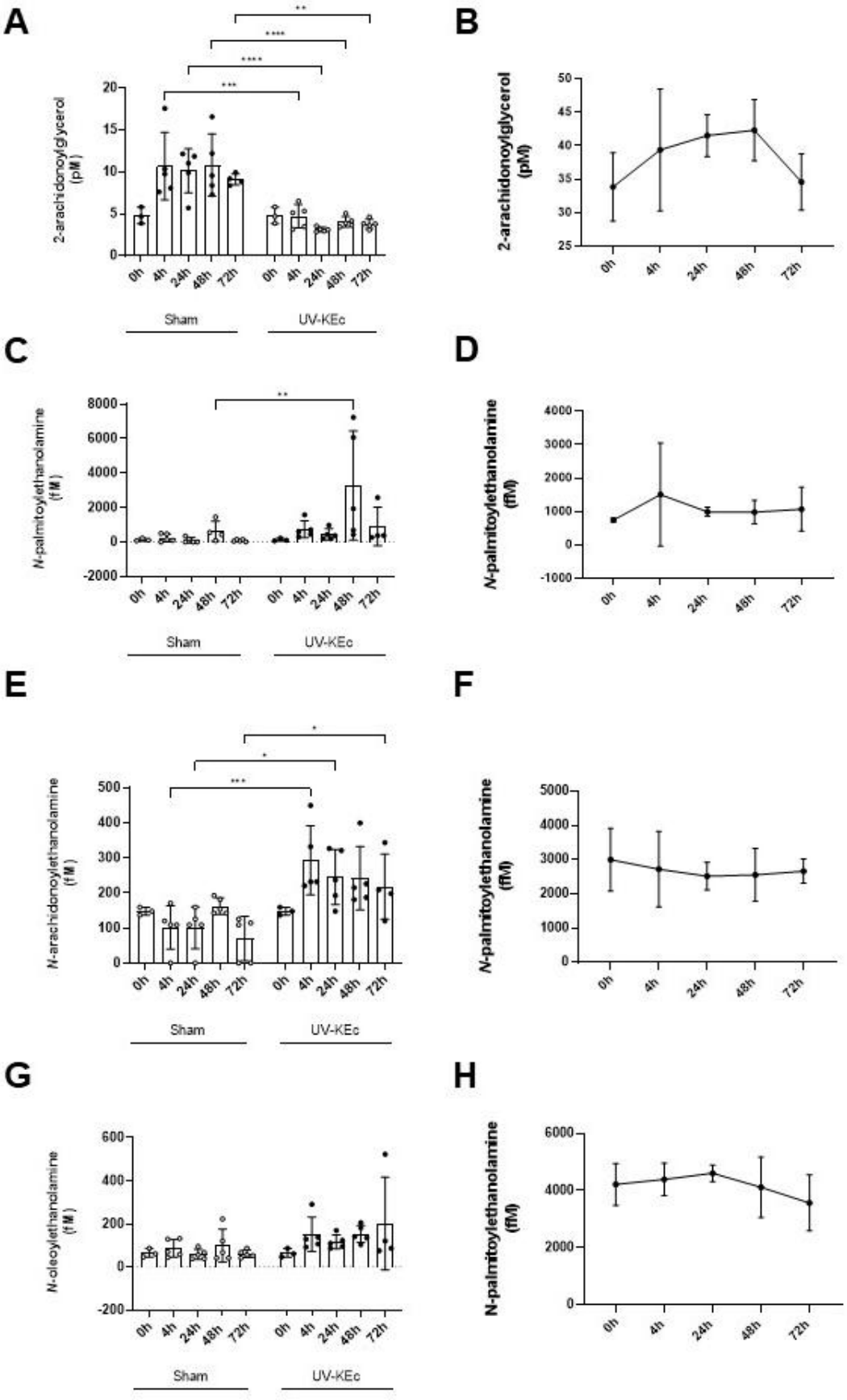
A
B
C
D
E
F
G
H
2-arachidonoylglycerol (pM)
N-palmitoylethanolamine (fM)
N-arachidonoylethanolamine (fM)
N-oleoylethanolamine (fM)
0h
4h
24h
48h
72h
Sham
UV-KEc

Figure 4.11. Temporal profile of endocannabinoids extracted from skin and plasma following UV-KEc-induced resolving dermal inflammation. Male C57BL/6J mice were anaesthetised and inoculated with two intradermal injections of 100 µL sterile saline containing 1.5 x 10^7 UV-KEc or sham (saline) control. Endocannabinoids were extracted from skin biopsies and plasma and levels determined at baseline (0h), 4h, 24h, 48h and 72h by HPLC-MS. Depicted are skin (A) and plasma (B) 2-arachidonoylglycerol (2-AG); skin (C) and plasma (D) *N*-palmitoylethanolamine (PEA); skin (E) and plasma (F) *N*-arachidonoylethanolamine (anandamide [AEA]) and skin (G) and plasma (H) *N*-oleoylethanolamine (OEA). Data are presented as individual data points and mean with SD; $n = 5$. *$p < 0.05$, **$p < 0.01$, ***$p < 0.001$, ****$p < 0.0001$.

4.4 Summary of findings

The key aim of this chapter was to characterise a resolving UV-KEc induced dermal model of inflammation.

To main conclusions of this chapter are:

- Injection of 1.5 x 10^7 UV-KEc into mouse skin causes a resolving inflammatory response in skin, characterised by the influx of neutrophils, which had entered the resolution phase of inflammation by 72h.
- Following UV-KEc injection into the skin of mice, there is a systemic inflammatory response detectable in circulating leucocytes, which had resolved by 72h.
- Intradermal injection of UV-KEc results in an expansion of intermediate monocytes.
- Similar changes are seen in bone marrow and circulating neutrophil subsets in response to UV-KEc, but to a lesser extent than seen with the higher dose.
- In addition to extracting and detecting endocannabinoids from inflamed murine skin, this methodology was also possible in both skin and plasma using HPLC-MS using the lower dose of UV-KEc.

4.5 Discussion

In this chapter, I developed a murine model of resolving dermal inflammation triggered by the intradermal injection of UV-KEc. This was characterised by the influx and subsequent clearance of neutrophils from the inflamed skin. As before, I have characterised immune cell profiles at the site of inflammation and those in circulation, focusing on monocyte subsets and both bone marrow and circulating neutrophil subsets. Unlike in the non-resolving model described in **Chapter 3**, most cell-types had returned to baseline in the inflamed mouse skin by the end of the time-course. I have also shown that key endocannabinoids can be extracted and quantified from plasma, in addition to the inflamed skin. Collectively, this can be used in conjunction with the non-resolving model to investigate the immune system of both mouse and human during steady state and disease, including autoimmune diseases such as RA. As with the higher dose non-resolving model, it can also be used alongside the human model of UV-KEc-triggered dermal inflammation (267).

4.5.1 Intradermal injection of 1.5 x 10^7 UV-KEc results in granulopoiesis and release of developmentally immature neutrophils into the circulation

It is known that during acute infections and inflammatory conditions, the haematopoietic system rapidly responds, turning from steady state to emergency granulopoiesis (340). Neutrophils are short-lived cells and develop from self-renewing haematopoietic stem cells (HSCs) (341). These give rise to the non-renewing differentiated cells, multi-potent progenitors (MPPs), which can differentiate into oligopotent common myeloid progenitors and further differentiate into GMPs (342). The process of differentiation from GMPs into mature, segmented neutrophils, is a highly complex and tightly regulated process. This involves the sensing of pathogens or other stimuli by haematopoietic and non-haematopoietic cells mediated *via* TLR/MyD88 pathways, the release of growth factors (including G-CSF, IL-6 and CXCL1) and activation of dormant HSCs to generate neutrophils in the bone marrow, dependent on GATA-1, CCAAT-enhancer-binding protein (C/EBP)-α (during steady state), C/EBP-β (during inflammation), growth factor independent-1 (Gfi-1), STAT1,

STAT3, STAT5 and c-Myelocytomatosis (c-Myc) (340). Using *Myd88*$^{-/-}$ knock-out germ-free mice, granulopoiesis has been shown to be dependent on TLR/MyD88 signalling, as evidenced by the failure to restore microbiota-driven granulopoiesis when transferred with microbiota or serum from colonised mice (343). It has also been shown in a murine model of endotoxaemia using non-haematopoietic background *TLR*$^{-/-}$ animals, that there was still a significant release of G-CSF and resulting emergency granulopoiesis (344). LPS, as found in the outer membrane of the UV-KEc cell envelope, is known to activate TLR4/MyD88 pathways to induce IL-17A and G-CSF to facilitate granulopoiesis (345). In both the resolving and non-resolving models, I have shown a gradual increment in GMP numbers across the time-course, suggesting an increase in granulopoiesis in response to UV-KEc. This process if therefore likely to be driven by LPS activation at the site of inflammation, TLR/MyD88 signalling to HSCs, mediated by G-CSF and IL-6 and dependent on C/EBP-β, Gfi-1, STAT1, STAT3, STAT5 and c-Myc. However, it is unclear whether the source of G-CSF is from the haematopoietic cells at the site of inflammation or other non-haematopoietic cells, such as fibroblasts.

In a model of sepsis, altered granulopoiesis has been shown to release immunosuppressive IL-1R2^{+} neutrophils, demonstrating inhibition of the proliferation and activation of CD4^{+} T cells and leading to a maladaptive immune response (346–348). Importantly, in septic patients this dysregulated immune response was shown to lead to poor clinical outcomes, across a range of infectious aetiologies (348). Given the significant numbers of pre-neutrophils and immature neutrophils released from the bone marrow in the non-resolving model, it is therefore possible that this too leads to a maladaptive immune response, which can be further investigated using this model, particularly important given the role of neutrophils in the development of autoimmune disease, including RA (349).

4.5.2 Intradermal injection of 1.5 x 10^7 UV-KEc causes a transient expansion in Ly6C^{int} monocytes

Ly6C^{hi} monocytes are thought to be analogous to human classical monocytes (CD14^{++}, CD16^{-}) and Ly6C^{lo} monocytes to human non-classical monocytes (CD14^{-}, CD16^{+}) (350). In humans, intermediate monocytes (CD14^{+}, CD16^{+}) have been described and shown to bear a distinct transcriptomic profile (*LYZ, S100A8, CD14, S100A10, HLA-DRA, CD74, IFI30, HLA-DPB1, CPV*) (351, 352). Intermediate monocytes display similar inflammatory characteristics to classical monocytes in terms of phagocytosis and ROS production, but with increased HLA-DR expression and increased production of IL-1β, IL-6, TNF-α and IL-12 upon TLR stimulation (351). In mouse, there is growing evidence that Ly6C^{int} monocytes similarly represent a third, functionally distinct subtype, although they remain relatively understudied (353). As shown in **Chapter 3** in the non-resolving model of inflammation, in this resolving model, there was again an expansion of the phenotypically distinct Ly6C^{int} monocyte population. Unlike the non-resolving model, both absolute numbers of Ly6C^{int} monocytes and relative proportions to the other monocyte subsets returned to baseline levels at the end of the time-course. Using principal component analysis, Mildner *et al.* (2017) have previously shown that the murine Ly6C^{int} population is heterogenous, with two phenotypically similar populations displaying distinct transcriptomes (309). One cluster showed increased expression of MHC II and CD209, whilst the other showed intermediate expression of genes related to Ly6C^{lo} monocytes. Additionally, the Ly6C^{lo} monocyte-like cluster of Ly6C^{int} monocytes were comparatively short-lived. Given the functional similarity in human classical and non-classical monocytes with murine Ly6C^{hi} and Ly6C^{lo} monocytes, respectively, it is tempting to speculate that human intermediate monocytes and the expanded Ly6C^{int} monocyte population seen in both models reported here are similar in function, retaining the inflammatory capacity of Ly6C^{hi} monocytes as well as the endothelial surveillance, wound healing and anti-inflammatory properties of Ly6C^{lo} monocytes (353). Additionally, in the non-resolving model, there was a significant increase in MHC II expression by infiltrating Ly6C^{int} and Ly6C^{lo} monocytes at 24h, suggesting that these cells may also play a role in antigen presentation within the inflamed tissue, in keeping with both human and murine transcriptomic data (351, 352). Ly6C^{lo}

monocytes have traditionally been considered ‘patrolling’ monocytes, remaining in circulation, acting as scavengers and orchestrating tissue repair (353, 354). Contrary to published literature, I have also shown that Ly6C^{lo} monocytes are able infiltrate inflamed tissue following the intradermal injection of UV-KEc at both high and low dose, albeit not until 72h in the non-resolving model. Overall, this would suggest a role for Ly6C^{lo} monocytes in tissue repair at the site of inflammation in this resolving model.

In humans, there is an expansion of intermediate monocytes in RA patients, leading to increased levels of Th-17 cells which produce pro-inflammatory cytokines, including IL-17, IL-6, IL-21, IL-22 and TNF-α thought to be important in the pathogenesis of the disease (355). It is also known that an expansion of intermediate monocytes also drives atherosclerosis and metabolic disease and is associated with increased cardiovascular risk (356), as well as in SLE (320), Crohn’s disease (321), Graves’ disease (322) and sarcoidosis (323). To better understand the significance of Ly6C^{int} monocytes in inflammatory diseases, these models can be used in parallel to gain further insights into the function of these cells and their role in the development of chronic inflammatory diseases.

4.5.3 Injection of 1.5 x 10^7 UV-KEc into mouse skin causes a significant eosinophilia at 72h

The only immune cell-type to peak at 72h in the resolving model of inflammation were eosinophils. It has been shown in murine skin that following the application of peptidoglycan from *S. aureus* that there was a late eosinophil recruitment to the site of inflammation and that this process is mediated through Regulated upon Activation, Normal T cell Expressed and presumably Secreted (RANTES [CCL5]), but not eotaxin, eotaxin-2 or MCP-1 (357). The same group also showed that RANTES is produced by Langerhans cells. Eosinophil trafficking requires several adhesion molecules, including P-selectin, E-selectin, ICAM-1 and VCAM-1, which mediate transient or firm adhesion to and subsequent interaction with the inflamed endothelium

(358). Migration to sites of inflammation also requires chemoattractants such as platelet-activating factor and LTB_4 and several chemokines, including RANTES, eotaxin, eotaxin-2 and MCP-3 (359, 360). In another murine model of *S. aureus* dermal inflammation, eosinophils were shown to have a comparable contribution to inflammation to T cells, dependent on eosinophil-derived IL-17A and IL-17F production and that keratinocyte-derived IL-36 and CCL7-mediated signalling was critical for eosinophil recruitment to the inflamed skin (361). Therefore, it is possible that the late high numbers of eosinophils seen in this resolving model of dermal inflammation reported here may be mediated through RANTES-mediated chemoattraction. As both neutrophils and mononuclear phagocytes had mostly returned to basal levels by 72h in both the inflamed skin and circulation, it is likely that the T cell population was the source of RANTES or other chemoattractant(s), such as T cell-derived ecalectin (362), which remained elevated at 72h. However, dermal Langerhans cell and macrophage numbers had not returned to baseline levels, so they may have also contributed to this process. Eosinophils are involved in a range of biological functions, including wound healing, host defence against parasitic infection and allergic inflammation but increasing evidence has also implicated them in the control of bacterial and viral infections (363–365). They are commonly thought of as mediators of tissue damage with destructive effector functions, exerting a cytotoxic effect through the release of a range of mediators, including granule protein, eosinophil peroxidase and eosinophil cationic protein and are also able to generate mitochondrial DNA-containing traps to engulf microorganisms (366). From a disease perspective, eosinophils have also been implicated in the pathogenesis of allergic airway inflammation, atopic dermatitis, hypereosinophilic syndromes, eosinophilic gastrointestinal disease and demyelinating diseases such as multiple sclerosis and neuromyelitis optica (367, 368). In addition, eosinophils have more recently been described as regulators of local immunity (369) and play important roles in wound healing and epithelial remodelling and have been shown to contribute to the resolution of airway inflammation (370, 371). Given the significant increase in eosinophils, it is likely that these cells may play a role in tissue repair in resolving inflammation.

4.5.4 Ly6C^{hi} and Ly6C^{int} monocyte subsets give rise to a second pool of short-term Langerhans cells

When analysing circulating monocyte subsets expression of Langerin (CD207) by MFI, both infiltrating Ly6C^{hi} and Ly6C^{lo} monocytes upregulated Langerin from 24h. Langerhans cells comprise around 2-3% of epidermal cells and possess an exceptionally long life cycle (372). Owing to their specialised location in the skin, along with dendritic cells, they constitute the first immune barrier for invading pathogens and it has been suggested they are key to the induction of immune tolerance (373). During steady state, bone marrow-derived Langerhans cells are maintained in the tissue by local, long-lived precursors that seed skin during embryonic development and are able to self-renew (374). During inflammation, Langerhans cells become activated and leave the skin, trafficking towards the draining lymph nodes and are replaced by circulating Gr-1 (Ly6C/Ly6G)^{hi} monocytic Langerhans cell precursors (375). Using *ld2*$^{-/-}$ knock-out mice, it has been shown that during ontogeny and steady state, the development of long-term Langerhans cells is dependent on ligand 2 (ld2), whereas during inflammation, this process is independent of ld2 and results in a pool of short-lived Langerhans cells (376). These cells differ phenotypically and morphologically from their long-term counterparts with differential expression of Langerin, CD24, CD205, increased CD11b and CX3CR1 and with more dendrites in epidermal sheets (377). Therefore, I propose that using the resolving model reported here, the increase in Langerin-expressing Ly6C^{hi} and Ly6C^{int} monocytes within the inflamed tissue from 24h onwards represent monocyte-derived Langerhans cells, serving as short-term replacements for tissue-resident Langerhans cells who have migrated to the lymph node. Furthermore, there were negligble Langerhans cells in the circulation except for a significant peak at 24h, suggesting that these were the true tissue-resident activated Langerhans cells emigrating from the inflamed skin to the draining lymph nodes. If this hypothesis were to be true, it is therefore likely that there would be a second, later wave of Langerhans cells in the inflamed skin with further replacement with longer-term, steady state Langerhans cells derived from local or bone marrow precursors, in an ld2-dependent manner.

Langerhans cells have also been implicated in the development of immune tolerance by the uptake of autoantigens mediated by Langerin and suppression of autoimmunity by expanding regulatory T cells (378). Historically, work has focussed on secondary lymphoid organs as the centre of T cells immunity, with the established dogma of naïve T cells being primed by migratory dendritic cells allowing for the differentiation and effector function of T cells recruited to sites of inflammation (379). Philips *et al.* (2015) demonstrated that ablation of Langerhans cells led to the increased production of autoantibodies in a murine model of lupus dermatitis, suggesting that under steady state conditions, Langerhans cells may also regulate activation of $CD4^+$ T follicular helper cells (380). Given the immune sentinel role of Langerhans cells, it may be that these cells act as immune regulators *in situ* and that local environmental interactions between Langerhans cells and T cells may also be important in understanding the development of autoimmune diseases. The model of dermal inflammation reported here provides a platform in which to further evaluate the role of Langerhans cells in the development of autoimmune disease and their contribution to immune tolerance.

4.5.5 Resolution of UV-KEc-triggered dermal inflammation can be quantified using indices of resolution

The clearance of apoptotic neutrophils by professional mononuclear phagocytes is the cellular hallmark of inflammatory resolution in tissue (381). I set out to assess the feasability of applying previously described resolution indices that can be used to pinpoint the time of resolution of inflammation, in terms of immune cell trafficking (44). When using models of inflammation, the time-points chosen only give a snapshot of the immune response at that moment and clearly there is ongoing cellular and molecular activity between these times. Given my aim of identifying anti-inflamamtory/pro-resolution signals which may be key in the maintenance of remission in RA, it was important to be able to identify the exact time of resolution, so that when using the model and translating the work into humans, this moment could be selected as an experimental time-point allowing the investigation of critical soluble mediators. In the inflamed skin, I was able to identify the T_{max} (24h) and T_{50} (36.9h), showing a decrease in neutrophil numbers by 50%. At 42.3h, the number of

neutrophils equalled the infiltrating mononuclear cell numbers, representing the intersection point, or $I_{PMN=mono}$, and therefore the time of inflammatory resolution. Thus, this resolving model of dermal inflammation can be used in conjunction with resolution indices, to provide operative and unbiased assessments of resolution.

4.5.6 Low dose UV-KEc exerts a biological effect on skin endocannabinoid concentrations but does not affect plasma levels

Following the intradermal injection of 1.5 x 10^7 UV-KEc, marked changes were seen in endocannabinoid levels extracted from the inflamed skin. As observed with the non-resolving model of inflammation described in **Chapter 3**, there were significant differences seen with 2-AG and PEA. However, unexpectedly, animals injected with UV-KEc showed significantly lower concentrations of 2-AG in the inflamed skin at all time-points. A similarly contrasting finding was seen with PEA at the lower dose of UV-KEc with significantly higher levels seen at 48h. In addition, significant changes were seen in the concentration of AEA extracted from the inflamed skin, the most abundant endocannabinoid. 2-AG, AEA and WIN 55,212-2, a full agonist of the CB-$_1$ receptor, have been shown to have neuroprotective activity using *in vitro* and *in vivo* models of ischaemic brain injury (382). CB-$_1$ receptor knock-out mice have been shown to have increased mortality from cerebral ischemia with increased infarct size, more severe neurological deficits and decreased cerebral blood flow, compared with wild type controls subjected to the same insult (383). Despite this, treatment with high dose but not low dose WIN 55,212-2 in a rat model of middle cerebral artery occlusion had no protective effect on cerebral function (384). It is also known that activation of CB-$_1$ receptors in the brain can lead to inhibition or the release of both inhibitory and excitatory neurotransmitters (385). Furthemore, in a murine model of physiological and behavioural assays, AEA at low dose induced leucocyte phagocytosis and stimulated behavioural activities, whilst high dose AEA inhibited phagocytosis (386). The authors suggested that the dose effect observed may be due to the differential involvement of a Gs and a Gi protein, activated at low and high doses, respectively, as well as allosteric modulation of AEA. Thus, it is clear that many of the actions of endocannainoids and their receptor agonists are dose-dependently biphasic (385). In

addition, Ben-Shabat *et al.* (1988) have suggested that endocannabinoids can also exhibit an "entourage effect", whereby there is enhancement of their activity by structurally related, biologically inactive, endogenous constituents, which may have also played a role (387). Clearly, there are dosing considerations in the biological activity of endocannabinoids both in terms of the inflammatory stimulus and their interactions with the CB_1 and CB_2 receptors, which could in part explain the contrasting results seen using the resolving and non-resolving models in terms of endocannabinoid levels at the site of inflammation.

It was observed that in the resolving model of inflammation, that PEA concentrations in the inflamed skin were significantly elevated at 48h, whereas they were significantly reduced in the non-resolving model. During inflammation, PEA has been shown to reduce neutrophil recruitment (388), inhibit pro-inflammatory cytokines (IL1-β, IL-6 and TNF-α) and chemokines (MCP-1, MIP-Iα and MIP-2) (335) and that this was mediated through decreased activation of the NK-κB system (336). Others have shown that PEA treatment was associated with reduced levels of P-selectin and IL-2 (337). Given that the significant rise in PEA at 48h coincided with the resolution of inflammation in the skin using the resolving model of inflammation as defined by clearance of neutrophils, it is likely that PEA plays a role in reducing neutrophil recruitment and the inhibition of pro-inflammatory cytokines, bringing about inflammatory resolution. In addition, 2-AG levels were increased in the inflamed skin at all time-points. In the resolving model of inflammation, AEA levels peaked at 4h and remained elevated at all time-points following the intradermal injection, but no significant changes were seen using the non-resolving model. Given that AEA has been implicated in enhanced phagocytosis at low dose, the attenuation of inflammasome (NLRP3, NLR family caspase activation and recruitment domain-containing 4 [NLRC4], adapter protein apoptosis associated speck-like protein containing a CARD [ASC], IL-18) activation and the consequent reduction in production of IL-1β (386, 389), it is likely that a significant increase at this time using the resolving model is important to initiate phagocytosis of UV-KEc and a reduction in pro-inflammatory cytokine production to facilitate inflammatory resolution.

The immunosuppressant and anti-inflammatory properties of cannabinoids are also highly relevant for human autoimmune disease, including RA. Ajulemic acid is a synthetic cannabinoid and high-affinity agonist for human cannabinoid receptors. It is an analogue of the acid metabolites of tetrahydrocannabinol and cannabidiol and has been shown to have anti-inflammatory effects in animal models of arthritis (390, 391), and suppressed PG production *in vitro* above that of the potent non-steroidal anti-inflammatory drug, indomethacin (392, 393). Ajulemic acid also induces apoptosis in human T lymphocytes (394) and suppresses IL-1β production in human monocytes (395). Furthemore, treatment with cannabidiol attenuated LPS-induced TNF-α production and blocked the progression of collagen-induced arthritis in mice (396). Overall, the anti-inflamamtory/pro-resolution role of endocannabinoids in RA remains understudied, although evidence is growing to suggest their beneficial effect in reducing autoimmune disease activity, particularly in animal models. I have shown for the first time using novel models of resolving and non-resolving inflammation that dermal and plasma endocannabinoids can successfully extracted and quantifed. These models can be used to further investigate their role in the onset, resolution and post-resolution phases of inflammation both in health and disease.

Having successfully developed novel murine models of resolving and non-resolving inflammation following using a high and a low dose of intradermal UV-KEc, I next wanted to translate the animal work into humans to continue with the ultimate aim of investigating anti-inflammatory/pro-resolution pathways in patients with RA, which may be important for the maintenance of remission.

5 Effects of ATB-346 and naproxen on a resolving model of human dermal inflammation

5.1 Introduction

Having developed and characterised models of resolving and non-resolving inflammation in murine skin following the injection of UV-KEc, attention turned to *in vivo* human models. One such model, described by Motwani *et al*. (2016) is akin to the models described in **Chapter 3** and **4**, using the same UV-KEc inflammatory stimulus (252). Unlike the mouse models where inflamed dermal tissue is enzymatically and mechanically digested to yield a single-cell suspension, this model utilises a negative pressure suction cup to generate a blister by gently separating the dermal and epidermal layers. This blister contains an inflammatory exudate consisting of infiltrating immune cells into the site of inflammation and can be sampled in a temporal manner, analogously mapping out the immune response over time.

I aimed to ascertain whether this model of dermal inflammation can be used safely in humans to investigate anti-inflammatory/pro-resolution signals and to show that the model responds to therapeutic intervention for use in longer term translational studies. As such, naproxen, a traditional NSAID commonly prescribed for symptom control in active RA, was selected. Following discussion with Antibe Therapeutics Inc., a novel H_2S-releasing NSAID, ATB-346, was made available to me with potential clinical advantages over traditional NSAIDs in terms of reduced GI adverse effect in animal studies (397), improved pain scores and reduced GI ulcer formation in clinical trials (197). Therefore, both drugs were included in the study design.

5.2 Hypothesis

These experiments will address the hypothesis that: **NSAIDs (naproxen and ATB-346) can safely hasten the resolution of inflammation in a human UV-KEc-triggered model of resolving dermal inflammation.**

The aims of this chapter were:

1. Conduct a study in healthy volunteers to determine the effects of naproxen and ATB-346 on immune cells and soluble mediators of acute inflammation.
2. Investigate clinical parameters of acute inflammation in these volunteers including pain, tenderness and temperature.
3. Quantify the blood flow/vascular hyper-reactivity at the site of inflammation using laser Doppler imaging.

5.3 Results

5.3.1 Study volunteer baseline characteristics

All volunteers in this study were male. As shown in **Table 5.1**, the mean age for the untreated control group, naproxen and ATB-346 groups was 27, 23 and 22 years, respectively and there were no significant differences across the groups. In terms of ethnicity, most participants identified as white British across all groups (66.7%) with no significant differences seen between groups.

Table 5.1 Baseline characteristics of study participants. Age and ethnicity shown for all 21 healthy, male volunteers recruited. No significant differences were seen between participants for either age or ethnicity; $n = 7$.

Treatment Group		Age (Years)	Ethnicity
Untreated	1	32	African British
	2	25	White British
	3	19	White British
	4	24	White British
	5	32	White British
	6	29	Mixed white/African
	7	31	White British
Mean		**27**	
Naproxen	1	28	White Irish
	2	22	British Pakistani
	3	23	White British
	4	23	White British
	5	20	British Pakistani
	6	22	White British
	7	28	White British
Mean		**23**	
ATB-346	1	26	White British
	2	20	Chinese
	3	25	White British
	4	26	White British
	5	20	Mixed White/African
	6	20	White British
	7	20	White British
Mean		**22**	

5.3.2 Blister volumes

Mean blister volumes at 4h and 48h for untreated controls were 0.1059 mL and 0.1201 mL, respectively. Mean blister volumes at 4h and 48h for the naproxen group were 0.1391 mL and 0.1304 mL, respectively. Mean blister volumes at 4h and 48h for the ATB-346 group were 0.1442 mL and 0.1558 mL, respectively (**Figure 5.1**). There were no significant differences in blister volumes between groups at any time-point.

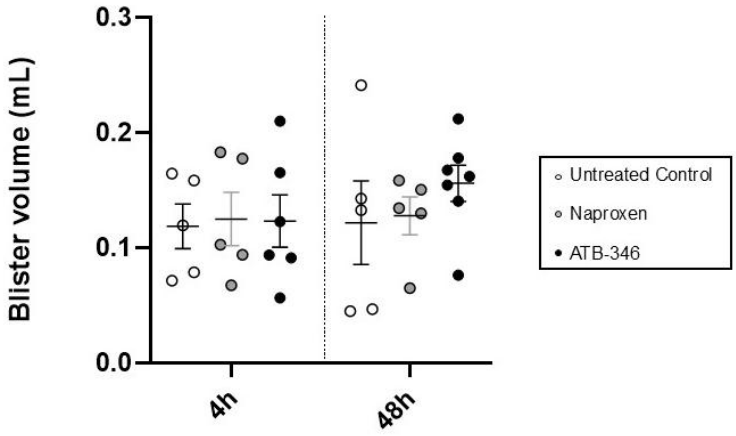

Figure 5.1. Blister volumes following UV-KEc-triggered inflammation. Healthy, male volunteers were randomised to receive either ATB-346 (250 mg daily), naproxen (500 mg twice daily) or no drug (untreated control) prior to UV-KEc injection. Following the intradermal injection of 1.5 x 10^7 UV-KEc into the volar aspect of each forearm for all participants, blisters were formed using a negative pressure suction cup at two time-points (4h and 48h), one per forearm for each volunteer. Data are expressed as individual values with the mean with SD at each time-point; $n = 7$

5.3.3 ATB-346 is potently anti-inflammatory in a UV-KEc-triggered model of inflammation

Polychromatic flow cytometric characterisation of inflammatory cell infiltrate following injection of UV-KEc into the skin revealed a robust inflammatory response with infiltration of neutrophils peaking at 4h in healthy volunteers and clearing by 48h (**Figure 5.2A**). While naproxen significantly inhibited numbers of neutrophils in the blister at 4h ($p < 0.05$), the effects of ATB-346 compared to healthy controls was more

significant ($p < 0.001$) (**Figure 5.2A**), although there was no difference between naproxen and ATB-346. There were significantly fewer classical monocytes in the ATB-346 group compared to untreated controls ($p < 0.01$) at 48h, whilst naproxen exerted a trend towards a reduction in numbers of these cells at this time-point (**Figure 5.2B**). There was a trend towards significant reduction of intermediate monocytes in both ATB-346 and naproxen treated participants (**Figure 5.1C**). Non-classical monocytes were comparatively fewer in this model, with a trend towards reduction in numbers at both time-points (**Figure 5.2D)**. Dendritic cells were also highest in the blisters at 48h in all groups, with those treated with ATB-346 showing a trend toward a reduction in numbers of these cells at 48h (**Figure 5.2E)**. Finally, as the flow panel was designed to focus on granulocytes and mononuclear phagocytes, other population of cells were grouped together such as T cells and NK cells, which showed a collective, significant reduction in response to ATB-346 at 48h ($p < 0.01$) (**Figure 5.2F**). Neither drug influenced B lymphocyte numbers, which were also highest at 48h in the blister (**Figure 5.2G)**.

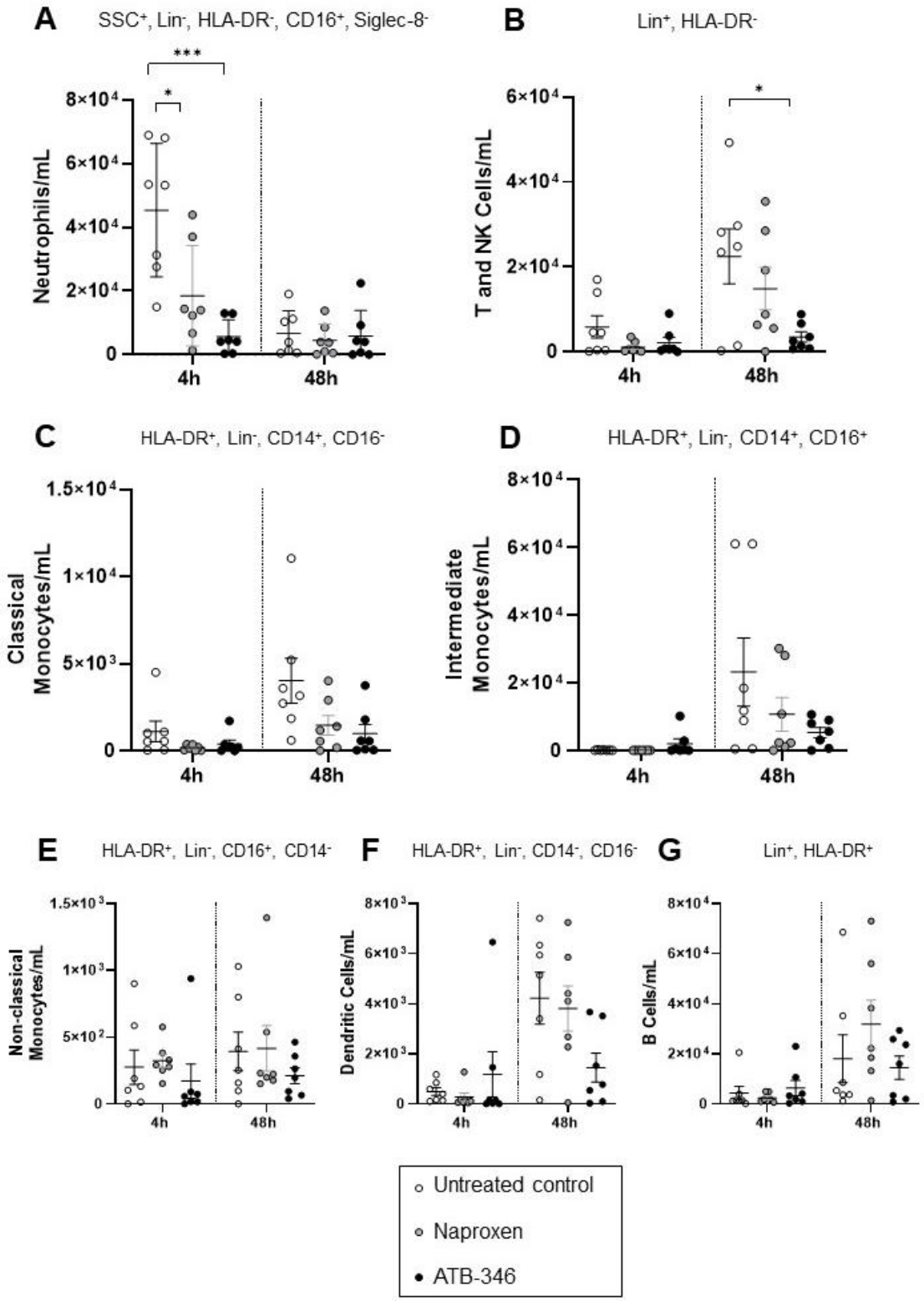
A
SSC+, Lin-, HLA-DR-, CD16+, Siglec-8-
***
*
Neutrophils/mL
8×10⁴
6×10⁴
4×10⁴
2×10⁴
0
4h
48h
B
Lin+, HLA-DR-
*
T and NK Cells/mL
6×10⁴
4×10⁴
2×10⁴
0
4h
48h
C
HLA-DR+, Lin-, CD14+, CD16-
Classical Monocytes/mL
1.5×10⁴
1×10⁴
5×10³
0
4h
48h
D
HLA-DR+, Lin-, CD14+, CD16+
Intermediate Monocytes/mL
8×10⁴
6×10⁴
4×10⁴
2×10⁴
0
4h
48h
E
HLA-DR+, Lin-, CD16+, CD14-
Non-classical Monocytes/mL
1.5×10³
1×10³
5×10²
0
4h
48h
F
HLA-DR+, Lin-, CD14-, CD16-
Dendritic Cells/mL
8×10³
6×10³
4×10³
2×10³
0
4h
48h
G
Lin+, HLA-DR+
B Cells/mL
8×10⁴
6×10⁴
4×10⁴
2×10⁴
0
4h
48h
Untreated control
Naproxen
ATB-346

Figure 5.2. Imme cells profiles at the site of UV-KEc-triggered resolving dermal inflammation. Healthy, male volunteers were randomised to receive either ATB-346 (250 mg daily), naproxen (500 mg twice daily) or no drug (untreated control) for 72h prior to UV-KEc injection. Following the intradermal injection of 1.5 x 10^7 UV-KEc into the volar aspect of each forearm for all participants, inflammatory exudate was obtained using a negative pressure suction cup at two time-points (4h and 48h), one per forearm for each volunteer. Cells were separated from the soluble mediator-containing supernatant by centrifugation and incubated with a fluorochrome-tagged antibody cocktail. Stained cells were acquired using the LSR Fortessa™ and analysed using Flowjo software. Depicted are (A) neutrophils, (B) T and NK cells, (C) classical monocytes, (D) intermediate monocytes, (E) non-classical monocytes, (F) dendritic cells and (G) B cells were identified. Cell numbers are shown as cell count per millilitre. Data are expressed as individual values with the mean with SD at each time-point; $n = 7$. *$p < 0.05$, **$p < 0.01$, ***$p < 0.001$, ****$p < 0.0001$.

5.3.4 Effects of ATB-346 on immune cell phenotype

Further analysis was performed to look for changes in the MFI for each cell surface marker. Having noted a trend towards a reduction in all monocyte subtypes at 48h following intradermal UV-KEc in both drug groups compared to healthy control, I investigated the expression of CD14, a co-receptor for TLR4 needed for LPS detection. I also examined the expression of CD62L given the reduction in neutrophils levels seen in the blister at 4h. Finally, I wanted to determine whether ATB-346 was aiding neutrophil clearance and so investigated the expression CCR7, a mediator of neutrophil migration from the site of inflammation to lymph nodes. At 48h, both classical and intermediate monocytes exhibited a significant reduction in their expression of CD14 based on the MFI in both naproxen ($p < 0.05$) and ATB-346 ($p < 0.05$) treated groups compared to healthy controls (**Figures 5.3A-C**). There was significantly lower neutrophil CD62L expression in volunteers treated with both naproxen ($p < 0.05$) and ATB-346 ($p < 0.05$) at 4h compared to healthy controls (**Figure 5.3D**). Infiltrating neutrophils showed higher expression of CCR7 based on MFI in volunteers treated with ATB-346 compared to the untreated group (**Figure 5.3E**), although this was not significant.

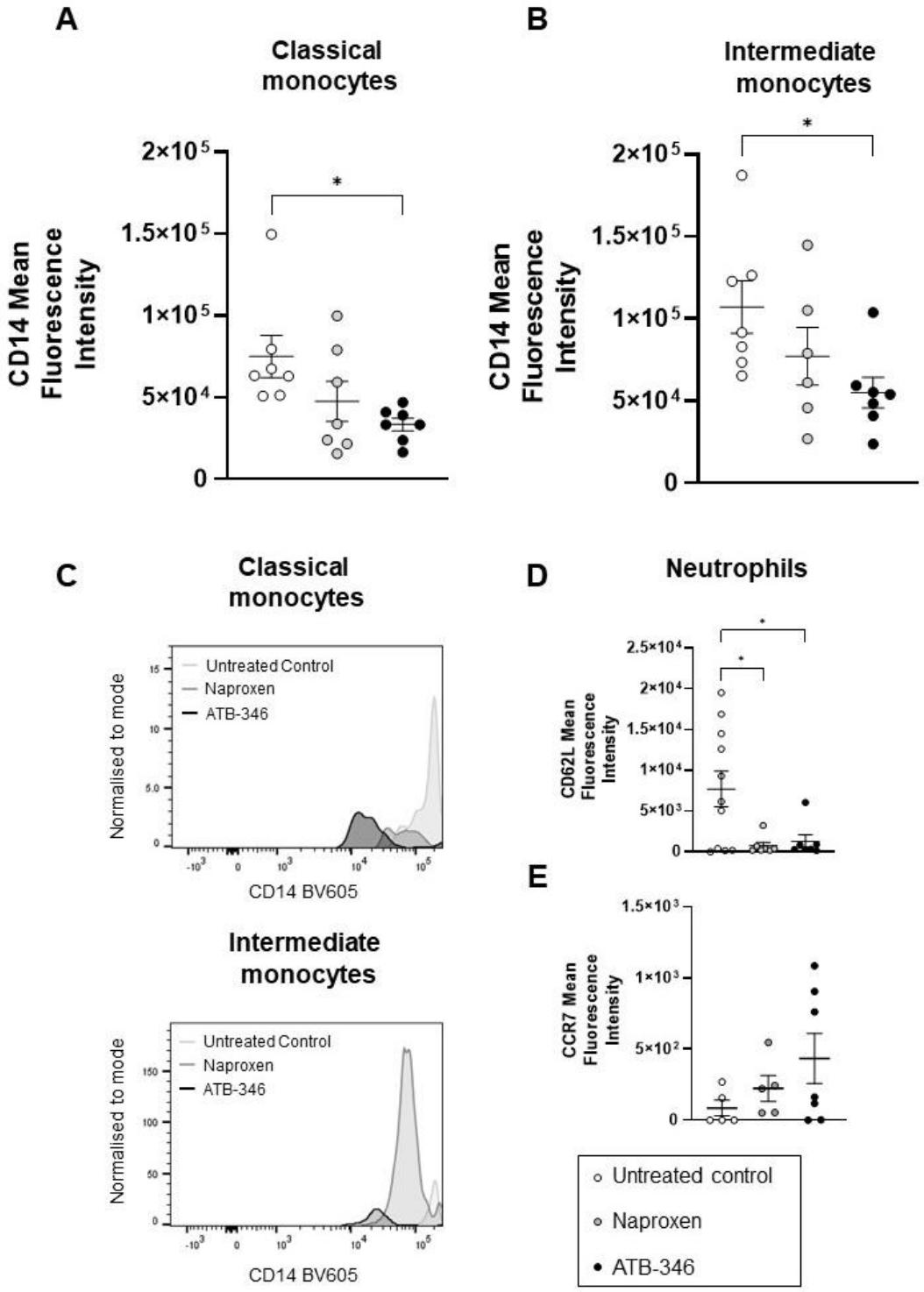
A
Classical monocytes
CD14 Mean Fluorescence Intensity
2×10^5
1.5×10^5
1×10^5
5×10^4
0
*
B
Intermediate monocytes
CD14 Mean Fluorescence Intensity
2×10^5
1.5×10^5
1×10^5
5×10^4
0
*
C
Classical monocytes
Normalised to mode
Untreated Control
Naproxen
ATB-346
CD14 BV605
Intermediate monocytes
Normalised to mode
Untreated Control
Naproxen
ATB-346
CD14 BV605
D
Neutrophils
CD62L Mean Fluorescence Intensity
2.5×10^4
2×10^4
1.5×10^4
1×10^4
5×10^3
0
*
*
E
CCR7 Mean Fluorescence Intensity
1.5×10^3
1×10^3
5×10^2
0
Untreated control
Naproxen
ATB-346

Figure 5.3. MFI values for blister fluid immune cells following intradermal UV-KEc. Healthy, male volunteers were randomised to receive either ATB-346 (250 mg daily), naproxen (500 mg twice daily) or no drug (untreated control) for 72h prior to UV-KEc injection. Following the intradermal injection of 1.5 x 10^7 UV-KEc into the volar aspect of each forearm for all participants, inflammatory exudate was obtained using a negative pressure suction cup at two time-points (4h and 48h), one per forearm for each volunteer. Cells were separated from the soluble mediator-containing supernatant by centrifugation and incubated with a fluorochrome-tagged antibody cocktail. Stained cells were acquired using the LSR Fortessa™ and analysed using Flowjo software. Geometric median MFI data are also shown for CD14 expressed as individual data points for (A) classical monocytes and (B) intermediate monocytes at the 48h time-point and depicted as histograms (C) for both monocyte subsets. Geometric median MFI data are shown for (D) CD62L and (E) CCR7 expression on blister neutrophils at 4h. Data are expressed as individual values with means with SD; $n = 7$. *$p < 0.05$, **$p < 0.01$, ***$p < 0.001$, ****$p < 0.0001$.

5.3.5 ATB-346 does not significantly alter vascular hyper-reactivity

Using laser Doppler imaging, blood flow at the site of UV-KEc-triggered inflammation was assessed. As previously shown by Motwani *et al.* (2016) (267), vascular hyper-reactivity (perfusion units), peaked at 24h in all groups, declining back to baseline by 48h (**Figure 5.4A**). At 4h and 24h, there was a trend towards increased hyper-reactivity in the ATB-346 group compared to naproxen and healthy control, although this was not significant and did not persist at other time-points (**Figure 5.4B**). A representative Doppler image time-course and accompanying photograph is shown in **Figure 5.4C**, showing the onset of inflammation at 4h with increasing vascular hyper-reactivity, peaking at 24h and decreasing to levels like that at baseline at 48h.

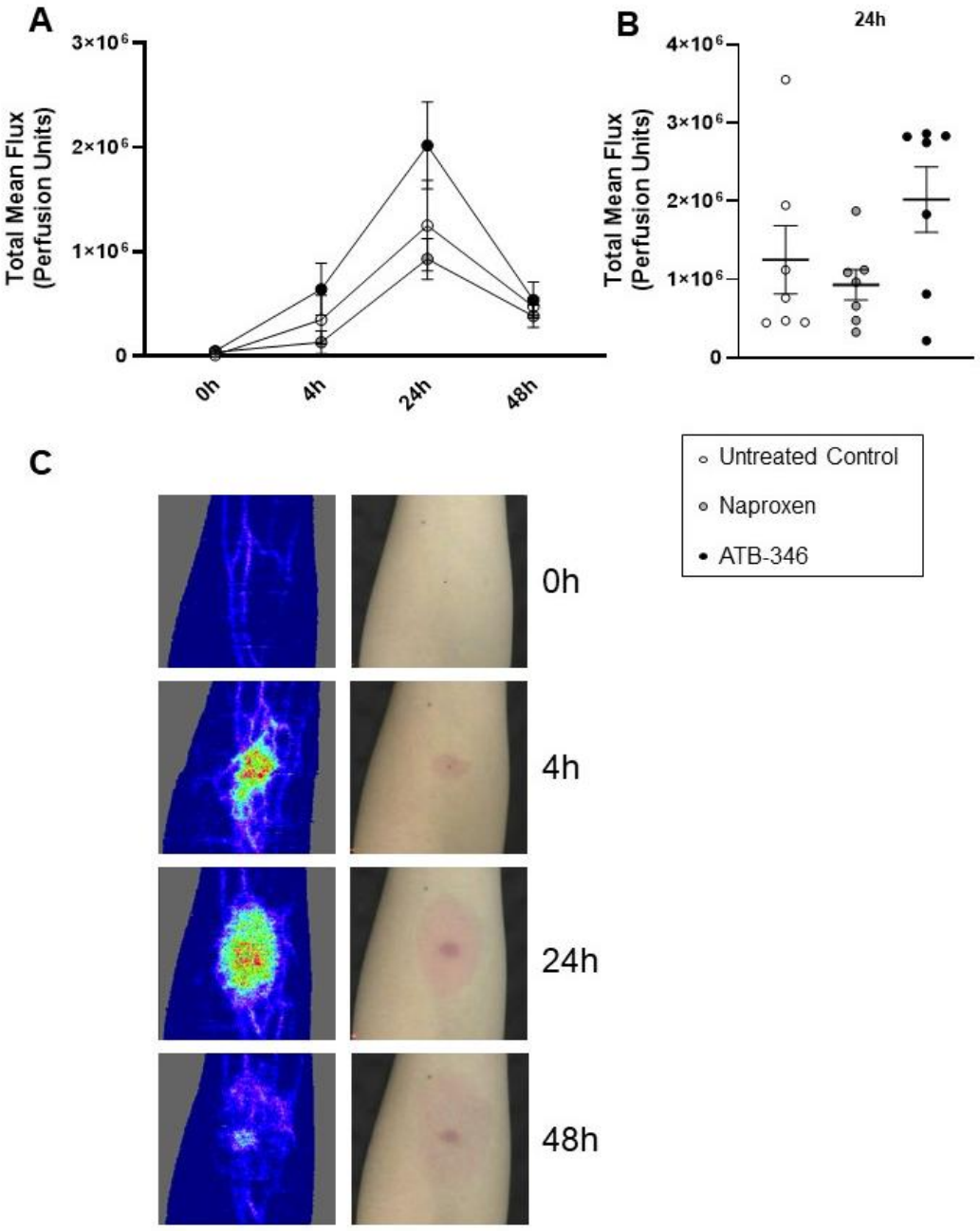

Figure 5.4. Assessment of vascular hyper-reactivity at the site of UV-KEc-triggered resolving dermal resolution. Healthy, male volunteers were randomised to receive either ATB-346 (250 mg daily), naproxen (500 mg twice daily) or no drug (untreated control) for 72h prior to UV-KEc injection. Acute inflammation was triggered by the intradermal injection of 1.5 x 10^7 UV-KEc suspended in 100 µL 0.9% sodium chloride. (A) Vascular response and total blood flow were assessed using a laser Doppler imager (moorLDI-HIR) and are shown here as total mean perfusion units, (B) total mean flux at 24h is shown as individual data points and (C) representative Doppler image and accompanying photograph is shown. Data are expressed as mean values with SD. *n* = 7.

5.3.6 ATB-346 and naproxen reduce pain and tenderness scores

A volunteer-reported visual analogue score was used to assess pain and elicited tenderness at the site of inflammation. Volunteers treated with ATB-346 reported significantly lower pain scores at the time-point of maximal neutrophil infiltration ($p < 0.001$), effects also observed with naproxen ($p < 0.001$) (**Figure 5.5A**). Volunteers exposed to ATB-346 also reported lower tenderness scores, following the application of a 100 g weight at the site of inflammation ($p < 0.05$). This represents the perceived pain on the application of the weight as opposed to the subjective sensation of pain without an external force applied.

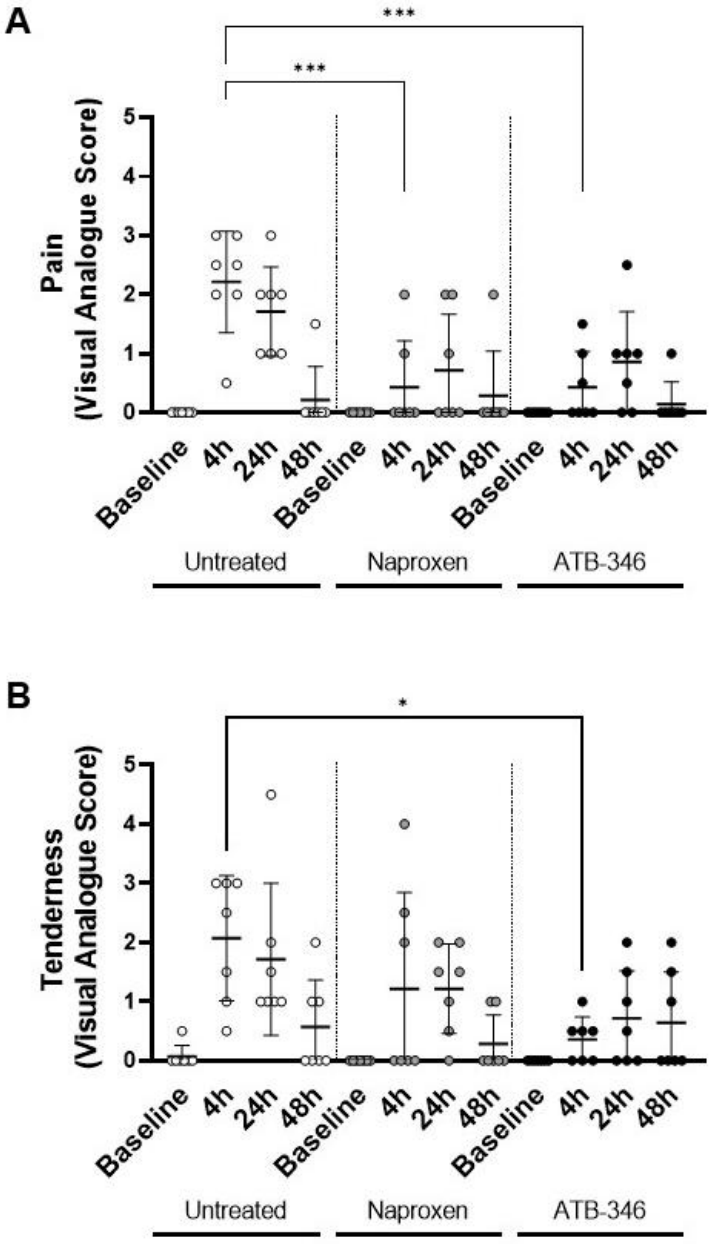

Figure 5.5. Clinical scores for pain and tenderness at the site of UV-KEc-triggered resolving dermal resolution. Healthy, male volunteers were randomised to receive either ATB-346 (250 mg daily), naproxen (500 mg twice daily) or no drug (untreated control) for 72h prior to UV-KEc injection. Volunteers were asked to rate the level of pain experienced at the site of acute inflammation, triggered by intradermal injection of 1.5 x 10^7 UV-KEc suspended in 100 µL 0.9% sodium chloride. Scores were given from 0 – 10, with 10 being the worst pain imaginable and 0 being no pain at all. (A) Pain scores are shown and (B) tenderness scores were also obtained using the same scale, following the application of a 100 g weight at the site. This represents the perceived pain on the application of the weight as opposed to the subjective sensation of pain without an external force applied. Data are presented as individual values mean with SD; $n = 7$. *$p < 0.05$, **$p < 0.01$, ***$p < 0.001$, ****$p < 0.0001$.

5.3.7 ATB-346 has no effect on temperature

Temperature at the site of inflammation measured using a digital thermometer (Thermofocus®) as well as centrally (forehead measurement). Temperature at the site of inflammation peaked at 24h in both drug-treated groups and 4h in untreated controls. (**Figure 5.6A**). No significant differences were detected when measuring central temperature at any time-point (**Figure 5.6B**). The ambient room temperature was measured at each throughout the study to control for background heat, with no significant differences were seen at any timepoint (**Figure 5.6C**). Neither drug significantly affected temperature throughout the study.

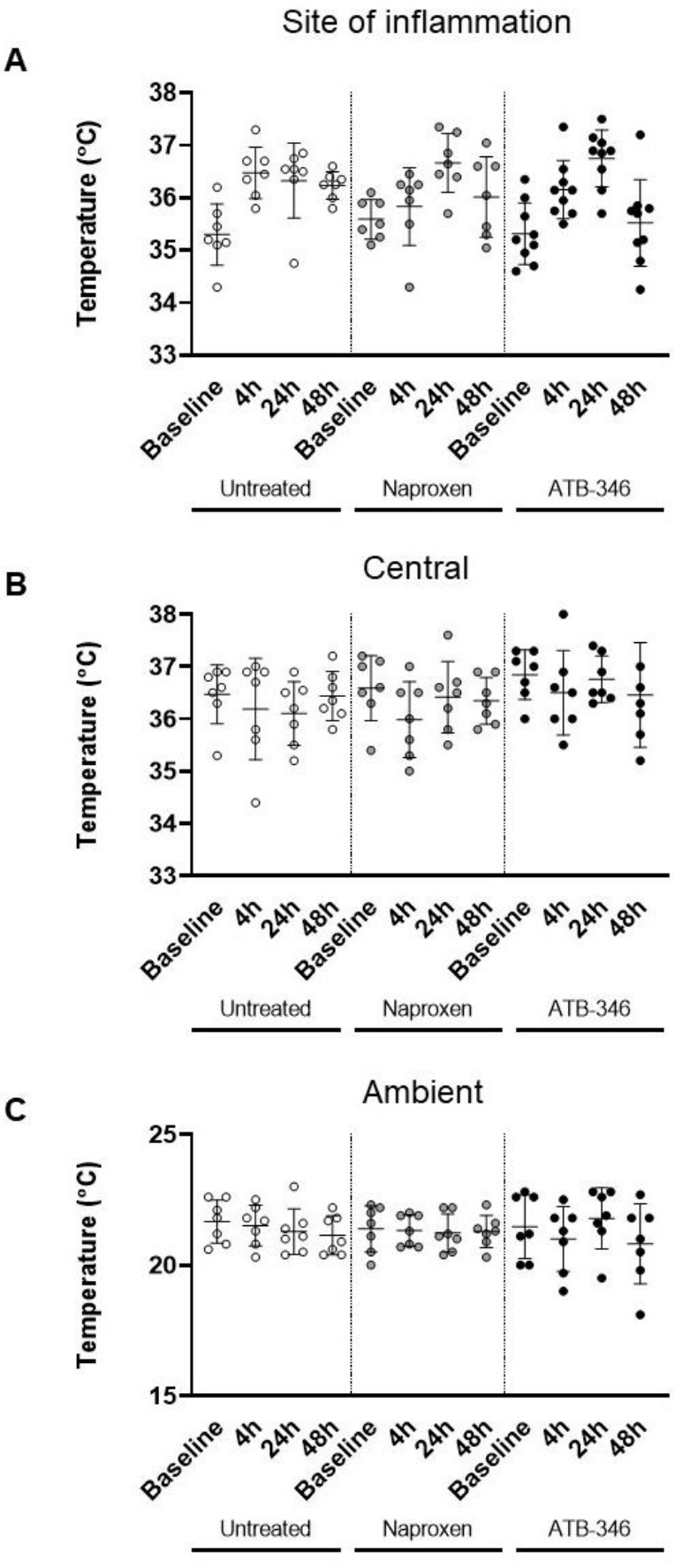
A
Site of inflammation
Temperature (°C)
38
37
36
35
34
33
Baseline
4h
24h
48h
Untreated
Naproxen
ATB-346
B
Central
C
Ambient
25
20
15

Figure 5.6. Central, mean site of inflammation and ambient temperature during UV-KEc-triggered dermal inflammation. Healthy, male volunteers were randomised to receive either ATB-346 (250 mg daily), naproxen (500 mg twice daily) or no drug (untreated control) 72h prior to UV-KEc injection. Inflammation was triggered by intradermal injection of 1.5 x 10^7 UV-KEc suspended in 100 µL 0.9% sodium chloride into each forearm. Temperature was taken using a digital thermometer (Thermofocus®) at (A) the site of inflammation (mean from both forearms), (B) centrally (forehead) and (C) ambient room temperature. Results for all clinical scores are shown here from baseline, 4h, 24h and 48h. Data are expressed as individual values with means with SD; n = 7.

5.3.8 ATB-346 and naproxen suppress PGE_2 equally but have no significant effect on TNF-α or IL-10 levels

Following UV-KEc-triggered inflammation, cell-free inflammatory blister exudate was probed for differences in relevant cytokines and lipid mediators. PGE_2 was chosen as a readout of COX activity, as the most abundant PG in humans. TNF-α and IL-10 were chosen as representative pro- and anti-inflammatory cytokines, respectively. As ATB-346 and naproxen alter lipid pathways, this brings about a differential alteration in TNF-α and IL-10 and affects phagocytosis, so in addition I also measured endotoxin levels as a readout of bacterial clearance. PGE_2 levels were significantly reduced in the blister at 4h in both ATB-346 ($p < 0.05$) and naproxen-treated volunteers ($p < 0.05$) compared to healthy control (**Figure 5.7A**). While there was a trend towards an increase in TNF-α (**Figure 5.7A**) and a reduction in IL-10 in both treatment groups, these were not significant (**Figure 5.7B**). ATB-346 ($p < 0.05$) and untreated volunteers ($p < 0.05$) demonstrated significantly lower endotoxin levels in the blister fluid at 4h compared to the naproxen group. Endotoxin had cleared in all groups by 48h (**Figure 5.7C**).

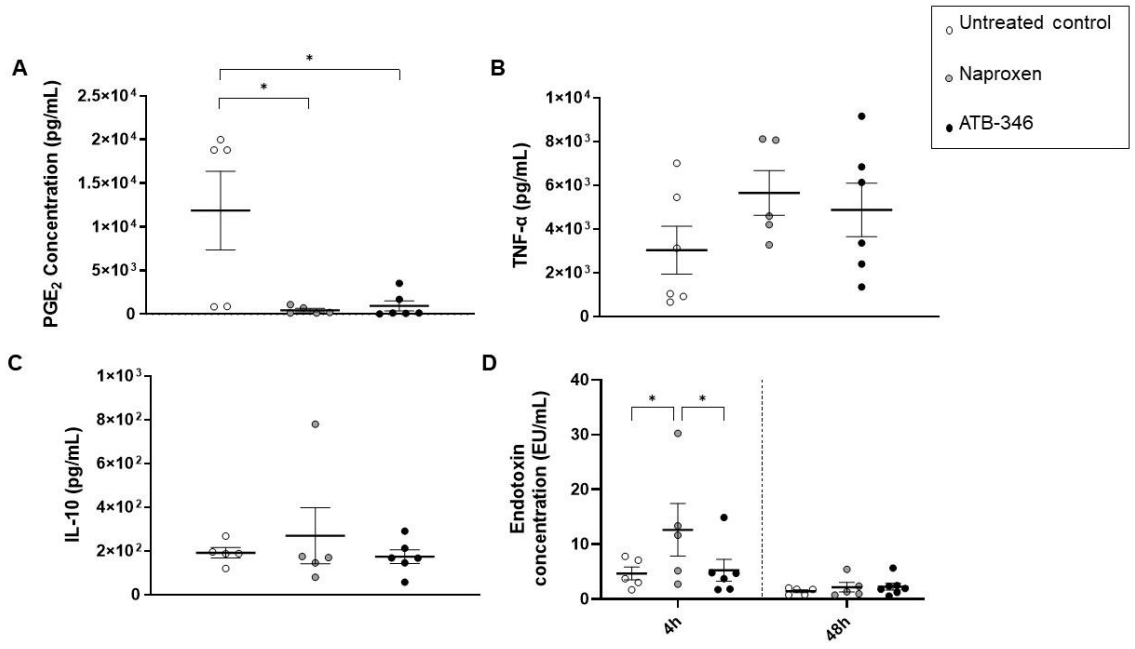

Figure 5.7. Soluble mediators and endotoxin concentrations at the site of UV-KEc-triggered resolving dermal inflammation. Healthy, male volunteers were randomised to receive either ATB-346 (250 mg daily), naproxen (500 mg twice daily) or no drug (untreated control) 72h prior to UV-KEc injection. Inflammation was triggered by intradermal injection of 1.5 x 10^7 UV-KEc suspended in 100 µL 0.9% sodium chloride into each forearm. Inflammatory exudate was obtained using a negative pressure suction cup at two time-points (4h and 48h), one per forearm for each volunteer. Cells were separated from the soluble mediator-containing supernatant by centrifugation. Supernatant PGE_2 concentration at 4h (A) was determined using an ELISA. Cytokines (TNF-α and IL-10) in the cell-free exudate were probed using a customised multiplex ELISA (B-C), respectively. Blister endotoxin levels (D) in blister fluid was measured using the *Limulus* amoebocyte lysate assay. Data are expressed as individual values with means with SD; *$p < 0.05$, **$p < 0.01$, ***$p < 0.001$, ****$p < 0.0001$.

5.4 Summary of findings

The key aim of this chapter was to investigate whether anti-inflammatory drugs could be safely used in a human dermal model of resolving acute inflammation following the injection of UV-KEc and whether the system was responsive to them. Additionally, I aimed to investigate the anti-inflammatory role of these drugs at a clinical level, looking at pain and tenderness scores, temperature and measuring vascular hyper-reactivity by laser Doppler imaging.

The main findings of this chapter are:

- The UV-KEc-triggered model of resolving dermal inflammation was responsive to the use of NSAIDs and can be used to investigate inflammatory responses in humans.
- Both ATB-346 and naproxen were able to hasten the resolution of inflammation as evidenced by a significant reduction in neutrophils at 4h compared to healthy controls.
- ATB-346 significantly reduced T/NK cells at 48h compared to untreated controls.
- ATB-346 significantly increased the expression of CD14 on both classical and intermediate monocyte subsets at 48h.
- There was a trend towards an increase in vascular hyper-reactivity at 4h and 24h in subjects treated with ATB-346.
- Naproxen and ATB-346 significantly reduced pain scores at 4h, and ATB-346 significantly reduced tenderness scores at 4h.
- Neither naproxen of ATB-346 altered temperature centrally or at the inflammatory site.
- Both naproxen and ATB-346 were able to suppress COX enzymes equally, as measured by a significant reduction in PGE_2 at 4h.

5.5 Discussion

In this chapter, I have established that the UV-KEc-triggered model of dermal inflammation can be used safely in humans, with no significant adverse events reported throughout the duration of the study. I have also shown that the model is responsive to both naproxen and ATB-346 and these drugs can be used in this system to investigate changes in inflammatory responses in terms of cellular trafficking, soluble mediators and clinical parameters. Whilst the investigation of the anti-inflammatory capacity of ATB-346 was not the primary aim of this chapter, several interesting findings were borne from this study.

5.5.1 ATB-346 is potently anti-inflammatory without compromising host immunity

PGE_2 is generated from AA by COX-1 and COX-2 enzymes and by the actions of different isoforms of PGES (398). PGE_2 is the most abundant PG detected in almost all tissues and exerts versatile physiological and pathological responses mediated through four PGE_2 receptors (EP1-4) (399, 400). Upon stimulation by pro-inflammatory stimuli, such as LPS, IL-1β and TNF-α, PGE_2 is upregulated by the expression of COX and *E. coli*-derived LPS in particular is known to potently induce PGE_2 production by macrophages in both mouse and human (401). Activation and infiltration of neutrophils has been shown to be inhibited by PGE_2 in animal models (402, 403). Furthermore, in a murine model of *Pseudomonas aeruginosa* infection, inhibition of EP2 signalling improved neutrophil migration and bacterial clearance by phagocytosis, suggesting this process if EP2-dependent (404). In addition to attracting macrophages in the early stages of inflammation, PGE_2 also inhibits macrophage activation through EP2 signalling (405). Phagocytic properties of alveolar macrophages have been shown to be inhibited in an EP2-dependent manner during infection with *Klebsiella pneumoniae* and *S. pneumoniae* in rat and mouse models, respectively, with phagocytosis restored through the inhibition of PGE_2 synthesis with non-selective COX inhibitors such as indomethacin (406, 407). In addition, PGE_2 also alters the cytokine response of macrophages and promotes an immunosuppressive

phenotype (408). Of note, PGE_2 induces the production of immunoregulatory cytokines, such as IL-10 and IL-17 (409, 410). Thus, using this model of dermal inflammation in humans, both naproxen and ATB-346 exert potent anti-inflammatory actions by the inhibition of COX activity and subsequent suppression of PGE_2 production, likely mediated *via* EP2 signalling. In turn, this leads to a reduction in pain, redness, swelling and temperature seen in volunteers treated with NSAIDs (411). Overall, the significant decrease in PGE_2 at 4h at the site of inflammation in both ATB-346 and naproxen-treated volunteers suggests that both drugs are equally capable of suppressing COX enzymes, however, neither drug influenced IL-10 concentration using this model. This finding is in agreement with another group that has shown that ATB-346 is as effective as naproxen at suppressing COX activity over a 24h period with a single dose, compared to the standard twice-daily regimen for naproxen (196).

In the inflamed skin at 4h there was also significantly lower levels of endotoxin in volunteers treated with ATB-346 compared to those treated with naproxen. By 48h, endotoxin had been cleared in both groups. H_2S has been shown to inhibit p38 MAPK signalling *in vitro* following doxorubicin-induced cardiotoxicity, resulting in increased cell viability (412), likely due to suppression of NF-κB signalling and subsequently reduced IL-1β production (413). *In vitro,* H_2S treatment in LPS-stimulated microglia and astrocytes has been shown to have an anti-inflammatory effect in terms of reduced NO and TNF-α production, due to H_2S inhibition of iNOS and p38 MAPK signalling pathways (120). It has also been proposed that H_2S polarises macrophages to the 'M2' phenotype macrophages, whose functions are largely anti-inflammatory playing a role in wound healing, tissue repair and the resolution of inflammation (414). In addition, macrophage scavenger receptors (SR), including SR-A1, SR-B2 (CD36), SR-D1 (CD68), SR-E1 (LOX-1), SR-E2 (CLEC7A), SR-E3 (CD206) and SR-11 (CD163), can bind to a range of ligands and enhance the elimination of non-self-targets (415). They are considered PRRs, recognising not only DAMPs but also PAMPs (416). They have an important role in host defence, by the recognition, internalisation and elimination of microbial antigens. H_2S is known to mediate the SR-A signalling pathway (110), which has a broad ligand specificity, including LPS found in Gram-negative bacteria such as *E. coli* (415). In a

rat model, exogenous H_2S treatment has been shown to reduce renal ischaemia-reperfusion injury by up-regulating endoplasmic reticulum stress-induced autophagy. Recently, de Maeyer *et al.* (2020) have shown in humans that inhibition of p38 MAPK in a human model of cantharidin-induced dermal inflammation rescued TIM-4 expression and improved efferocytic function of macrophages, promoting a pro-resolution phenotype (261). Thus, collectively this would suggest that the increased bacteria clearance seen in volunteers treated with ATB-346 compared to naproxen, as demonstrated by reduced endotoxin levels at the site of inflammation, may be due to H_2S-driven enhanced efferocytosis due to inhibition of p38 MAPK signalling and activation of macrophage SR-mediated autophagy. In addition, H_2S is also known to regulate the production and release of ROS and nitrogen species, including superoxide, hydrogen peroxide, hydroxyl radical, peroxynitrite and hypochlorous acid by neutrophils, which are involved in bacterial killing and clearance by phagocytosis (417). This could further contribute to the enhanced endotoxin clearance seen in ATB-346-treated volunteers.

Our group have previously shown that inhibiting COX activity with NSAIDs primes innate immune responses, increasing phagocytosis and NADPH oxidase-mediated bacterial clearing and that this was associated with elevated TNF-α (418). In this model, measurement of TNF-α in the inflammatory blister exudate, revealed comparably increased levels of this pro-inflammatory cytokine in the blister fluid in volunteers treated with both ATB-346 and naproxen, highlighting that ATB-346 does not compromise host immunity, unlike corticosteroids, where their use is associated with significantly increased risk of infection.

5.5.2 ATB-346 may affect neutrophil numbers at the site of inflammation by more than one mechanism

NSAIDs are known to reduce tissue inflammation by suppressing COX activity, resulting in a reduction in PG synthesis, promoting apoptosis (121), activating PPAR-α and PPAR-γ and inhibiting neutrophil aggregation and granulation (419). They can also disrupt normal signalling events and modify processes necessary for immune function, including cell adhesion (195, 420). In humans, it has been shown that H_2S significantly downregulates neutrophil CD62L in an ADAM-17-dependent manner, as well as inhibitory effects on the production of pro-inflammatory cytokines, including IL-17, TNF-α and IFN-γ (421). ADAM-17, also known as TNF-α-converting enzyme (TACE), mediates the shedding of inflammatory cytokines and cytokine receptors and thus plays a central role in inflammation (422). Activation of p38 MAPK phosphorylates TACE and CD62L is then released from its interaction with tissue inhibitor of metalloproteinase-3 (TIMP3). In the absence of p38 MAPK signalling, the activity of TACE is inhibited by the formation of dimers and its interaction with TIMP3 (423). Overall, upon pro-inflammatory stimulation, the activity of TACE is increased by p38 MAPK signalling leading to the cleavage of CD62L (423). NSAIDs have also been shown to interfere with the ability of neutrophils to initiate interaction with endothelial cells, by triggering CD62L shedding through the production of ROS (420). Specifically, using neutrophils from patients with chronic granulomatous disease (a hereditary defect in the NADPH oxidase complex that results in the reduction of ROS production), Dominguez-Luis *et al*. (2013) demonstrated that NSAIDs require NADPH oxidase-dependent generation of superoxide anion to trigger L-selectin shedding (424). Given that NSAIDs inhibit p38 MAPK activity, the significant decrease in neutrophil CD62L expression at 4h in the blister fluid of volunteers treated with ATB-346 and naproxen was unlikely mediated through p38 MAPK signalling but could be due to NADPH oxidase-dependent ROS production. As there was no significant difference between the drug-treated groups in terms of neutrophil numbers, this effect is also unlikely to be mediated *via* H_2S. Overall, the significant reduction in CD62L in volunteers taking naproxen and ATB-346 at the site of inflammation at 4h and subsequent reduced capacity for interaction at the endothelium, may contribute to the significant reduction in infiltrating neutrophils at this time.

On further assessment of the phenotype of infiltrating cells to the site of UV-KEc stimulated inflammation, I have identified a further possible novel mode of action of ATB-346. Neutrophils, being the most abundant of human circulating phagocytes, are well known to be the first cells to infiltrate into sites of acute inflammation (425). Their purpose is to phagocytose microorganisms and immune cell debris. The dogma dictates that to 'switch off' inflammation, these effete cells then undergo programmed cell death by apoptosis and are cleared by mononuclear phagocytes, beginning the resolution phase of inflammation (426, 427). Beauvillain *et al*. (2009) have shown that CCR7 is rapidly expressed at the neutrophil membrane following stimulation and that these cells migrate in response to the CCR7 ligands CCL19 and CCL21 *in vitro* (428). They further demonstrated *in vivo,* following the injection of complete Fruend adjuvant, a rapid recruitment of neutrophils to the lymph nodes in wild-type mice, but not in *Ccr7*$^{-/-}$ animals, suggesting this process is CCR7-dependent. More recently it has been shown that certain populations of neutrophils may re-enter the circulation following the initial extravasation into inflamed tissue in process of reverse migration (429–431). These cells subsequently migrate to lymph nodes to facilitate antigen presentation, thereby bridging the innate and adaptive immune system with this subset of neutrophils having been shown to express CCR7, taking on a more dendritic cell-like phenotype (432). Given that I have shown, in the presence of ATB-346, a significant reduction in neutrophil numbers at 4h at the site of inflammation, in combination with an increase in CCR7 expression on these cells, it is tempting to speculate that H_2S acts directly on neutrophils, not only to reduce their infiltration into the site of inflammation by COX-mediated PG inhibition, but to also increase their expression of CCR7. In doing so, this promotes their migration to secondary lymphoid tissue and subsequent antigen presentation. It is therefore perhaps not surprising that between 4h and 24h, 29% of volunteers treated with ATB-346 reported a heaviness in their axillae associated with erythematous, lymphatic tracking towards the axillary lymph nodes; the first major draining lymphoid tissue in proximity to the site of UV-KEc injection. This phenomenon was not observed in any untreated controls or those taking naproxen.

Whilst numerous biological processes likely contribute to the significant reduction in neutrophil numbers seen in this model of inflammation, reported mechanisms of

neutrophil inhibition vary between different NSAIDs (433). This further suggests that different NSAIDs may have direct effects on neutrophil activation and accumulation, as well as their effects on phagocytosis and endotoxin clearance, independent of their shared inhibition of PG synthesis.

5.5.3 Gasotransmitter-induced vascular dilatation is a pro-resolution effect

At both 4h and 24h, there was notably increased vascular dilatation in volunteers treated with ATB-346 compared to untreated controls and those treated with naproxen, albeit not significant. Counterintuitively, this represented increased blood flow at the site of UV-KEc injection and hence an increase in inflammation in those treated with an anti-inflammatory drug. Paradoxically, this increased vascular hyper-reactivity correlated with significantly reduced pain and tenderness scores in these volunteers. H_2S is one of the three classical gaseous mediators, along with NO and CO, which both play important roles in physiological and pathophysiological processes. There has long been conflicting literature as to whether H_2S is either pro- or anti-inflammatory (107, 115, 434). It is feasible that the H_2S moiety released from ATB-346 induces vasodilatation at the site of UV-KEc-triggered inflammation, accounting for the difference between the two drug treatment groups. Whilst this did not meet statistical significance for ATB-346, I propose this may represent a novel mode of action of ATB-346 in that this vasodilatory effect may facilitate extravasation of neutrophils. This could therefore also contribute to the reduction in numbers of neutrophils seen here in those treated with ATB-346 at 4h. The biological significance of H_2S in this system remains unclear but would suggest that the presence of H_2S itself may reduce neutrophil infiltration into the site of inflammation. It is conceivable that the dose of H_2S liberated from the standard 250 mg once daily dosing of ATB-346 was insufficient to induce a significant physiological vasodilation detectable using laser Doppler imaging as a surrogate marker of vascular hyper-reactivity. It would therefore be interesting to see if a higher dose of ATB-346 and consequent increased concentration of liberated H_2S would lead to a further increase in vascular hyper-reactivity at the site of inflammation. Unfortunately, the 250 mg once daily dosing of ATB-346 used in this study was the maximum dose investigated in clinical trials to

date (197, 435) and therefore there is no safety data available at a higher dose so this would not be possible. Another strategy would be to employ a H_2S donor, such as a sulfide salt (including sodium hydrosulfide or sodium sulfide) (436). These can give access to biologically relevant amounts of H_2S and have been used successfully both *in vitro* and in rodent studies, although have not been safely used *in vivo* in humans at the time of writing. Sulfide salts hydrolyse instantly on dissolution in water with equilibrium forming between H_2S, HS^- and S^{2-} species, thus allowing volatilisation of H_2S (436, 437). This lowers the overall concentration of sulfur species and with further oxidation of HS^- and the concentration of H_2S in solution reduces further. Therefore, this means that it is challenging to deliver meaningful concentrations of H_2S in a biological system, making donors unsuitable for use in this model. Another further strategy would be to deliver inhaled H_2S given the accessible and non-invasive nature of this route of administration. Unfortunately, the gas can be toxic and is also highly flammable, meaning administration and storage of the gas itself limits this as a viable method of H_2S delivery in humans.

5.5.4 ATB-346 may modulate the pro-inflammatory role of monocytes

There were significantly fewer classical monocytes in the ATB-346 group at 48h with a trend towards fewer in the naproxen group, compared to untreated controls. It is known that CD14 is involved in LPS-induced monocyte activation and plays a crucial role in fighting infection and inflammation, as well as regulating numerous cellular responses (438, 439). A significant reduction in expression of CD14 on both classical and intermediate monocytes at this time of inflammation resolution suggests exposure to both ATB-346-containing naproxen and native naproxen alters the phenotype of these cells and is therefore likely a PG-mediated event. A reduction in CD14 may confer a less inflammatory phenotype, perhaps with reduced phagocytic and scavenging capability, reduced production of ROS, antigen presentation and proliferation or stimulation of T cell responses. Given that that endotoxin and therefore bacteria had cleared by this time, it is also possible that these cells downregulated CD14 expression in response to reduced LPS levels at the site of inflammation. As PGs (PGE_1, PGE_2 and PGA_1) increase CD14 expression *via* cAMP-dependent protein

kinase A (440), it is likely that the use of both ATB-346 and naproxen led to a COX-mediated reduction in the expression of CD14, as seen in both drug-treated groups. *In vitro*, IL-4 has also been shown to downregulate CD14 expression on human monocytes and that an LPS-induced increase in CD14 expression rescued monocytes from apoptosis, whereas IL-4 treatment evoked apoptosis (441, 442) The data presented here therefore suggests that this observation was due to exposure to an NSAID and PG suppression rather than a drug-specific effect of ATB-346, likely mediated *via* IL-4 signalling and cAMP-dependent protein kinase A.

5.5.5 Clinical significance

From a clinical perspective, both ATB-346 and naproxen significantly reduced pain at the site of inflammation at 4h, the time-point of maximal neutrophil infiltration. This suggests that a reduction in infiltrating immune cells contributed to the analgesic effect of both drugs in addition to the role of soluble mediators. The mechanism by which pain is ameliorated by both ATB-346 and naproxen can in part be explained by inhibition of COX and reduction in PG synthesis. Whilst mononuclear phagocytes and fibroblasts are the predominant cells producing PGs, neutrophils also provide a source of these. PG-mediated pain is mainly conferred indirectly by PGE_2, one the most abundant PGs, through EP1 (and to lesser extent EP3) receptor signalling, that acts on peripheral sensory neurones at the site of inflammation, as well as on central neuronal sites, leading to the characteristic redness, swelling and pain (443). PGI_2 is also an important mediator in the development of tissue oedema, with the swelling itself activating local baroreceptors and subsequent increased nociceptive signalling pathways (443). Therefore, a significant reduction in PG-producing neutrophils, as well as the direct effect of both drugs on COX activity and on other PG-producing cells, is likely the cause for reduced pain scores in both drug-treated groups.

Independent of inhibition of PG synthesis, ATB-346 may also interfere with G-protein-mediated signal transduction leading to a reduction in pro-inflammatory cytokines, including IL-1β, IL-6 and TNF-α (444). Several animal studies have shown

exposure to H_2S, for example in mice with osteoarthritis, reduces pain but the mechanism for this remains poorly understood (445). It is suggested that the anti-nociceptive actions of H_2S may be mediated by the opening of potassium-ATP channels (K-ATP) (446, 447), activation of Kv7 (448) and the Nrf2 transcription factor signalling pathways (445). These PG-independent mechanisms could explain why ATB-346 resulted in significantly lower tenderness scores at 4h compared to healthy control, the effect of which was not seen in those treated with naproxen. Clearly the generation of pain following the acute inflammatory insult and the effect of the two drugs investigated in this model is complex, involving numerous biologic pathways. Therefore, both ATB-346 and naproxen used here demonstrated analgesic effect mediated through the suppression of COX and PG synthesis through EP1 and EP3, whereas the addition of H_2S gave additional analgesic effect, likely through the inhibition of NF-κB, p38 MAPK, Kv7, K-ATP, Nrf2 and other pathways.

Pro-inflammatory cytokines, through their binding to receptors on brain endothelial cells, evoke fever by eliciting PGE_2 synthesis in these cells (449). PGE_2 is known to be the final mediator of fever, which binds to the EP3 receptor in the preoptic hypothalamus and initiates thermogenesis. Vane (1971) was the first to show that NSAIDs exert their antipyretic action by inhibition of PG synthesis (450). Temperature, one of the other cardinal signs of acute inflammation, was not significantly different between groups at any time-point, however, it was of interest that both ATB-346 and naproxen delayed the peak temperature at the site of inflammation from 4h as seen in untreated controls, until 24h. COX-2 is rapidly inducible by inflammatory signals including bacterial endotoxin and pyrogenic cytokines including IL-1β, TNF-α and IL-6 (451), so this delay in peak temperature was likely due to suppression of PGs by both NSAIDs.

As the opioid crisis continues in the developed world (201, 202), it is vitally important that we can find new therapeutics that are both efficacious, but also agreeable to patients in terms of adverse effects. This is especially important, particularly long-term, given major issues with tolerance and dependence with opioid medication (202).

Conventional NSAIDs are effective at reducing the signs of inflammation, but have been limited in their use, predominantly due to GI, cardiovascular and renal complications (191–194). From a clinical point of view, it has been shown that after oral administration of ATB-346, plasma levels of naproxen derived from the compound were much lower than equimolar doses of naproxen but maintained cyclooxygenase (COX) inhibition and analgesic effects equally, allowing reduced exposure to the GI irritant, but with equivalent anti-inflammatory effects (115, 196). More recently, in a recent Phase 2b safety clinical trial in healthy volunteers, the incidence of upper GI ulceration in subjects taking standard dose twice-daily naproxen was over 42%; significantly greater than the rate of ulceration of only 2.5% ($p < 0.001$) in subjects taking an equi-effective (in terms of COX inhibition) dose of ATB-346 once daily (435). ATB-346 is therefore an attractive alternative to traditional NSAIDs, whose long-term use is limited by significant GI and cardiovascular adverse effect.

A further double-blind, placebo-controlled Phase 2b efficacy trial in patients with knee osteoarthritis showed significantly greater improvement in the Western Ontario and McMaster Universities Arthritis Index (WOMAC) relative to the average NSAID efficacy (435) and a Phase 3 multi-arm trial using ATB-346 in acute pain is soon to open for recruitment. Overall, the data presented here supports the use of ATB-346 in further clinical trials for the treatment of inflammation, including in RA patients.

In this chapter, I have established that the UV-KEc-triggered model of dermal inflammation can be used safely in humans, with no significant adverse events reported throughout the duration of the study. The use of both naproxen and ATB-346 were well tolerated by all volunteers following the injection of UV-KEc. I propose that ATB-346 represents a novel H_2S-NSAID as a viable alternative to conventional NSAIDs, suitable for longer term use with reduced GI adverse effects. ATB-346 exerts its effect through numerous signalling pathways and I have described a potential novel mode of action mediated through the release of H_2S.

Having shown that that the human UV-KEc-triggered dermal model of inflammation is responsive to the use of a traditional NSAID and a novel H_2S-NSAID, I next wanted

to investigate the immune responses of patients with RA. Before using pharmacological agents in the system, I first wanted to assess the acceptability of RA patients to the model so set out to recruit RA patients not currently on medication and without active disease, aiming to identify any anti-inflammatory/pro-resolution signals which may be important for maintaining disease remission.

6 Characterising the immune response of RA patients using a UV-KEc-triggered resolving dermal model of inflammation

6.1 Introduction

Using UV-KEc as the inflammatory stimulus, I have developed novel resolving and non-resolving models of murine inflammation and shown that the use of conventional and novel RA therapies can be used safely in a complementary human UV-KEc-triggered model of dermal inflammation in healthy volunteers. I next wanted to use the same human dermal model of inflammation in RA patients, with the aim of identifying anti-inflammatory/pro-resolution signals which may inform on the pathways involved in the biological maintenance of disease remission. In doing so, I aimed to develop a platform in which novel and existing pharmacological agents can be used to further our understanding of RA pathophysiology, but also identify druggable targets for the development of new treatments for RA. Most studies looking at immune responses in patients with autoimmune disease are limited in that RA patients are routinely on immunosuppressive treatment, meaning that the underlying dysregulation of immune response and development of pathophysiological processes are confounded by treatment effects on immune cell function. Similarly, most studies are *ex vivo* and have been performed on blood in steady state or using *in vitro* stimulation. As such, there is a paucity of translational, experimental medicine studies to date addressing the fundamental differences *in vivo* of the immune response of RA patients.

6.2 Hypothesis

Using the skin blister model as a window into the immune system of patients with RA, I set out to complete a human study looking at the immune response of these patients, but importantly those patients that are either off treatment or treatment naïve. The aim being to identify anti-inflammatory/pro-resolution signals. To understand whether pain pathways are also aberrant in patients with RA, I also wanted to quantify pain and tenderness scores along with other clinical parameters of acute inflammation. These experiments will address the hypothesis that: **patients with RA have a dysregulated inflammatory response following the intradermal injection of UV-KEc.**

The aims of this chapter were:

1. Conduct a human study to investigate the underlying immune defects in patients with RA, specifically looking at cellular profiles and cell surface marker expression.
2. Investigate clinical parameters of acute inflammation in these volunteers including pain, tenderness and temperature.
3. Quantify the blood flow/vascular hyper-reactivity at the site of inflammation using laser Doppler imaging.

6.3 Results

6.3.1 Study volunteer baseline characteristics

Most volunteers in this study were female (91.6%). The mean age for the healthy control group was 44.3 years and 53.8 years for the RA group. There were no significant differences in terms of age, height or weight. Most participants identified as white (58.3%), followed by southeast Asian (25.0%) and then mixed ethnicity (16.6%).

Table 6.1 Baseline characteristics of RA study participants. Gender, age, ethnicity, height and weight for all volunteers are shown. No significant differences were seen between participants within in each group or between groups for either age, height or weight. Depicted are healthy controls (HC) and rheumatoid arthritis (RA), female (F) and male (M)

	Group	Gender	Age (years)	Ethnicity	Height (cm)	Weight (kg)
HC	1	F	64	White British	157	66.7
	2	F	46	Southeast Asian	160	69.0
	3	F	51	Southeast Asian	160	62.0
	4	F	36	White British	163	66.0
	5	M	38	White New Zealand	178	76.0
	Naïve	F	31	Southeast Asian	160	62.0
		Mean	**44.3**	**-**	**163**	**67.0**
RA	1	F	54	White British	172	68.5
	2	F	34	White British	182	58.0
	3	F	55	White British	174	67.1
	4	F	61	Mixed (white/Caribbean)	175	58.0
	5	F	64	Mixed (white/Caribbean)	168	57.0
	Naïve	F	55	White British	174	67.1
		Mean	**53.8**	**-**	**174.2**	**62.6**

6.3.2 Blister volumes, total blister immune cell and circulating immune leucocyte numbers

Blister volume was higher at 24h compared to 48h in both RA and healthy controls, with no significant differences between the groups (**Figure 6.1A**). In both groups, total immune cell numbers were higher at 48h compared to 24h, with no significant differences between the groups (**Figure 6.1B**). Cell counts from ACK lysed peripheral blood peaked at 4h in healthy controls and 24h in RA patients, although there were no significant differences at any time-point (**Figure 6.1C**).

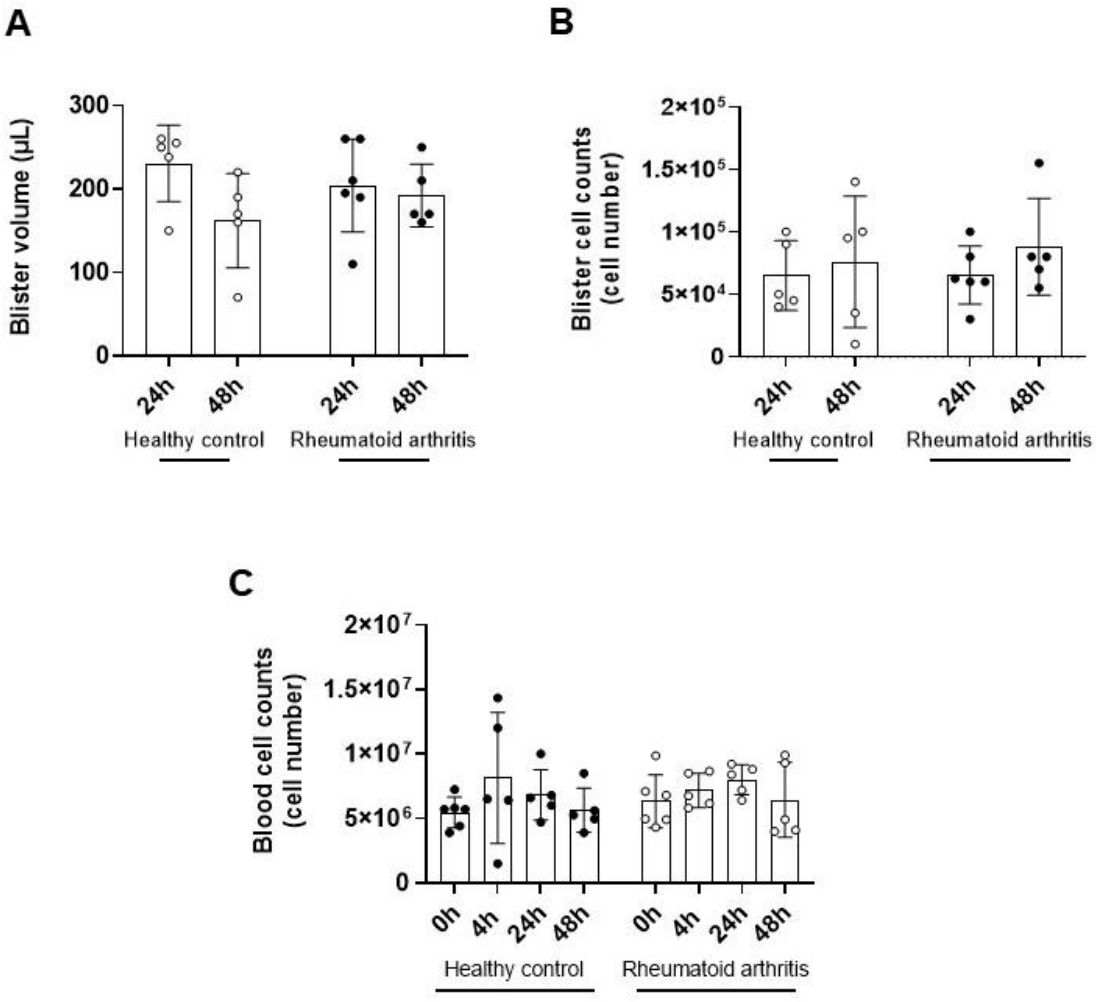

Figure 6.1. Inflammatory parameters following UV-KE-triggered dermal inflammation. Following the intradermal injection of 1.5 x 10^7 UV-KEc into the volar aspect of each forearm of RA patients and healthy controls. Inflammatory exudate was obtained using a negative pressure suction cup at two time-points (24h and 48h), for each volunteer with single cell suspensions obtained by ACK lysis. Blister volume was determined and blister and blood cells counted using a manual haemocytometer. Depicted are (A) blister volume (24h and 48h), (B) blister cell counts (24h and 48h) and (C) blood cell counts (0h, 4h, 24h and 48h). Data are expressed as individual values with the mean with SD at each time-point; n = 5.

6.3.3 Temporal profiles of immune cell infiltration into the blister and circulating blood following injection with 1.5 x 10^7 UV-KEc

6.3.3.1 Blood immune cell profiles following the intradermal injection of UV-KEc

Instead of using polychromatic flow cytometry as utilised in **Chapter 5**, for this study I employed time of flight mass cytometry (CyTOF). Unlike flow cytometry, this allows the simultaneous assessment of up to 50 cell surfaces markers, along with intracellular markers and is not limited in spectral overlap and difficulties with compensation as antibodies are conjugated to heavy metal isotopes rather than fluorophores. The Maxpar® Direct Immune Profiling Assay (MDIPA) kit was used with the addition of additional drop-in intracellular and surface markers.

In blood, neutrophil numbers were maximal at 4h in healthy controls and at 24h in RA patients following intradermal UVK-Ec injection, although no signficant differences were seen at any time-point (**Figure 6.2A**). Eosinophils were maximal at 24h in both groups, but were fewer in RA patients at all time-points, although not significant (**Figure 6.2B**). Basophil numbers were significantly higher at baseline in RA patients ($p < 0.05$), compared to healthy controls with no significant differences seen at any other time-point (**Figure 6.2C**).

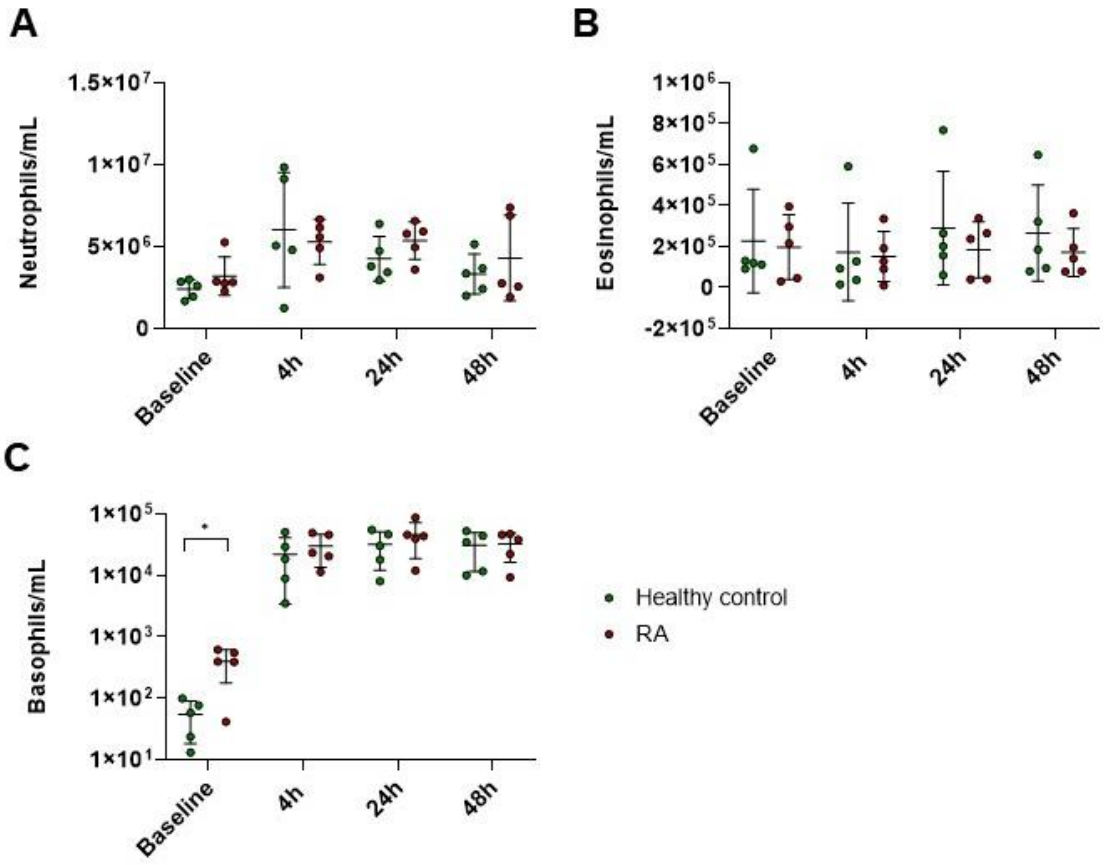

Figure 6.2. Temporal profiles of circulating granulocytes following UV-KEc-triggered dermal inflammation. Following the intradermal injection of 1.5 x 10^7 UV-KEc into the volar aspect of each forearm of RA patients and healthy controls, single cell suspensions were obtained by ACK lysis of peripheral blood at baseline (0h), 4h, 24h and 48h. Cells were incubated with a metal isotope-tagged antibody cocktail. Stained cells were acquired using the Helios XT SAE 20W-50 system and analysed using Flowjo software. Depicted are (A) neutrophils, (B) eosinophils and (C) basophils. Cell numbers are shown as cell count per millilitre. Data are expressed as individual values with the mean with SD at each time-point; $n = 5$. *$p < 0.05$, **$p < 0.01$, ***$p < 0.001$, ****$p < 0.0001$.

At baseline, RA patients had significantly higher numbers of circulating total monocytes ($p < 0.05$) (**Figure 6.3A**), intermediate monocytes ($p < 0.05$) (**Figure 6.3C**) and non-classical monocytes ($p < 0.01$) (**Figure 6.3D**), compared to healthy controls. Total monocytes, classical, intermediate and non-classical moncytes increased from baseline at 4h and remained elevated at 72h (**Figure 6.3A-D**).

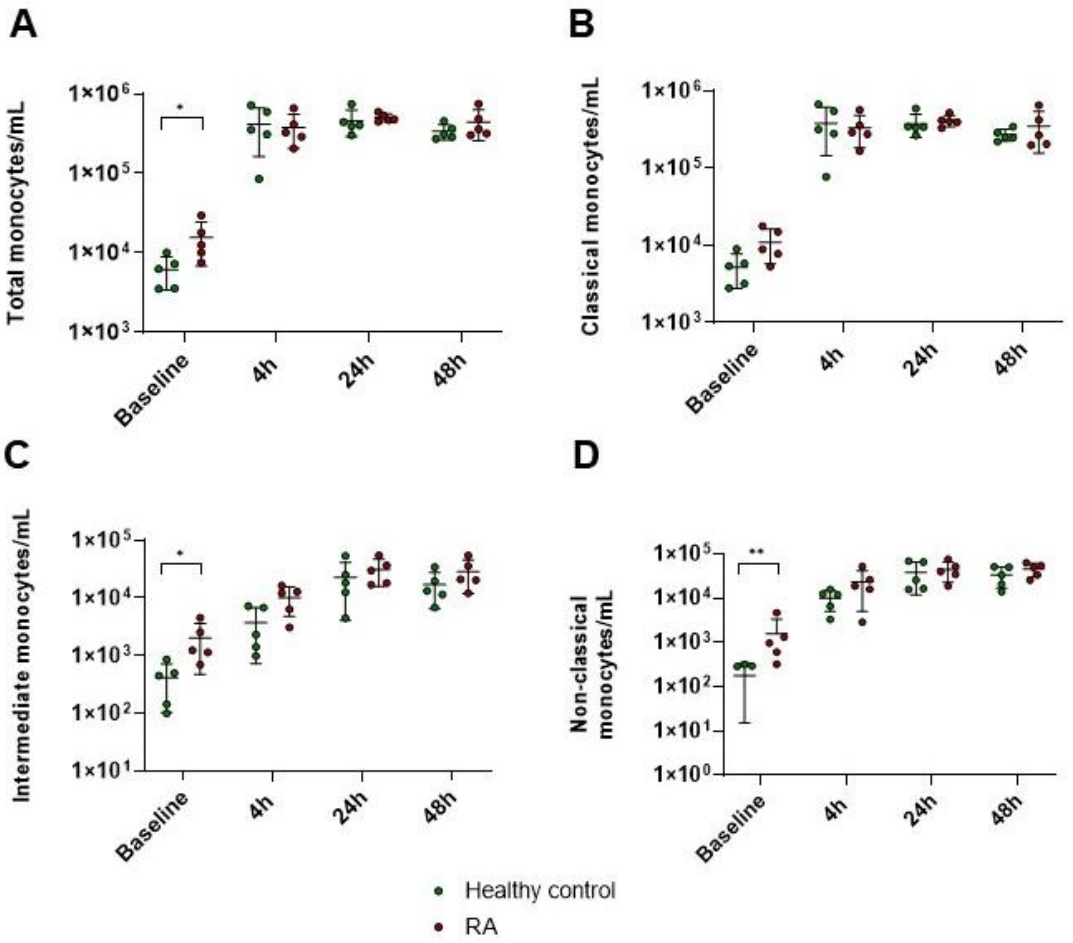

Figure 6.3. Temporal profiles of circulating monocyte subsets following UV-KEc-triggered dermal inflammation. Following the intradermal injection of 1.5 x 10^7 UV-KEc into the volar aspect of each forearm of RA patients and healthy controls, single cell suspensions were obtained by ACK lysis of peripheral blood at baseline (0h), 4h, 24h and 48h. Cells were incubated with a metal isotope-tagged antibody cocktail. Stained cells were acquired using the Helios XT SAE 20W-50 system and analysed using Flowjo software. Depicted are (A) total monocytes, (B) classical monocytes, (C) intermediate monocytes and (D) non-classical monocytes. Cell numbers are shown as cell count per millilitre. Data are expressed as individual values with the mean with SD at each time-point; $n = 5$. *$p < 0.05$, **$p < 0.01$, ***$p < 0.001$, ****$p < 0.0001$.

There were signficantly higher numbers of myeloid dendritic cells in circulation in the RA group at baseline compared to healthy controls ($p < 0.05$) (**Figure 6.4C**). No significant differences were seen in total dendritic cells or dendritic cell subsets at any other time-point (**Figure 6.4A-D**).

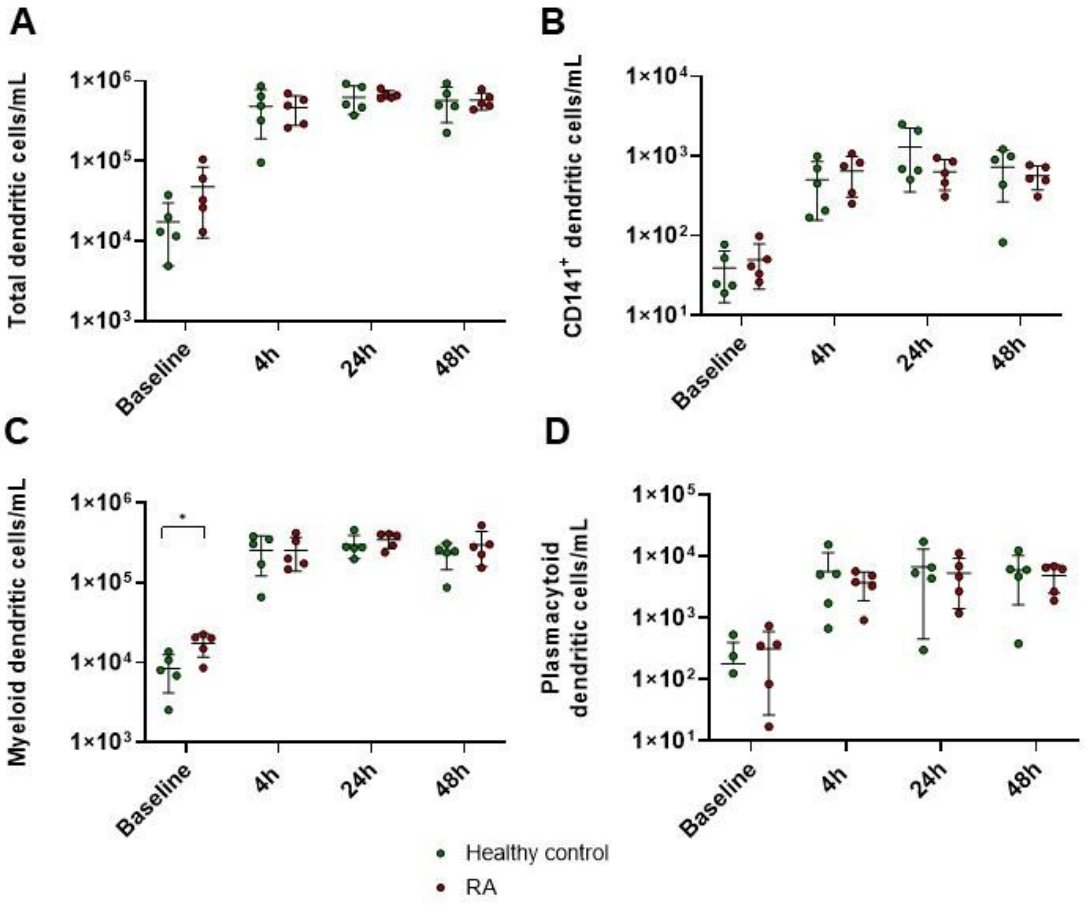

Figure 6.4. Temporal profiles of circulating dendritic cell subsets following UV-KEc-triggered dermal inflammation. Following the intradermal injection of 1.5 x 10^7 UV-KEc into the volar aspect of each forearm of RA patients and healthy controls, single cell suspensions were obtained by ACK lysis of peripheral blood at baseline (0h), 4h, 24h and 48h. Cells were incubated with a metal isotope-tagged antibody cocktail. Stained cells were acquired using the Helios XT SAE 20W-50 system and analysed using Flowjo software. Depicted are (A) total dendritic cells, (B) $CD141^+$ dendritic cells, (C) myeloid dendritic cells and (D) plasmacytoid dendritic cells. Cell numbers are shown as cell count per millilitre. Data are expressed as individual values with the mean with SD at each time-point; $n = 5$. *$p < 0.05$, **$p < 0.01$, ***$p < 0.001$, ****$p < 0.0001$.

No significant differences were seen in total αβ or γδ T cell numbers at any time-point (**Figure 6.5A-B**). Baseline circulating total $CD4^+$ T cells were significantly higher in RA patients compared to healthy controls ($p < 0.05$) (**Figure 6.5C**), but no significant differences were identified at any other time-point. There were significantly fewer $CD8^+$ T cells in RA patients at 48h compared to healthy controls ($p < 0.05$) (**Figure 6.5D**).

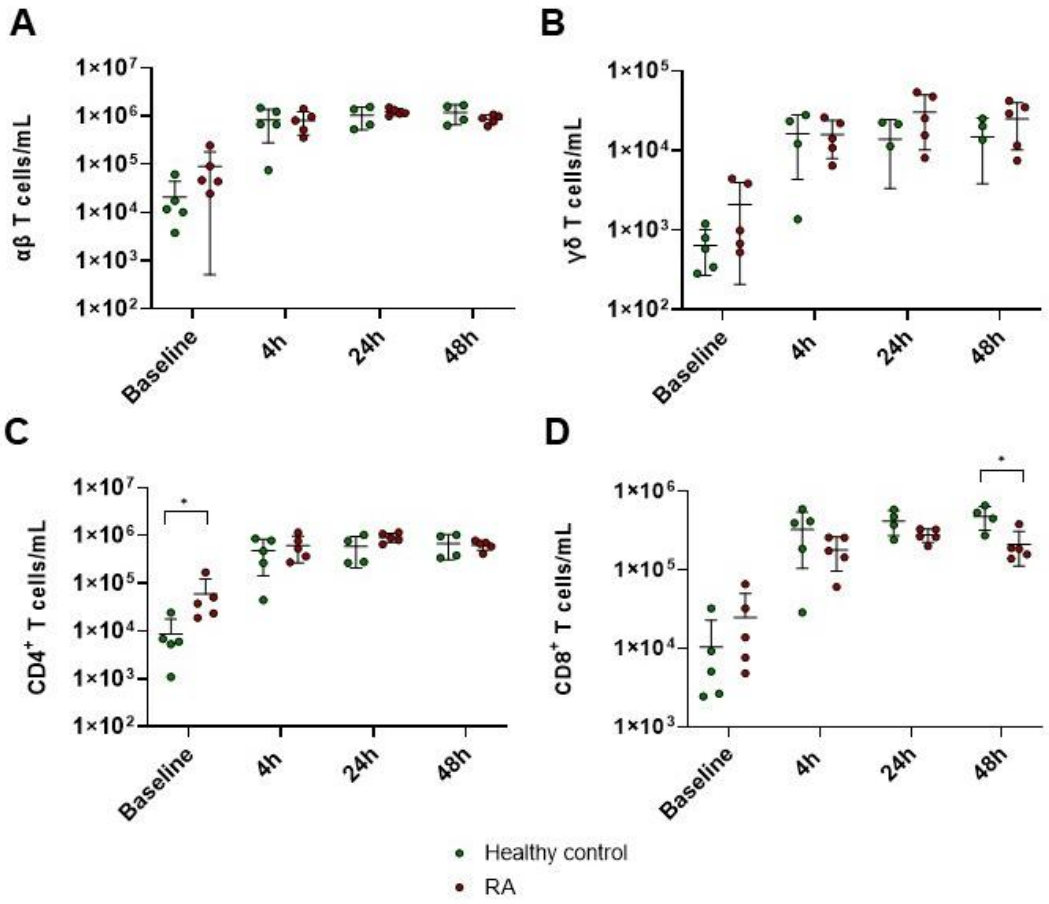

Figure 6.5. Temporal profiles of circulating T cell subsets following UV-KEc-triggered dermal inflammation. Following the intradermal injection of 1.5 x 10^7 UV-KEc into the volar aspect of each forearm of RA patients and healthy controls, single cell suspensions were obtained by ACK lysis of peripheral blood at baseline (0h), 4h, 24h and 48h. Cells were incubated with a metal isotope-tagged antibody cocktail. Single cell suspensions were obtained by ACK lysis at baseline (0h), 4h, 24h and 48h. Cells were separated from the soluble mediator-containing supernatant by centrifugation and incubated with a metal isotope-tagged antibody cocktail. Stained cells were acquired using the Helios XT SAE 20W-50 system and analysed using Flowjo software. Depicted are (A) αβ T cells, (B) γδ T cells, (C) total $CD4^+$ T cells and (D) total $CD8^+$ T cells. Cell numbers are shown as cell count per millilitre. Data are expressed as individual values with the mean with SD at each time-point; $n = 5$. *$p < 0.05$, **$p < 0.01$, ***$p < 0.001$, ****$p < 0.0001$.

At baseline RA patients had significantly higher naïve $CD4^+$ T cells ($p < 0.01$) (**Figure 6.6A**), central memory $CD4^+$ T cells ($p < 0.05$) (**Figure 6.6B**), effector memory $CD4^+$ T cells ($p < 0.05$) (**Figure 6.6C**) and terminal effector memory $CD4^+$ T cells ($p < 0.05$) (**Figure 6.6D**), compared to healthy controls. No significant differences were seen at any other time-point.

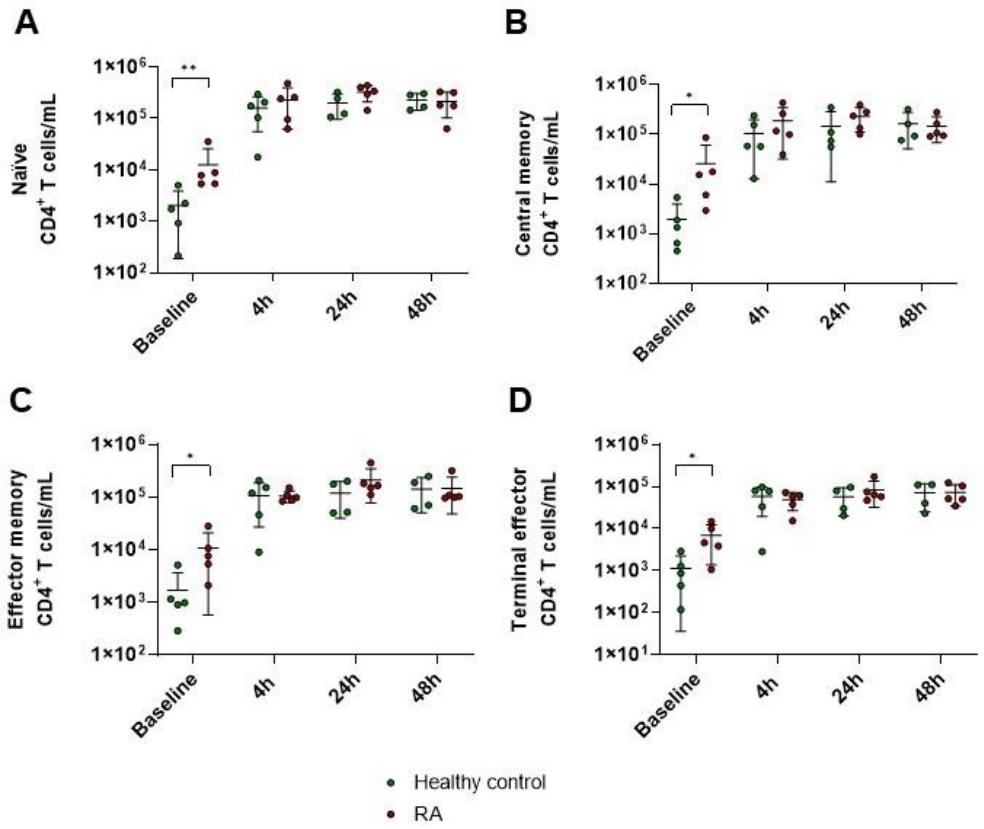

Figure 6.6. Temporal profiles of circulating CD4$^+$ T cell subsets following UV-KEc-triggered dermal inflammation. Following the intradermal injection of 1.5 x 10^7 UV-KEc into the volar aspect of each forearm of RA patients and healthy controls, single cell suspensions were obtained by ACK lysis of peripheral blood at baseline (0h), 4h, 24h and 48h. Cells were incubated with a metal isotope-tagged antibody cocktail. Stained cells were acquired using the Helios XT SAE 20W-50 system and analysed using Flowjo software. Depicted are (A) naïve CD4$^+$ T cells, (B) central memory CD4$^+$ T cells, (C) effector memory CD4$^+$ T cells and (D) terminal effector CD4$^+$ T cells. Cell numbers are shown as cell count per millilitre. Data are expressed as individual values with the mean with SD at each time-point; $n = 5$. *$p < 0.05$, **$p < 0.01$, ***$p < 0.001$, ****$p < 0.0001$.

Naïve, central memory, effector memory and terminal effector CD8$^+$ T cells increased in number following intradermal UV-KEc, peaking around 24h in both groups and appearing to decline thereafter (**Figure 6.7A-D**). Terminal effector CD8$^+$ T cells were significantly fewer in RA patients compared to healthy controls at all time-points following the intradermal injection of UV-KEc ($p < 0.05$) (**Figure 6.7D**).

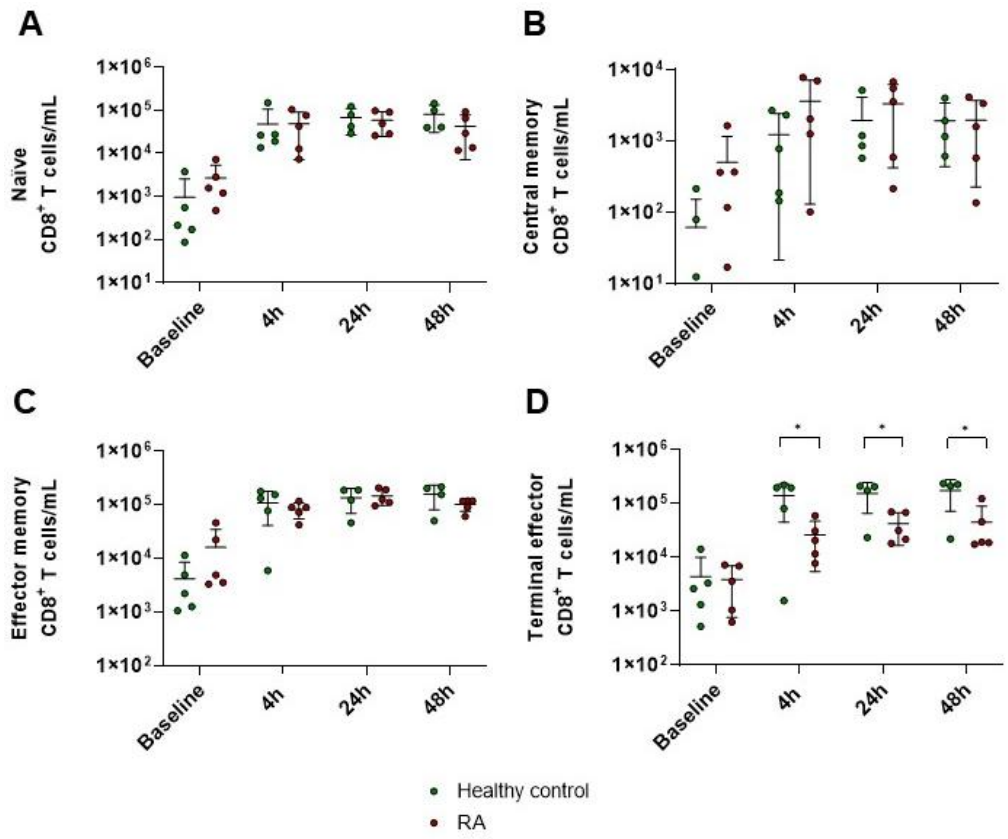

Figure 6.7. Temporal profiles of circulating CD8$^+$ T cell subsets following UV-KEc-triggered dermal inflammation. Following the intradermal injection of 1.5 x 10^7 UV-KEc into the volar aspect of each forearm of RA patients and healthy controls, single cell suspensions were obtained by ACK lysis of peripheral blood at baseline (0h), 4h, 24h and 48h. Cells were incubated with a metal isotope-tagged antibody cocktail. Stained cells were acquired using the Helios XT SAE 20W-50 system and analysed using Flowjo software. Depicted are (A) naïve CD8$^+$ T cells, (B) central memory CD8$^+$ T cells, (C) effector memory CD8$^+$ T cells and (D) terminal effector CD8$^+$ T cells. Cell numbers are shown as cell count per millilitre. Data are expressed as individual values with the mean with SD at each time-point; $n = 5$. *$p < 0.05$, **$p < 0.01$, ***$p < 0.001$, ****$p < 0.0001$.

At baseline, RA patients had significantly higher levels of Th-2 cells ($p < 0.05$) (**Figure 6.8B**), Th-17 cells ($p < 0.01$) (**Figure 6.8C**) and T_{regs} ($p < 0.01$) (**Figure 6.8D**), compared to healthy controls. Circulating Th-1, Th-2 and Th-17 as well as T_{regs} increased in number following intradermal UV-KEc, peaking at around 24h in both groups and appearing to decline thereafter (**Figure 6.8A-D**).

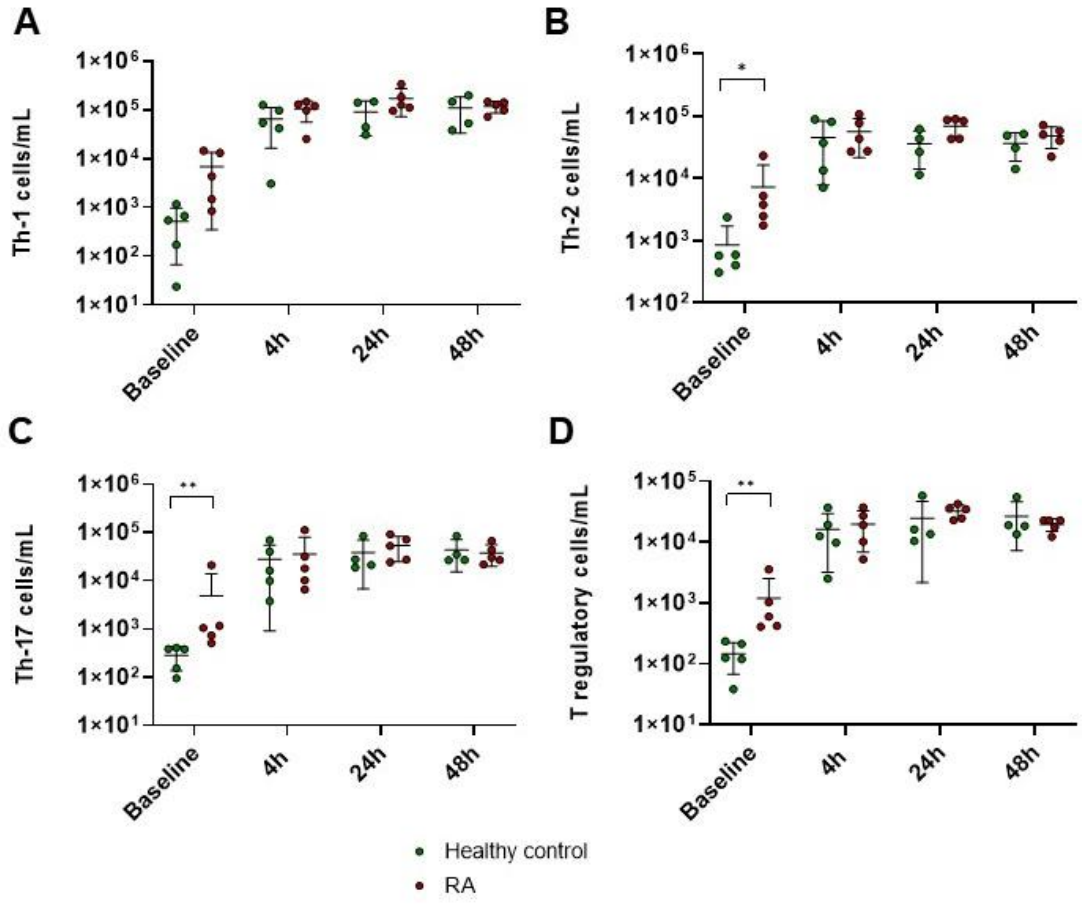

Figure 6.8. Temporal profiles of circulating T helper cell subset and T regulatory cells following UV-KEc-triggered dermal inflammation. Following the intradermal injection of 1.5 x 10^7 UV-KEc into the volar aspect of each forearm of RA patients and healthy controls, single cell suspensions were obtained by ACK lysis of peripheral blood at baseline (0h), 4h, 24h and 48h. Cells were incubated with a metal isotope-tagged antibody cocktail. Stained cells were acquired using the Helios XT SAE 20W-50 system and analysed using Flowjo software. Depicted are (A) Th-1 cells, (B) Th-2 cells, (C) Th-17 cells and (D) T_{regs}. Cell numbers are shown as cell count per millilitre. Data are expressed as individual values with the mean with SD at each time-point; n = 5. *p < 0.05, **p < 0.01, ***p < 0.001, ****p < 0.0001.

At baseline, circulating total B cells and naïve B cells were significantly higher in RA patients (p < 0.05) compared to healthy controls (**Figure 6.9A-B**). Total B cells, naïve B cells, memory B cell and plasmablast numbers peaked at around 4h in both groups, although no significant differences were seen at any time-point following the intradermal injection of UV-KEc (**Figure 6.9A-D**).

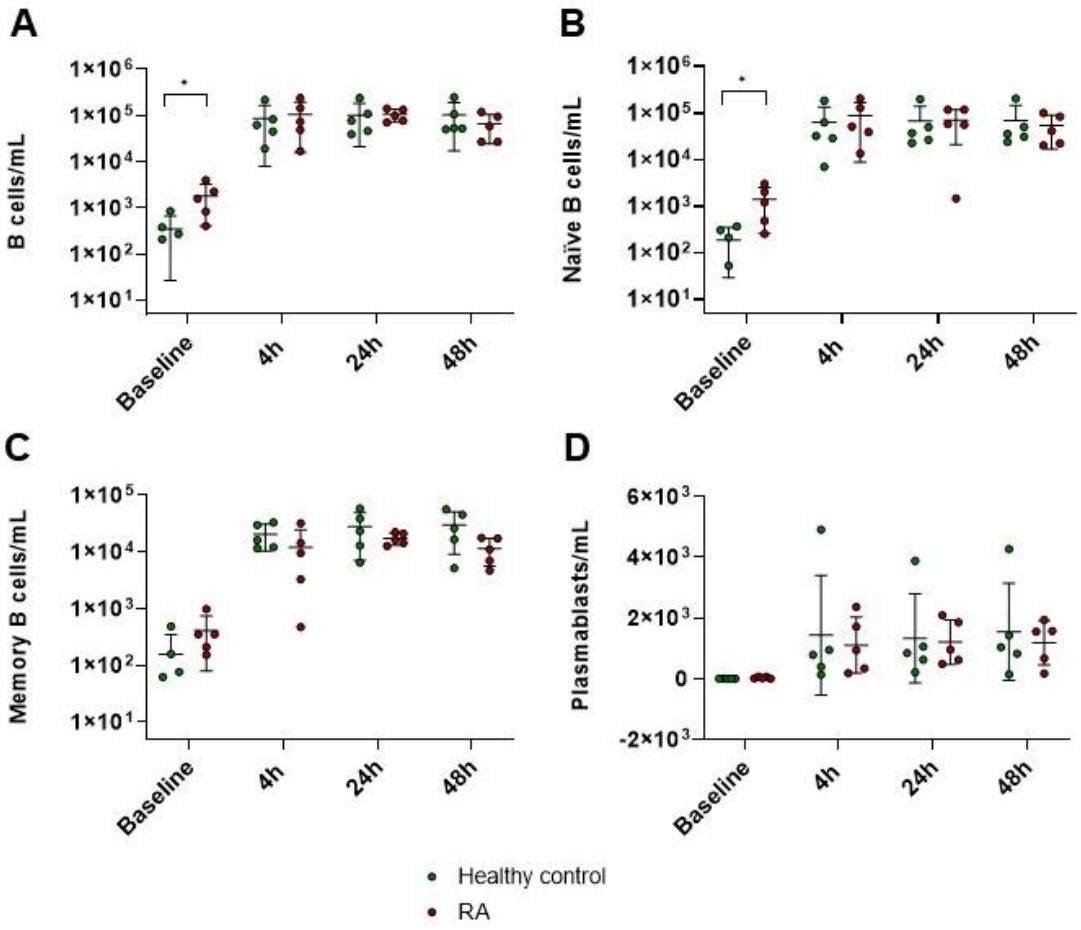

Figure 6.9. Temporal profiles of circulating B cell subsets following UV-KEc-triggered dermal inflammation. Following the intradermal injection of 1.5 x 10^7 UV-KEc into the volar aspect of each forearm of RA patients and healthy controls, single cell suspensions were obtained by ACK lysis of peripheral blood at baseline (0h), 4h, 24h and 48h. Cells were incubated with a metal isotope-tagged antibody cocktail. Stained cells were acquired using the Helios XT SAE 20W-50 system and analysed using Flowjo software. Depicted are (A) total B cells, (B) naïve B cells, (C) memory B cells and (D) plasmablasts. Cell numbers are shown as cell count per millilitre. Data are expressed as individual values with the mean with SD at each time-point; $n = 5$. *$p < 0.05$, **$p < 0.01$, ***$p < 0.001$, ****$p < 0.0001$.

Total NK cells, early NK cells, late NK cells and NKT cells all peaked at around 24h with levels maintained at 72h in both groups (**Figure 6.10A-D**). There were significantly fewer NKT cells in RA patients at 72h ($p < 0.05$), compared to healthy controls (**Figure 6.10D**).

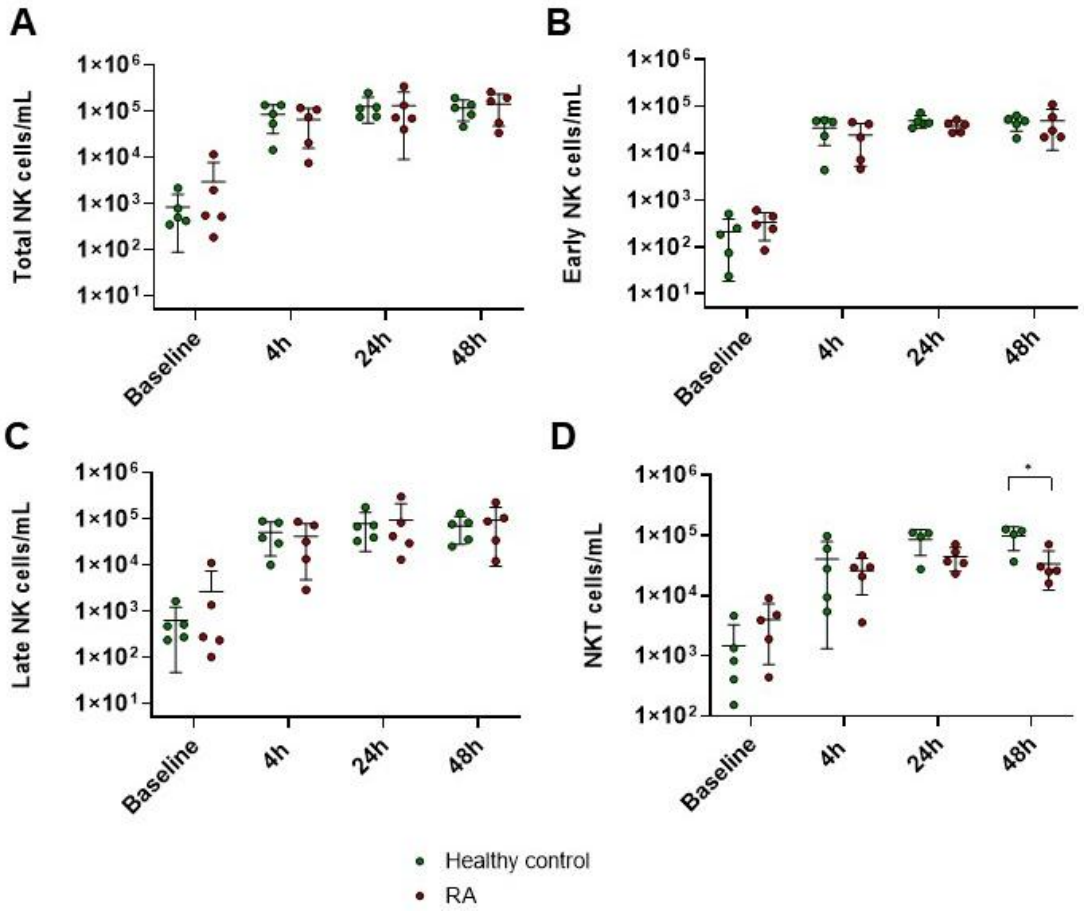

Figure 6.10. Temporal profiles of circulating NK subsets and NKT cells following UV-KEc-triggered dermal inflammation. Following the intradermal injection of 1.5 x 10^7 UV-KEc into the volar aspect of each forearm of RA patients and healthy controls, single cell suspensions were obtained by ACK lysis at baseline (0h), 4h, 24h and 48h. Cells were incubated with a metal isotope-tagged antibody cocktail. Stained cells were acquired using the Helios XT SAE 20W-50 system and analysed using Flowjo software. Depicted are (A) total NK cells, (B) early NK cells, (C) late NK cells and (D) NKT cells. Cell numbers are shown as cell count per millilitre. Data are expressed as individual values with the mean with SD at each time-point; $n = 5$. *$p < 0.05$, **$p < 0.01$, ***$p < 0.001$, ****$p < 0.0001$.

6.3.3.2 Blister cell profiles

Having analysed the circulating immune cell-types, next the inflammatory exudate aspirated from the blister formed by negative pressure suction at the site of dermal inflammation was investigated. In the blister fluid, no significant differences were seen in neutrophil numbers (**Figure 6.11A**), eosinophils (**Figure 6.11B**) or basophils (**Figure 6.11C**).

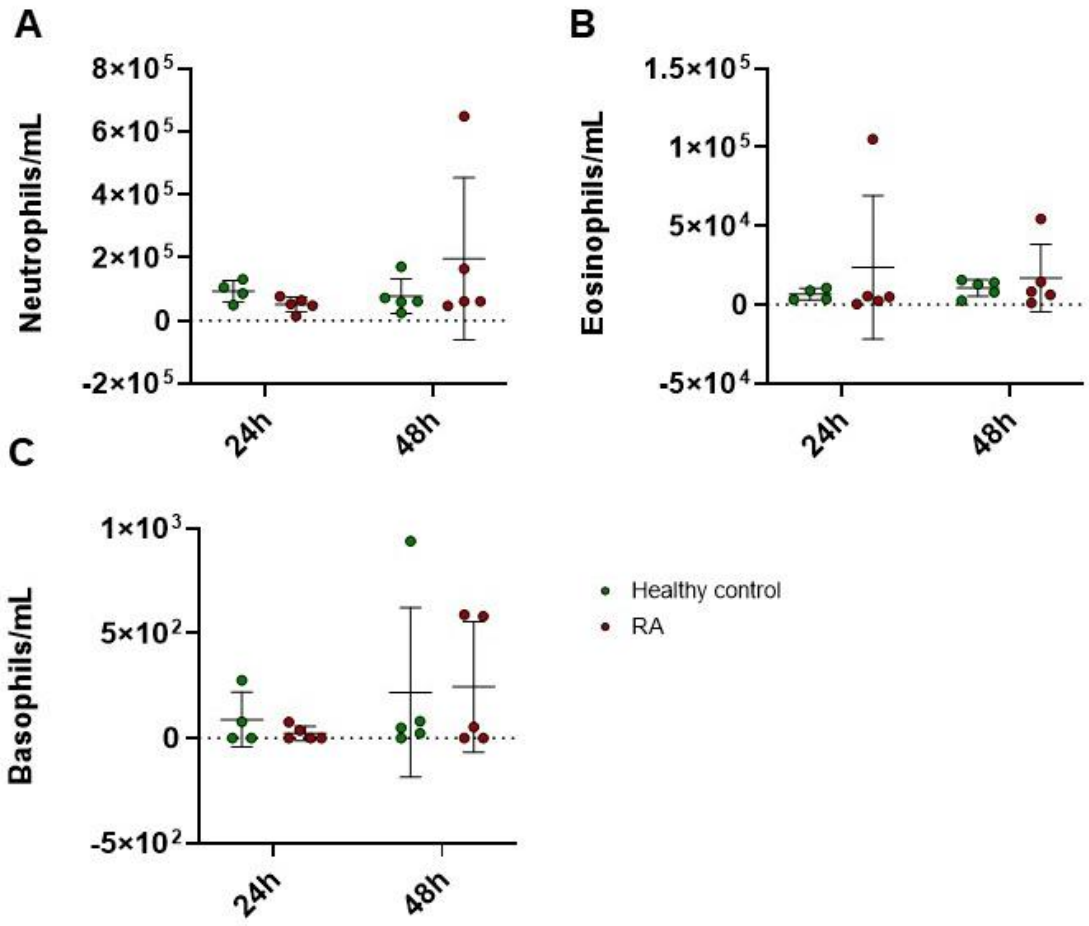

Figure 6.11. Temporal profiles of blister granulocytes following UV-KEc-triggered dermal inflammation. Following the intradermal injection of 1.5 x 10^7 UV-KEc into the volar aspect of each forearm of RA patients and healthy controls, blisters were formed at 24h and 48h using a negative pressure suction cup. Single cell suspensions were obtained by ACK lysis and cells were incubated with a metal isotope-tagged antibody cocktail. Stained cells were acquired using the Helios XT SAE 20W-50 system and analysed using Flowjo software. Depicted are (A) neutrophils, (B) eosinophils and (C) basophils. Cell numbers are shown as cell count per millilitre. Data are expressed as individual values with the mean with SD at each time-point; $n = 5$. *$p < 0.05$, **$p < 0.01$, ***$p < 0.001$, ****$p < 0.0001$.

No significant differerences were seen between RA patients and healthy controls for total monocyte (**Figure 6.12A**), classical monocyte (**Figure 6.12B**), intermediate monocyte (**Figure 6.12C**) or non-classical monocyte (**Figure 6.12D**) numbers at either time-point.

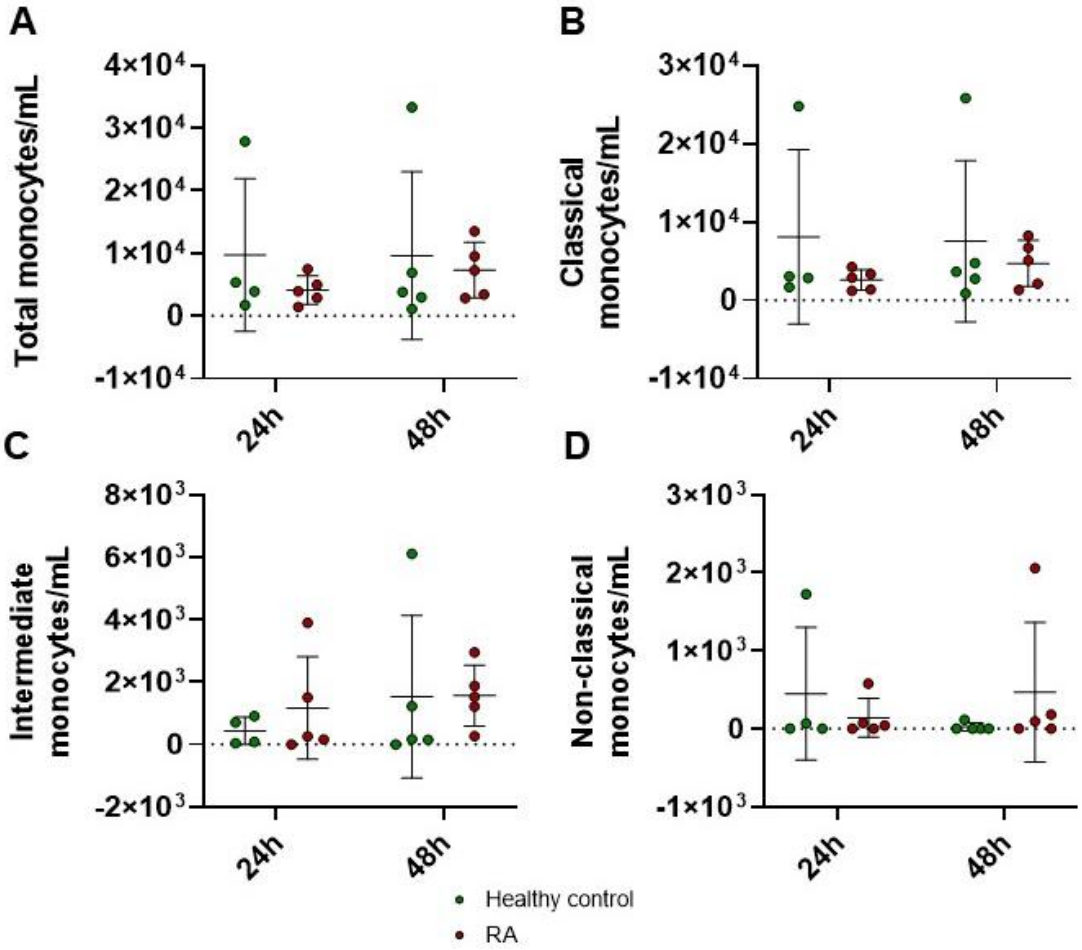

Figure 6.12. Temporal profiles of blister monocyte subsets following UV-KEc-triggered dermal inflammation. Following the intradermal injection of 1.5 x 10^7 UV-KEc into the volar aspect of each forearm of RA patients and healthy controls, blisters were formed at 24h and 48h using a negative pressure suction cup. Single cell suspensions were obtained by ACK lysis and cells were incubated with a metal isotope-tagged antibody cocktail. Stained cells were acquired using the Helios XT SAE 20W-50 system and analysed using Flowjo software. Depicted are (A) total monocytes, (B) classical monocytes, (C) intermediate monocytes and (D) non-classical monocytes. Cell numbers are shown as cell count per millilitre. Data are expressed as individual values with the mean with SD at each time-point; $n = 5$. *$p < 0.05$, **$p < 0.01$, ***$p < 0.001$, ****$p < 0.0001$.

There were no significant differences seen for blister numbers of total dendritic cells (**Figure 6.13A**), $CD141^+$ dendritic cells (**Figure 6.13B**) or myeloid dendritic cells (**Figure 6.13C**) between groups at either time-point. Plasmacytoid dendritic cells were

undetectable in the 24h blister in both groups, but significantly increased in the RA group at 48h compared to healthy controls ($p < 0.01$) (**Figure 6.13D**).

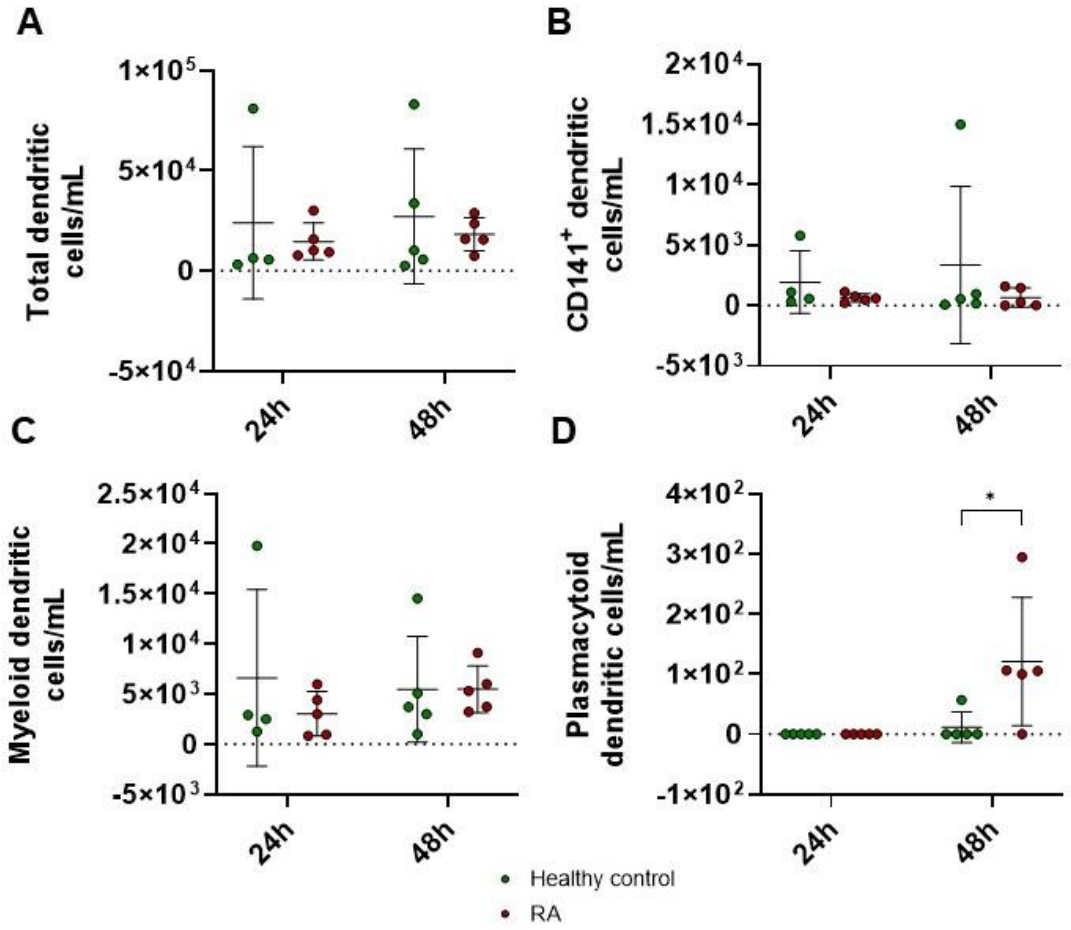

Figure 6.13. Temporal profiles of blister dendritic cell subsets following UV-KEc-triggered dermal inflammation. Following the intradermal injection of 1.5 x 10^7 UV-KEc into the volar aspect of each forearm of RA patients and healthy controls, blisters were formed at 24h and 48h using a negative pressure suction cup. Single cell suspensions were obtained by ACK lysis and cells were incubated with a metal isotope-tagged antibody cocktail. Stained cells were acquired using the Helios XT SAE 20W-50 system and analysed using Flowjo software. Depicted are (A) total dendritic cells, (B) $CD141^+$ dendritic cells, (C) myeloid dendritic cells and (D) plasmacytoid dendritic cells. Cell numbers are shown as cell count per millilitre. Data are expressed as individual values with the mean with SD at each time-point; $n = 5$. *$p < 0.05$, **$p < 0.01$, ***$p < 0.001$, ****$p < 0.0001$.

There were no significant differences in blister αβ T cells (**Figure 6.14A**), γδ T cells (**Figure 6.14B**), total $CD4^+$ T cells (**Figure 6.14C**) or total $CD8^+$ T cells (**Figure 6.14D**) at either time-point between the groups.

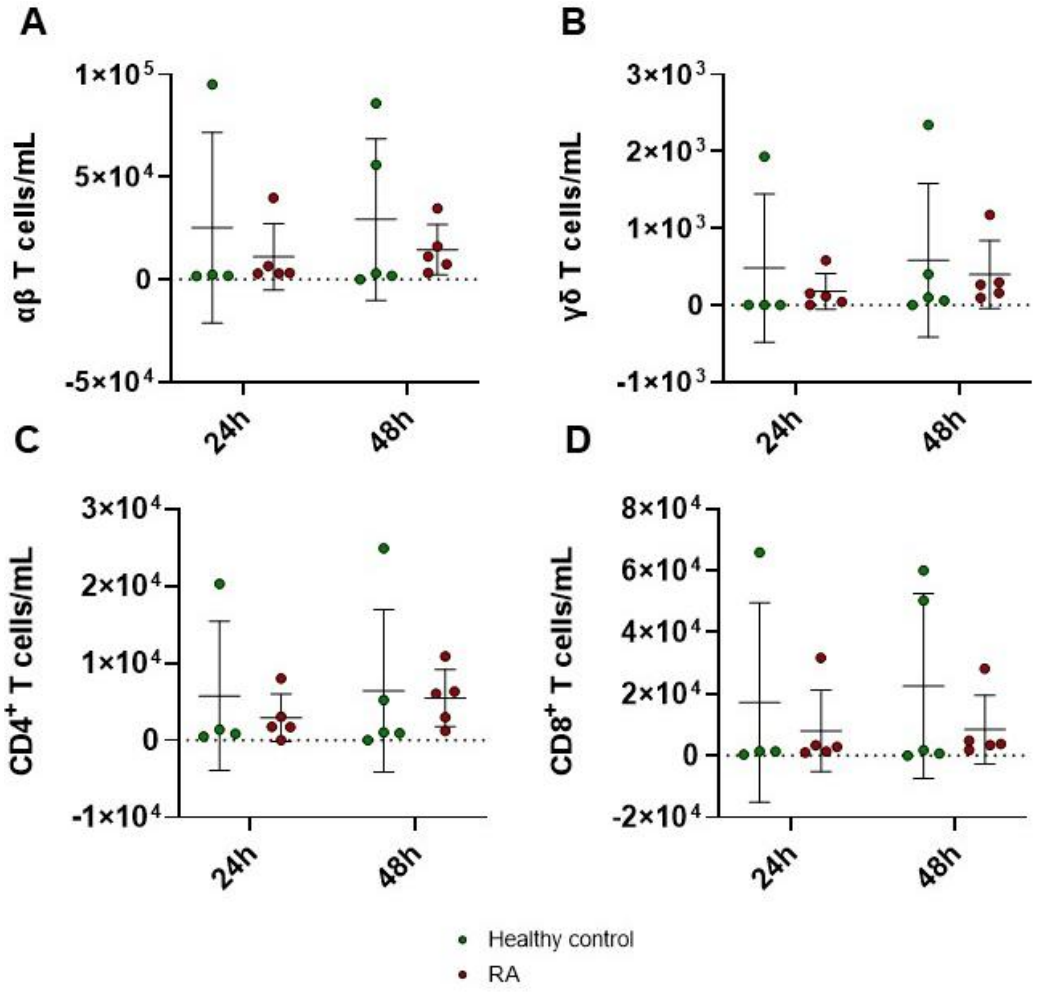

Figure 6.14. Temporal profiles of blister T cell subsets following UV-KEc-triggered dermal inflammation. Following the intradermal injection of 1.5 x 10^7 UV-KEc into the volar aspect of each forearm of RA patients and healthy controls, blisters were formed at 24h and 48h using a negative pressure suction cup. Single cell suspensions were obtained by ACK lysis and cells were incubated with a metal isotope-tagged antibody cocktail. Stained cells were acquired using the Helios XT SAE 20W-50 system and analysed using Flowjo software. Depicted are (A) αβ T cells, (B) γδ T cells, (C) total $CD4^+$ T cells and (D) total $CD8^+$ T cells. Cell numbers are shown as cell count per millilitre. Data are expressed as individual values with the mean with SD at each time-point; $n = 5$. *$p < 0.05$, **$p < 0.01$, ***$p < 0.001$, ****$p < 0.0001$.

No significant differences were seen in any $CD4^+$ T cell subset (naïve [**Figure 6.15A**], central memory [**Figure 6.15B**], effector memory [**Figure 6.15C**] or terminal effector [**Figure 6.15D**]) any either time-point. Naïve and central memory $CD4^+$ T cells were low or undetectable at 24h and 48h in both RA patients and healthy controls.

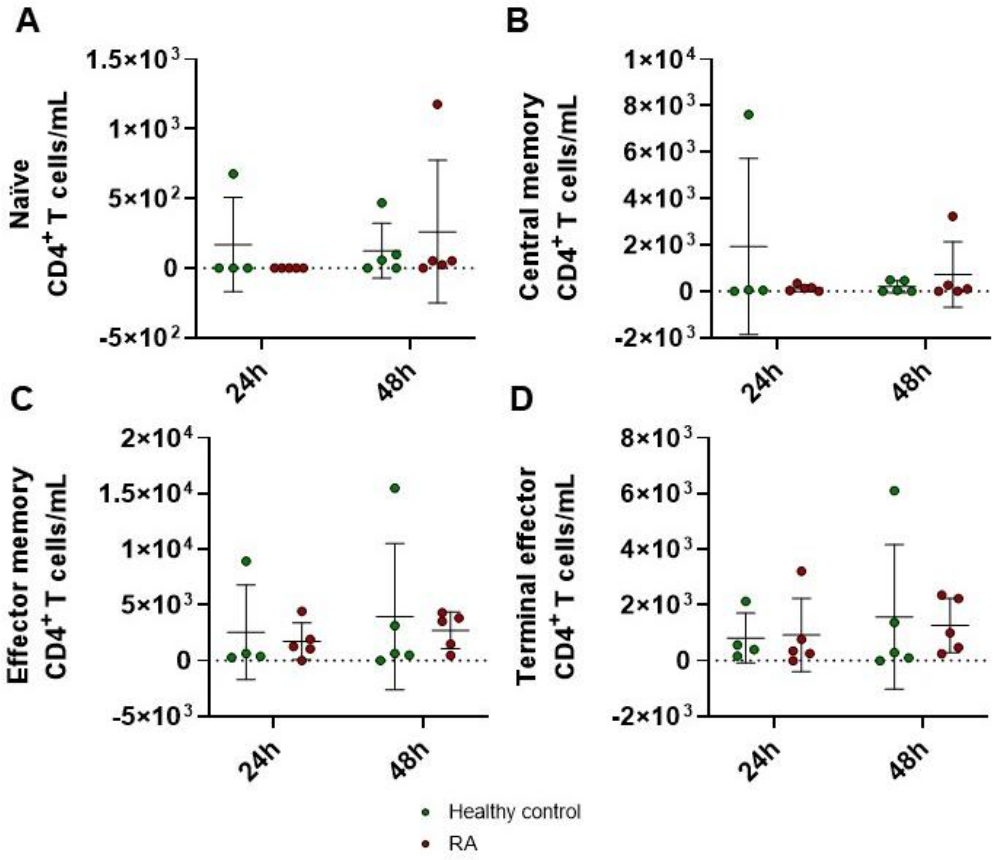

Figure 6.15. Temporal profiles of blister $CD4^+$ T cell subsets following UV-KEc-triggered dermal inflammation. Following the intradermal injection of 1.5 x 10^7 UV-KEc into the volar aspect of each forearm of RA patients and healthy controls, blisters were formed at 24h and 48h using a negative pressure suction cup. Single cell suspensions were obtained by ACK lysis and cells were incubated with a metal isotope-tagged antibody cocktail. Stained cells were acquired using the Helios XT SAE 20W-50 system and analysed using Flowjo software. Depicted are (A) naïve $CD4^+$ T cells, (B) central memory $CD4^+$ T cells, (C) effector memory $CD4^+$ T cells and (D) terminal effector $CD4^+$ T cells. Cell numbers are shown as cell count per millilitre. Data are expressed as individual values with the mean with SD at each time-point; $n = 5$. *$p < 0.05$, **$p < 0.01$, ***$p < 0.001$, ****$p < 0.0001$.

As for $CD4^+$ T cell subsets, there were no significant differences seen in any $CD8^+$ T cell subset (naïve [**Figure 6.16A**], central memory [**Figure 6.16B**], effector memory [**Figure 6.16C**] or terminal effector [**Figure 6.16D**]) at either time-point. Naïve and central memory $CD8^+$ T cells were low or undetectable at 24h and 48h in both groups.

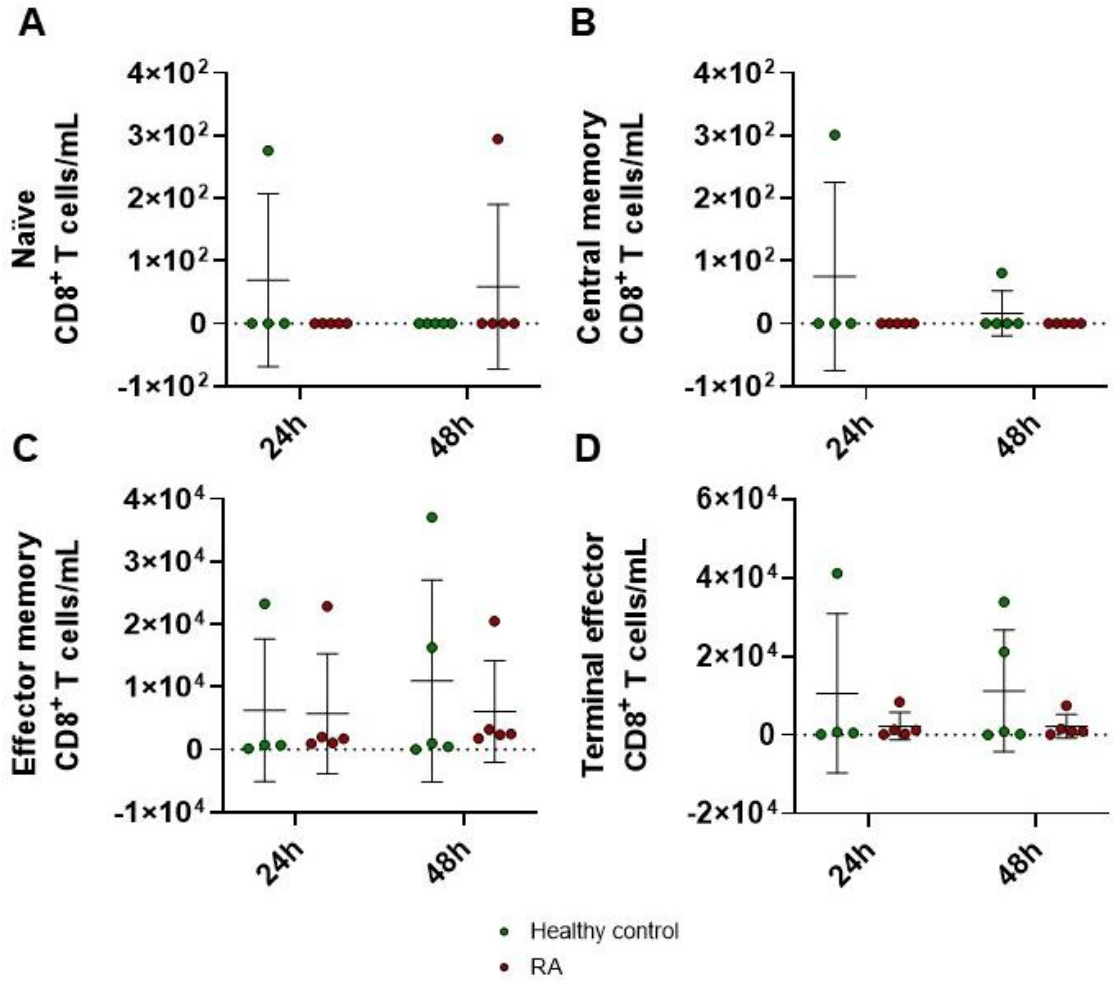

Figure 6.16. Temporal profiles of blister $CD8^+$ T cell subsets following UV-KEc-triggered dermal inflammation. Following the intradermal injection of 1.5 x 10^7 UV-KEc into the volar aspect of each forearm of RA patients and healthy controls, blisters were formed at 24h and 48h using a negative pressure suction cup. Single cell suspensions were obtained by ACK lysis and cells were incubated with a metal isotope-tagged antibody cocktail. Stained cells were acquired using the Helios XT SAE 20W-50 system and analysed using Flowjo software. Depicted are (A) naïve $CD8^+$ T cells, (B) central memory $CD8^+$ T cells, (C) effector memory $CD8^+$ T cells and (D) terminal effector $CD8^+$ T cells. Cell numbers are shown as cell count per millilitre. Data are expressed as individual values with the mean with SD at each time-point; $n = 5$. *$p < 0.05$, **$p < 0.01$, ***$p < 0.001$, ****$p < 0.0001$.

No signficant differences were identified in Th-1 cells (**Figure 6.17A**), Th-2 cells (**Figure 6.17.B**), Th-17 cells (**Figure 6.17C**) or T_{regs} (**Figure 6.17D**) at either time-point.

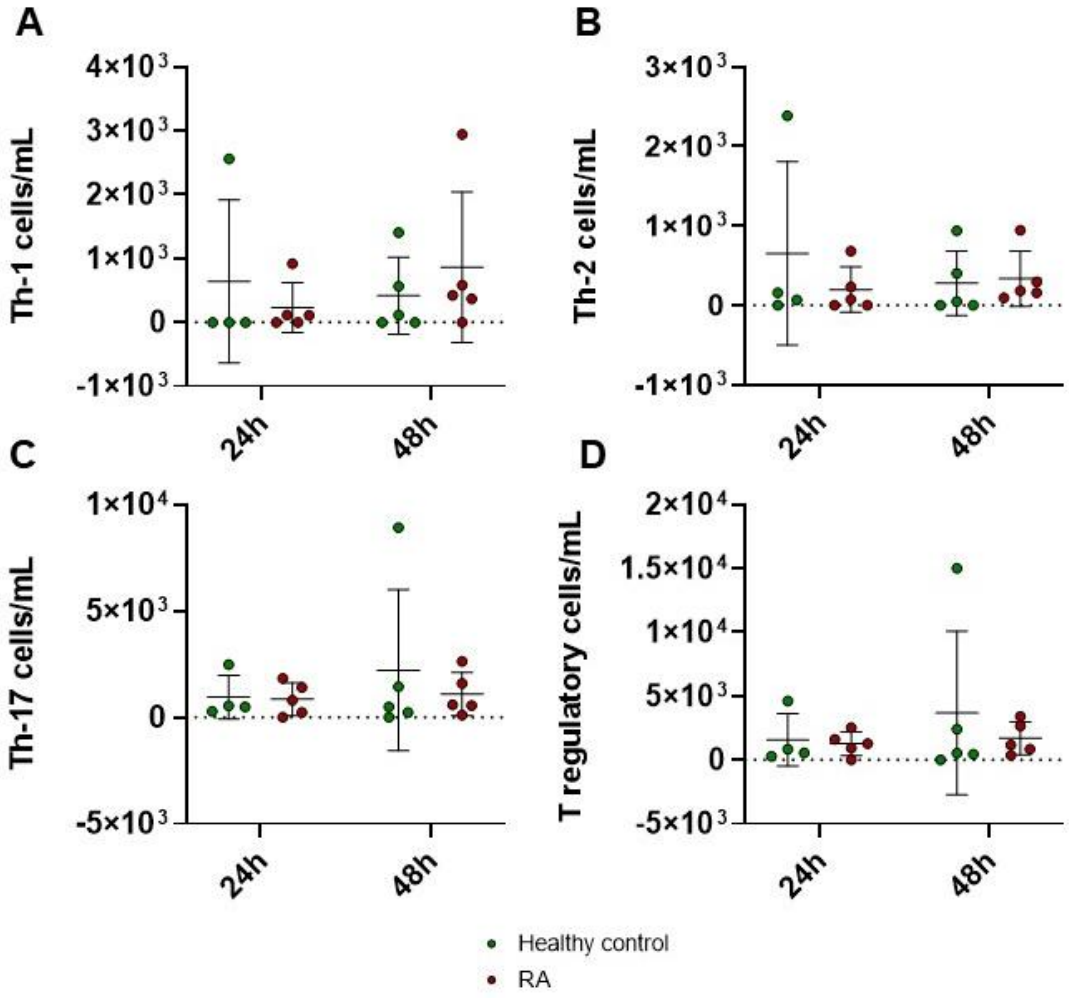

Figure 6.17. Temporal profiles of blister T helper cell subsets and T regulatory cells following UV-KEc-triggered dermal inflammation. Following the intradermal injection of 1.5 x 10^7 UV-KEc into the volar aspect of each forearm of RA patients and healthy controls, blisters were formed at 24h and 48h using a negative pressure suction cup. Single cell suspensions were obtained by ACK lysis and cells were incubated with a metal isotope-tagged antibody cocktail. Stained cells were acquired using the Helios XT SAE 20W-50 system and analysed using Flowjo software. Depicted are (A) Th-1 cells, (B) Th-2 cells, (C) Th-17 cells and (D) T_{regs}. Cell numbers are shown as cell count per millilitre. Data are expressed as individual values with the mean with SD at each time-point; $n = 5$. *$p < 0.05$, **$p < 0.01$, ***$p < 0.001$, ****$p < 0.0001$.

There were no significant differences seen in numbers of total B cells (**Figure 6.18A**) or naïve B cells (**Figure 6.18B**) at either time-point. Memory B cells were undetectable in the blister fluid of RA patients at 24h and no significant differences were seen between groups at 48h (**Figure 6.18C**). Plasmablasts were not detected in the blister fluid in either group at either time-point (**Figure 6.18D**).

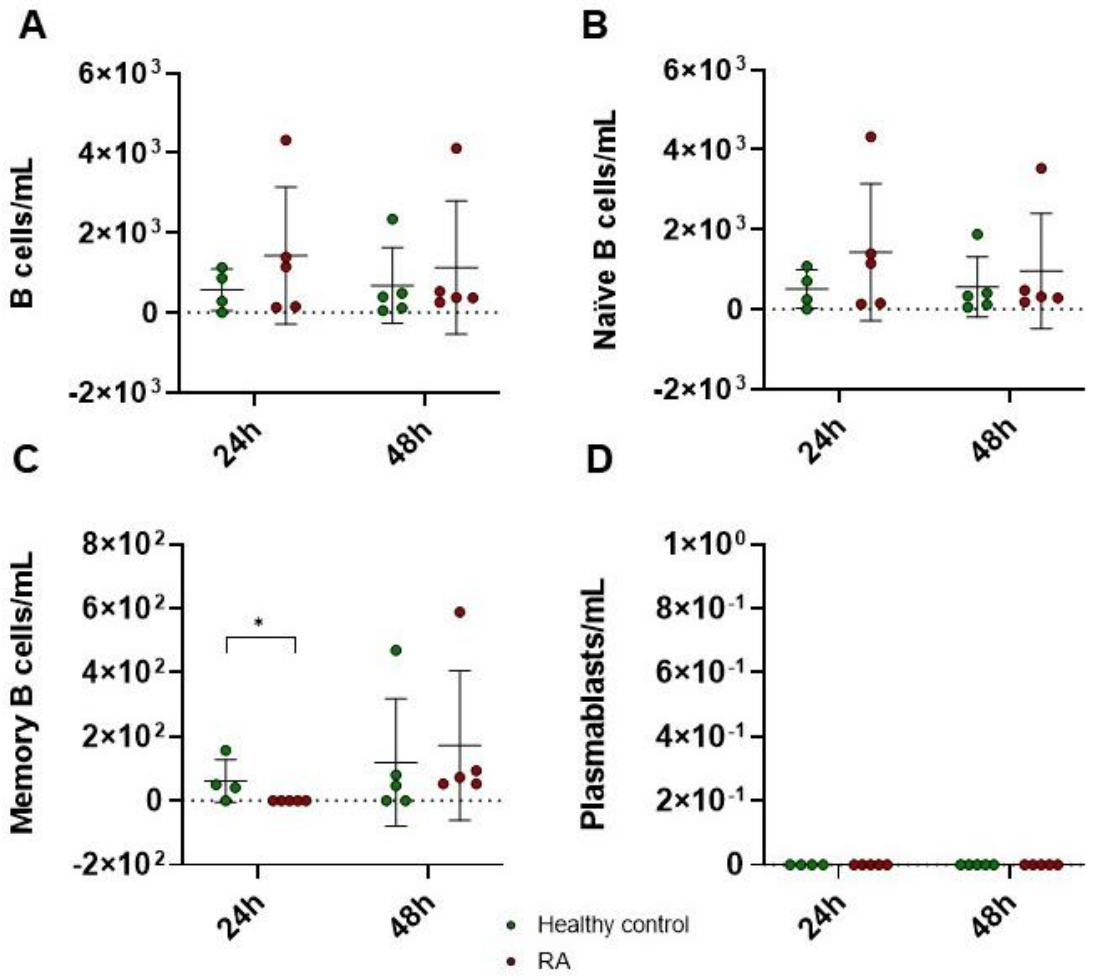

Figure 6.18. Temporal profiles of blister B cells following UV-KEc-triggered dermal inflammation. Following the intradermal injection of 1.5 x 10^7 UV-KEc into the volar aspect of each forearm of RA patients and healthy controls, blisters were formed at 24h and 48h using a negative pressure suction cup. Single cell suspensions were obtained by ACK lysis and cells were incubated with a metal isotope-tagged antibody cocktail. Stained cells were acquired using the Helios XT SAE 20W-50 system and analysed using Flowjo software. Depicted are (A) total B cells, (B) naïve B cells, (C) memory B cells and (D) plasmablasts. Cell numbers are shown as cell count per millilitre. Data are expressed as individual values with the mean with SD at each time-point; $n = 5$. *$p < 0.05$, **$p < 0.01$, ***$p < 0.001$, ****$p < 0.0001$.

No significant differences were seen in blister fluid total NK cell numbers (**Figure 6.19A**), early NK cells (**Figure 6.19B**), late NK cells (**Figure 6.19C**) or NKT cells (**Figure 6.19D**) at either time-point.

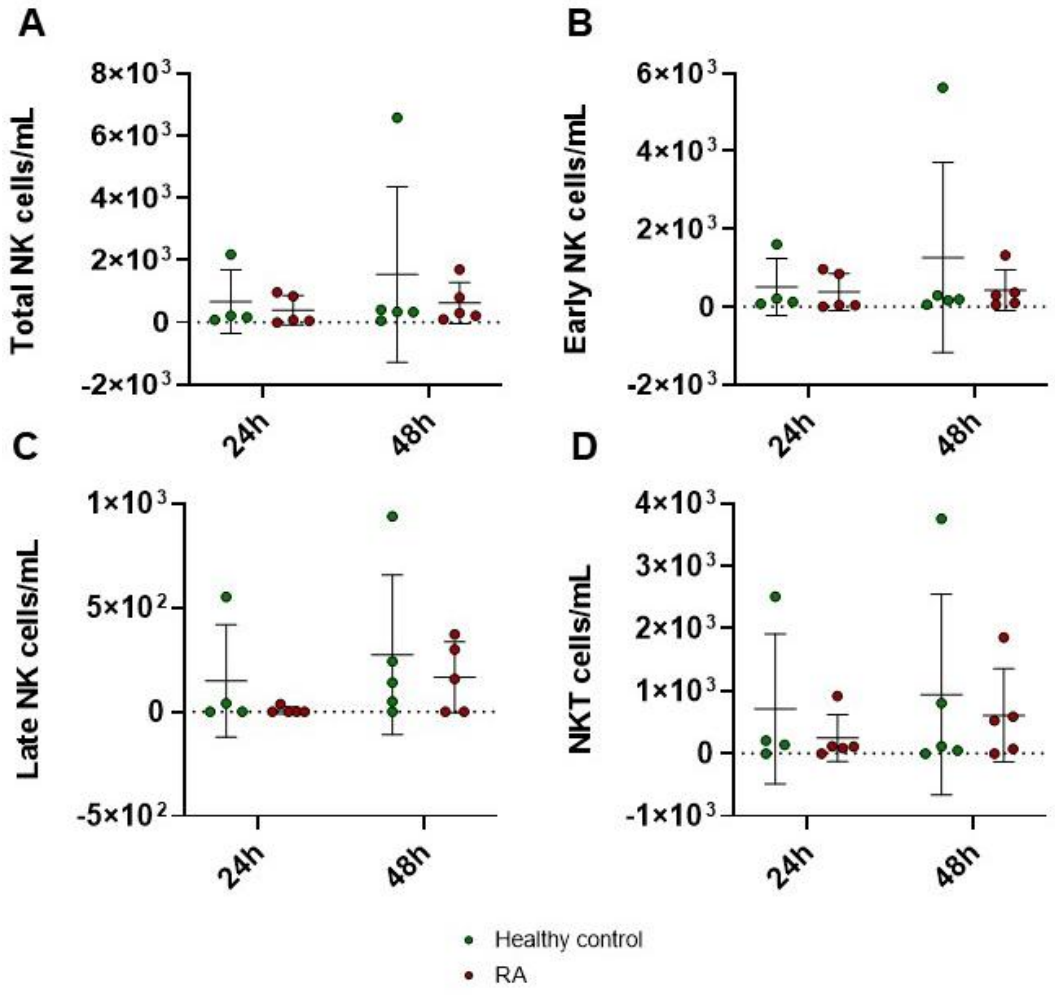

Figure 6.19. Temporal profiles of blister NK cell subsets and NKT cells following UV-KEc-triggered dermal inflammation. Following the intradermal injection of 1.5 x 10^7 UV-KEc into the volar aspect of each forearm for all participants, single cell suspensions were obtained by ACK lysis at baseline (0h), 4h, 24h and 48h. Cells were incubated with a metal isotope-tagged antibody cocktail. Stained cells were acquired using the Helios XT SAE 20W-50 system and analysed using Flowjo software. Depicted are (A) total NK cells, (B) early NK cells, (C) late NK cells and (D) NKT cells. Cell numbers are shown as cell count per millilitre. Data are expressed as individual values with the mean with SD at each time-point; $n = 5$. *$p < 0.05$, **$p < 0.01$, ***$p < 0.001$, ****$p < 0.0001$.

6.3.4 UMAP analysis

Having initially identified immune cells in the blood and blister fluid of RA patients using manual gating in FlowJo, I wanted to utilise all 40 antigens used in the mass cytometry panel to identify any unique cell populations in RA patients. UMAP analysis constructs a high dimensional graphical representation of data and shows the connectedness of, in this case, antigen expression by immune cell-types. UMAPs were generated to allow the easy identification of different cell-type clusters to identify any unique populations in either group. When performing the UMAP analysis, the number of clusters to be represented is assigned, which determines how spread out the data points are. 30 clusters gave the best representation of the data; fewer would have meant I would have not seen certain less frequent cell-types and more would have resulted in distinct clusters representing the same cell-type. Of the 30 discrete clusters, six were excluded as likely represented doublets or debris, leaving 24 clusters, which were phenotyped. **Figure 6.20** depicts a UMAP showing the 24 clusters, each representing a unique cell-type with data combined for both healthy control and RA patients at both 24h and 48h. Broadly speaking, the clusters towards the bottom of the plot represents granulocytes, whilst the upper left shows mononuclear phagocytes and the upper right cells of the lymphoid lineage.

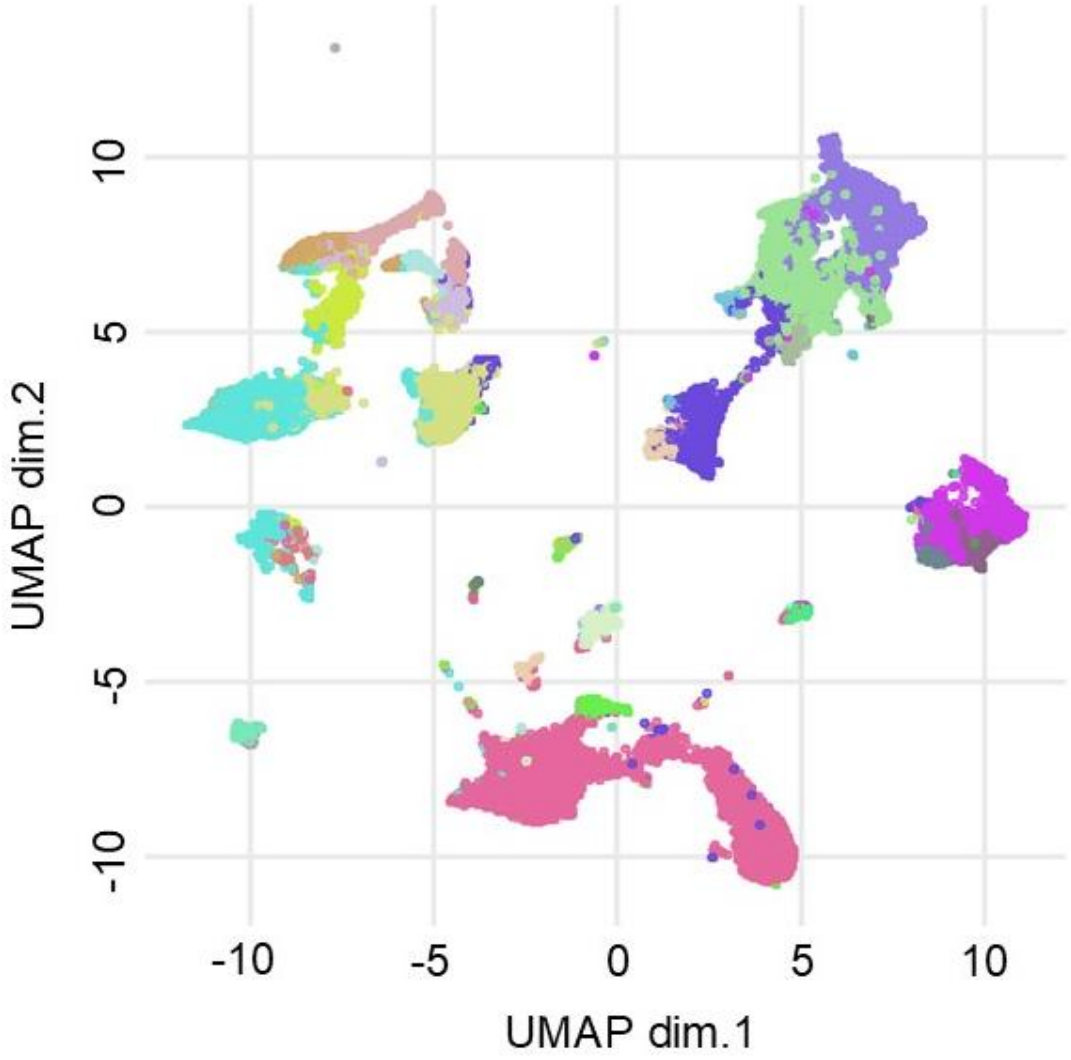

Populations

- Activated NK cells
- B cells
- Basophils
- CD127⁺ dendritic cells
- CD127⁺ macrophages
- CD1c⁺ dendritic cells
- CD4⁺ T cells
- CD4⁺ γδ T cells
- CD4⁺ T cells
- CD8⁺ γδ T cells
- CD8⁺ T cells
- CD8⁺ TEMRA cells
- Classical monocytes
- Transitioning classical monocytes
- Eosinophils
- γδ T cells
- Innate lymphoid cells
- Intermediate monocytes
- Naïve CD4⁺ T cells
- Naïve CD8⁺ T cells
- Neutrophils
- NK cells
- Non-classical monocytes
- Plasmacytoid dendritic cells

Figure 6.20. UMAP analysis showing combined cell-types identified in the blister fluid at the site of inflammation following the intradermal injection of UV-KEc. Following the intradermal injection of 1.5 x 10^7 UV-KEc into the volar aspect of each forearm of RA patients and healthy controls, blisters were formed at 24h and 48h using a negative pressure suction cup. Blisters were also formed on the skin of one healthy control and one RA patient who did not undergo the intradermal injection with UV-KEc. Single cell suspensions were obtained by ACK lysis and cells were incubated with a metal isotope-tagged antibody cocktail. Stained cells were acquired using the Helios XT SAE 20W-50 system and analysed using Cytobank Premium Software and R software programming language. Depicted is a combined UMAP showing all cell-types identified in healthy controls and RA patients. *n* = 5.

6.3.4.1 RA patients have a unique population of $CD127^+$ macrophages at the site of UV-KEc-triggered inflammation

Figure 6.21 shows UMAP analyses of the clusters of defined immune cells at 24h and 48h for naïve (*n* = 2), RA (n = 5) and healthy controls (n = 5). Two striking differences were noted in the $CD127^+$ macrophage population and neutrophil populations at both time-points. The discrete $CD127^+$ macrophage cluster was identified in RA patients but was not seen in any healthy controls at either time-point. The phenotype of these cells was $CD45^+$, $CD11c^+$, HLA-DR^+, $CD14^{int}$, $CD16^{int}$, $CD38^+$, $CD141^+$, $CD127^+$. These cells therefore share phenotypic similarities with intermediate monocytes, dendritic cells and macrophages. Additionally, the discrete neutrophil cluster was identified in all groups, but as shown in **Figure 6.21**, there are clear differences between RA patients and healthy controls at both 24h and 48h.

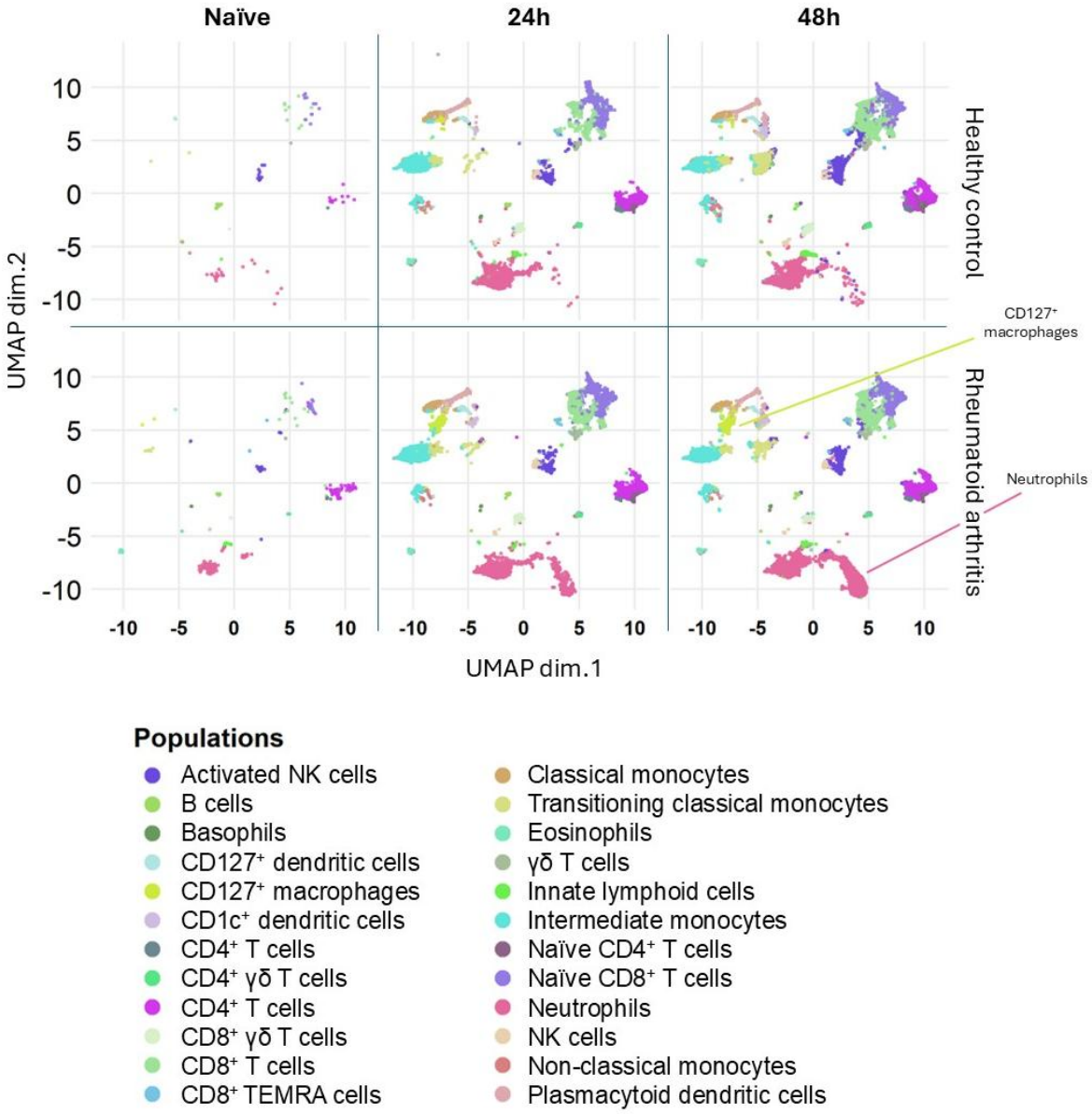

Figure 6.21. UMAP of immune cells accumulating in the skin of RA patients and healthy controls following the intradermal injection of UV-KEc. Following the intradermal injection of 1.5 x 10^7 UV-KEc into the volar aspect of each forearm of RA patients and healthy controls, blisters were formed at 24h and 48h using a negative pressure suction cup. Blisters were also formed on the skin of one healthy control and one RA patient who did not undergo the intradermal injection with UV-KEc. Single cell suspensions were obtained by ACK lysis and cells were incubated with a metal isotope-tagged antibody cocktail. Stained cells were acquired using the Helios XT SAE 20W-50 system and analysed using Cytobank Premium Software and R software programming language. Depicted are UMAPs from naïve, healthy controls and RA patients, separated into 30 discrete clusters. Cluster 4 is shown in lavender and cluster 10 in red; n = 6.

A combined heatmap showing median antigen expression by cell-type for RA patients and healthy controls at 24h and 48h is depicted in **Figure 6.22**. A total of 40 antigenic markers were used in the unbiased UMAP analysis and scaled median representation is shown for each of the discrete 24 cell clusters generated by the analysis. The heatmap represents the characteristics of the 24 annotated cell populations from each cluster, with median marker intensities with clustered columns (antigens) and rows (cell-types), colour-coded with red for higher expression and blue for lower expression.

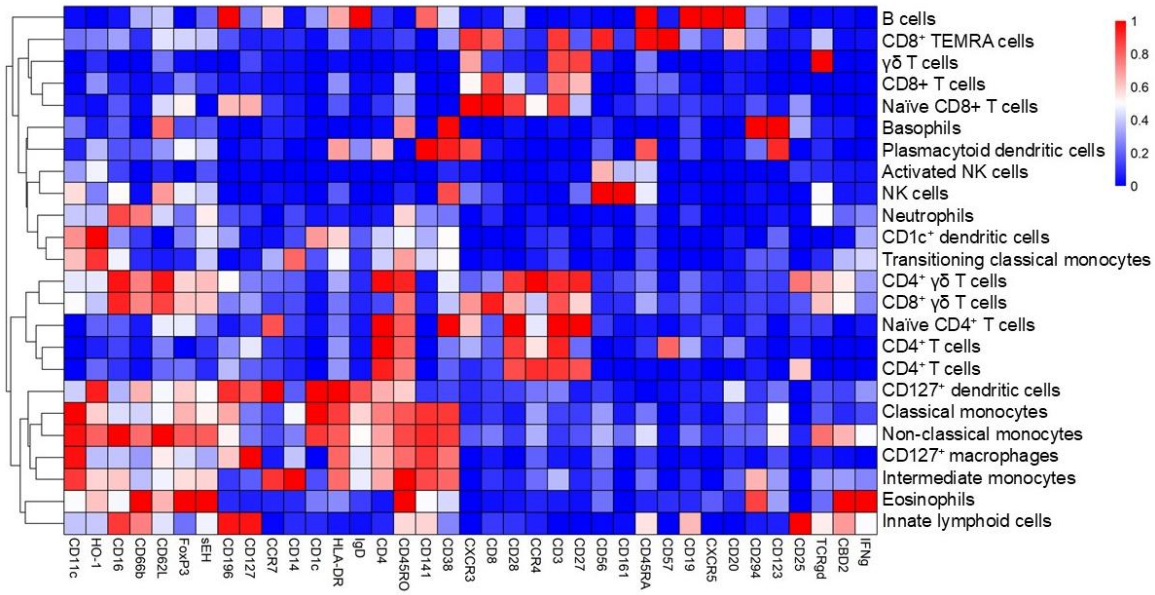

Figure 6.22. Heatmap showing combined antigen expression by cell-type for RA patients and healthy controls from immune cells accumulating in the skin following the intradermal injection of UV-KEc. Following the intradermal injection of 1.5 x 10^7 UV-KEc into the volar aspect of each forearm of RA patients and healthy controls, blisters were formed at 24h and 48h using a negative pressure suction cup. Single cell suspensions were obtained from peripheral blood and blisters by ACK lysis and cells incubated with a metal isotope-tagged antibody cocktail. Stained cells were acquired using the Helios XT SAE 20W-50 system and analysed using Cytobank Premium Software and R software programming language. Depicted is a combined heatmap showing median antigen expression for by cell-type for RA patients and healthy controls at both 24h and 48h. Dendrograms are also shown representing clustering of cell-types (rows) and antigens (columns) based on hierarchical clustering between 24 megaclusters with Euclidean distance metric and average linkage; n = 5.

To investigate further differences in numbers of immune cells present in the blister fluid at the site of UV-KEc-triggered dermal inflammation, the proportion of each cell-type was calculated for both RA and healthy controls at 24h (**Figure 6.23**) and 48h (**Figure 6.24**). As shown in **Figure 6.23**, in the blister fluid at 24h there was a trend towards fewer classical monocytes in RA patients compared to healthy controls (p = 0.0546). A similar trend was seen for innate lymphoid cells in RA patients (p = 0.0973). There were significantly fewer neutrophils ($p < 0.05$) and eosinophils ($p <$ 0.05) in the blister fluid of RA patients at 24h, compared to healthy controls.

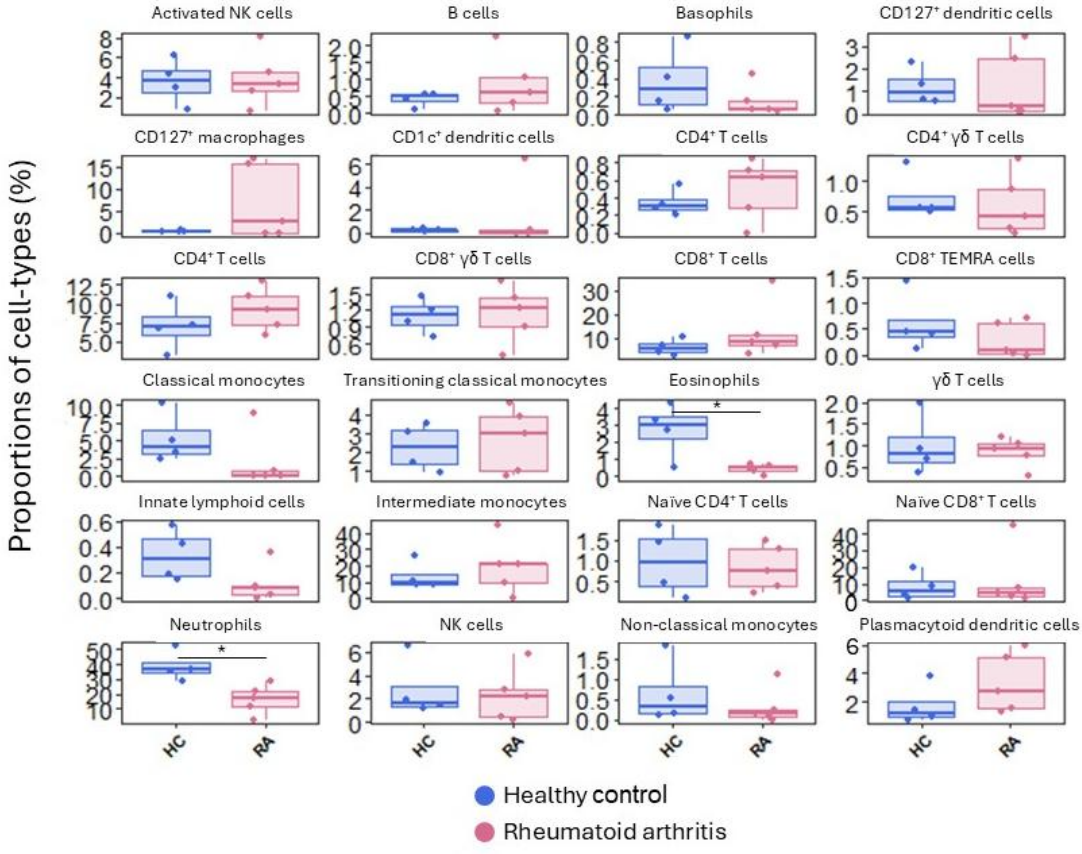

Figure 6.23. Relative proportions of cell-types accumulating in the skin of RA patients and healthy controls at 24h following the intradermal injection of UV-KEc. Following the intradermal injection of 1.5 x 10^7 UV-KEc into the volar aspect of each forearm of RA patients and healthy controls, blisters were formed at 24h and 48h using a negative pressure suction cup. Single cell suspensions were obtained by ACK lysis and cells were incubated with a metal isotope-tagged antibody cocktail. Stained cells were acquired using the Helios XT SAE 20W-50 system and analysed using Cytobank Premium Software and R software programming language. Depicted are proportions of each cell-type in the blister fluid at 24h; n = 5.

As shown in **Figure 6.24**, in the blister fluid at 48h there were significantly fewer classical monocytes ($p < 0.05$) and innate lymphoid cells ($p < 0.05$) in RA patients compared to healthy controls.

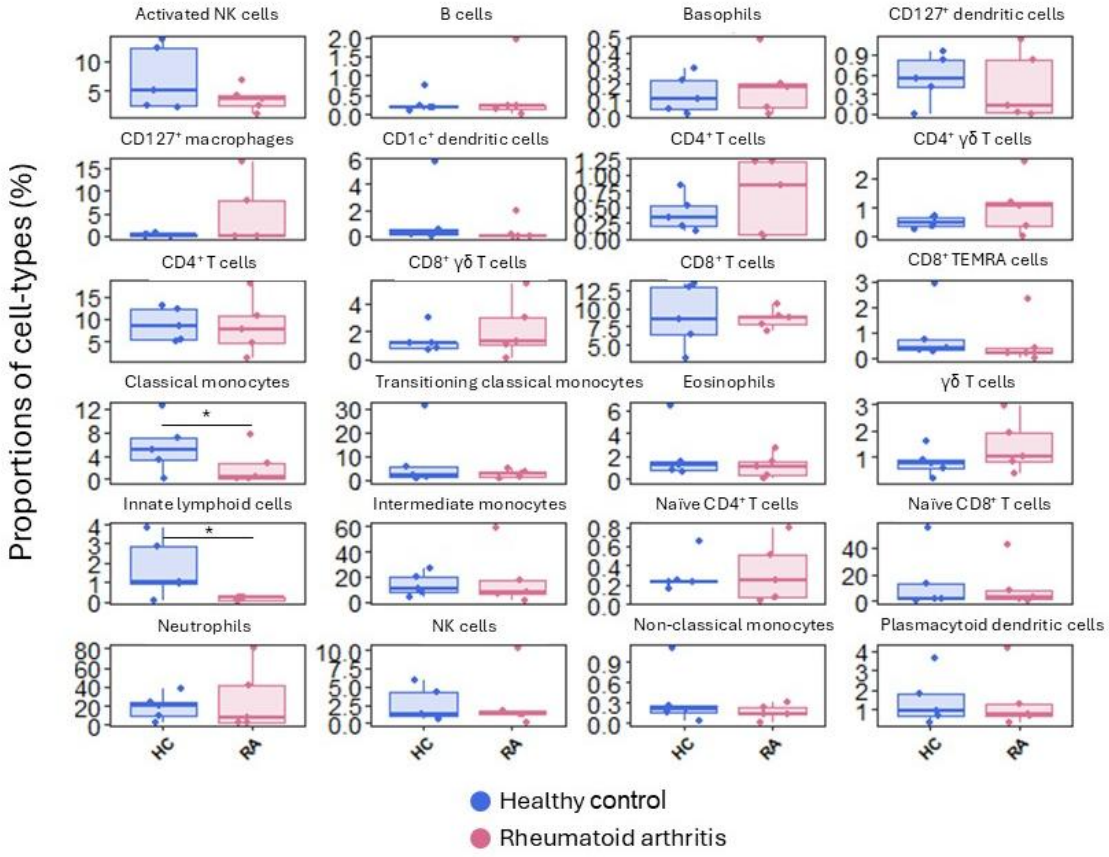

Figure 6.24. Relative proportions of cell-types accumulating in the skin of RA patients and healthy controls at 48h following the intradermal injection of UV-KEc. Following the intradermal injection of 1.5 x 10^7 UV-KEc into the volar aspect of each forearm of RA patients and healthy controls, blisters were formed at 24h and 48h using a negative pressure suction cup. Single cell suspensions were obtained by ACK lysis and cells were incubated with a metal isotope-tagged antibody cocktail. Stained cells were acquired using the Helios XT SAE 20W-50 system and analysed using Cytobank Premium Software and R software programming language. Depicted are proportions of each cell-type in the blister fluid at 48h; $n = 5$.

When looking at the individual UMAPs for each volunteer, it became clear that whilst there were no CD127$^+$ macrophages detectable in the blister fluid of healthy controls, there was variation between RA patients. Three out of the five enrolled in the study

showed significantly elevated levels of this cell-type at 24h ($p < 0.05$) (**Figure 6.25A**) and a trend towards signficantly increased numbers at 48h (**Figure 6.25B**) ($p = 0.0637$). The other two RA patients had no $CD127^+$ macrophages detectable in the blister fluid at either time-point, as observed in the healthy controls. There were significantly fewer neutrophils in the 24h blister of RA patients compared to healthy controls ($p < 0.05$) (**Figure 6.25C**) with no significant difference seen at 48h (**Figure 6.25D**). In the blister fluid at 24h, there were significantly fewer eosinophils in RA patients compared to healthy controls ($p < 0.05$) (**Figure 6.25E**) with no significant difference seen at 48h (**Figure 6.25F**). There was a trend towards fewer innate lymphoid cells (ILCs) in the 24h blister for RA patients (**Figure 6.25G**) with significantly fewer seen in the blister at 48h ($p < 0.05$) compared to healthy controls (**Figure 6.25H**). Unlike the blister fluid, there were no discernable differences in cluster differentiation between healthy controls and RA circulating immune cells at any time-point.

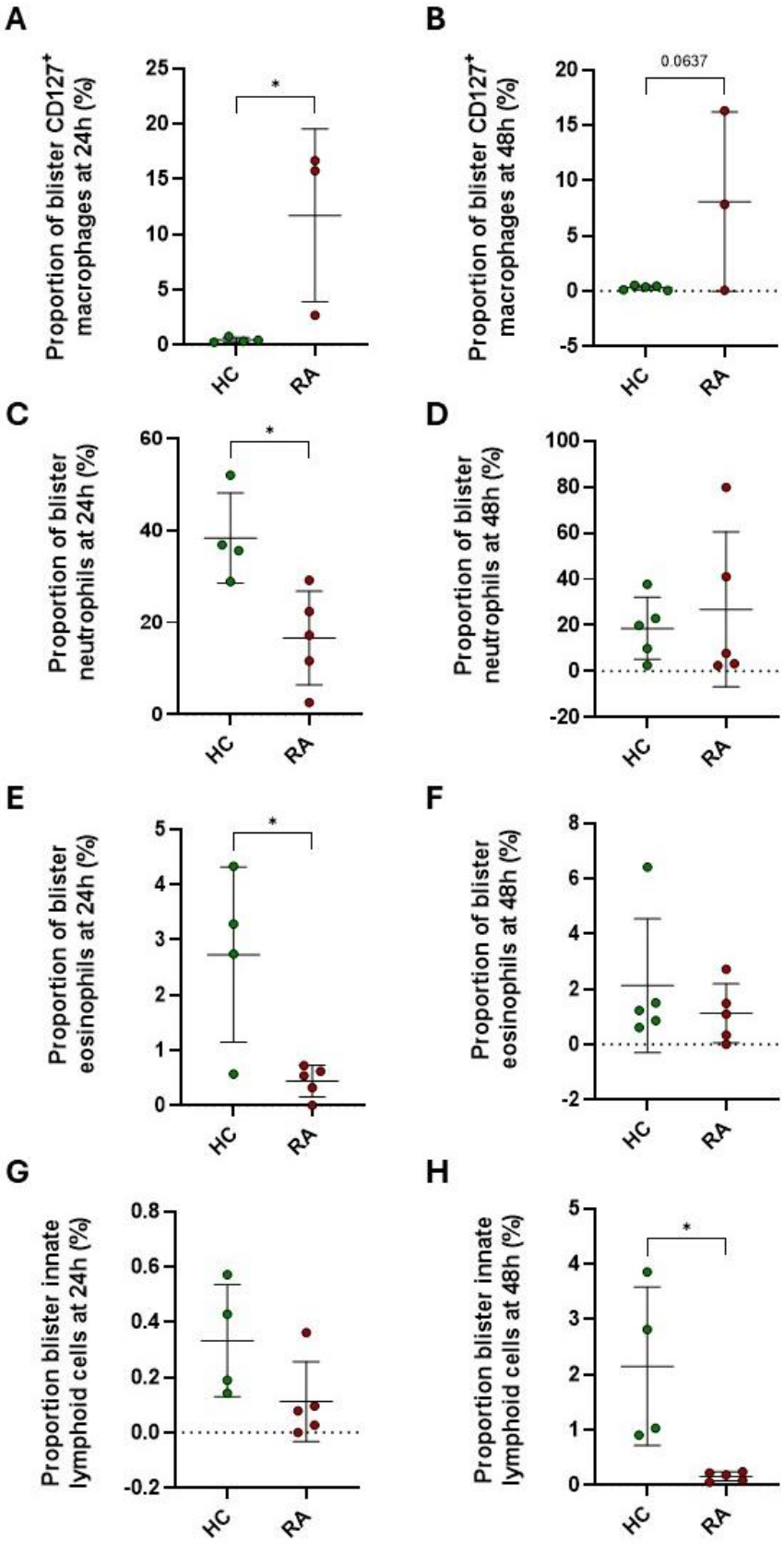
A
Proportion of blister CD127+ macrophages at 24h (%)
25
20
15
10
5
0
*
HC
RA
B
Proportion of blister CD127+ macrophages at 48h (%)
20
15
10
5
0
-5
0.0637
HC
RA
C
Proportion of blister neutrophils at 24h (%)
60
40
20
0
*
HC
RA
D
Proportion of blister neutrophils at 48h (%)
100
80
60
40
20
0
-20
HC
RA
E
Proportion of blister eosinophils at 24h (%)
5
4
3
2
1
0
*
HC
RA
F
Proportion of blister eosinophils at 48h (%)
8
6
4
2
0
-2
HC
RA
G
Proportion blister innate lymphoid cells at 24h (%)
0.8
0.6
0.4
0.2
0.0
-0.2
HC
RA
H
Proportion blister innate lymphoid cells at 48h (%)
5
4
3
2
1
0
*
HC
RA

Figure 6.25. Relative proportions of cell-types accumulating in the skin of RA patients and healthy controls at 48h following the intradermal injection of UV-KEc. Following the intradermal injection of 1.5 x 10^7 UV-KEc into the volar aspect of each forearm of RA patients and healthy controls, blisters were formed at 24h and 48h using a negative pressure suction cup. Single cell suspensions were obtained by ACK lysis and cells were incubated with a metal isotope-tagged antibody cocktail. Stained cells were acquired using the Helios XT SAE 20W-50 system and analysed using Cytobank Premium Software and R software programming language. Depicted are proportions of blister (A) $CD127^+$ macrophages at 24h for non-flaring RA patients (n = 3) and healthy controls (n = 5), (B) $CD127^+$ macrophages at 48h for non-flaring RA patients (n = 3) and healthy controls (n = 5), (C) neutrophils at 24h for all volunteers (n = 5), (D) neutrophils at 48h for all volunteers (n = 5), (E) eosinophils at 24h for all volunteers (n = 5), (F) eosinophils at 48h for all volunteers (n = 5), (G) innate lymphoid cells at 24h for all volunteers (n = 5) and (H) innate lymphoid cells at 48h for all volunteers (n = 5). *p < 0.05, **p < 0.01, ***p < 0.001, ****p < 0.0001.

6.3.5 RA patients have a faster onset and resolution of vascular hyper-reactivity

Using laser Doppler imaging, the blood flow at the site of UV-KEc-triggered inflammation was assessed. As previously shown in the Gilroy group, the onset of vascular hyper-reactivity was at 4h, as demonstrated by perfusion units, peaking at 24h in all groups and returning to baseline at 48h (**Figure 6.26**). This increase at 4h was significant in the RA group compared to baseline. In both groups, vascular hyper-reactivity reduced significantly between 24h and 48h. A representative Doppler image time-course and accompanying photograph is shown in **Figure 6.26B** and **Figure 6.26C**, respectively. Macroscopically, the skin of RA patients was more erythematous at both 4h and 24h. Overall, this would suggest that the onset and resolution of inflammation is accelerated and greater in RA compared the healthy controls.

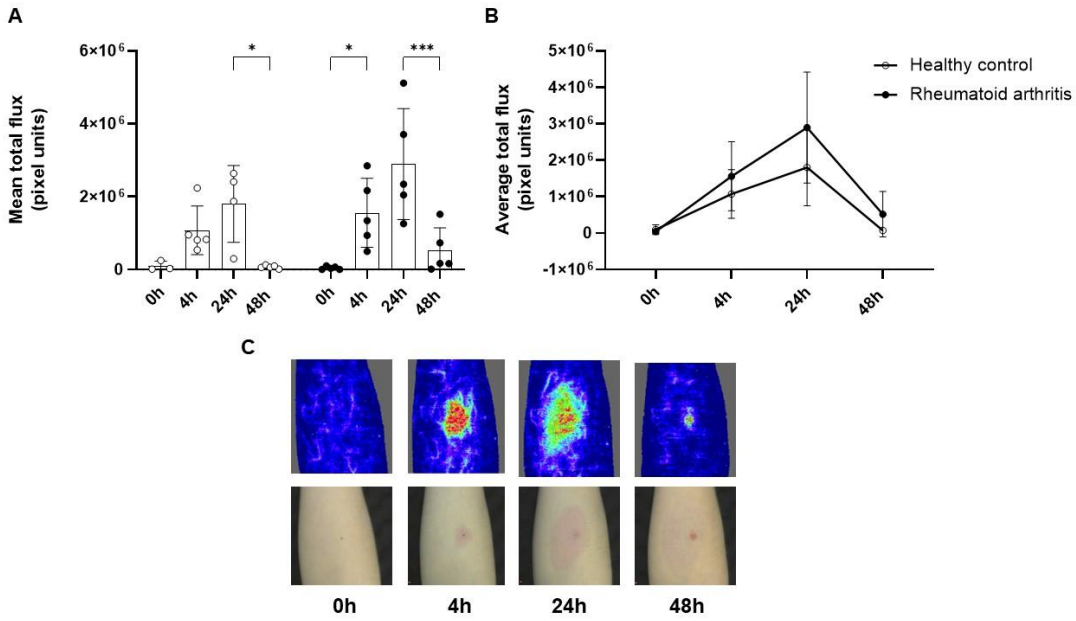

Figure 6.26. Vascular hyper-reactivity at the site of UV-KEc-triggered resolving acute resolution. Following the intradermal injection of 1.5 x 10^7 UV-KEc into the volar aspect of each forearm of RA patients and healthy controls, vascular hyper-reactivity was assessed using a laser Doppler imager (moorLDI-HIR) at baseline (0h), 4h, 24h and 48h. Depicted are (A) mean total flux (pixel units), (B) timeline of total mean flux and (C) representative Doppler image and accompanying photograph. Data are individual data points and mean values with SD; $n = 5$. *$p < 0.05$, **$p < 0.01$, ***$p < 0.001$, ****$p < 0.0001$.

6.3.6 Perception of pain and tenderness is significantly reduced in RA patients

A volunteer-reported visual analogue score was used to assess pain and elicited tenderness at the site of inflammation. Pain onset in the healthy control group was at 4h ($p < 0.01$), with no pain experienced by RA patients at this time (**Figure 6.27A**). Pain peaked at 24h in healthy controls ($p < 0.0001$), but did not return to baseline levels at 48h. RA patients only experienced pain at 24h following UV-KEc injection and this was significantly lower than healthy controls ($p < 0.05$). A similar trend was seen for elicited tenderness scores in both groups (**Figure 6.27B**).

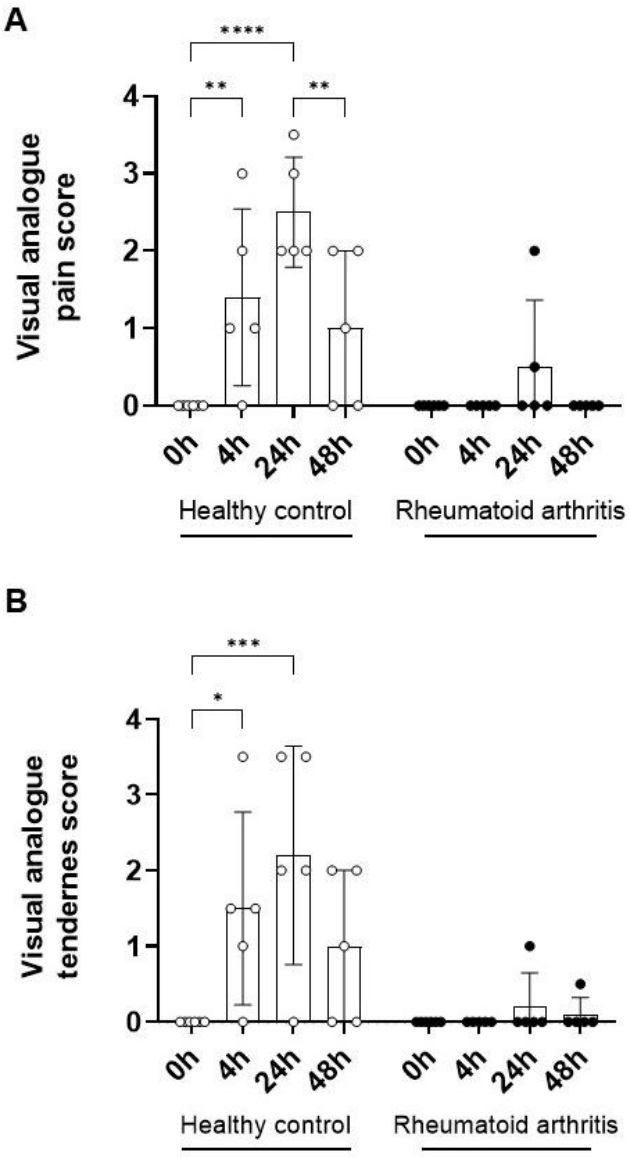

Figure 6.27. Clinical scores for pain and tenderness at the site of UV-KEc-triggered resolving acute resolution. Following the intradermal injection of 1.5 x 10^7 UV-KEc into the volar aspect of each forearm of RA patients and healthy controls pain scores (0 – 10; 10 = the worst pain imaginable, 0 = no pain at all) and tenderness scores (obtained using the same scale, following the application of a 100 g weight at the inflamed site) were assessed. Depicted are (A) mean volunteer reported pain scores and (B) mean tenderness scores. Data are presented as individual values mean with SD; $n = 5$. *$p < 0.05$, **$p < 0.01$, ***$p < 0.001$, ****$p < 0.0001$.

6.3.7 Central and site of inflammation temperature is equivalent in healthy controls and RA patients

Central body temperature, ambient room temperature and temperature at the site of inflammation was measured using a digital thermometer (Thermofocus®). No significant differences were detected when measuring central temperature at any time-point (**Figure 6.28A**). The ambient room temperature was measured at each throughout the study to control for background heat, with no significant differences seen at any timepoint (**Figure 6.28B**). Temperature at the site of UV-KEc-triggered inflammation peaked at 4h in healthy controls and 24h in RA patients although these differences were no significant (**Figure 6.28C**). Neither group returned to baseline temperature by 48h.

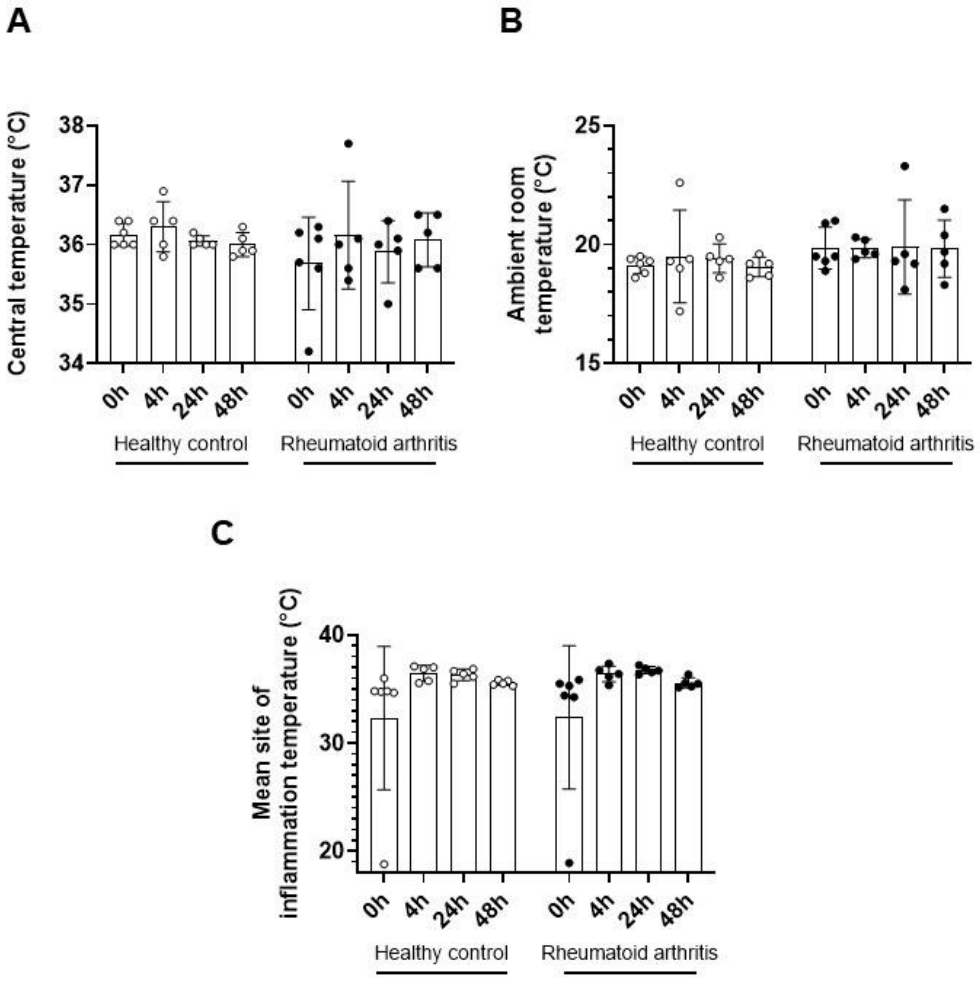

Figure 6.28. Central, mean site of inflammation and ambient temperature during UV-KEc-triggered dermal inflammation. Following the intradermal injection of 1.5 x 10^7 UV-KEc into the volar aspect of each forearm of RA patients and healthy controls, temperature was assessed at baseline (0h), 4h, 24h and 48h using a digital thermometer at the site of inflammation (Thermofocus®). Depicted are (A) central temperature (forehead), (B) ambient room temperature and (C) temperature at the site of inflammation (mean from both inflamed forearms). Data are expressed as individual values with means and SD; n = 5.

6.4 Summary of findings

The key aim of this chapter was to investigate the immune response of RA patients not on immunosuppressive therapy using a human, dermal model of resolving acute inflammation following the injection of UV-KEc. Additionally, I aimed to investigate inflammation at a clinical level, looking at pain and tenderness scores, temperature and measuring vascular hyper-reactivity by laser Doppler imaging.

The main conclusions of this chapter are:

- RA did not affect blister volume, blister cell numbers or blood cell numbers at any time-point.
- RA patients had significantly different baseline levels of both circulating myeloid and lymphoid cells by flow cytometric analysis.
- RA patients had significantly increased levels of plasmacytoid dendritic cells in the blister formed at 48h by flow cytometric analysis.
- RA patients had significantly fewer neutrophils and eosinophils in the blister fluid at 24h by UMAP analysis.
- RA patients had significantly fewer classical monocytes and innate lymphoid cells in the blister fluid at 48h by UMAP analysis.
- RA patients had a unique population of $CD127^{+}$ macrophages at the site of inflammation at 48h UMAP analysis.
- RA patients experienced significantly reduced pain and tenderness throughout the inflammatory time-course, with significantly lower scores at 4h and 24h, the peak of inflammation in this model.

6.5 Discussion

6.5.1 Utilisation of the UV-KEc model of dermal inflammation to investigate immune dysregulation in RA

Most scientific research into the underlying dysregulated immune system in RA has relied on cell-based techniques, animal models or by profiling tissue both in steady state and disease, but these are limited in their inability to inflame tissue *in vivo*. Whilst humans and mice share over 90% gene homology, the wide-ranging soluble mediator, cellular, genetic and epigenetic factors at play means that such models do not truly represent what happens in humans, *in vivo* (306). Indeed, whilst several murine models of inflammatory arthritis exist, including the collagen-induced arthritis model (233) and transgenic serum-transfer K/BxN model (452), these are not fully representative of the complex and multi-factorial pathogenesis leading to the development of RA in humans (168).

One of the unique strengths of this study is that all RA patients recruited were not taking disease-modifying treatment. Only a limited number of studies have been performed using treatment-naïve RA patients or those who are not on any treatment (453–458). This is in part due to the difficulty in recruiting these patients, given that most RA patients will be on treatment in the form of a DMARD, biologic drug or corticosteroids. Furthermore, higher infection rates have been reported in RA compared to non-diseased controls, but it is unclear whether this is due to the immunomodulatory effects of RA or due to the immunosuppressive effects of the drugs, thus confounding the results of these studies (459, 460). At the time of writing, this is the first human, experimental model of acute, resolving inflammation in RA patients not taking immunosuppressive medications, thus this model may be used to the investigate pro-resolution/anti-inflammatory signals without the confounding effects of such drugs.

6.5.2 Volunteer baseline characteristics

The healthy control group was approximately gender-matched with just one male participant (20%) and the rest being female. The majority of RA participants identified as white (60%), which is in keeping with UK prevalence data where 55-65% of RA patients are reported as white (461). In the UK, RA can occur at any stage of life but increases with age and the prevalence peaks in the third and fifth decades (137). The mean age of RA patients enrolled in this study was 53.8 years and 44.3 years for healthy controls, again in keeping with UK prevalence data. The groups were also well matched in terms of baseline characteristics, with no significant differences identified in terms of age, height or weight. As such, participants in this study were representative of the RA population in the UK

6.5.3 Baseline circulating immune cells in RA patients

Analysis by using manual gating in Flowjo revealed several key differences in circulating immune cells in RA patients compared to healthy controls. From the myeloid lineage, there were significantly higher total monocytes, intermediate monocytes, non-classical monocytes and myeloid dendritic cells in the blood of RA patients compared to healthy controls. From the lymphoid lineage, there were increased numbers of total $CD4^+$ T cells and all $CD4^+$ T cell subsets (naïve, central memory, effector memory and terminal effector) as well as total B cells, naïve B cells, T_{regs}, Th-2 and Th-17 cells. Additionally, there were fewer circulating NKT and $CD8^+$ T cells at 48h and fewer $CD8^+$ terminal effector T cells at 4h, 24h and 48h following the intradermal injection of UV-KEc. T_{regs} play a vital role in maintaining self-tolerance and regulate the immune response through intercellular interactions or by inhibiting pro-inflammatory cytokine release and inducing negative regulatory signalling molecules to suppress excessive immune responses (462). T_{regs} are also capable of generating anti-inflammatory cytokines, including TGF-β, IL-35 and IL-10 (463). Circulating T_{regs} are typically found in fewer numbers in patients with RA and their frequency is fewer still in patients with high levels of disease activity (464). Furthermore, it has been shown that the number and inhibitory activity of T_{regs} are

higher in clinical remission compared to active RA and that T_{reg} inhibitory activity is inversely correlated with clinical disease activity scores (465). T_{regs} have also been shown to be low in RA patients in the early stages of the disease (466). Interestingly, the frequency of T_{regs} in the synovium of RA patients with active joint inflammation is higher than those without the disease (467). Whilst I did not investigate immune cells from the synovial fluid or membrane in this study, a significantly elevated circulating T_{reg} population in RA patients compared to healthy controls suggests that these cells may play a role in maintaining disease remission. Thus, increasing T_{reg} numbers or improving the function of existing T_{regs} in RA may be a potential treatment strategy to reduce disease activity and prevent damage to joints (462, 468). In addition to higher T_{reg} numbers in RA patients, there were also higher baseline levels of Th-2 but not Th-1 cells. Th-1 cells induce pro-inflammatory cytokines, including IFN-γ, IL-2 and TNF-α, whereas Th-2 cells primarily secrete IL-4, IL-5 and IL-13, which are anti-inflammatory and anti-osteoclastogenic (469). Furthermore, Th-2 cytokine-mediated processes include further activation of Th-2 cells by IL-4 and IL-13, IL-5-induced eosinophil expansion, IL-33-mediated macrophage polarisation and the production of IL-10 and IL-27 by B cells (470). Overall, it would seem that the RA patients in this study demonstrated an anti-inflammatory repertoire of cells which together play a role in maintaining disease remission.

$CD8^+$ T cells are known to contribute to the development of RA amongst other autoimmune diseases, including SLE, anti-neutrophil cytoplasmic antibody-associated vasculitis, multiple sclerosis and type 1 diabetes mellitus (471–473). Using the K/BxN murine model of arthritis, $CD8^+$ T cells have been shown to be increased in both the peripheral blood and synovium of arthritic mice, findings which have also been shown in the circulation and inflamed joints of RA patients (474, 475). Taken together, this indicates that $CD8^+$ T cells are enriched in RA patients with active disease both in blood and the inflamed joint. Carvalheiro *et al.* (2015) showed that $CD8^+$ T cells are reduced in RA patients in disease remission compared to both healthy controls and RA patients with active disease, suggesting a role for $CD8^+$ T cells as a biomarker of disease activity (476). They also showed that these cells produced less pro-inflammatory IL-6, TNF-α, IL-17A and IFN-γ and that this correlated with disease

activity scores. In addition, it has also been shown that these $CD8^+$ T cells are effector T cells and not central memory T cells (477). Given that $CD8^+$ terminal effector T cells were significantly reduced in RA patients in this study following the intradermal injection of UV-KEc, I suggest that fewer circulating (and likely synovial) $CD8^+$ terminal effector T cells in these patients enable the maintenance of disease remission, conferring a reduced pro-inflammatory cytokine signature, unlike those with active disease.

NKT cells have been described as T lymphocytes expressing NK receptors, such as NK1.1 and CD161, recognising glycolipid antigens unlike conventional T cells (478). A unique feature of NKT cells is that their T cell receptor (TCR) repertoire is highly skewed with an invariant TCR-α rearrangement, Vα24 (479). NKT cells are thought to play important roles in the regulation of immune response as they are known to rapidly produce large quantities of both pro-inflammatory Th-1 (IL-1β, IL-6 and TNF-α) and anti-inflammatory Th-2 cytokines (IL-4, GM-CSF and IL-13) on activation and can therefore enhance or suppress inflammation (480). Reduced numbers of NKT cells have also been implicated in the development of autoimmune disease including lupus-prone (NZB × NZW) F1 mice (481). In humans, Vα24 NKT cell numbers are reduced in the peripheral blood of patients with a variety of organ-specific and systemic autoimmune conditions including RA (482, 483). There are, however, conflicting findings and a decrease in Vα24 NKT cell numbers is not found in all autoimmune diseases, as it is not observed in Graves' disease, myasthenia gravis or celiac disease (480, 482). Overall, as with $CD8^+$ effector cells, it is therefore likely that the significant decrease in circulating NKT cells following intradermal injection of UV-KEc in RA patients compared to healthy controls is a mechanism by which RA patients maintain disease remission, likely due to a diminished Th-1 cytokine response. Whilst the production of high levels of both IFN-γ and IL-4 cytokines by Vα24 NKT cells following TCR stimulation remains a challenge for understanding their mode of action, manipulation of Vα24 NKT cell responses is an exciting potential target for autoimmune disease therapies, including RA.

6.5.4 RA patients have a unique population of CD127^{+} macrophages

The most striking finding from the UMAP analysis of immune cells present in RA and healthy control blister fluid was the presence of a unique CD127^{+} population of macrophages found only in RA patients who were in disease remission. CD127 is an IL-7 receptor subunit, with IL-7 being a member of common γ chain receptor cytokine family (484). IL-7 receptor is a heterodimer and is composed of the common γ chain receptor and IL-7-specific α chain (CD127) (485). The degree of CD127 expression determines the extent of signal through the IL-7/IL-7 receptor complex, which activates two major pathways, JAK/STAT5 and Akt/phosphatidylinositol 3-kinase (Akt/PI3K), as well as being a weak activator of the MAPK/ERK pathway (486, 487). IL-7 is known to modulate CD127 expression with two known forms of CD127, including immune cell membrane-bound and soluble CD127 in peripheral blood (488). It is known that both IL-1β and TNF-α increase stromal production of IL-7 and in turn IL-7 upregulates TNF-α production by macrophages, inducing the production of osteoclastogenic cytokines by T cells and leading to the maturation of osteoclasts and subsequent bone destruction seen in RA (489). Indeed, treatment with IL-7 has been shown to increase STAT5 phosphorylation, pro-inflammatory cytokine secretion, promote cellular proliferation and enhance monocyte activation of CD4^{+} T cells (490). However, PI3K/AKT has also been shown to be a major effector of IL-7 with IL-7 induced PI3K-dependent phosphorylation of Akt and its downstream targets GSK-3, FOXO1, and FOXO3a (487) and IL-7 regulates autophagy *via* PI3K/AKT signalling in lung cancer cells (491). In addition to the pro-inflammatory actions, IL-7 is also important for naïve T cell differentiation and survival, as well as memory T cell development and homeostasis (484). IL-7 and CD127 are also critical for B cell development in mice, as well as differentiation and survival of naïve T cells and generation of memory T cells (485). IL-7 regulates the rearrangement of immunoglobulin genes in immature B cell subsets and T cell receptor genes in precursor T cell subsets *via* the CD127 signalling pathway to ensure primary antibody repertoire and T cell diversity (492). Furthermore, IL-7 controls the survival of mature and memory T cells by upregulating the expression of anti-apoptotic Bcl-2 family proteins and the glycerol channel aquaporin-9, thus promoting long-term immunity, again mediated *via* PI3K signalling (493, 494). Additionally, IL-7 is also known to

have anti-virus and anti-tumour functions and plays important roles in the restoration of immune function (495). IL-7 is also known to modulate the responses of immune cells, such as NK cells, dendritic cells, B cells, and T cells, against pathogens (496–499) and IL-7 treatment has been shown to promote Th-2 cell immune responses, increasing the production of neutralising antibodies and increasing the cytotoxicity of antigen-specific cytotoxic T cells (500). As described, IL-7 PI3K/AKT signalling confers several anti-inflammatory actions and informs on the development of T cell memory, but it is also known that increased PI3K/AKT signalling can reduce the anti-inflammatory function of T_{regs}, as unlike effector T cells, T_{regs} rely on minimal activation of this pathway to develop and maintain their characteristic phenotype, function, and metabolic state (501). Taken together, I therefore propose that the significantly higher levels of $CD127^+$ macrophages at the site of inflammation in RA without ongoing disease activity represents a mechanism by which RA patients maintain disease remission. I propose that the upregulation of CD127 by macrophages at the site of inflammation, such as the skin used here (and likely in the synovium) in RA patients, leads to an increase in PI3K/AKT but not JAK-STAT5 signalling, skewing the immune response to an anti-inflammatory/pro-resolution phenotype. In turn, this leads to increased $CD4^+$ T cell differentiation, as shown by increased baseline circulating total $CD4^+$ T cell, as well as $CD4^+$ naïve, central memory, effector memory and terminal effector T cell subsets in RA patients compared to healthy controls using this model. More recently in mouse, Feehan *et al.* (2024) has shown that in animals exposed to *S. pneumoniae*-induced lung inflammation, differential gene expression of alveolar macrophages implicated CD127 in the facilitation of macrophage-T cell interaction in the post-resolution phase (260). Therefore, post-resolution phase macrophages can directly interact with T cells in their environment to shape their phenotype and function and IL-7 may provide a key link between the innate and adaptive immune systems. Using models in which tissue is inflamed, as described here, further insight can be gained into the interplay between innate and adaptive immune responses in RA patients.

Cells of the myeloid lineage cells are not historically well-recognised CD127-expressing cells (502), although have more recently been shown to have highly

inducible expression upon activation (503). However, the functional significance and biological importance of IL-7 receptor signalling remains unknown. From a clinical perspective, recently, Zhang *et al*. (2022) identified an anti-inflammatory $CD127^+$ population of mononuclear phagocytes in COVID-19 patients in inflamed lung tissue, as well as in RA patients and that these cells rendered otherwise inert monocytes responsive to IL-7 (504). They showed that active IL-7 signalling engaged epigenetically coupled, STAT5-coordinated transcriptional programmes to restrain inflammatory gene expression, leading to an inverse correlation between CD127 expression and inflammatory phenotype of these cells. Thus, the $CD127^+$ macrophages identified in this model may similarly represent an anti-inflammatory phenotype. Additionally, they were unable to detect CD127 expression in mouse. CD127 has previously been shown to be downregulated postnatally following foetal monocyte expression, although one group has been able to demonstrate transient expression, and therefore murine models of inflammation may not suitable to investigate IL-7/IL-7 receptor signalling, giving further strength to the *in vivo* human model reported here to investigate the significance $CD127^+$ macrophages in RA (505). Synovial fluid-derived monocytes from patients with spondyloarthritis (both axial spondyloarthritis and psoriatic arthritis) have been shown to be enriched for $CD127^+$ cells with a unique transcriptional profile that overlaps with IL-7-induced gene sets (*LTB, CD14, CCL5, IL32* and *TCF7*) (506). These cells were found at a lower frequency in PBMCs isolated from peripheral blood, suggesting a role for these cells at the site of inflammation. Conversely, whilst Chen *et al.* (2013) showed increased expression of IL-7 and CD127 in the circulating monocytes of RA patients, higher levels correlated with increased disease activity and TNF-α levels, suggesting this represents a positive feedback regulation between IL-7/IL-7 receptor and TNF-α pathways by producing and responding to TNF-α (507). However, only seven of the 76 patients investigated in this study were on no treatment. Kim *et al.* (2020) described IL-7R/CD127 expression by 'M1' macrophages as the hallmark of RA and that these cells are highly responsive to IL-7-driven osteoclastogenesis. Furthermore, they established that LPS, IFN-γ and TNF-α enhanced IL-7R expression in RA and murine macrophages and that IL-7-induced arthritis is dependent on $F480^+iNOS^+IL\text{-}7R^+CCL5^+$ cell function, which activates Th-1 cells to amplify myeloid IL-7R expression and disease severity (508). Pickens *et al.* (2011) have also shown that IL-

7 and CD127 were co-expressed on RA synovial tissue lining, macrophages and endothelial cells and were significantly elevated in RA synovial fluid, circulating mononuclear phagocytes and fibroblasts (509). In addition, they showed that both LPS and TNF-α stimulation modulated expression of IL-7 and CD127 on RA macrophages and human lung microvascular endothelial cells (HMVECs), but only CD127 in RA fibroblasts. IL-7 also mediated RA pathogenesis by inducing production of potent proangiogenic factors from macrophages and endothelial cells implicating a novel role for IL-7 signalling in RA angiogenesis (509). Overall, the role of IL-7/CD127 signalling in RA is complex with both anti-inflammatory, as suggested using the model of dermal inflammation here, and pro-inflammatory functions and warrants further investigation to understand the contributions of both the JAK/STAT5 and PI3K/AKT pathways in inflammatory resolution. IL-7/CD127 signalling represents an exciting target for the treatment of RA by decreasing JAK/STAT5 activation to switch off pro-inflammatory, osteoclastogenic and angiogenic pathways or by augmenting PI3K/AKT activity to facilitate a switch to a pro-resolution phenotype

6.5.5 RA patients have fewer blister neutrophils, classical monocytes, ILCs and plasmacytoid dendritic cells

Dendritic cells play crucial roles in the pathogenesis of RA. Whilst conventional dendritic cells are professional antigen-presenting cells, plasmacytoid dendritic cells are enriched in the RA synovium and when activated show both enhanced migratory capacity and increased T cell activation (510). They are the most potent producer of type I IFNs in humans and are likely to be tolerogenic in RA (511). The type I IFN family, including IFN-α and IFN-β, stimulate macrophages and NK cells to elicit an anti-viral response, but is also crucial to trigger an adaptive immune response (512, 513). Whilst plasmacytoid dendritic cells were not detectable in the blister fluid at the site of inflammation at 24h, numbers increased significantly at 48h in RA patients compared to healthy controls. In this model, it is likely that plasmacytoid dendritic cells are involved in TLR4-mediated recognition of UV-KEc-derived LPS and produce high levels of IFNs. This in turn stimulates dendritic cell maturation and the subsequent expression of pro-inflammatory cytokines and costimulatory molecules,

leading to the transition to adaptive immunity (514). This may suggest local dysregulation in immune response in RA patients at the site of UK-KEc-triggered inflammation, equivalent to the aberrant process seen in the synovium and subsequent clinical manifestation of inflammatory arthritis in the joints of RA patients. Having seen an expanded population of plasmacytoid dendritic cells at the site of inflammation, this model can therefore be used as a tool to investigate the importance of the dendritic cell-driven type I IFN responses in RA patients.

More recently, the discovery of the innate lymphoid cell (ILC) family was accompanied by recognition that IL-7 was also essential for development and maintenance of many of its members, and consequently the generation of lymphoid structures and barrier defence mechanisms mediated by these cells (515). However, it remains unclear exactly how IL-7 controls the development of ILCs, although is thought to be dependent on key transcription factors such as NFIL3, whose activation is dependent on IL-7 signalling (516). The presence of $CD127^+$ macrophages at the site of UV-KEc-triggered dermal inflammation in RA patients in disease remission, but not those who were about to flare, was paradoxically accompanied by fewer ILCs at 24h in the blister fluid and significantly fewer at 48h, compared to healthy controls. Previous studies have shown that ILCs accumulate in the synovial tissues of RA patients with active disease, which produce more IFN-γ than their peripheral blood counterparts and promote TNF-α production by $CD14^+$ monocytes in the joints following activation with IL-12, IL-15, and IL-18 (517). Pro-inflammatory ILCs enriched in the synovial fluid of RA patients have also been shown to positively correlate with disease activity (518). Therefore, the decrease in ILCs at the inflamed skin in RA patients compared to healthy controls would suggest that, even in the presence of high levels of CD127, ILCs are not a predominant inflammatory cell-type in RA patients in disease remission.

Mononuclear phagocytes are of particular interest in RA, as macrophages are known to be enriched in the synovium of active RA, providing a major source of pro-inflammatory cytokines, including TNF-α (519). Therefore, following the intradermal injection of UV-KEc, an increase in pro-inflammatory infiltrating monocytes would

have been expected. However, using this model of inflammation, there were fewer blister classical monocytes at both 24h and 48h in RA patients, compared to healthy controls. This finding is in keeping with previous work from our group by Dr Julia Flint (MD thesis) who has also shown using the UV-KEc model of dermal inflammation in RA patients significantly fewer blister classical monocytes at 24h, although no blisters were formed at 48h. Flint also showed that blister IFN-γ and IFN-γ inducible protein-10 (IP-10/CXCL10), both involved in monocyte activation and chemotaxis, were decreased at the site of inflammation whilst other monocyte chemoattracts including MCP-1 and MCP-4 were present at equivalent levels in both RA patients and healthy controls. Classical monocytes are the dominant blood population, expressing CCR2, a receptor involved in migration from bone marrow and recruitment to sites of inflammation by MCP-1 (520). IP-10 is produced by monocytes, endothelial cells and fibroblasts in response to IFN-γ and promotes chemoattraction of mononuclear phagocytes, T cells, NK cells and dendritic cells *via* its ligand, CXCR3, to sites of inflammation (521). Flint also showed that CXCR3 was decreased on classical monocytes of RA patients compared to healthy controls, suggesting defective IP-10/CXCR3 signalling may be involved in the reduced numbers seen in both studies. What is not clear is whether the reduced numbers of classical monocytes seen was due to decreased IFN-γ and IP-10 and subsequent decrease in monocyte chemotaxis, or whether low levels of IFN-γ and IP-10 was a consequence of fewer monocytes at the site of inflammation and warrants further investigation. In addition, elevated levels of IL-7 in RA synovial tissue have been shown to be involved in attracting monocytes into the inflammatory joints and remodelling them into pro-inflammatory macrophages and mature osteoclasts (522). Whilst I did not perform cytokine analysis on the blister fluid, given high levels of CD127 it seems unlikely this would have contributed to reduced classical monocyte numbers. There were also significantly fewer neutrophils in the blister at 24h in RA patients compared to healthy controls, suggesting that there was no impairment to neutrophil clearance by these cells. It is therefore also feasible, that in RA patients, there is enhanced phagocytic capacity of inflammatory monocytes as has previously been reported (523, 524) and that the neutrophils have been cleared by classical monocytes efferocytosis by 24h, subsequent conversion to a pro-resolution 'M2' phenotype and emigration from the site of inflammation (2, 21). Overall, the

mechanisms by which fewer classical monocytes seen in the blister fluid of RA patients following intradermal injection of UV-KEc are complex but could be mediated *via* a combination of reduced IP-10/CXCL10 chemoattraction and/or accelerated resolution of inflammation, conversion of inflammatory monocytes to an anti-inflammatory and emigration.

6.5.6 RA patients have a faster onset and resolution of vascular hyper-reactivity

In keeping with previous work in the Gilroy group by Dr Julia Flint (MD thesis), the onset of vascular hyper-reactivity was at 4h, peaking at 24h in all groups. Whilst not statically significant, this was higher at both 4h and 24h in the RA group, suggesting a more rapid and robust inflammatory response in RA patients compared to healthy controls following inoculation with UV-KEc. It can thus be postulated that in patients with RA, the onset of inflammation is more rapid and the rate of resolution is faster than that seen in healthy controls. The biological significance of enhanced inflammatory resolution could suggest that RA patients have a 'primed' immune response which can activate more rapidly compared to healthy controls but is never truly switched off creating an environment in which tolerance can be lost and autoimmunity develops. This observation would also be in keeping with the visibly less red skin seen in RA patients at the site of inflammation and the significant reduction in both neutrophils and classical monocytes seen at 24h.

6.5.7 Perception of pain and tenderness is significantly lower in RA patients

One of the most striking findings in this study was that RA patients experienced significantly less pain and tenderness at the site of UV-KEc-triggered inflammation, the symptomatic response the inflammatory stimulus. Pain remains on the of the most important symptoms of disease activity in RA patients as commonly cited in patient-reported outcome and experience measures (525). Pain in RA is complex and arises

from multiple mechanisms, including inflammation, peripheral and central pain processing, psychological factors, coexisting disease (multimorbidity), as well as structural changes to the anatomy of the arthritic joint (526). Given that the subjective experience of pain is included in several disease activity scores used in clinical practice to assess patients and inform on the need for treatment escalation, it is paramount we understand the significance of this debilitating symptom in RA patients (527). Overall, the two likely explanations for reduced pain levels in RA patients would be either the local inflammatory response leading to decreased production of pain mediators and subsequent reduced activation of nociceptors, or that UV-KEc-triggered inflammation pain receptors were activated to a similar degree in both RA patients and healthy control and that chronicity of disease and the development of tolerance to pain over time could have developed, involving central modulation of ascending pain pathways (528). However, several studies have shown a reduced pain threshold in patients with RA rather than increased (529–532) and that this pain threshold reduces further with longer disease duration (533). Importantly these studies do not report pain in RA patients at sites of triggered inflammation, distal from the inflamed index tissue; the synovium. Thus, at the time of writing, this is the first report of decreased pain in RA patients following experimental inflammation at a site distal to the inflamed joint and may point to an adapted immune response and diminished nociceptor activation at the site of inflammation in these patients. Whilst the RA patients enrolled in this study were in disease remission, it is known that pro-inflammatory mediators at the site of inflammation are important in mediating the pain response in RA (534). As in the joint of RA patients, at the site of UV-KEc-triggered inflammation there is likely production of inflammatory cytokines (IL-1β, IL-6, TNF-α, IL-8), anti-inflammatory cytokines (IL-4, IL-6, IL-10, IL-12, IL-13) and PGs (including PGE_2), all of which have a recognised potential to trigger nociceptors (535). It is also possible that the lower pain scores reported by RA patients in this study could also be mediated *via* a reduction in soluble pain mediators such as vasopressin, angiotensin II, vasoactive intestinal peptide, substance P, histamine, bradykinin or eicosanoids (including PGs), however, these were not quantified in this study (534). Overall, RA patients experienced less pain and tenderness at the site of UV-KEc-triggered dermal inflammation compared to healthy controls and this model provides a platform in which these pathways can be further investigated including the contribution of soluble mediators of pain.

6.5.8 Study limitations

One of the biggest challenges and thus limitations of this study was the recruitment of RA patients. In order to enrol RA patients who were not taking any immunomodulatory medication, these had to be either patients who were very early in their disease course i.e. those who were yet to start treatment, or those who had chosen not to take medication for personal reasons, such as those who wish to control their disease activity through lifestyle/dietary modification or those preferring to use complementary therapy such as homeopathy. A further group included those whose disease had simply burnt out with no ongoing need for regular medication. Additionally, all national and international guidelines put great emphasis on the need to treat patients early and aggressively with corticosteroids and disease modifying drugs, to halt disease progression and prevent permanent joint damage and ultimately disability (536). As informed by the study's ethical approval, patients were recruited with low disease activity (DAS28 less than 3.2), so whilst the sample represents the underlying immune dysregulation present in those recruited, it did not capture those with significantly active disease at the time of the study. The immunological activity at this time is likely to be different to subjects who are not presenting with clinically active disease.

Furthermore, this study was conducted before, during and after the peak of the COVID-19 pandemic. The government-enforced 'lockdown' meant that during this time, patients and healthy volunteers alike were either legally not permitted to travel or understandably were anxious to do so, even as restrictions were lifted. UCL's policy also prohibited human studies for a significant period of time and the Gilroy laboratory was closed, meaning that even those volunteers who had consented to partake in the study, were unable to do so. Nevertheless, the small sample size underpowers the study and further work needs to be done to increase numbers for future studies.

Overall, I have shown for the first time in RA patients not on treatment, an experimental and translational model of inflammation that the UV-KEc can be used to investigate pro-resolution and anti-inflammatory signal important for maintaining

disease remission. Collectively, these data suggest that RA patients may have a more rapid onset and resolution of inflammation and that they experience less pain at sites of inflammation distal to the index tissue. In addition, I have identified a unique population of $CD127^{+}$ macrophages in RA patients in remission, which can be further investigated using this model and may represent a novel, druggable target for the treatment of RA.

7 Final conclusions and future directions

7.1 Summary of thesis findings

The data presented in this thesis highlights key differences in the immune response of RA patients both during steady state (baseline) and experimental inflammation. I have demonstrated, for the first time in humans, that the UV-KEc dermal model of inflammation and subsequent analysis by mass cytometry can be safely used in RA patients who are in disease remission. I have also shown that the anti-inflammatory drugs, naproxen and ATB-346, can be used in this system to investigate anti-inflammatory and pro-resolution signals in humans. In addition, I have shown that RA patients not only have a more rapid onset of inflammation following the intradermal injection of UV-KEc but can resolve inflammation faster than healthy controls. My overarching hypothesis was that RA patients in remission maintain low levels of clinically active disease by the upregulation of protective, pro-resolution/anti-inflammatory pathways and I have suggested a mechanism by which this is achieved. Specifically, I have shown a unique population of $CD127^{+}$ macrophages in RA patients at the site of inflammation and propose that upregulation of CD127 by macrophages results in an increase in PI3K/AKT but not JAK-STAT5 signalling, skewing the immune response to an anti-inflammatory/pro-resolution phenotype and that this was characterised by a reduction in neutrophils and classical monocytes in the inflamed skin. The proposed mechanism has been summarised and shown in **Figure 7.1**.

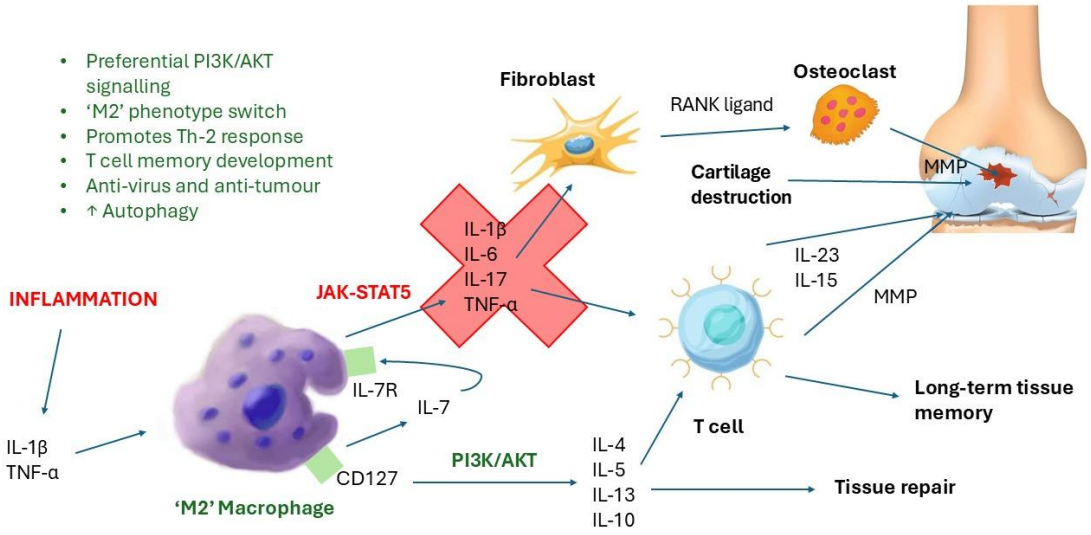

Figure 7.1. Summary figure showing proposed mechanism by which CD127$^+$ macrophages maintain disease remission in RA. Following the initiation of inflammation, IL-1β and TNF-α lead to an increase in IL-7 signalling. Upregulation of CD127 by macrophages leads to an increase in PI3K/AKT but not JAK-STAT5 signalling, thus promoting a switch in phenotype to 'M2' macrophages and skewing the immune response to one which is anti-inflammatory and pro-resolution, thus leading to improved tissue repair as opposed to the joint damage typical of RA.

Circulating anti-inflammatory T_{regs}, and Th-2 cells were higher in RA patients in remission at baseline as well all CD4$^+$ T cell subsets (naïve, central memory, effector memory and terminal effector) suggesting these patients have a repertoire of anti-inflammatory cells, which together play a role in maintaining disease remission and immune memory. In addition, following the intradermal injection of UV-KEc, there were fewer circulating pro-inflammatory CD8$^+$ terminal effector and NKT cells. I therefore suggest that during inflammation, fewer circulating (and likely synovial) CD8$^+$ terminal effector T cells and NKT cells in these patients contribute to the maintenance of disease remission, conferring a reduced pro-inflammatory cytokine signature, unlike that seen in RA patients with active disease. These data therefore provide a novel link between the innate and adaptive arms of the immune system and this model can be used to further investigate anti-inflammatory/pro-resolution signals important in maintaining disease remission.

I have also developed novel murine models of both resolving and non-resolving dermal inflammation, using the same inflammatory stimulus as used in the human models; UV-KEc. At high dose of UV-KEc, I have shown that there was formation of granuloma-like tissue at the site of inflammation and that infiltrating Ly6C^{hi} and Ly6C^{int} monocytes may be important for the initial formation of this granuloma with its maintenance dependent on T cells, NK cells and neutrophils. Additionally, at the high dose of UV-KEc, emergency granulopoiesis and release of both mature and developmentally immature neutrophil subsets from the bone marrow was observed. These neutrophils showed variation in CD11b expression, which may represent a possible mechanism to enhance initial capture of neutrophils at the endothelium and subsequent transmigration into the inflamed site, but also reduced CD16 expression, suggesting intrinsic low functionality of the emergency release of neutrophils. Importantly using this model, I have been able to confirm the expansion of a phenotypically distinct subset of intermediate monocytes, Ly6C^{int} monocytes, analogous to the intermediate monocytes found in humans. Using these models, I have also shown for the first time that endocannabinoids can be extracted and quantified from inflamed mouse skin and plasma and that these are responsive to UV-KEc. I propose that both 2-AG and PEA may have a role in pro-resolution events, potentially mediated through reduced activation of the NF-κB signalling and AEA may contribute to increased phagocytosis. Collectively, these murine models of inflammation can be used as a tool, in parallel with the human model, to investigate the role of granuloma formation, emergency granulopoiesis, Ly6C^{int} monocytes and endocannabinoids in the resolution of inflammation and the development of autoimmune diseases.

7.2 Clinical relevance

The mechanisms behind the anti-inflammatory effects of NSAIDs are well-established and both naproxen and ATB-346 likely exerted potent anti-inflammatory actions in this model by the inhibition of COX activity and subsequent suppression of PGE_2 production, mediated *via* EP2 signalling (398). I have shown that the addition of H_2S to a conventional NSAID, naproxen, may have additional anti-inflammatory actions, potentially through the polarisation of macrophages at the site of inflammation to the

'M2' phenotype and by H_2S-driven enhancement of efferocytosis due to inhibition of p38 MAPK signalling and activation of macrophage SR-mediated autophagy. ATB-346 is therefore an attractive alternative to traditional NSAIDs, whose long-term use is limited by significant GI and cardiovascular adverse effect. Often, patients with RA in severe pain turn to opioids, which are not hampered by GI adverse effect as with NSAIDs. As the opioid crisis continues in the developed world (201, 202), it is vitally important that we can find new anti-inflammatory therapeutics that are both efficacious, but also agreeable to patients in terms of adverse effects. This is especially important, particularly long-term, given major issues with tolerance and dependence with opioid medication (202). Contrary to the literature (533), RA patients reported significantly lower pain and tenderness scores at the site of inflammation, compared to healthy controls. However, this is the first report of decreased pain in RA patients following experimental inflammation at a site distal to the inflamed joint. Given the potential for dysregulated immune responses at the site of inflammation and therefore the potential involvement of local soluble pain mediators, this warrants further investigation to identify potential targets to attenuate local pain signals important during inflammation.

7.3 Future directions

As described, the expansion of intermediate monocytes and their contribution to the pathogenesis of chronic inflammation and development of autoimmune diseases in humans is well known (317, 325, 327, 537). Future work should therefore include investigating the mechanism associated with the expansion of $Ly6C^{int}$ monocytes in the non-resolving model of inflammation, including the p38 MAPK pathway and whether this can be manipulated, for example, with the use of losmapimod, an orally available, potent p38 MAPK inhibitor, in RA patients. Losmapimod could also be used in RA patients using the human model and has safely been used in RA patients in a pharmacokinetic study (538) and a randomised, double-blind, placebo-controlled Phase 2b trial in facioscapulohumeral muscular dystrophy (539). Thus, both the murine and human models reported here can be used together to further investigate

murine Ly6C^{int}/human intermediate monocytes *in vivo*, following experimental inflammation.

Given the small sample size in the RA study, it is important that the novel findings described here are confirmed in larger numbers of RA patients in remission. To avoid the confounding factor of immunosuppressive drugs in the study, RA patients were recruited who were not on treatment and in disease remission at the time of enrolment. As most RA patients are on immunosuppressive treatment, leading to the relatively small sample size, future studies would require a multicentre approach to maximise recruitment. In addition, it is likely that increased CD127^{+} macrophages may be relevant in other autoimmune diseases and at different times of life, so it would be important to use this model to investigate other autoimmune diseases, including juvenile idiopathic arthritis (onset before 16 years), axial spondyloarthritis, psoriatic arthritis and SLE and include younger volunteers in recruitment. Given that I only sampled the blisters formed at the inflamed site at 24h and 48h, it will also be informative to include a 4h timepoint to investigate the onset of inflammation, as well as a later timepoint, such as 14 days, to better understand the interplay of these innate immune cells with the adaptive immune response and their role in adapted homeostasis. Furthermore, I was not able to quantify resolution indices at the site of dermal inflammation in the human studies described here as only two time-points were used. To apply these principles and pinpoint the time of inflammatory resolution following the injection of UV-KEc into the skin, further time-points are needed to complete the landscape of inflammatory resolution, as shown in the resolving mouse model in **Chapter 4**.

Additionally, the Maxpar® Direct Immune Profiling Assay (MDIPA) kit used in the RA study is primarily designed to investigate cells of the adaptive immune system, with a focus on T cell subpopulations. Thus, modifying the antibody cocktail used in mass cytometry in this model can be used to further phenotype the CD127^{+} macrophage population identified in RA patients in remission, tailored towards cells of the innate immune system to give further insight into the function of these cells and their role in maintaining disease remission. This could also be complemented with

temporal single-cell transcriptomic analysis of isolated PBMCs, however, this would require the use of flow cytometry for blister cells, as mass cytometry is a destructive technique, meaning cells cannot be sorted for further analysis (540, 541). Having identified a novel immune signature of RA patients which may be important in maintaining disease remission, it will be important to demonstrate mechanistically the impact of these cells on the immune response. At the time of writing, no IL-7 knock-out mice are commercially available and so a Cre/lox macrophage-specific knock-out mouse would need to be generated and utilised to investigate the role of CD127/IL-7 signalling using the resolving and non-resolving models of murine inflammation described in **Chapter 3** and **Chapter 4**.

7.4 Concluding remarks

This thesis aimed to develop a toolkit, as summarised in **Figure 7.2**, in which to identify protective, pro-resolution/anti-inflammatory pathways in RA patients in remission, which contribute to low levels of clinically active disease. Specifically, I sought to develop and characterise murine and human models of inflammation, allowing the investigation of the onset, resolution and post-resolution phases. Overall, I have characterised an experimental model of inflammation in which to safely investigate pathways leading to and maintaining remission in patients with inactive RA. I have identified a unique cell population which may be important in this process and shown that the model is responsive to pharmacological manipulation. I have also developed corresponding resolving and non-resolving murine model of dermal inflammation, unified by the same inflammatory stimulus, UV-KEc. At the time of writing, no complementary experimental models of inflammation exist in mouse and human using the same inflammatory stimulus, allowing direct comparative analysis. Overall, the data reported here would suggest RA patients have a more rapid onset of inflammation and can resolve inflammation faster than healthy controls and that both the innate and adaptive immune response are therefore fundamental in the pathogenesis of autoimmune disease including RA.

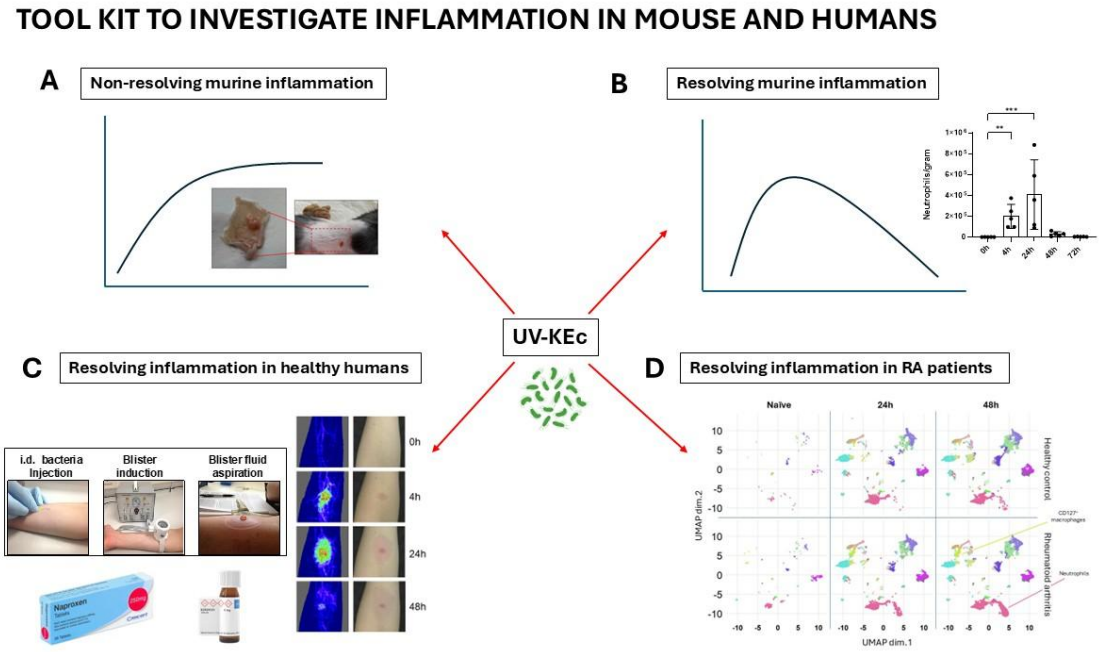

Figure 7.2. Summary figure of thesis. The data reported in this thesis collectively form a toolkit with which to investigate inflammatory pathways in both mouse and human. All inflammatory models described are unified by the same intradermal inflammatory stimulus: UV-KEc. A) **Chapter 3** describes a novel non-resolving model of inflammation which can be used to investigate immune cell profiles (the understudied Ly6C^{int} monocyte subtype), granuloma formation, granulopoiesis and for the first time extract endocannabinoids from inflamed murine skin. B) Additionally, **Chapter 4** describes a resolving model of inflammation which can be used to investigate neutrophil subsets (including bone marrow) and define indices of resolution. C) **Chapter 5** describes a model of resolving human skin inflammation in healthy volunteers, which can be safely used to investigate drugs both in clinical trials and mechanistic studies. D) **Chapter 6** describes a model of resolving inflammation which can be safely used in RA patients to investigate and identify anti-inflammatory/pro-resolution pathways.

8 References

1. Nathan, C. (2002) Points of control in inflammation. *Nature* **420**, 846–852

2. Buckley, C. D., Gilroy, D. W., Serhan, C. N., Stockinger, B., and Tak, P. P. (2013) The resolution of inflammation. *Nat. Rev. Immunol.* **13**, 59–66

3. Fullerton, J. N. and Gilroy, D. W. (2016) Resolution of inflammation: a new therapeutic frontier. *Nat. Rev. Drug Discov.* **15**, 551–567

4. Feehan, K. T. and Gilroy, D. W. (2019) Is Resolution the End of Inflammation? *Trends Mol. Med.* **25**, 198–214

5. Heidland, A., Klassen, A., Rutkowski, P., and Bahner, U. (2006) The contribution of Rudolf Virchow to the concept of inflammation: what is still of importance? *J. Nephrol.* **19 Suppl 10**, S102-9

6. Serhan, C. N. and Savill, J. (2005) Resolution of inflammation: the beginning programs the end. *Nat. Immunol.* **6**, 1191–1197

7. Baker, K. F., McDonald, D., Hulme, G., Hussain, R., Coxhead, J., Swan, D., Schulz, A. R., Mei, H. E., MacDonald, L., Pratt, A. G., Filby, A., Anderson, A. E., and Isaacs, J. D. (2024) Single-cell insights into immune dysregulation in rheumatoid arthritis flare versus drug-free remission. *Nat. Commun. 2024 151* **15**, 1–16

8. Medzhitov, R. and Janeway, C. A. (1997) Innate immunity: impact on the adaptive immune response. *Curr. Opin. Immunol.* **9**, 4–9

9. Schaefer, L. (2014) Complexity of Danger: The Diverse Nature of Damage-associated Molecular Patterns. *J. Biol. Chem.* **289**, 35237–35245

10. Savill, J. and Haslett, C. (1995) Granulocyte clearance by apoptosis in the resolution ofinflammation. *Semin. Cell Biol.* **6**, 385–393

11. Savill, J. (1997) Apoptosis in resolution of inflammation. *J. Leukoc. Biol.* **61**, 375–380

12. Maini, A. A., George, M. J., Motwani, M. P., Day, R. M., Gilroy, D. W., and O'Brien, A. J. (2016) A Comparison of Human Neutrophils Acquired from

Four Experimental Models of Inflammation. *PLoS One* **11**, e0165502

13. Gilroy, D. and De Maeyer, R. (2015) New insights into the resolution of inflammation. *Semin. Immunol.* **27**, 161–168

14. Gilroy, D. W. and Bishop-Bailey, D. (2019) Lipid mediators in immune regulation and resolution. *Br. J. Pharmacol.* **176**, 1009–1023

15. Esnault, S., Khosravi, M., Kelly, E. A., Liu, L. Y., Bochkov, Y. A., Tattersall, M. C., and Jarjour, N. N. (2021) Increased IL-6 and Potential IL-6 trans-signalling in the airways after an allergen challenge. *Clin. Exp. Allergy* **51**, 564–573

16. Hampton, H. R., Bailey, J., Tomura, M., Brink, R., and Chtanova, T. (2015) Microbe-dependent lymphatic migration of neutrophils modulates lymphocyte proliferation in lymph nodes. *Nat. Commun. 2015 61* **6**, 1–11

17. Line Beauvillain, C., Cunin, P., Doni, A., Scotet, M., Bastien Jaillon, S., Loiry, M.-L., Magistrelli, G., Masternak, K., Chevailler, A., Delneste, Y., and Jeannin, P. (2011) CCR7 is involved in the migration of neutrophils to lymph nodes. *Blood* **117**, 1196–1204

18. Fadok, V. A., Bratton, D. L., and Henson, P. M. (2001) Phagocyte receptors for apoptotic cells: recognition, uptake, and consequences. *J. Clin. Invest.* **108**, 957

19. Miyanishi, M., Tada, K., Koike, M., Uchiyama, Y., Kitamura, T., and Nagata, S. (2007) Identification of Tim4 as a phosphatidylserine receptor. *Nature* **450**, 435–439

20. Kobayashi, N., Karisola, P., Peña-Cruz, V., Dorfman, D. M., Jinushi, M., Umetsu, S. E., Butte, M. J., Nagumo, H., Chernova, I., Zhu, B., Sharpe, A. H., Ito, S., Dranoff, G., Kaplan, G. G., Casasnovas, J. M., Umetsu, D. T., DeKruyff, R. H., and Freeman, G. J. (2007) TIM-1 and TIM-4 glycoproteins bind phosphatidylserine and mediate uptake of apoptotic cells. *Immunity* **27**, 927–940

21. Funk, C. D. (2001) Prostaglandins and leukotrienes: Advances in eicosanoid biology. *Science (80-.).* **294**, 1871–1875

22. Zhao, J., Jiang, P., Guo, S., Schrodi, S. J., and He, D. (2021) Apoptosis, Autophagy, NETosis, Necroptosis, and Pyroptosis Mediated Programmed Cell Death as Targets for Innovative Therapy in Rheumatoid Arthritis. *Front. Immunol.* **12**

23. Baier, A., Meineckel, I., Gay, S., and Pap, T. (2003) Apoptosis in rheumatoid arthritis. *Curr. Opin. Rheumatol.* **15**, 274–279

24. Munoz, L. E., Van Bavel, C., Franz, S., Berden, J., Herrmann, M., and Van Der Vlag, J. (2008) Apoptosis in the pathogenesis of systemic lupus erythematosus. *Lupus* **17**, 371–375

25. Liu, T., Zhang, L., Joo, D., and Sun, S. C. (2017) NF-κB signaling in inflammation. *Signal Transduct. Target. Ther.* **2**, 17023

26. Akira, S. and Takeda, K. (2004) Toll-like receptor signalling. *Nat. Rev. Immunol. 2004 47* **4**, 499–511

27. Swanson, L., Katkar, G. D., Tam, J., Pranadinata, R. F., Chareddy, Y., Coates, J., Anandachar, M. S., Castillo, V., Olson, J., Nizet, V., Kufareva, I., Das, S., and Ghosh, P. (2020) TLR4 signaling and macrophage inflammatory responses are dampened by GIV/Girdin. *Proc. Natl. Acad. Sci. U. S. A.* **117**, 26895–26906

28. Harayama, T. and Shimizu, T. (2020) Roles of polyunsaturated fatty acids, from mediators to membranes. *J. Lipid Res.* **61**, 1150–1160

29. Dyall, S. C., Balas, L., Bazan, N. G., Brenna, J. T., Chiang, N., da Costa Souza, F., Dalli, J., Durand, T., Galano, J. M., Lein, P. J., Serhan, C. N., and Taha, A. Y. (2022) Polyunsaturated fatty acids and fatty acid-derived lipid mediators: Recent advances in the understanding of their biosynthesis, structures, and functions. *Prog. Lipid Res.* **86**

30. Simmons, D. L., Botting, R. M., and Hla, T. (2004) Cyclooxygenase Isozymes: The Biology of Prostaglandin Synthesis and Inhibition. *Pharmacol. Rev.* **56**, 387–437

31. Burke, J. E. and Dennis, E. A. (2009) Phospholipase A 2 structure/function, mechanism, and signaling. *J. Lipid Res.* **50**, S237–S242

32. Ricciotti, E. and Fitzgerald, G. A. (2011) Prostaglandins and Inflammation. *Arterioscler. Thromb. Vasc. Biol.* **31**, 986

33. Gomez, I., Foudi, N., Longrois, D., and Norel, X. (2013) The role of prostaglandin E2 in human vascular inflammation. *Prostaglandins. Leukot. Essent. Fatty Acids* **89**, 55–63

34. Legler, D. F., Bruckner, M., Uetz-von Allmen, E., and Krause, P. (2010) Prostaglandin E2 at new glance: Novel insights in functional diversity offer therapeutic chances. *Int. J. Biochem. Cell Biol.* **42**, 198–201

35. Murrant, C. L., Dodd, J. D., Foster, A. J., Inch, K. A., Muckle, F. R., Ruiz, D. A., Simpson, J. A., and Scholl, J. H. P. (2014) Prostaglandins induce vasodilatation of the microvasculature during muscle contraction and induce vasodilatation independent of adenosine. *J. Physiol.* **592**, 1267

36. Serezani, C. H., Chung, J., Ballinger, M. N., Moore, B. B., Aronoff, D. M., and Peters-Golden, M. (2007) Prostaglandin E2 suppresses bacterial killing in alveolar macrophages by inhibiting NADPH oxidase. *Am. J. Respir. Cell Mol. Biol.* **37**, 562–570

37. Baker, P. E., Fahey, J. V., and Munck, A. (1981) Prostaglandin inhibition of T-cell proliferation is mediated at two levels. *Cell. Immunol.* **61**, 52–61

38. Trivedi, S. G., Newson, J., Rajakariar, R., Jacques, T. S., Hannon, R., Kanaoka, Y., Eguchi, N., Colville-Nash, P., and Gilroy, D. W. (2006) Essential role for hematopoietic prostaglandin D2 synthase in the control of delayed type hypersensitivity. *Proc. Natl. Acad. Sci. U. S. A.* **103**, 5179–5184

39. Pahl, A. (2007) Lipoxygenase. *xPharm Compr. Pharmacol. Ref.* 1–7

40. Borgeat, P. and Samuelsson, B. (1979) Arachidonic acid metabolism in polymorphonuclear leukocytes: effects of ionophore A23187. *Proc. Natl. Acad. Sci. U. S. A.* **76**, 2148–2152

41. Maddox, J. F., Colgan, S. P., Clish, C. B., Petasis, N. A., Fokin, V. V., and Serhan, C. N. (1998) Lipoxin B 4 regulates human monocyte/neutrophil adherence and motility: design of stable lipoxin B 4 analogs with increased biologic activity . *FASEB J.* **12**, 487–494

42. Chiang, N., Gronert, K., Clish, C. B., O'Brien, J. A., Freeman, M. W., and Serhan, C. N. (1999) Leukotriene B4 receptor transgenic mice reveal novel protective roles for lipoxins and aspirin-triggered lipoxins in reperfusion. *J. Clin. Invest.* **104**, 309–316

43. Morris, T., Stables, M., Hobbs, A., de Souza, P., Colville-Nash, P., Warner, T., Newson, J., Bellingan, G., and Gilroy, D. W. (2009) Effects of low-dose aspirin on acute inflammatory responses in humans. *J. Immunol.* **183**, 2089–2096

44. Bannenberg, G. L., Chiang, N., Ariel, A., Arita, M., Tjonahen, E., Gotlinger, K. H., Hong, S., and Serhan, C. N. (2005) Molecular circuits of resolution: formation and actions of resolvins and protectins. *J. Immunol.* **174**, 5884c – 5884

45. Maddox, J. F. and Serhan, C. N. (1996) Lipoxin A4 and B4 are potent stimuli for human monocyte migration and adhesion: selective inactivation by dehydrogenation and reduction. *J. Exp. Med.* **183**, 137–146

46. Mathis, S., Jala, V. R., and Haribabu, B. (2007) Role of leukotriene B4 receptors in rheumatoid arthritis. *Autoimmun. Rev.* **7**, 12–17

47. Yousefi, B., Jadidi-Niaragh, F., Azizi, G., Hajighasemi, F., and Mirshafiey, A. (2014) The role of leukotrienes in immunopathogenesis of rheumatoid arthritis. *Mod. Rheumatol.* **24**, 225–235

48. Shi, Z., He, Z., and Wang, D. W. (2022) CYP450 Epoxygenase Metabolites, Epoxyeicosatrienoic Acids, as Novel Anti-Inflammatory Mediators. *Molecules* **27**, 3873

49. Zhao, M., Ma, J., Li, M., Zhang, Y., Jiang, B., Zhao, X., Huai, C., Shen, L., Zhang, N., He, L., and Qin, S. (2021) Cytochrome P450 Enzymes and Drug Metabolism in Humans. *Int. J. Mol. Sci.* **22**

50. Enayetallah, A. E., French, R. A., Thibodeau, M. S., and Grant, D. F. (2004) Distribution of soluble epoxide hydrolase and of cytochrome P450 2C8, 2C9, and 2J2 in human tissues. *J. Histochem. Cytochem.* **52**, 447–454

51. Konkel, A. and Schunck, W. H. (2011) Role of cytochrome P450 enzymes in

the bioactivation of polyunsaturated fatty acids. *Biochim. Biophys. Acta* **1814**, 210–222

52. Althurwi, H. N., Elshenawy, O. H., and El-Kadi, A. O. S. (2014) Fenofibrate modulates cytochrome P450 and arachidonic acid metabolism in the heart and protects against isoproterenol-induced cardiac hypertrophy. *J. Cardiovasc. Pharmacol.* **63**, 167–177

53. Imig, J. D., Zou, A. P., Stec, D. E., Harder, D. R., Falck, J. R., and Roman, R. J. (1996) Formation and actions of 20-hydroxyeicosatetraenoic acid in rat renal arterioles. *Am. J. Physiol.* **270**

54. Fan, F., Ge, Y., Lv, W., Elliott, M. R., Muroya, Y., Hirata, T., Booz, G. W., and Roman, R. J. (2016) Molecular mechanisms and cell signaling of 20-hydroxyeicosatetraenoic acid in vascular pathophysiology. *Front. Biosci. (Landmark Ed.* **21**, 1427

55. Hoxha, M. and Zappacosta, B. (2020) CYP-derived eicosanoids: Implications for rheumatoid arthritis. *Prostaglandins Other Lipid Mediat.* **146**, 106405

56. Cheng, Y. and Rong, J. (2019) Pro-resolving lipid mediators as therapeutic leads for cardiovascular diseases. *Expert Opin. Ther. Targets* **23**, 423–436

57. Basil, M. C. and Levy, B. D. (2015) Specialized pro-resolving mediators: endogenous regulators of infection and inflammation. *Nat. Rev. Immunol. 2015 161* **16**, 51–67

58. Arita, M., Ohira, T., Sun, Y.-P., Elangovan, S., Chiang, N., and Serhan, C. N. (2007) Resolvin E1 selectively interacts with leukotriene B4 receptor BLT1 and ChemR23 to regulate inflammation. *J. Immunol.* **178**, 3912–3917

59. Krishnamoorthy, S., Recchiuti, A., Chiang, N., Yacoubian, S., Lee, C. H., Yang, R., Petasis, N. A., and Serhan, C. N. (2010) Resolvin D1 binds human phagocytes with evidence for proresolving receptors. *Proc. Natl. Acad. Sci. U. S. A.* **107**, 1660–1665

60. Motwani, M. P., Newson, J., Kwong, S., Richard-Loendt, A., Colas, R., Dalli, J., and Gilroy, D. W. (2017) Prolonged immune alteration following resolution of acute inflammation in humans. *PLoS One* **12**, e0186964

61. Homer, N. Z., Andrew, R., and Gilroy, D. W. (2023) Re-analysis of lipidomic data reveals Specialised Pro-Resolution Lipid Mediators (SPMs) to be lower than quantifiable limits of assay in a human model of resolving inflammation. *bioRxiv* 2023.03.06.530669

62. Wang, J. and Ueda, N. (2009) Biology of endocannabinoid synthesis system. *Prostaglandins Other Lipid Mediat.* **89**, 112–119

63. Di Marzo, V. (2006) Endocannabinoids: synthesis and degradation. 1–24

64. Marinelli, S., Pacioni, S., Bisogno, T., Di Marzo, V., Prince, D. A., Huguenard, J. R., and Bacci, A. (2008) The Endocannabinoid 2-Arachidonoylglycerol Is Responsible for the Slow Self-Inhibition in Neocortical Interneurons. *J. Neurosci.* **28**, 13532

65. Barrie, N. and Manolios, N. (2017) The endocannabinoid system in pain and inflammation: Its relevance to rheumatic disease. *Eur. J. Rheumatol.* **4**, 210

66. Zou, S. and Kumar, U. (2018) Cannabinoid Receptors and the Endocannabinoid System: Signaling and Function in the Central Nervous System. *Int. J. Mol. Sci.* **19**

67. Di Marzo, V., Stella, N., and Zimmer, A. (2014) Endocannabinoid signalling and the deteriorating brain. *Nat. Rev. Neurosci. 2014 161* **16**, 30–42

68. Godlewski, G., Offertáler, L., Wagner, J. A., and Kunos, G. (2009) Receptors for acylethanolamides—GPR55 and GPR119. *Prostaglandins Other Lipid Mediat.* **89**, 105

69. Iannotti, F. A. and Vitale, R. M. (2021) The Endocannabinoid System and PPARs: Focus on Their Signalling Crosstalk, Action and Transcriptional Regulation. *Cells* **10**, 1–22

70. Gui, H., Tong, Q., Qu, W., Mao, C. M., and Dai, S. M. (2015) The endocannabinoid system and its therapeutic implications in rheumatoid arthritis. *Int. Immunopharmacol.* **26**, 86–91

71. Gonçalves, E. D. and Dutra, R. C. (2019) Cannabinoid receptors as therapeutic targets for autoimmune diseases: where do we stand? *Drug*

Discov. Today **24**, 1845–1853

72. Werth, V. P., Hejazi, E., Pena, S. M., Haber, J., Zeidi, M., Reddy, N., Okawa, J., Feng, R., Bashir, M. M., Gebre, K., Jadoo, A. S., Concha, J. S. S., Dgetluck, N., Constantine, S., and White, B. (2022) Safety and Efficacy of Lenabasum, a Cannabinoid Receptor Type 2 Agonist, in Dermatomyositis Patients with Refractory Skin: Disease A Randomized Clinical Trial. *J. Invest. Dermatol.* **142**, 2651

73. Spiera, R., Kuwana, M., Khanna, D., Hummers, L., Frech, T. M., Stevens, W., Matucci-Cerinic, M., Kafaja, S., Distler, O., Jun, J. B., Levy, Y., Leszczyński, P., Gordon, J., Steen, V., Lee, E. B., Jankowski, T., Litinsky, I., Chung, L., Hsu, V., Mayes, M., Sandorfi, N., Simms, R. W., Finzel, S., de Vries-Bouwstra, J., Constantine, S., Dgetluck, N., Dinh, Q., Bloom, B. J., Furst, D. E., White, B., and Denton, C. P. (2023) Efficacy and Safety of Lenabasum, a Cannabinoid Type 2 Receptor Agonist, in a Phase 3 Randomized Trial in Diffuse Cutaneous Systemic Sclerosis. *Arthritis Rheumatol.* **75**, 1608–1618

74. Lowe, H., Toyang, N., Steele, B., Bryant, J., and Ngwa, W. (2021) The Endocannabinoid System: A Potential Target for the Treatment of Various Diseases. *Int. J. Mol. Sci. 2021, Vol. 22, Page 9472* **22**, 9472

75. Kaur, I., Behl, T., Bungau, S., Zengin, G., Kumar, A., El-Esawi, M. A., Khullar, G., Venkatachalam, T., and Arora, S. (2020) The endocannabinoid signaling pathway as an emerging target in pharmacotherapy, earmarking mitigation of destructive events in rheumatoid arthritis. *Life Sci.* **257**, 118109

76. Tiwary, A. K., Kothiwala, S. K., and Kumar, P. (2019) JAK-STAT pathway and JAK inhibitors: A primer for dermatologists. *Iran. J. Dermatology* **22(88)**, 71–78

77. Wallace, J. L., Ianaro, A., Flannigan, K. L., and Cirino, G. (2015) Gaseous mediators in resolution of inflammation. *Semin. Immunol.* **27**, 227–233

78. Wallace, J. L. and Wang, R. (2015) Hydrogen sulfide-based therapeutics: Exploiting a unique but ubiquitous gasotransmitter. *Nat. Rev. Drug Discov.* **14**, 329–345

79. Wallace, J. L., Ianaro, A., Flannigan, K. L., and Cirino, G. (2015) Gaseous mediators in resolution of inflammation. *Semin. Immunol.* **27**, 227–233

80. Wallace, J. L. (2007) Hydrogen sulfide-releasing anti-inflammatory drugs. *Trends Pharmacol. Sci.* **28**, 501–505

81. Jerkic, M., Rivas-Elena, J. V., Prieto, M., Carrón, R., Sanz-Rodríguez, F., Pérez-Barriocanal, F., Rodríguez-Barbero, A., Bernabéu, C., and López-Novoa, J. M. (2004) Endoglin regulates nitric oxide-dependent vasodilatation. *FASEB J.* **18**, 609–611

82. Kolb, H. and Kolb-Bachofen, V. (1998) Nitric oxide in autoimmune disease: cytotoxic or regulatory mediator? *Immunol. Today* **19**, 556–561

83. Fang, F. C. and Vazquez-Torres, A. (2002) Nitric oxide production by human macrophages: there's NO doubt about it. *https://doi.org/10.1152/ajplung.00017.2002* **282**

84. Andrabi, S. M., Sharma, N. S., Karan, A., Shatil Shahriar, S. M., Cordon, B., Ma, B., Xie, J., Andrabi, S. M., Sharma, N. S., Karan, A., Shahriar, S. M. S., Cordon, B., Xie, J., and Ma, B. (2023) Nitric Oxide: Physiological Functions, Delivery, and Biomedical Applications. *Adv. Sci.* **10**, 2303259

85. Bogdan, C. (2001) Nitric oxide and the immune response. *Nat. Immunol.* **2**, 907–916

86. Papapetropoulos, A., Foresti, R., and Ferdinandy, P. (2015) Pharmacology of the 'gasotransmitters' NO, CO and H_2S: translational opportunities. *Br. J. Pharmacol.* **172**, 1395–1396

87. Pechánová, O., Varga, Z. V., Cebová, M., Giricz, Z., Pacher, P., and Ferdinandy, P. (2015) Cardiac NO signalling in the metabolic syndrome. *Br. J. Pharmacol.* **172**, 1415–1433

88. Yetik-Anacak, G. and Catravas, J. D. (2006) Nitric oxide and the endothelium: History and impact on cardiovascular disease. *Vascul. Pharmacol.* **45**, 268–276

89. Yetik-Anacak, G., Sorrentino, R., Linder, A. E., and Murat, N. (2015) Gas

what: NO is not the only answer to sexual function. *Br. J. Pharmacol.* **172**, 1434–1454

90. Santos, A. I., Martínez-Ruiz, A., and Araújo, I. M. (2015) S-nitrosation and neuronal plasticity. *Br. J. Pharmacol.* **172**, 1468–1478

91. Ryter, S. W., Alam, J., and Choi, A. M. K. (2006) Heme oxygenase-1/carbon monoxide: From basic science to therapeutic applications. *Physiol. Rev.* **86**, 583–650

92. Tenhunen, R., Marver, H. S., and Schmid, R. (1968) The enzymatic conversion of heme to bilirubin by microsomal heme oxygenase. *Proc. Natl. Acad. Sci. U. S. A.* **61**, 748–755

93. Tenhunen, R., Marver, H. S., and Schmid, R. (1969) Microsomal heme oxygenase. Characterization of the enzyme. *J. Biol. Chem.* **244**, 6388–6394

94. Tenhunen, R., Marver, H. S., and Schmid, R. (1970) The enzymatic catabolism of hemoglobin: Stimulation of microsomal heme oxygenase by hemin. *J. Lab. Clin. Med.* **75**, 410–421

95. YOSHIDA, T., BIRO, P., COHEN, T., MULLER, R. M., and SHIBAHARA, S. (1988) Human heme oxygenase cDNA and induction of its mRNA by hemin. *Eur. J. Biochem.* **171**, 457–461

96. Maines, M. D. (1997) THE HEME OXYGENASE SYSTEM:A Regulator of Second Messenger Gases. *Annu. Rev. Pharmacol. Toxicol.* **37**, 517–554

97. Ryter, S. W., Kvam, E., and Tyrrell, R. M. (2000) Heme oxygenase activity. Current methods and applications. *Methods Mol. Biol.* **99**, 369–391

98. Chiang, S. K., Chen, S. E., and Chang, L. C. (2021) The Role of HO-1 and Its Crosstalk with Oxidative Stress in Cancer Cell Survival. *Cells* **10**

99. Maines, M. D., Eke, B. C., and Zhao, X. (1996) Corticosterone promotes increased heme oxygenase-2 protein and transcript expression in the newborn rat brain. *Brain Res.* **722**, 83–94

100. Willis, D., Moore, A. R., Frederick, R., and Willoughby, D. A. (1996) Heme oxygenase: A novel target for the modulation of the inflammatory response.

Nat. Med. **2**, 87–90

101. Wegiel, B., Hedblom, A., Li, M., Gallo, D., Csizmadia, E., Harris, C., Nemeth, Z., Zuckerbraun, B. S., Soares, M., Persson, J. L., and Otterbein, L. E. (2014) Heme oxygenase-1 derived carbon monoxide permits maturation of myeloid cells. *Cell Death Dis.* **5**, e1139–e1139

102. Wegiel, B., Nemeth, Z., Correa-Costa, M., Bulmer, A. C., and Otterbein, L. E. (2014) Heme oxygenase-1: A metabolic nike. *Antioxidants Redox Signal.* **20**, 1709–1722

103. Toro, A., Ruiz, M. S., Lage-Vickers, S., Sanchis, P., Sabater, A., Pascual, G., Seniuk, R., Cascardo, F., Ledesma-Bazan, S., Vilicich, F., Vazquez, E., and Gueron, G. (2022) A Journey into the Clinical Relevance of Heme Oxygenase 1 for Human Inflammatory Disease and Viral Clearance: Why Does It Matter on the COVID-19 Scene? *Antioxidants 2022, Vol. 11, Page 276* **11**, 276

104. Biernacki, W. A., Kharitonov, S. A., and Barnes, P. J. (2001) Exhaled carbon monoxide in patients with lower respiratory tract infection. *Respir. Med.* **95**, 1003–1005

105. Shi, Y., Pan, F., Li, H., Pan, J., Qin, S., and Shen, C. (2000) Role of carbon monoxide and nitric oxide in newborn infants with postasphyxial hypoxic-ischemic encephalopathy. *Pediatrics* **106**, 1447–1451

106. Takaki, S., Takeyama, N., Kajita, Y., Yabuki, T., Noguchi, H., Miki, Y., Inoue, Y., Nakagawa, T., and Noguchi, H. (2010) Beneficial effects of the heme oxygenase-1/carbon monoxide system in patients with severe sepsis/septic shock. *Intensive Care Med.* **36**, 42–48

107. Wang, R. (2003) The gasotransmitter role of hydrogen sulfide. *Antioxidants Redox Signal.* **5**, 493–501

108. Morra, M. J. and Dick, W. A. (1991) Mechanisms of H2S Production from Cysteine and Cystine by Microorganisms Isolated from Soil by Selective Enrichment. *Appl. Environ. Microbiol.* **57**, 1413

109. Kimura, H. (2000) Hydrogen sulfide induces cyclic AMP and modulates the NMDA receptor. *Biochem. Biophys. Res. Commun.* **267**, 129–133

110. Ling, Q., Yu, X., Wang, T., Wang, S. G., Ye, Z. Q., and Liu, J. H. (2017) Roles of the Exogenous H2S-Mediated SR-A Signaling Pathway in Renal Ischemia/ Reperfusion Injury in Regulating Endoplasmic Reticulum Stress-Induced Autophagy in a Rat Model. *Cell. Physiol. Biochem.* **41**, 2461–2474

111. Kolluru, G. K., Shen, X., Bir, S. C., and Kevil, C. G. (2013) Hydrogen sulfide chemical biology: Pathophysiological roles and detection. *Nitric Oxide* **35**, 5–20

112. Bos, E. M., van Goor, H., Joles, J. A., Whiteman, M., and Leuvenink, H. G. D. (2015) Hydrogen sulfide: physiological properties and therapeutic potential in ischaemia. *Br. J. Pharmacol.* **172**, 1479–1493

113. Agyemang, C., Kieft, S., Snijder, M. B., Beune, E. J., Van Den Born, B. J., Brewster, L. M., Ujcic-Voortman, J. J., Bindraban, N., Van Montfrans, G., Peters, R. J., and Stronks, K. (2015) Hypertension control in a large multi-ethnic cohort in Amsterdam, The Netherlands: The HELIUS study. *Int. J. Cardiol.* **183**, 180–189

114. D'Emmanuele Di Villa Bianca, R., Mitidieri, E., Donnarumma, E., Tramontano, T., Brancaleone, V., Cirino, G., Bucci, M., and Sorrentino, R. (2015) Hydrogen sulfide is involved in dexamethasone-induced hypertension in rat. *Nitric Oxide - Biol. Chem.* **46**, 80–86

115. Wallace, J. L. (2007) Hydrogen sulfide-releasing anti-inflammatory drugs. *Trends Pharmacol. Sci.* **28**, 501–505

116. Wang, R. (2002) Two's company, three's a crowd: can H 2 S be the third endogenous gaseous transmitter? . *FASEB J.* **16**, 1792–1798

117. Tang, G., Wu, L., Liang, W., and Wang, R. (2005) Direct stimulation of KATP channels by exogenous and endogenous hydrogen sulfide in vascular smooth muscle cells. *Mol. Pharmacol.* **68**, 1757–1764

118. Li, L., Rossoni, G., Sparatore, A., Lee, L. C., Del Soldato, P., and Moore, P. K. (2007) Anti-inflammatory and gastrointestinal effects of a novel diclofenac derivative. *Free Radic. Biol. Med.* **42**, 706–719

119. Oh, G. S., Pae, H. O., Lee, B. S., Kim, B. N., Kim, J. M., Kim, H. R., Jeon, S.

B., Jeon, W. K., Chae, H. J., and Chung, H. T. (2006) Hydrogen sulfide inhibits nitric oxide production and nuclear factor-κB via heme oxygenase-1 expression in RAW264.7 macrophages stimulated with lipopolysaccharide. *Free Radic. Biol. Med.* **41**, 106–119

120. Hu, L.-F., Wong, P. T.-H., Moore, P. K., and Bian, J.-S. (2007) Hydrogen sulfide attenuates lipopolysaccharide-induced inflammation by inhibition of p38 mitogen-activated protein kinase in microglia. *J. Neurochem.* **100**, 1121–1128

121. Rinaldi, L., Gobbi, G., Pambianco, M., Micheloni, C., Mirandola, P., and Vitale, M. (2006) Hydrogen sulfide prevents apoptosis of human PMN via inhibition of p38 and caspase 3. *Lab. Investig.* **86**, 391–397

122. Whiteman, M., Cheung, N. S., Zhu, Y. Z., Chu, S. H., Siau, J. L., Wong, B. S., Armstrong, J. S., and Moore, P. K. (2005) Hydrogen sulphide: A novel inhibitor of hypochlorous acid-mediated oxidative damage in the brain? *Biochem. Biophys. Res. Commun.* **326**, 794–798

123. Kashiba, M., Kajimura, M., Goda, N., and Suematsu, M. (2002) From O2 to H2S: A landscape view of gas biology. *Keio J. Med.* **51**, 1–10

124. Bannenberg, G. L., Chiang, N., Ariel, A., Arita, M., Tjonahen, E., Gotlinger, K. H., Hong, S., and Serhan, C. N. (2005) Molecular circuits of resolution: formation and actions of resolvins and protectins. *J. Immunol.* **174**, 4345–4355

125. Newson, J., Stables, M., Karra, E., Arce-Vargas, F., Quezada, S., Motwani, M., Mack, M., Yona, S., Audzevich, T., and Gilroy, D. W. (2014) Resolution of acute inflammation bridges the gap between innate and adaptive immunity. *Blood* **124**, 1748–1764

126. Gilroy, D. W., Edin, M. L., Maeyer, R. P. H. D., Bystrom, J., Newson, J., Lih, F. B., Stables, M., Zeldin, D. C., and Bishop-Bailey, D. (2016) CYP450-derived oxylipins mediate inflammatory resolution. *Proc. Natl. Acad. Sci. U. S. A.* **113**, E3240–E3249

127. Newson, J., Motwani, M. P., Kendall, A. C., Nicolaou, A., Muccioli, G. G.,

Alhouayek, M., Bennett, M., Van De Merwe, R., James, S., De Maeyer, R. P. H., and Gilroy, D. W. (2017) Inflammatory Resolution Triggers a Prolonged Phase of Immune Suppression through COX-1/mPGES-1-Derived Prostaglandin E2. *Cell Rep.* **20**, 3162–3175

128. Stables, M. J., Newson, J., Ayoub, S. S., Brown, J., Hyams, C. J., and Gilroy, D. W. (2010) Priming innate immune responses to infection by cyclooxygenase inhibition kills antibiotic-susceptible and -resistant bacteria. *Blood* **116**, 2950–2959

129. Feehan, Karen T., Bridgewater Hannah E., Stenkiewicz-Witeska, Jan., De Maeyer. Roel P. H., Ferguson, John., Mack, Matthias., Brown, Jeremy., Ercoli, Giuseppe., Mawer, Connar M., Akbar, Arne N., Glanville, James R. W., Jalali, Parinaaz., Bracken, OFeehan, D. W. (2024) Post-resolution macrophage-derived lipids shapes long-term tissue immunity and integrity.

130. Fonseca, D. M. Da, Hand, T. W., Han, S. J., Gerner, M. Y., Zaretsky, A. G., Byrd, A. L., Harrison, O. J., Ortiz, A. M., Quinones, M., Trinchieri, G., Brenchley, J. M., Brodsky, I. E., Germain, R. N., Randolph, G. J., and Belkaid, Y. (2015) Microbiota-Dependent Sequelae of Acute Infection Compromise Tissue-Specific Immunity. *Cell* **163**, 354–366

131. Collins, N., Hochheiser, K., Carbone, F. R., and Gebhardt, T. (2017) Sustained accumulation of antigen-presenting cells after infection promotes local T-cell immunity. *Immunol. Cell Biol.* **95**, 878–883

132. Davidson, A. and Diamond, B. (2001) Autoimmune Diseases. *N. Engl. J. Med.* **345**

133. Rosenblum, M. D., Remedios, K. A., and Abbas, A. K. (2015) Mechanisms of human autoimmunity. *J. Clin. Invest.* **125**, 2228–2233

134. Schett, G. (2019) Resolution of inflammation in arthritis. *Semin. Immunopathol.* **41**, 675–679

135. Conrad, N., Misra, S., Verbakel, J. Y., Verbeke, G., Molenberghs, G., Taylor, P. N., Mason, J., Sattar, N., McMurray, J. J. V., McInnes, I. B., Khunti, K., and Cambridge, G. (2023) Incidence, prevalence, and co-occurrence of

autoimmune disorders over time and by age, sex, and socioeconomic status: a population-based cohort study of 22 million individuals in the UK. *Lancet* **401**, 1878–1890

136. Kahlenberg, J. M. and Fox, D. A. (2011) Advances in the medical treatment of rheumatoid arthritis. *Hand Clin.* **27**, 11–20

137. Symmons, D. P. M. (2002) Epidemiology of rheumatoid arthritis: determinants of onset, persistence and outcome. *Best Pract. Res. Clin. Rheumatol.* **16**, 707–722

138. Allan Gibofsky, M. J. (2014) Epidemiology, Pathophysiology, and Diagnosis of Rheumatoid Arthritis: A Synopsis. **20**

139. De Almeida, D. E., Ling, S., Pi, X., Hartmann-Scruggs, A. M., Pumpens, P., and Holoshitz, J. (2010) Immune dysregulation by the rheumatoid arthritis shared epitope. *J. Immunol.* **185**, 1927–1934

140. Cooles, F. A. H. and Isaacs, J. D. (2011) Pathophysiology of rheumatoid arthritis. *Curr. Opin. Rheumatol.* **23**, 233–240

141. van Delft, M. A. M. and Huizinga, T. W. J. (2020) An overview of autoantibodies in rheumatoid arthritis. *J. Autoimmun.* **110**

142. Alvarez, I., Collado, J., Daura, X., Colomé, N., Rodríguez-García, M., Gallart, T., Canals, F., and Jaraquemada, D. (2008) The rheumatoid arthritis-associated allele HLA-DR10 (DRB1*1001) shares part of its repertoire with HLA-DR1 (DRB1*0101) and HLA-DR4 (DRB*0401). *Arthritis Rheum.* **58**, 1630–1639

143. Saad, M. N., Mabrouk, M. S., Eldeib, A. M., and Shaker, O. G. (2016) Identification of rheumatoid arthritis biomarkers based on single nucleotide polymorphisms and haplotype blocks: A systematic review and meta-analysis. *J. Adv. Res.* **7**, 1

144. Svendsen, A. J., Kyvik, K. O., Houen, G., Junker, P., Christensen, K., Christiansen, L., Nielsen, C., Skytthe, A., and Hjelmborg, J. V. (2013) On the Origin of Rheumatoid Arthritis: The Impact of Environment and Genes—A Population Based Twin Study. *PLoS One* **8**

145. Hoffmann, M., Hayer, S., and Steiner, G. (2009) Immmunopathogenesis of rheumatoid arthritis; induction of arthritogenic autoimmune responses by proinflammatory stimuli. *Ann. N. Y. Acad. Sci.* **1173**, 391–400

146. Svendsen, A. J., Westergaard, M. C. W., Draborg, A. H., Holst, R., Kyvik, K. O., Jakobsen, M. A., Junker, P., and Houen, G. (2021) Altered Antibody Response to Epstein-Barr Virus in Patients With Rheumatoid Arthritis and Healthy Subjects Predisposed to the Disease. A Twin Study. *Front. Immunol.* **12**, 650713

147. Ingegnoli, F., Castelli, R., and Gualtierotti, R. (2013) Rheumatoid Factors: Clinical Applications. *Dis. Markers* **35**, 727

148. Takahashi, Y., Murai, C., Shibata, S., Munakata, Y., Ishii, T., Ishii, K., Saitoh, T., Sawai, T., Sugamura, K., and Sasaki, T. (1998) Human parvovirus B19 as a causative agent for rheumatoid arthritis. *Proc. Natl. Acad. Sci. U. S. A.* **95**, 8227

149. Arleevskaya, M. I., Kravtsova, O. A., Lemerle, J., Renaudineau, Y., and Tsibulkin, A. P. (2016) How Rheumatoid Arthritis Can Result from Provocation of the Immune System by Microorganisms and Viruses. *Front. Microbiol.* **7**

150. Brand, D. D., Kang, A. H., and Rosloniec, E. F. (2004) The mouse model of collagen-induced arthritis. *Methods Mol. Med.* **102**, 295–312

151. Möttönen, T., Hannonen, P., Oka, M., Rautiainen, J., Jokinen, I., Arvilommi, H., Palosuo, T., and Aho, K. (1988) Antibodies against native type II collagen do not precede the clinical onset of rheumatoid arthritis. *Arthritis Rheum.* **31**, 776–779

152. Rowley, M., Tait, B., Mackay, I. R., Cunningham, T., and Phillips, B. (1986) Collagen antibodies in rheumatoid arthritis. Significance of antibodies to denatured collagen and their association with HLA-DR4. *Arthritis Rheum.* **29**, 174–184

153. Glossop, J. R., Emes, R. D., Nixon, N. B., Packham, J. C., Fryer, A. A., Mattey, D. L., and Farrell, W. E. (2015) Genome-wide profiling in treatment-

naive early rheumatoid arthritis reveals DNA methylome changes in T and B lymphocytes. *http://dx.doi.org/10.2217/epi.15.103* **8**, 209–224

154. Glossop, J. R., Emes, R. D., Nixon, N. B., Packham, J. C., Fryer, A. A., Mattey, D. L., and Farrell, W. E. (2016) Genome-wide profiling in treatment-naive early rheumatoid arthritis reveals DNA methylome changes in T and B lymphocytes. *Epigenomics* **8**, 209–224

155. Nemtsova, M. V., Zaletaev, D. V., Bure, I. V., Mikhaylenko, D. S., Kuznetsova, E. B., Alekseeva, E. A., Beloukhova, M. I., Deviatkin, A. A., Lukashev, A. N., and Zamyatnin, A. A. (2019) Epigenetic Changes in the Pathogenesis of Rheumatoid Arthritis. *Front. Genet.* **10**

156. James, E. A., Moustakas, A. K., Bui, J., Papadopoulos, G. K., Bondinas, G., Buckner, J. H., and Kwok, W. W. (2010) HLA-DR1001 presents "altered-self" peptides derived from joint-associated proteins by accepting citrulline in three of its binding pockets. *Arthritis Rheum.* **62**, 2909–2918

157. Kurowska, W., Kuca-Warnawin, E. H., Radzikowska, A., and Maslinski, W. (2017) The role of anti-citrullinated protein antibodies (ACPA) in the pathogenesis of rheumatoid arthritis. *Cent. J. Immunol.* **42**, 390

158. Lu, M. C., Lai, N. S., Yu, H. C., Huang, H. Bin, Hsieh, S. C., and Yu, C. L. (2010) Anti-citrullinated protein antibodies bind surface-expressed citrullinated Grp78 on monocyte/macrophages and stimulate tumor necrosis factor alpha production. *Arthritis Rheum.* **62**, 1213–1223

159. Conigliaro, P., Chimenti, M. S., Triggianese, P., Sunzini, F., Novelli, L., Perricone, C., and Perricone, R. (2016) Autoantibodies in inflammatory arthritis. *Autoimmun. Rev.* **15**, 673–683

160. Ospelt, C., Camici, G. G., Engler, A., Kolling, C., Vogetseder, A., Gay, R. E., Michel, B. A., and Gay, S. (2014) Smoking induces transcription of the heat shock protein system in the joints. *Ann. Rheum. Dis.* **73**, 1423–1426

161. Hedström, A. K., Stawiarz, L., Klareskog, L., and Alfredsson, L. (2018) Smoking and susceptibility to rheumatoid arthritis in a Swedish population-based case–control study. *Eur. J. Epidemiol.* **33**, 415

162. Liao, K. P., Alfredsson, L., and Karlson, E. W. (2009) Environmental influences on risk for rheumatoid arthritis. *Curr. Opin. Rheumatol.* **21**, 279

163. Kostoglou-Athanassiou, I., Athanassiou, L., and Athanassiou, P. (2020) The Effect of Omega-3 Fatty Acids on Rheumatoid Arthritis. *Mediterr. J. Rheumatol.* **31**, 190

164. Dong, L., Zou, H., Yuan, C., Hong, Y. H., Kuklev, D. V., and Smith, W. L. (2016) Different Fatty Acids Compete with Arachidonic Acid for Binding to the Allosteric or Catalytic Subunits of Cyclooxygenases to Regulate Prostanoid Synthesis. *J. Biol. Chem.* **291**, 4069

165. Lund-Olesen, K. (1970) Oxygen tension in synovial fluids. *Arthritis Rheum.* **13**, 769–776

166. Akhavani, M. A., Madden, L., Buysschaert, I., Sivakumar, B., Kang, N., and Paleolog, E. M. (2009) Hypoxia upregulates angiogenesis and synovial cell migration in rheumatoid arthritis. *Arthritis Res. Ther.* **11**, R64

167. Kennedy, A., Fearon, U., Veale, D. J., and Godson, C. (2011) Macrophages in synovial inflammation. *Front. Immunol.* **2**, 12744

168. McInnes, I. B. and Schett, G. (2011) The Pathogenesis of Rheumatoid Arthritis. *N. Engl. J. Med.* **365**, 2205–2219

169. Pope, R. M. and Huang, Q. Q. (2009) The role of toll-like receptors in rheumatoid arthritis. *Curr. Rheumatol. Rep.* **11**, 357–364

170. Tu, J., Huang, W., Zhang, W., Mei, J., and Zhu, C. (2021) A Tale of Two Immune Cells in Rheumatoid Arthritis: The Crosstalk Between Macrophages and T Cells in the Synovium. *Front. Immunol.* **12**, 655477

171. Goh, F. G. and Midwood, K. S. (2012) Intrinsic danger: activation of Toll-like receptors in rheumatoid arthritis. *Rheumatology* **51**, 7–23

172. Weissmann, G. (2004) Pathogenesis of rheumatoid arthritis. *J. Clin. Rheumatol.* **10**

173. Nardella, F. A., Dayer, J. M., Roelke, M., Krane, S. M., and Mannik, M. (1983) Self-associating IgG rheumatoid factors stimulate monocytes to release

prostaglandins and mononuclear cell factor that stimulates collagenase and prostaglandin production by synovial cells. *Rheumatol. Int.* **3**, 183–186

174. Weissmann, G. and Korchak, H. (1984) Rheumatoid arthritis. The role of neutrophil activation. *Inflammation* **8 Suppl**

175. van Venrooij, W. J., B C van Beers, J. J., M Pruijn, G. J., van Venrooij wvanvenrooij, W. J., van Venrooij, W. J., B C van Beers, J. J., and M Pruijn, G. J. (2011) Anti-CCP antibodies: the past, the present and the future. *Nat. Publ. Gr.* **7**, 391–398

176. Vencovský, J., Macháček, S., Šedová, L., Kafková, J., Gatterová, J., Pešáková, V., and Růžičková, Š. (2003) Autoantibodies can be prognostic markers of an erosive disease in early rheumatoid arthritis. *Ann. Rheum. Dis.* **62**, 427–430

177. Kondo, N., Kuroda, T., and Kobayashi, D. (2021) Cytokine Networks in the Pathogenesis of Rheumatoid Arthritis. *Int. J. Mol. Sci.* **22**, 10922

178. Lebre, M. C., Jongbloed, S. L., Tas, S. W., Smeets, T. J. M., McInnes, I. B., and Tak, P. P. (2008) Rheumatoid arthritis synovium contains two subsets of CD83-DC-LAMP- dendritic cells with distinct cytokine profiles. *Am. J. Pathol.* **172**, 940–950

179. Podojil, J. R. and Miller, S. D. (2009) Molecular mechanisms of T-cell receptor and costimulatory molecule ligation/blockade in autoimmune disease therapy. *Immunol. Rev.* **229**, 337–355

180. Lohr, J., Knoechel, B., Caretto, D., and Abbas, A. K. (2009) Balance of Th1 and Th17 effector and peripheral regulatory T cells. *Microbes Infect.* **11**, 589

181. Corvaisier, M., Delneste, Y., Jeanvoine, H., Preisser, L., Blanchard, S., Garo, E., Hoppe, E., Barré, B., Audran, M., Bouvard, B., Saint-André, J. P., and Jeannin, P. (2012) IL-26 is overexpressed in rheumatoid arthritis and induces proinflammatory cytokine production and Th17 cell generation. *PLoS Biol.* **10**

182. Wu, F., Gao, J., Kang, J., Wang, X., Niu, Q., Liu, J., and Zhang, L. (2021) B Cells in Rheumatoid Arthritis：Pathogenic Mechanisms and Treatment

Prospects. *Front. Immunol.* **12**

183. Sobhani, K., Li, J., and Cortes, M. (2023) Nonsteroidal Anti-Inflammatory Drugs (NSAIDs). *First Aid Perioper. Ultrasound Acute Pain Man. Surg. Proced.* 127–138

184. Morita, I. (2002) Distinct functions of COX-1 and COX-2. *Prostaglandins Other Lipid Mediat.* **68**–**69**, 165–175

185. Davies, N. M., Roøseth, A. G., Appleyard, C. B., Mcknight, W., Del Soldato, P., Calignano, A., Cirino, G., and Wallace, J. L. (1997) NO-naproxen vs. naproxen: ulcerogenic, analgesic and anti-inflammatory effects. *Aliment. Pharmacol. Ther.* **11**, 69–79

186. Todd, P., Drugs, S. C.-, and 1990, undefined. Naproxen. *Springer*

187. Davies, N. M. and Anderson, K. E. (1997) Clinical pharmacokinetics of naproxen. *Clin. Pharmacokinet.* **32**, 268–293

188. KASS, E. H. and FINLAND, M. (1958) Corticosteroids and infections. *Adv. Intern. Med.* **9**, 45–80

189. Dixon, W. G., Suissa, S., and Hudson, M. (2011) The association between systemic glucocorticoid therapy and the risk of infection in patients with rheumatoid arthritis: systematic review and meta-analyses. *Arthritis Res. Ther.* **13**, R139

190. Zink, A., Askling, J., Dixon, W. G., Klareskog, L., Silman, A. J., and Symmons, D. P. M. (2009) European biologicals registers: methodology, selected results and perspectives. *Ann. Rheum. Dis.* **68**, 1240–1246

191. Chan, F. K. (2006) Primer: managing NSAID-induced ulcer complications—balancing gastrointestinal and cardiovascular risks. *Nat. Clin. Pract. Gastroenterol. Hepatol.* **3**, 563–573

192. Graham, D. J. (2006) COX-2 Inhibitors, Other NSAIDs, and Cardiovascular Risk. *JAMA* **296**, 1653

193. White, W. B. (2007) Cardiovascular risk, hypertension, and NSAIDs. *Curr. Rheumatol. Rep.* **9**, 36–43

194. Ng, S. C. and Chan, F. K. (2010) NSAID-induced gastrointestinal and cardiovascular injury. *Curr. Opin. Gastroenterol.* **26**, 611–617

195. Rostom, A., Dube, C., Wells, G. A., Tugwell, P., Welch, V., Jolicoeur, E., McGowan, J., and Lanas, A. (2002) Prevention of NSAID-induced gastroduodenal ulcers. *Cochrane Database Syst. Rev.*

196. Wallace, J. L., Vaughan, D., Dicay, M., Macnaughton, W. K., and De Nucci, G. (2018) Hydrogen Sulfide-Releasing Therapeutics: Translation to the Clinic. *Antioxidants Redox Signal.* **28**, 1533–1540

197. Wallace, J. L., Nagy, P., Feener, T. D., Allain, T., Ditrói, T., Vaughan, D. J., Muscara, M. N., de Nucci, G., and Buret, A. G. (2019) A proof-of-concept, Phase 2 clinical trial of the gastrointestinal safety of a hydrogen sulfide-releasing anti-inflammatory drug. *Br. J. Pharmacol.*

198. Greaves, M. W. (1976) Anti-inflammatory action of corticosteroids. *Postgrad. Med. J.* **52**, 631–633

199. Richards, R. N. (2008) Side Effects of Short-Term Oral Corticosteroids. *https://doi.org/10.2310/7750.2008.07029* **12**, 77–81

200. Youssef, J., Novosad, S. A., and Winthrop, K. L. (2016) Infection Risk and Safety of Corticosteroid Use. *Rheum. Dis. Clin. North Am.* **42**, 157–176

201. Bailey, C. P. and Connor, M. (2005) Opioids: cellular mechanisms of tolerance and physical dependence. *Curr. Opin. Pharmacol.* **5**, 60–68

202. Christie, M. J. (2009) Cellular neuroadaptations to chronic opioids: tolerance, withdrawal and addiction. *Br. J. Pharmacol.* **154**, 384–396

203. Scott, D. L. (2012) Biologics-Based Therapy for the Treatment of Rheumatoid Arthritis. *Clin. Pharmacol. Ther.* **91**, 30–43

204. Choy, E. H. S. and Panayi, G. S. (2001) Cytokine Pathways and Joint Inflammation in Rheumatoid Arthritis. *N. Engl. J. Med.* **344**, 907–916

205. Lopez-Olivo, M. A., Siddhanamatha, H. R., Shea, B., Tugwell, P., Wells, G. A., and Suarez-Almazor, M. E. (2014) Methotrexate for treating rheumatoid arthritis. *Cochrane Database Syst. Rev.* **2014**

206. Friedman, B. and Cronstein, B. (2019) Methotrexate mechanism in treatment of rheumatoid arthritis. *Jt. Bone Spine* **86**, 301–307

207. Cronstein, B. N. and Aune, T. M. (2020) Methotrexate and its mechanisms of action in inflammatory arthritis. *Nat. Rev. Rheumatol.* **16**, 145–154

208. Onda, K., Honma, T., and Masuyama, K. (2023) Methotrexate-related adverse events and impact of concomitant treatment with folic acid and tumor necrosis factor-alpha inhibitors: An assessment using the FDA adverse event reporting system. *Front. Pharmacol.* **14**, 1030832

209. Liptay, S., Fulda, S., Schanbacher, M., Bourteele, S., Ferri, K. F., Kroemer, G., Adler, G., Debatin, K. M., and Schmid, R. M. (2002) Molecular mechanisms of sulfasalazine-induced T-cell apoptosis. *Br. J. Pharmacol.* **137**, 608–620

210. Smedegård, G. and Björk, J. (1995) Sulphasalazine: Mechanism of Action in Rheumatoid Arthritis. *Rheumatology* **XXXIV**, 7–15

211. Schrezenmeier, E. and Dörner, T. (2020) Mechanisms of action of hydroxychloroquine and chloroquine: implications for rheumatology. *Nat. Rev. Rheumatol. 2020 163* **16**, 155–166

212. Breedveld, F. C. and Dayer, J. M. (2000) Leflunomide: mode of action in the treatment of rheumatoid arthritis. *Ann. Rheum. Dis.* **59**, 841–849

213. Firestein, G. S., Xu, W. D., Townsend, K., Broide, D., Alvaro-Gracia, J., Glasebrook, A., and Zvaifler, N. J. (1988) Cytokines in chronic inflammatory arthritis. I. Failure to detect T cell lymphokines (interleukin 2 and interleukin 3) and presence of macrophage colony-stimulating factor (CSF-1) and a novel mast cell growth factor in rheumatoid synovitis. *J. Exp. Med.* **168**, 1573–1586

214. Elliott, M. J., Maini, R. N., Feldmann, M., Long-Fox, A., Charles, P., Katsikis, P., Brennan, F. M., Walker, J., Bijl, H., Ghrayeb, J., and Woody, J. N. (1993) Treatment of rheumatoid arthritis with chimeric monoclonal antibodies to tumor necrosis factor alpha. *Arthritis Rheum.* **36**, 1681–1690

215. Bartok, B. and Firestein, G. S. (2010) Fibroblast-like synoviocytes: key effector cells in rheumatoid arthritis. *Immunol. Rev.* **233**, 233

216. Isomäki, P., Punnonen, J., Isomaki', P., and Punnonen'>, J. (1997) Pro-and Anti-inflammatory Cytokines in Rheumatoid Arthritis. *Ann. Med.* **29**, 499–507

217. Khader, Y., Beran, A., Ghazaleh, S., Lee-Smith, W., and Altorok, N. (2022) Predictors of remission in rheumatoid arthritis patients treated with biologics: a systematic review and meta-analysis. *Clin. Rheumatol.* **41**, 3615–3627

218. Fleischmann, R. (2013) Back to the future: oral small molecule kinases. *Rheumatology* **52**, 1153–1154

219. Massalska, M., Maslinski, W., and Ciechomska, M. (2020) Small Molecule Inhibitors in the Treatment of Rheumatoid Arthritis and Beyond: Latest Updates and Potential Strategy for Fighting COVID-19. *Cells* **9**

220. Hu, X., li, J., Fu, M., Zhao, X., and Wang, W. (2021) The JAK/STAT signaling pathway: from bench to clinic. *Signal Transduct. Target. Ther.* **6**

221. Seif, F., Khoshmirsafa, M., Aazami, H., Mohsenzadegan, M., Sedighi, G., and Bahar, M. (2017) The role of JAK-STAT signaling pathway and its regulators in the fate of T helper cells. *Cell Commun. Signal. 2017 151* **15**, 1–13

222. Hoisnard, L., Lebrun-Vignes, B., Maury, S., Mahevas, M., El Karoui, K., Roy, L., Zarour, A., Michel, M., Cohen, J. L., Amiot, A., Claudepierre, P., Wolkenstein, P., Grimbert, P., and Sbidian, E. (2022) Adverse events associated with JAK inhibitors in 126,815 reports from the WHO pharmacovigilance database. *Sci. Reports 2022 121* **12**, 1–10

223. Tong, Y., Li, X., Deng, Q., Shi, J., Feng, Y., and Bai, L. (2023) Advances of the small molecule drugs regulating fibroblast-like synovial proliferation for rheumatoid arthritis. *Front. Pharmacol.* **14**

224. Fugger, L., Jensen, L. T., and Rossjohn, J. (2020) Leading Edge Perspective Challenges, Progress, and Prospects of Developing Therapies to Treat Autoimmune Diseases.

225. Webb, D. R. (2014) Animal models of human disease: Inflammation. *Biochem. Pharmacol.* **87**, 121–130

226. Masopust, D., Sivula, C. P., and Jameson, S. C. (2017) Of Mice, Dirty Mice, and Men: Using Mice to Understand Human Immunology. *J. Immunol.* **199**, 383

227. Zhang, B., Duan, Z., and Zhao, Y. (2009) Mouse models with human immunity and their application in biomedical research. *J. Cell. Mol. Med.* **13**, 1043

228. Tsuchida, T., Wada, T., Mizugaki, A., Oda, Y., Kayano, K., Yamakawa, K., and Tanaka, S. (2022) Protocol for a Sepsis Model Utilizing Fecal Suspension in Mice: Fecal Suspension Intraperitoneal Injection Model. *Front. Med.* **9**, 765805

229. Bergamini, G., Perico, M. E., Palma, S. Di, Sabatini, D., Andreetta, F., Defazio, R., Felici, A., and Ferrari, L. (2021) Mouse pneumonia model by Acinetobacter baumannii multidrug resistant strains: Comparison between intranasal inoculation, intratracheal instillation and oropharyngeal aspiration techniques. *PLoS One* **16**, e0260627

230. Barone, M., Chain, F., Sokol, H., Brigidi, P., Bermúdez-Humarán, L. G., Langella, P., and Martín, R. (2018) A versatile new model of chemically induced chronic colitis using an outbred murine strain. *Front. Microbiol.* **9**, 326524

231. Larkin, J., Clayton, M., Sun, B., Perchonock, C. E., Morgan, J. L., Siracusa, L. D., Michaels, F. H., and Feitelson, M. A. (1999) Hepatitis B virus transgenic mouse model of chronic liver disease. *Nat. Med. 1999 58* **5**, 907–912

232. Jabeen, M., Boisgard, A. S., Danoy, A., Kholti, N. El, Salvi, J. P., Boulieu, R., Fromy, B., Verrier, B., and Lamrayah, M. (2020) Advanced Characterization of Imiquimod-Induced Psoriasis-Like Mouse Model. *Pharmaceutics* **12**, 1–18

233. Brand, D. D., Latham, K. A., and Rosloniec, E. F. (2007) Collagen-induced arthritis. *Nat. Protoc. 2007 25* **2**, 1269–1275

234. Brand, D. D., Latham, K. A., and Rosloniec, E. F. (2007) Collagen-induced arthritis. *Nat. Protoc. 2007 25* **2**, 1269–1275

235. Myers, L. K., Rosloniec, E. F., Cremer, M. A., and Kang, A. H. (1997) Collagen-induced arthritis, an animal model of autoimmunity. *Life Sci.* **61**, 1861–1878

236. Yu, Y.-R. A., O'koren, E. G., Hotten, D. F., Kan, M. J., Kopin, D., Nelson, E. R., Que, L., and Gunn, M. D. (2016) A Protocol for the Comprehensive Flow Cytometric Analysis of Immune Cells in Normal and Inflamed Murine Non-Lymphoid Tissues.

237. Lintner, K. E., Patwardhan, A., Rider, L. G., Abdul-Aziz, R., Wu, Y. L., Lundstrom, E., Padyukov, L., Zhou, B., Alhomosh, A., Newsom, D., White, P., Jones, K. B., O'Hanlon, T. P., Miller, F. W., Spencer, C. H., and Yu, C. Y. (2016) Gene copy-number variations (CNVs) of complement C4 and C4A deficiency in genetic risk and pathogenesis of juvenile dermatomyositis. *Ann. Rheum. Dis.* **75**, 1599–1606

238. Sakamoto, K., Goel, S., Funakoshi, A., Honda, T., and Nagao, K. (2021) Flow cytometry analysis of the subpopulations of mouse keratinocytes and skin immune cells. *STAR Protoc.* **3**

239. Kugelberg, E., Norström, T., Petersen, T. K., Duvold, T., Andersson, D. I., and Hughes, D. (2005) Establishment of a superficial skin infection model in mice by using Staphylococcus aureus and Streptococcus pyogenes. *Antimicrob. Agents Chemother.* **49**, 3435–3441

240. Rafiyan, M., Sadeghmousavi, S., Akbarzadeh, M., and Rezaei, N. (2023) Experimental animal models of chronic inflammation. *Curr. Res. Immunol.* **4**, 100063

241. Calum, H., Høiby, N., and Moser, C. (2014) Burn mouse models. *Methods Mol. Biol.* **1149**, 793–802

242. Perlman, R. L. (2016) Mouse models of human disease: An evolutionary perspective. *Evol. Med. Public Heal.* **2016**, 170

243. Junhee Seok, H. Shaw Warren, Alex, G. C., Michael, N. M., Henry, V. B., Xu, W., Richards, D. R., McDonald-Smith, G. P., Gao, H., Hennessy, L., Finnerty, C. C., López, C. M., Honari, S., Moore, E. E., Minei, J. P.,

Cuschieri, J., Bankey, P. E., Johnson, J. L., Sperry, J., Nathens, A. B., Billiar, T. R., West, M. A., Jeschke, M. G., Klein, M. B., Gamelli, R. L., Gibran, N. S., Brownstein, B. H., Miller-Graziano, C., Calvano, S. E., Mason, P. H., Cobb, J. P., Rahme, L. G., Lowry, S. F., Maier, R. V., Moldawer, L. L., Herndon, D. N., Davis, R. W., Xiao, W., and Tompkins, R. G. (2013) Genomic responses in mouse models poorly mimic human inflammatory diseases. *Proc. Natl. Acad. Sci. U. S. A.* **110**, 3507–3512

244. Patel, A. A., Zhang, Y., Fullerton, J. N., Boelen, L., Rongvaux, A., Maini, A. A., Bigley, V., Flavell, R. A., Gilroy, D. W., Asquith, B., Macallan, D., and Yona, S. (2017) The fate and lifespan of human monocyte subsets in steady state and systemic inflammation. *J. Exp. Med.* **214**, 1913–1923

245. van Lier, D., Geven, C., Leijte, G. P., and Pickkers, P. (2019) Experimental human endotoxemia as a model of systemic inflammation. *Biochimie* **159**, 99–106

246. Andreasen, A., Krabbe, K., Krogh-Madsen, R., Taudorf, S., Pedersen, B., and Moller, K. (2008) Human endotoxemia as a model of systemic inflammation. *Curr. Med. Chem.* **15**, 1697–1705

247. Kamisoglu, K., Haimovich, B., Calvano, S. E., Coyle, S. M., Corbett, S. A., Langley, R. J., Kingsmore, S. F., and Androulakis, I. P. (2015) Human metabolic response to systemic inflammation: assessment of the concordance between experimental endotoxemia and clinical cases of sepsis/SIRS. *Crit. Care* **19**

248. Hietbrink, F., Besselink, M. G. H., Renooij, W., De Smet, M. B. M., Draisma, A., Van Der Hoeven, H., and Pickkers, P. (2009) Systemic inflammation increases intestinal permeability during experimental human endotoxemia. *Shock* **32**, 374–378

249. Mayr, F. B. and Jilma, B. (2006) Coagulation interventions in experimental human endotoxemia. *Transl. Res.* **148**, 263–271

250. Visser, T., Pillay, J., Pickkers, P., Leenen, L. P. H., and Koenderman, L. (2012) Homology in systemic neutrophil response induced by human

experimental endotoxemia and by trauma. *Shock* **37**, 145–151

251. Kiers, D., Koch, R. M., Hamers, L., Gerretsen, J., Thijs, E. J. M., Van Ede, L., Riksen, N. P., Kox, M., and Pickkers, P. (2017) Characterization of a model of systemic inflammation in humans in vivo elicited by continuous infusion of endotoxin. *Sci. Reports 2017 71* **7**, 1–10

252. Motwani, M. P., Flint, J. D., De Maeyer, R. P., Fullerton, J. N., Smith, A. M., Marks, D. J., and Gilroy, D. W. (2016) Novel translational model of resolving inflammation triggered by UV-killed *E. coli*. *J. Pathol. Clin. Res.* **2**, 154–165

253. Jenner, W., Motwani, M., Veighey, K., Newson, J., Audzevich, T., Nicolaou, A., Murphy, S., MacAllister, R., and Gilroy, D. W. (2014) Characterisation of Leukocytes in a Human Skin Blister Model of Acute Inflammation and Resolution. *PLoS One* **9**, e89375

254. Glanville, J. R. W., Jalali, P., Flint, J. D., Patel, A. A., Maini, A. A., Wallace, J. L., Hosin, A. A., and Gilroy, D. W. (2021) Potent anti-inflammatory effects of an H2S-releasing naproxen (ATB-346) in a human model of inflammation. *FASEB J.* **35**, e21913

255. Chambers, E. S., Vukmanovic-Stejic, M., Shih, B. B., Trahair, H., Subramanian, P., Devine, O. P., Glanville, J., Gilroy, D., Rustin, M. H. A., Freeman, T. C., Mabbott, N. A., and Akbar, A. N. (2021) Recruitment of inflammatory monocytes by senescent fibroblasts inhibits antigen-specific tissue immunity during human aging. *Nat. aging* **1**, 101–113

256. Akbar, A. N., Reed, J. R., Lacy, K. E., Jackson, S. E., Vukmanovic-Stejic, M., and Rustin, M. H. A. (2013) Investigation of the cutaneous response to recall antigen in humans in vivo. *Clin. Exp. Immunol.* **173**, 163–172

257. Szylar, G., Wysoczanski, R., Marshall, H., Marks, D. J. B., José, R., Ehrenstein, M. E., and Brown, J. S. (2022) A novel Streptococcus pneumoniae human challenge model demonstrates Treg lymphocyte recruitment to the infection site. *Sci. Rep.* **12**, 3990

258. Marks, D. J. B., Harbord, M. W. N., MacAllister, R., Rahman, F. Z., Young, J., Al-Lazikani, B., Lees, W., Novelli, M., Bloom, S., and Segal, A. W. (2006)

Defective acute inflammation in Crohn's disease: A clinical investigation. *Lancet* **367**, 668–678

259. Marks, D. J. B., Rahman, F. Z., Novelli, M., Yu, R. C., McCartney, S., Bloom, S., and Segal, A. W. (2006) An exuberant inflammatory response to E coli: implications for the pathogenesis of ulcerative colitis and pyoderma gangrenosum. *Gut* **55**, 1662

260. Feehan, K. T., Bridgewater, H. E., Stenkiewicz-Witeska, J., De Maeyer, R. P. H., Ferguson, J., Mack, M., Brown, J., Ercoli, G., Mawer, C. M., Akbar, A. N., Glanville, J. R. W., Jalali, P., Bracken, O. V., Nicolaou, A., Kendall, A. C., Sugimoto, M. A., and Gilroy, D. W. (2024) Post-resolution macrophages shape long-term tissue immunity and integrity in a mouse model of pneumococcal pneumonia. *Nat. Commun. 2024 151* **15**, 1–17

261. De Maeyer, R. P. H., van de Merwe, R. C., Louie, R., Bracken, O. V., Devine, O. P., Goldstein, D. R., Uddin, M., Akbar, A. N., and Gilroy, D. W. (2020) Blocking elevated p38 MAPK restores efferocytosis and inflammatory resolution in the elderly. *Nat. Immunol.* **21**, 615

262. van Riel, P. L. C. M. (2014) The development of the disease activity score (DAS) and the disease activity score using 28 joint counts (DAS28). *Clin. Exp. Rheumatol.* **32**, S65–S74

263. Lou, F., Sun, Y., and Wang, H. Protocol for Flow Cytometric Detection of Immune Cell Infiltration in the Epidermis and Dermis of a Psoriasis Mouse Model.

264. Bannenberg, G. L., Chiang, N., Ariel, A., Arita, M., Tjonahen, E., Gotlinger, K. H., Hong, S., and Serhan, C. N. (2005) Molecular circuits of resolution: formation and actions of resolvins and protectins. *J. Immunol.* **174**, 4345–4355

265. Olga, L., Bobeldijk-Pastorova, I., Bas, R. C., Seidel, F., Snowden, S. G., Furse, S., Ong, K. K., Kleemann, R., and Koulman, A. (2022) Lipid profiling analyses from mouse models and human infants. *STAR Protoc.* **3**, 101679

266. Franco, J., Rajwa, B., Ferreira, C. R., Sundberg, J. P., and Hogenesch, H.

(2020) Lipidomic Profiling of the Epidermis in a Mouse Model of Dermatitis Reveals Sexual Dimorphism and Changes in Lipid Composition before the Onset of Clinical Disease. *Metabolites* **10**, 1–18

267. Motwani, M. P., Flint, J. D., De Maeyer, R. P., Fullerton, J. N., Smith, A. M., Marks, D. J., and Gilroy, D. W. (2016) Novel translational model of resolving inflammation triggered by UV-killed *E. coli*. *J. Pathol. Clin. Res.* **2**, 154–165

268. Haworth, O. and Buckley, C. D. (2015) Pathways involved in the resolution of inflammatory joint disease. *Semin. Immunol.* **27**, 194–199

269. Toshchakov, V., Jones, B. W., Perera, P. Y., Thomas, K., Cody, M. J., Zhang, S., Williams, B. R. G., Major, J., Hamilton, T. A., Fenton, M. J., and Vogel, S. N. (2002) TLR4, but not TLR2, mediates IFN-beta-induced STAT1alpha/beta-dependent gene expression in macrophages. *Nat. Immunol.* **3**, 392–398

270. Kowalski, E. J. A. and Li, L. (2017) Toll-interacting protein in resolving and non-resolving inflammation. *Front. Immunol.* **8**, 268335

271. Morris, M. C., Gilliam, E. A., and Li, L. (2014) Innate Immune Programing by Endotoxin and Its Pathological Consequences. *Front. Immunol.* **5**

272. Begka, C., Pattaroni, C., Mooser, C., Nancey, S., McCoy, K. D., Velin, D., and Maillard, M. H. (2020) Toll-Interacting Protein Regulates Immune Cell Infiltration and Promotes Colitis-Associated Cancer. *iScience* **23**, 100891

273. Unterberger, S., Davies, K. A., Rambhatla, S. B., and Sacre, S. (2021) Contribution of Toll-Like Receptors and the NLRP3 Inflammasome in Rheumatoid Arthritis Pathophysiology. *ImmunoTargets Ther.* **10**, 285

274. Monnet, E., Choy, E. H., McInnes, I., Kobakhidze, T., De Graaf, K., Jacqmin, P., Lapeyre, G., and De Min, C. (2020) Efficacy and safety of NI-0101, an anti-toll-like receptor 4 monoclonal antibody, in patients with rheumatoid arthritis after inadequate response to methotrexate: a phase II study. *Ann. Rheum. Dis.* **79**, 316–323

275. Nagai, Y., Akashi, S., Nagafuku, M., Ogata, M., Iwakura, Y., Akira, S., Kitamura, T., Kosugi, A., Kimoto, M., and Miyake, K. (2002) Essential role

of MD-2 in LPS responsiveness and TLR4 distribution. *Nat. Immunol. 2002 37* **3**, 667–672

276. Moore, K. J., Andersson, L. P., Ingalls, R. R., Monks, B. G., Li, R., Arnaout, M. A., Golenbock, D. T., and Freeman, M. W. (2000) Divergent Response to LPS and Bacteria in CD14-Deficient Murine Macrophages. *J. Immunol.* **165**, 4272–4280

277. Ling, G. S., Bennett, J., Woollard, K. J., Szajna, M., Fossati-Jimack, L., Taylor, P. R., Scott, D., Franzoso, G., Cook, H. T., and Botto, M. (2014) Integrin CD11b positively regulates TLR4-induced signalling pathways in dendritic cells but not in macrophages. *Nat. Commun. 2014 51* **5**, 1–12

278. Pagán, A. J. and Ramakrishnan, L. (2018) The Formation and Function of Granulomas. *Annu. Rev. Immunol.* **36**, 639–665

279. Shah, K. K., Pritt, B. S., and Alexander, M. P. (2017) Histopathologic review of granulomatous inflammation. *J. Clin. Tuberc. Other Mycobact. Dis.* **7**, 1–12

280. Terziroli Beretta-Piccoli, B., Mainetti, C., Peeters, M. A., and Laffitte, E. (2018) Cutaneous Granulomatosis: a Comprehensive Review. *Clin. Rev. Allergy Immunol.* **54**, 131–146

281. Suya, H., Fujioka, A., Pincelli, C., Fukuyama, K., and Epstein, W. L. (1988) Skin Granuloma Formation in Mice Immunosuppressed by Cyclosporine. *J. Invest. Dermatol.* **90**, 430–433

282. Iida, T., Sato, N., Fukuyama, K., Lau, D. T., and Epstein, W. L. (1991) Immunogenetic influences on skin granuloma formation in mice. *Exp. Mol. Pathol.* **54**, 172–180

283. Leal, R. O., Simpson, K., Fine, M., Husson, J. C., and Hernandez, J. (2017) Granulomatous colitis: more than a canine disease? A case of Escherichia coli-associated granulomatous colitis in an adult cat. *J. Feline Med. Surg. Open Reports* **3**

284. Manchester, A. C., Dogan, B., Guo, Y., and Simpson, K. W. (2021) Escherichia coli-associated granulomatous colitis in dogs treated according to

antimicrobial susceptibility profiling. *J. Vet. Intern. Med.* **35**, 150–161

285. Bettke, J. A., Tam, J. W., Montoya, V., Butler, B. P., and van der Velden, A. W. M. (2022) Inflammatory Monocytes Promote Granuloma-Mediated Control of Persistent Salmonella Infection. *Infect. Immun.* **90**

286. Weeratunga, P., Moller, D. R., and Ho, L. P. (2024) Immune mechanisms of granuloma formation in sarcoidosis and tuberculosis. *J. Clin. Invest.* **134**

287. Hiranuma, R., Sato, R., Yamaguchi, K., Nakamizo, S., Asano, K., Shibata, T., Fukui, R., Furukawa, Y., Kabashima, K., and Miyake, K. (2024) Aberrant monocytopoiesis drives granuloma development in sarcoidosis. *Int. Immunol.* **36**, 183–196

288. Alves da Silva, D. A., Da Silva, M. V., Oliveira Barros, C. C., Dias Alexandre, P. B., Timóteo, R. P., Catarino, J. S., Sales-Campos, H., Machado, J. R., Rodrigues, D. B. R., Oliveira, C. J., and Rodrigues, V. (2018) TNF-α blockade impairs in vitro tuberculous granuloma formation and down modulate Th1, Th17 and Treg cytokines. *PLoS One* **13**

289. Sorobetea, D., Matsuda, R., Peterson, S. T., Grayczyk, J. P., Rao, I., Krespan, E., Lanza, M., Assenmacher, C. A., Mack, M., Beiting, D. P., Radaelli, E., and Brodsky, I. E. (2023) Inflammatory monocytes promote granuloma control of Yersinia infection. *Nat. Microbiol. 2023 84* **8**, 666–678

290. Lösslein, A. K., Lohrmann, F., Scheuermann, L., Gharun, K., Neuber, J., Kolter, J., Forde, A. J., Kleimeyer, C., Poh, Y. Y., Mack, M., Triantafyllopoulou, A., Dunlap, M. D., Khader, S. A., Seidl, M., Hölscher, A., Hölscher, C., Guan, X. L., Dorhoi, A., and Henneke, P. (2021) Monocyte progenitors give rise to multinucleated giant cells. *Nat. Commun. 2021 121* **12**, 1–22

291. Yoshioka, Y., Mizutani, T., Mizuta, S., Miyamoto, A., Murata, S., Ano, T., Ichise, H., Morita, D., Yamada, H., Hoshino, Y., Tsuruyama, T., and Sugita, M. (2016) Neutrophils and the S100A9 protein critically regulate granuloma formation. *Blood Adv.* **1**, 184

292. Silvestre-Roig, C., Fridlender, Z. G., Glogauer, M., and Scapini, P. (2019)

Neutrophil Diversity in Health and Disease. *Trends Immunol.* **40**, 565

293. Scapini, P., Marini, O., Tecchio, C., and Cassatella, M. A. (2016) Human neutrophils in the saga of cellular heterogeneity: insights and open questions. *Immunol. Rev.* **273**, 48–60

294. Christoffersson, G. and Phillipson, M. (2018) The neutrophil: one cell on many missions or many cells with different agendas? *Cell Tissue Res.* **371**, 415–423

295. Bai, M., Grieshaber-Bouyer, R., Wang, J., Schmider, A. B., Wilson, Z. S., Zeng, L., Halyabar, O., Godin, M. D., Nguyen, H. N., Levescot, A., Cunin, P., Lefort, C. T., Soberman, R. J., and Nigrovic, P. A. (2017) CD177 modulates human neutrophil migration through activation-mediated integrin and chemoreceptor regulation. *Blood* **130**, 2092–2100

296. Welin, A., Amirbeagi, F., Christenson, K., Björkman, L., Björnsdottir, H., Forsman, H., Dahlgren, C., Karlsson, A., and Bylund, J. (2013) The human neutrophil subsets defined by the presence or absence of OLFM4 both transmigrate into tissue in vivo and give rise to distinct NETs in vitro. *PLoS One* **8**

297. Clemmensen, S. N., Bohr, C. T., Rørvig, S., Glenthøj, A., Mora-Jensen, H., Cramer, E. P., Jacobsen, L. C., Larsen, M. T., Cowland, J. B., Tanassi, J. T., Heegaard, N. H. H., Wren, J. D., Silahtaroglu, A. N., and Borregaard, N. (2012) Olfactomedin 4 defines a subset of human neutrophils. *J. Leukoc. Biol.* **91**, 495

298. Peng, Z., Liu, C., Victor, A. R., Cao, D. Y., Veiras, L. C., Bernstein, E. A., Khan, Z., Giani, J. F., Cui, X., Bernstein, K. E., and Okwan-Duodu, D. (2021) Tumors exploit CXCR4hiCD62Llo aged neutrophils to facilitate metastatic spread. *Oncoimmunology* **10**

299. Puellmann, K., Kaminski, W. E., Vogel, M., Nebe, C. T., Schroeder, J., Wolf, H., and Beham, A. W. (2006) A variable immunoreceptor in a subpopulation of human neutrophils. *Proc. Natl. Acad. Sci. U. S. A.* **103**, 14441–14446

300. Massena, S., Christoffersson, G., Vågesjö, E., Seignez, C., Gustafsson, K.,

Binet, F., Hidalgo, C. H., Giraud, A., Lomei, J., Weström, S., Shibuya, M., Claesson-Welsh, L., Gerwins, P., Welsh, M., Kreuger, J., and Phillipson, M. (2015) Identification and characterization of VEGF-A–responsive neutrophils expressing CD49d, VEGFR1, and CXCR4 in mice and humans. *Blood* **126**, 2016–2026

301. Song, Z., Bhattacharya, S., Huang, G., Greenberg, Z. J., Yang, W., Bagaitkar, J., Schuettpelz, L. G., and Dinauer, M. C. (2023) NADPH oxidase 2 limits amplification of IL-1β-G-CSF axis and an immature neutrophil subset in murine lung inflammation. *Blood Adv.* **7**, 1225–1240

302. Kim, H., Sierra, M. D. L. L., Williams, C., Blood, A. G.-, and 2006, undefined. G-CSF down-regulation of CXCR4 expression identified as a mechanism for mobilization of myeloid cells. *ashpublications.orgHK Kim, M La Luz Sierra, CK Williams, AV Gulino, G TosatoBlood, 2006•ashpublications.org*

303. Pillay, J., Kamp, V. M., Van Hoffen, E., Visser, T., Tak, T., Lammers, J. W., Ulfman, L. H., Leenen, L. P., Pickkers, P., and Koenderman, L. (2012) A subset of neutrophils in human systemic inflammation inhibits T cell responses through Mac-1. *J. Clin. Invest.* **122**, 327–336

304. Pillay, J., Ramakers, B. P., Kamp, V. M., Loi, A. L. T., Lam, S. W., Hietbrink, F., Leenen, L. P., Tool, A. T., Pickkers, P., and Koenderman, L. (2010) Functional heterogeneity and differential priming of circulating neutrophils in human experimental endotoxemia. *J. Leukoc. Biol.* **88**, 211–220

305. Zhou, X., Gao, X. P., Fan, J., Liu, Q., Anwar, K. N., Frey, R. S., and Malik, A. B. (2005) LPS activation, of Toll-like receptor 4 signals CD11b/CD18 expression in neutrophils. *Am. J. Physiol. - Lung Cell. Mol. Physiol.* **288**, 655–662

306. Lin, S., Lin, Y., Nery, J. R., Urich, M. A., Breschi, A., Davis, C. A., Dobin, A., Zaleski, C., Beer, M. A., Chapman, W. C., Gingeras, T. R., Ecker, J. R., and Snyder, M. P. (2014) Comparison of the transcriptional landscapes between human and mouse tissues. *Proc. Natl. Acad. Sci. U. S. A.* **111**, 17224–17229

307. Hackert, N. S., Radtke, F. A., Exner, T., Lorenz, H. M., Müller-Tidow, C., Nigrovic, P. A., Wabnitz, G., and Grieshaber-Bouyer, R. (2023) Human and mouse neutrophils share core transcriptional programs in both homeostatic and inflamed contexts. *Nat. Commun. 2023 141* **14**, 1–21

308. Zhu, Y. P., Thomas, G. D., and Hedrick, C. C. (2016) 2014 Jeffrey M. Hoeg award lecture: Transcriptional control of monocyte development. *Arterioscler. Thromb. Vasc. Biol.* **36**, 1722–1733

309. Mildner, A., Schönheit, J., Giladi, A., David, E., Lara-Astiaso, D., Lorenzo-Vivas, E., Paul, F., Chappell-Maor, L., Priller, J., Leutz, A., Amit, I., and Jung, S. (2017) Genomic Characterization of Murine Monocytes Reveals C/EBPβ Transcription Factor Dependence of Ly6C− Cells. *Immunity* **46**, 849-862.e7

310. Yona, S., Kim, K. W., Wolf, Y., Mildner, A., Varol, D., Breker, M., Strauss-Ayali, D., Viukov, S., Guilliams, M., Misharin, A., Hume, D. A., Perlman, H., Malissen, B., Zelzer, E., and Jung, S. (2013) Fate Mapping Reveals Origins and Dynamics of Monocytes and Tissue Macrophages under Homeostasis. *Immunity* **38**, 79–91

311. De Bruijn, M. F. T. R., Van, W., Ploemacher, R. E., Bakker-Woudenberg, I. A. J. M., Campbell, P. A., Van Ewijk, W., and Leenen, P. J. M. (1998) Bone marrow cellular composition in Listeria monocytogenes infected mice detected using ER-MP12 and ER-MP20 antibodies: a flow cytometric alternative to differential counting. *J. Immunol. Methods* **217**, 27–39

312. Kapellos, T. S., Bonaguro, L., Gemünd, I., Reusch, N., Saglam, A., Hinkley, E. R., and Schultze, J. L. (2019) Human monocyte subsets and phenotypes in major chronic inflammatory diseases. *Front. Immunol.* **10**, 2035

313. Smiljanovic, B., Radzikowska, A., Kuca-Warnawin, E., Kurowska, W., Grün, J. R., Stuhlmüller, B., Bonin, M., Schulte-Wrede, U., Sörensen, T., Kyogoku, C., Bruns, A., Hermann, S., Ohrndorf, S., Aupperle, K., Backhaus, M., Burmester, G. R., Radbruch, A., Grützkau, A., Maslinski, W., and Häupl, T. (2018) Extended report: Monocyte alterations in rheumatoid arthritis are dominated by preterm release from bone marrow and prominent triggering in

the joint. *Ann. Rheum. Dis.* **77**, 300

314. Gómez-Olarte, S., Bolaños, N. I., Echeverry, M., Rodríguez, A. N., Cuéllar, A., Puerta, C. J., Mariño, A., and González, J. M. (2019) Intermediate Monocytes and Cytokine Production Associated With Severe Forms of Chagas Disease. *Front. Immunol.* **10**, 1671

315. Rana, A. K., Li, Y., Dang, Q., and Yang, F. (2018) Monocytes in rheumatoid arthritis: Circulating precursors of macrophages and osteoclasts and, their heterogeneity and plasticity role in RA pathogenesis. *Int. Immunopharmacol.* **65**, 348–359

316. Wacleche, V. S., Tremblay, C. L., Routy, J. P., and Ancuta, P. (2018) The Biology of Monocytes and Dendritic Cells: Contribution to HIV Pathogenesis. *Viruses* **10**

317. Highton, J., Carlisle, B., and Palmer, D. G. (1995) Changes in the phenotype of monocytes/macrophages and expression of cytokine mRNA in peripheral blood and synovial fluid of patients with rheumatoid arthritis. *Clin. Exp. Immunol.* **102**, 541–546

318. Palmer, D. G., Hogg, N., Highton, J., Hessian, P. A., and Denholm, I. (1987) Macrophage migration and maturation within rheumatoid nodules. *Arthritis Rheum.* **30**, 729–736

319. Tsukamoto, M., Seta, N., Yoshimoto, K., Suzuki, K., Yamaoka, K., and Takeuchi, T. CD14 bright CD16+ intermediate monocytes are induced by interleukin-10 and positively correlate with disease activity in rheumatoid arthritis.

320. Hirose, S., Lin, Q., Ohtsuji, M., Nishimura, H., and Verbeek, J. S. (2019) Monocyte subsets involved in the development of systemic lupus erythematosus and rheumatoid arthritis. *Int. Immunol.* **31**, 687–696

321. Liao, X., Liu, J., Guo, X., Meng, R., Zhang, W., Zhou, J., Xie, X., and Zhou, H. (2024) Origin and Function of Monocytes in Inflammatory Bowel Disease. *J. Inflamm. Res.* **17**, 2897

322. Yin, Q., Song, D., Chen, J., Ning, G., Wang, W., and Wang, S. (2022) The

CD14++CD16+ monocyte subset is expanded and controls Th1 cell development in Graves' disease. *Clin. Immunol.* **245**, 109160

323. Lepzien, R., Liu, S., Czarnewski, P., Nie, M., Österberg, B., Baharom, F., Pourazar, J., Rankin, G., Eklund, A., Bottai, M., Kullberg, S., Blomberg, A., Grunewald, J., and Smed-Sörensen, A. (2021) Monocytes in sarcoidosis are potent tumour necrosis factor producers and predict disease outcome. *Eur. Respir. J.* **58**

324. Feinstein, M. J., Buzkova, P., Olson, N. C., Doyle, M. F., Sitlani, C. M., Fohner, A. E., Huber, S. A., Floyd, J., Sinha, A., Thorp, E. B., Landay, A., Freiberg, M. S., Longstreth, W. T., Tracy, R. P., Psaty, B. M., and Delaney, J. A. (2022) Monocyte subsets, T cell activation profiles, and stroke in men and women: The Multi-Ethnic Study of Atherosclerosis and Cardiovascular Health Study. *Atherosclerosis* **351**, 18–25

325. Chow, D. C., Saiki, K. M. W., Siriwardhana, C., Lozano-Gerona, J., Vanapruks, S., Ogle, J., Premeaux, T. A., Ndhlovu, L. C., and Boisvert, W. A. (2023) Increased transmigration of intermediate monocytes associated with atherosclerotic burden in people with HIV on antiretroviral therapy. *AIDS* **37**, 1177–1179

326. Wildgruber, M., Aschenbrenner, T., Wendorff, H., Czubba, M., Glinzer, A., Haller, B., Schiemann, M., Zimmermann, A., Berger, H., Eckstein, H. H., Meier, R., Wohlgemuth, W. A., Libby, P., and Zernecke, A. (2016) The "Intermediate" CD14++CD16+ monocyte subset increases in severe peripheral artery disease in humans. *Sci. Reports 2016 61* **6**, 1–8

327. Hirose, S., Lin, Q., Ohtsuji, M., Nishimura, H., and Verbeek, J. S. (2019) Monocyte subsets involved in the development of systemic lupus erythematosus and rheumatoid arthritis. *Int. Immunol.* **31**, 687

328. Navarini, L., Vomero, M., Di Donato, S., Currado, D., Berardicurti, O., Marino, A., Bearzi, P., Biaggi, A., Ferrito, M., Ruscitti, P., Fava, M., Leuti, A., Cipriani, P., Maccarrone, M., and Giacomelli, R. (2022) 2-Arachidonoylglycerol Reduces the Production of Interferon-Gamma in T Lymphocytes from Patients with Systemic Lupus Erythematosus.

Biomedicines **10**, 1675

329. Choubey, D. and Moudgil, K. D. (2011) Interferons in Autoimmune and Inflammatory Diseases: Regulation and Roles. *J. Interf. Cytokine Res.* **31**, 857

330. Selvi, E., Lorenzini, S., Garcia-Gonzalez, E., Maggio, R., Lazzerini, P. E., Capecchi, P. L., Balistreri, E., Spreafi Co, A., Niccolini, S., Pompella, G., Natale, M. R., Guideri, F., Pasini, F. L., Galeazzi, M., Marcolongo, R., Selvi, E., Lorenzini, S., Garcia-Gonzalez, E., Maggio, R., Lazzerini, P. E., Capecchi, L., Balistreri, E., Spreafi Co, A., Natale, M. R., Guideri, F., Franco, ;, Pasini, L., Galeazzi, M., and Marcolongo, R. (2008) Inhibitory effect of synthetic cannabinoids on cytokine production in rheumatoid fibroblast-like synoviocytes. *clinexprheumatol.orgE Selvi, S Lorenzini, E Garcia-Gonzalez, R Maggio, PE Lazzerini, PL Capecchi, E BalistreriClinical Exp. Rheumatol. 2008•clinexprheumatol.org* **26**, 574–581

331. Richardson, D., Pearson, R. G., Kurian, N., Latif, M. L., Garle, M. J., Barrett, D. A., Kendall, D. A., Scammell, B. E., Reeve, A. J., and Chapman, V. (2008) Characterisation of the cannabinoid receptor system in synovial tissue and fluid in patients with osteoarthritis and rheumatoid arthritis. *Arthritis Res. Ther.* **10**

332. Lourbopoulos, A., Grigoriadis, N., Lagoudaki, R., Touloumi, O., Polyzoidou, E., Mavromatis, I., Tascos, N., Breuer, A., Ovadia, H., Karussis, D., Shohami, E., Mechoulam, R., and Simeonidou, C. (2011) Administration of 2-arachidonoylglycerol ameliorates both acute and chronic experimental autoimmune encephalomyelitis. *Brain Res.* **1390**, 126–141

333. Lambert, D., Vandevoorde, S., Jonsson, K.-O., and Fowler, C. (2012) The Palmitoylethanolamide Family: A New Class of Anti-Inflammatory Agents ? *Curr. Med. Chem.* **9**, 663–674

334. Fessler, S. N., Liu, L., Chang, Y., Yip, T., and Johnston, C. S. (2022) Palmitoylethanolamide Reduces Proinflammatory Markers in Unvaccinated Adults Recently Diagnosed with COVID-19: A Randomized Controlled Trial. *J. Nutr.* **152**, 2218–2226

335. Impellizzeri, D., Esposito, E., Di Paola, R., Ahmad, A., Campolo, M., Peli, A., Morittu, V. M., Britti, D., and Cuzzocrea, S. (2013) Palmitoylethanolamide and luteolin ameliorate development of arthritis caused by injection of collagen type II in mice. *Arthritis Res. Ther.* **15**, 1–14

336. Esposito, E. and Cuzzocrea, S. (2013) Palmitoylethanolamide in homeostatic and traumatic central nervous system injuries. *CNS Neurol. Disord. Drug Targets* **12**, 55–61

337. Fessler, S. N., Liu, L., Chang, Y., Yip, T., and Johnston, C. S. (2022) Palmitoylethanolamide Reduces Proinflammatory Markers in Unvaccinated Adults Recently Diagnosed with COVID-19: A Randomized Controlled Trial. *J. Nutr.* **152**, 2218

338. Steels, E., Venkatesh, R., Steels, E., Vitetta, G., and Vitetta, L. (2019) A double-blind randomized placebo controlled study assessing safety, tolerability and efficacy of palmitoylethanolamide for symptoms of knee osteoarthritis. *Inflammopharmacology* **27**, 475–485

339. Singh, T. P., Zhang, H. H., Borek, I., Wolf, P., Hedrick, M. N., Singh, S. P., Kelsall, B. L., Clausen, B. E., and Farber, J. M. (2016) Monocyte-derived inflammatory Langerhans cells and dermal dendritic cells mediate psoriasis-like inflammation. *Nat. Commun. 2016 71* **7**, 1–18

340. Paudel, S., Ghimire, L., Jin, L., Jeansonne, D., and Jeyaseelan, S. (2022) Regulation of emergency granulopoiesis during infection. *Front. Immunol.* **13**

341. Trumpp, A., Essers, M., and Wilson, A. (2010) Awakening dormant haematopoietic stem cells. *Nat. Rev. Immunol.* **10**, 201–209

342. Pouzolles, M., Oburoglu, L., Taylor, N., and Zimmermann, V. S. (2016) Hematopoietic stem cell lineage specification. *Curr. Opin. Hematol.* **23**, 311–317

343. Balmer, M. L., Schürch, C. M., Saito, Y., and Geuking, M. B. (2014) Microbiota-derived compounds drive steady-state granulopoiesis via MyD88/TICAM signaling. *journals.aai.orgML Balmer, C. Schürch, Y Saito, MB Geuking, H Li, M Cuenca, LV Kovtonyuk, KD McCoyThe J. Immunol.*

2014•journals.aai.org **193**, 5273–5283

344. Boettcher, S., Ziegler, P., Schmid, M. A., Takizawa, H., van Rooijen, N., Kopf, M., Heikenwalder, M., and Manz, M. G. (2012) Cutting Edge: LPS-Induced Emergency Myelopoiesis Depends on TLR4-Expressing Nonhematopoietic Cells. *J. Immunol.* **188**, 5824–5828

345. Deshmukh, H. S., Liu, Y., Menkiti, O. R., Mei, J., Dai, N., O'Leary, C. E., Oliver, P. M., Kolls, J. K., Weiser, J. N., and Worthen, G. S. (2014) The microbiota regulates neutrophil homeostasis and host resistance to Escherichia coli K1 sepsis in neonatal mice. *Nat. Med.* **20**, 524–530

346. Kwok, I., Becht, E., Xia, Y., Ng, M., Teh, Y., Tan, L., Immunity, M. E.-, and 2020, undefined. Combinatorial single-cell analyses of granulocyte-monocyte progenitor heterogeneity reveals an early uni-potent neutrophil progenitor. *cell.comI Kwok, E Becht, Y Xia, M Ng, YC Teh, L Tan, M Evrard, JLY Li, HTN Tran, Y Tan, D LiuImmunity, 2020•cell.com*

347. Zekavat, S. M., Lin, S. H., Bick, A. G., Liu, A., Paruchuri, K., Wang, C., Uddin, M. M., Ye, Y., Yu, Z., Liu, X., Kamatani, Y., Bhattacharya, R., Pirruccello, J. P., Pampana, A., Loh, P. R., Kohli, P., McCarroll, S. A., Kiryluk, K., Neale, B., Ionita-Laza, I., Engels, E. A., Brown, D. W., Smoller, J. W., Green, R., Karlson, E. W., Lebo, M., Ellinor, P. T., Weiss, S. T., Daly, M. J., Koyama, S., Ito, K., Momozawa, Y., Matsuda, K., Yamanashi, Y., Furukawa, Y., Morisaki, T., Murakami, Y., Muto, K., Nagai, A., Obara, W., Yamaji, K., Takahashi, K., Asai, S., Takahashi, Y., Suzuki, T., Sinozaki, N., Yamaguchi, H., Minami, S., Murayama, S., Yoshimori, K., Nagayama, S., Obata, D., Higashiyama, M., Masumoto, A., Koretsune, Y., Palotie, A., Ziemann, A., Mitchell, A., Huertas-Vazquez, A., Salminen, A., Jussila, A., Havulinna, A., Mackay, A., Abbasi, A., Elliott, A., Cole, A., Shcherban, A., Mälarstig, A., Ganna, A., Loboda, A., Podgornaia, A., Lehtonen, A., Pitkäranta, A., Remes, A., Auranen, A., Hakanen, A., Palomäki, A., Jalanko, A., Loukola, A., Chhibber, A., Lertratanakul, A., Lehisto, A., Mannermaa, A., Hedman, Å., Chu, A., Madar, A., Ghazal, A., Challis, B., Sun, B., Cummings, B., Riley-Gillis, B., Fox, C., Chen, C. Y., Wang, C., Chatelain, C., Gordin, D., Quarless, D., Oh, D., Choy, D., Close, D., Pulford, D., Rice, D., Waterworth,

D., Rajpal, D., Baird, D., Jambulingam, D., Chang, D., Kulkarni, D., Paul, D., Liu, D., Teng, E., Punkka, E., Ekholm, E., Kangasniemi, E., Laakkonen, E., Wigmore, E., Järvensivu, E., Kilpeläinen, E., Widen, E., Tsai, E., Mohammed, E., Strauss, E., Kvikstad, E., Pitkänen, E., Kaiharju, E., Xu, E., Xu, F., Rahimov, F., Vaura, F., Auge, F., Brein, G., Lassi, G., Heap, G., Laivuori, H., Mattsson, H., Uusitalo-Järvinen, H., Kankaanranta, H., Uusitalo, H., Chen, H., Siirtola, H., Joensuu, H., Runz, H., Lehtonen, H., Heyne, H., Soininen, H., Jacob, H., Chen, H., Shen, H. Y., Xu, H., Vähätalo, I., Kalliala, I., Tachmazidou, I., Kaprio, J., Parkkinen, J., Jacob, J., Kumar, J., van Adelsberg, J., Laukkanen, J., Ritari, J., Garcia-Tabuenca, J., Waring, J., Schutzman, J., Liu, J., Lee, J., Betts, J., Rämö, J., Huhtakangas, J., Mäkelä, J., Mattson, J., Schleutker, J., Kettunen, J., Eicher, J., Zierer, J., Chung, J., Turunen, J. A., Gordillo, J. E., Maranville, J., Karjalainen, J., Mehtonen, J., Rinne, J., Sinisalo, J., Junttila, J., Koskela, J., Partanen, J., Peltola, J., Hunkapiller, J., Pihlajamäki, J., Wade, J., Partanen, J., Mäkikallio, K., Kaarniranta, K., Tasanen, K., Metsärinne, K., Pärn, K., King, K. S., Eklund, K., Linden, K., Nieminen, K., Hannula-Jouppi, K., Call, K., Klinger, K., Donner, K., Hyvärinen, K., Kristiansson, K., Kivinen, K., Kaukinen, K., Pylkäs, K., de Lange, K., Usiskin, K., Palin, K., Shkura, K., Auro, K., Kalpala, K., Sipilä, K., Elenius, K., Tsuo, K., Lahtela, L. E., Addis, L., Huilaja, L., Kotaniemi-Talonen, L., Mustaniemi, L., Pirilä, L., Morin-Papunen, L., Aaltonen, L., Koulu, L., Suominen, L., Kallio, L., McCarthy, L., Aoxing, L., Männikkö, L., Obeidat, M., Rivas, M., Hautalahti, M., Pelkonen, M., Kaunisto, M., Niemi, M. E., Siponen, M., Crohns, M., Kalaoja, M., Luodonpää, M., Vääräsmäki, M., Taskinen, M. R., Tuppurainen, M., McCarthy, M., Laakso, M., Laukkanen, M., Voutilainen, M., Juonala, M., Perola, M., Hochfeld, M., Färkkilä, M., Reeve, M. P., Kanai, M., Brauer, M., Gossel, M., Peura, M., Ehm, M., Miller, M., Liu, M., Aavikko, M., Koskinen, M., Helminen, M., Kähönen, M., Arvas, M., Hiltunen, M., Kiviniemi, M., Caliskan, M., Karjalainen, M., Raivio, M., Koivusalo, M., Kurki, M., Maasha, M., Bing, N., Bowers, N., Raghavan, N., Renaud, N., Välimäki, N., Hautala, N., Mars, N., Pitkänen, N., Smaoui, N., Kaipiainen-Seppänen, O., Carpén, O., Dada, O. A., Soylemez, O., Heikinheimo, O., Tuovila, O., Uimari, O.,

Gormley, P., Auvinen, P., Laiho, P., Mäntylä, P., Polo, P., Bronson, P., Kauppi, P., Karihtala, P., Nieminen, P., Tienari, P., Virolainen, P., Isomäki, P., Della Briotta Parolo, P., Pussinen, P., Palta, P., Pakkanen, R., Serpi, R., Mishra, R., Hinttala, R., Kälviäinen, R., Wong, R., Popovic, R., Siegel, R., Lahesmaa, R., Kajanne, R., Graham, R., Plenge, R., Yang, R., Kallionpää, R., Tian, R., Miller, R., Esmaeeli, S., Kauppila, S., John, S., Heikkinen, S., Koskelainen, S., Wadhawan, S., Pikkarainen, S., Heron, S., Ripatti, S., Seitsonen, S., Lahdenperä, S., Ruotsalainen, S., Pendergrass, S., Smith, S., Vuoti, S., Hassan, S., Biswas, S., Luo, S., Rüeger, S., Lähteenmäki, S., Peltonen, S., Soini, S., Petrovski, S., Ghosh, S., McDonough, S., Loomis, S., Greenberg, S., Eaton, S., Lemmelä, S., Xia, T. H., Laitinen, T., Tukiainen, T., Salmi, T., Niiranen, T., Paajanen, T., Kuopio, T., Kilpi, T., Ollila, T., Hiekkalinna, T., Jyrhämä, T., Harju, T., Luukkaala, T., Tuomi, T., Behrens, T., Lu, T., Blomster, T., Sipilä, T. P., Southerington, T., Mäkelä, T., Kiiskinen, T., Mantere, T., Meretoja, T., Bhangale, T., Salo, T., Sistonen, T., Palotie, U., Gursoy, U., Kujala, U., Julkunen, V., Salomaa, V., Kosma, V. M., Rathinakannan, V. S., Kurra, V., Aaltonen, V., Neduva, V., Llorens, V., Sinha, V., Anttonen, V., Zhou, W., Fleuren, W., Chen, X., Hu, X., Wu, Y., Huang, Y., Terao, C., Zhao, H., Ebert, B. L., Reilly, M. P., Ganna, A., Machiela, M. J., Genovese, G., and Natarajan, P. (2021) Hematopoietic mosaic chromosomal alterations increase the risk for diverse types of infection. *Nat. Med. 2021 276* **27**, 1012–1024

348. Kwok, A. J., Allcock, A., Ferreira, R. C., Cano-Gamez, E., Smee, M., Burnham, K. L., Zurke, Y. X., Novak, A., Darwent, M., Baron, T., Brown, C., Beer, S., Espinosa, A., Panduro, T., Georgiou, D., Martinez, J., Thraves, H., Perez, E., Fernandez, R., Sobrino, A., Sanchez, V., Magallano, R., Dineen, K., Wilson, J., McKechnie, S., Mentzer, A. J., Monaco, C., Udalova, I. A., Hinds, C. J., Todd, J. A., Davenport, E. E., and Knight, J. C. (2023) Neutrophils and emergency granulopoiesis drive immune suppression and an extreme response endotype during sepsis. *Nat. Immunol.* **24**, 767–779

349. O'Neil, L. J. and Kaplan, M. J. (2019) Neutrophils in Rheumatoid Arthritis: Breaking Immune Tolerance and Fueling Disease. *Trends Mol. Med.* **25**, 215–

227

350. Geissmann, F., Jung, S., and Littman, D. R. (2003) Blood monocytes consist of two principal subsets with distinct migratory properties. *Immunity* **19**, 71–82

351. Passlick, B., Flieger, D., and Ziegler-Heitbrock, H. (1989) Identification and characterization of a novel monocyte subpopulation in human peripheral blood.

352. Zawada, A. M., Rogacev, K. S., Rotter, B., Winter, P., Marell, R. R., Fliser, D., and Heine, G. H. (2011) SuperSAGE evidence for CD14++CD16+ monocytes as a third monocyte subset. *Blood* **118**

353. Mildner, A., Schönheit, J., Giladi, A., David, E., Lara-Astiaso, D., Lorenzo-Vivas, E., Paul, F., Chappell-Maor, L., Priller, J., Leutz, A., Amit, I., and Jung, S. (2017) Genomic Characterization of Murine Monocytes Reveals C/EBPβ Transcription Factor Dependence of Ly6C- Cells. *Immunity* **46**, 849-862.e7

354. Auffray, C., Fogg, D., Garfa, M., Elain, G., Join-Lambert, O., Kayal, S., Sarnacki, S., Cumano, A., Lauvau, G., and Geissmann, F. (2007) Monitoring of blood vessels and tissues by a population of monocytes with patrolling behavior. *Science (80-.).* **317**, 666–670

355. Azizi, G., Jadidi-Niaragh, F., and Mirshafiey, A. (2013) Th17 Cells in Immunopathogenesis and treatment of rheumatoid arthritis. *Int. J. Rheum. Dis.* **16**, 243–253

356. Sahbandar, I. N., Ndhlovu, L. C., Saiki, K., Kohorn, L. B., Peterson, M. M., D'antoni, M. L., Shiramizu, B., Shikuma, C. M., and Chow, D. C. (2020) Relationship between Circulating Inflammatory Monocytes and Cardiovascular Disease Measures of Carotid Intimal Thickness. *J. Atheroscler. Thromb.* **27**, 441–448

357. Matsui, K., Wirotesangthong, M., and Nishikawa, A. (2007) Percutaneous application of peptidoglycan from Staphylococcus aureus induces eosinophil infiltration in mouse skin. *Clin. Exp. Allergy* **37**, 615–622

358. Resnick, M. B. and Weller, P. F. (1993) Mechanisms of eosinophil recruitment. *Am. J. Respir. Cell Mol. Biol.* **8**, 349–355

359. Forssmann, U., Uguccioni, M., Loetscher, P., Dahinden, C. A., Langen, H., Thelen, M., and Baggiolini, M. (1997) Eotaxin-2, a Novel CC Chemokine that Is Selective for the Chemokine Receptor CCR3, and Acts Like Eotaxin on Human Eosinophil and Basophil Leukocytes. *J. Exp. Med.* **185**, 2171

360. Rot, A., Krieger, M., Brunner, T., Bischoff, S. C., Schall, T. J., and Dahinden, C. A. (1992) RANTES and macrophage inflammatory protein 1 alpha induce the migration and activation of normal human eosinophil granulocytes. *J. Exp. Med.* **176**, 1489–1495

361. Kline, S. N., Orlando, N. A., Lee, A. J., Wu, M. J., Zhang, J., Youn, C., Feller, L. E., Pontaza, C., Dikeman, D., Limjunyawong, N., Williams, K. L., Wang, Y., Cihakova, D., Jacobsen, E. A., Durum, S. K., Garza, L. A., Dong, X., and Archer, N. K. (2024) Staphylococcus aureus proteases trigger eosinophil-mediated skin inflammation. *Proc. Natl. Acad. Sci. U. S. A.* **121**, e2309243121

362. Hirashima, M. (1999) Ecalectin as a T cell-derived eosinophil chemoattractant. *Int. Arch. Allergy Immunol.* **120 Suppl 1**, 7–10

363. Hogan, S. P., Rosenberg, H. F., Moqbel, R., Phipps, S., Foster, P. S., Lacy, P., Barry Kay, A., and Rothenberg, M. E. (2008) Eosinophils: biological properties and role in health and disease. *Wiley Online Libr. Hogan, HF Rosenberg, R Moqbel, S Phipps, PS Foster. P Lacy, AB Kay, ME RothenbergClinical Exp. Allergy, 2008•Wiley Online Libr.* **38**, 709–750

364. Wen, T., spectrum, M. R.-M., and 2016, undefined. (2016) The regulatory function of eosinophils. *Am Soc MicrobiolT Wen, ME RothenbergMicrobiology spectrum, 2016•Am Soc Microbiol* **4**

365. Ramirez, G. A., Yacoub, M.-R., Ripa, M., Mannina, D., Cariddi, A., Saporiti, N., Ciceri, F., Castagna, A., Colombo, G., and Dagna, L. (2018) Eosinophils from physiology to disease: a comprehensive review. *Wiley Online Libr. Ramirez, MR Yacoub, M Ripa, D Mannina, A Cariddi, N Saporiti, F Ciceri, A CastagnaBioMed Res. Int. 2018•Wiley Online Libr.* **2018**

366. Kanda, A., Yun, Y., Bui, D. Van, Nguyen, L. M., Kobayashi, Y., Suzuki, K., Mitani, A., Sawada, S., Hamada, S., Asako, M., and Iwai, H. (2021) The multiple functions and subpopulations of eosinophils in tissues under steady-state and pathological conditions. *Allergol. Int.* **70**, 9–18

367. Kanda, A., Yasutaka, Y., Bui, D. Van, Suzuki, K., Sawada, S., Kobayashi, Y., Asako, M., and Iwai, H. (2020) Multiple biological aspects of eosinophils in host defense, eosinophil-associated diseases, immunoregulation, and homeostasis: is their role beneficial, detrimental. *jstage.jst.go.jpA Kanda, Y Yasutaka, D Van Bui, K Suzuki, S Sawada, Y Kobayashi, M Asako, H IwaiBiological Pharm. Bull. 2020•jstage.jst.go.jp* **43**, 20–30

368. Rosenberg, H., Dyer, K., Immunology, P. F.-N. R., and 2013, undefined. Eosinophils: changing perspectives in health and disease. *nature.comHF Rosenberg, KD Dye. PS Foster. Rev. Immunol. 2013•nature.com*

369. Coden, M., Biology, S. B.-J. of L., and 2020, undefined. Eosinophils in wound healing and epithelial remodeling: Is coagulation a missing link? *Acad. Coden, S BerdnikovsJournal Leucoc. Biol. 2020•academic.oup.com*

370. Chusid, M. J. (2018) Eosinophils: Friends or Foes? *J. Allergy Clin. Immunol. Pract.* **6**, 1439–1444

371. Takeda, K., Shiraishi, Y., Ashino, S., Han, J., Jia, Y., Wang, M., Lee, N. A., Lee, J. J., and Gelfand, E. W. (2015) Eosinophils contribute to the resolution of lung-allergic responses following repeated allergen challenge. *J. Allergy Clin. Immunol.* **135**, 451-460.e5

372. Romani, N., Holzmann, S., Tripp, C. H., Koch, F., and Stoitzner, P. (2003) Langerhans cells – dendritic cells of the epidermis. *APMIS* **111**, 725–740

373. Kissenpfennig, A., Immunology, B. M.-T. in, and 2006, undefined. Langerhans cells–revisiting the paradigm using genetically engineered mice. *cell.comA Kissenpfennig, B MalissenTRENDS Immunol. 2006•cell.com*

374. Merad, M., Manz, M., Karsunky, H., … A. W.-N., and 2002, undefined. Langerhans cells renew in the skin throughout life under steady-state conditions. *nature.comM Merad, MG Manz, H Karsunky, A Wagers, W*

Peters, I Charo, Weissman, JG CysterNature Immunol. 2002•nature.com

375. Ginhoux, F., Tacke, F., Angeli, V., … M. B.-N., and 2006, undefined. Langerhans cells arise from monocytes in vivo. *nature.comF Ginhoux, F Tacke, V Angeli, M Bogunovic, M Loubeau, XM Dai, ER Stanley, GJ RandolphNature Immunol. 2006•nature.com*

376. Seré, K., Baek, J. H., Ober-Blöbaum, J., Müller-Newen, G., Tacke, F., Yokota, Y., Zenke, M., and Hieronymus, T. (2012) Two Distinct Types of Langerhans Cells Populate the Skin during Steady State and Inflammation. *Immunity* **37**, 905–916

377. Chorro, L., Sarde, A., Li, M., … K. W.-J. of E., and 2009, undefined. Langerhans cell (LC) proliferation mediates neonatal development, homeostasis, and inflammation-associated expansion of the epidermal LC network. *rupress.orgL Chorro, A Sarde, M Li, KJ Woollard, P Chambon, B Malissen, A KissenpfennigJournal Exp. Med. 2009•rupress.org*

378. Kitashima, D. Y., Kobayashi, T., Woodring, T., Idouchi, K., Doebel, T., Voisin, B., Adachi, T., Ouchi, T., Takahashi, H., Nishifuji, K., Kaplan, D. H., Clausen, B. E., Amagai, M., and Nagao, K. (2018) Langerhans Cells Prevent Autoimmunity via Expansion of Keratinocyte Antigen-Specific Regulatory T Cells. *EBioMedicine* **27**, 293–303

379. West, H. C. and Bennett, C. L. (2018) Redefining the role of langerhans cells as immune regulators within the skin. *Front. Immunol.* **8**, 322056

380. King, J. K., Philips, R. L., Eriksson, A. U., Kim, P. J., Halder, R. C., Lee, D. J., and Singh, R. R. (2015) Langerhans Cells Maintain Local Tissue Tolerance in a Model of Systemic Autoimmune Disease. *J. Immunol.* **195**, 464–476

381. Mitchell, S., Thomas, G., Harvey, K., Cottell, D., Reville, K., Berlasconi, G., Petasis, N. A., Erwig, L., Rees, A. J., Savill, J., Brady, H. R., and Godson, C. (2002) Lipoxins, Aspirin-Triggered Epi-Lipoxins, Lipoxin Stable Analogues, and the Resolution of Inflammation: Stimulation of Macrophage Phagocytosis of Apoptotic. *journals.lww.com* **13**, 2497–2507

382. Nagayama, T., Sinor, A. D., Simon, R. P., Chen, J., Graham, S. H., Jin, K.,

and Greenberg, D. A. (1999) Cannabinoids and neuroprotection in global and focal cerebral ischemia and in neuronal cultures. *Soc Neurosci. Nagayama, AD Sinor, RP Simon, J Chen, SH Graham, K Jin, DA GreenbergJournal Neurosci. 1999•Soc Neurosci.*

383. Parmentier-Batteur, S., Jin, K., Mao, X. O., Xie, L., and Greenberg, D. A. (2002) Increased severity of stroke in CB1 cannabinoid receptor knock-out mice. *Soc Neurosci. Parmentier-Batteur, K Jin, XO Mao, L Xie, DA GreenbergJournal Neurosci. 2002•Soc Neurosci.*

384. Muthian, S., Rademacher, D., Roelke, C., Neuroscience, G. G.-, and 2004, undefined. (2004) Anandamide content is increased and CB1 cannabinoid receptor blockade is protective during transient, focal cerebral ischemia. *ElsevierS Muthian, DJ Rademacher, CT Roelke, GJ Gross, CJ HillardNeuroscience, 2004•Elsevier*

385. Mechoulam, R. and Parker, L. A. (2013) The endocannabinoid system and the brain. *Annu. Rev. Psychol.* **64**, 21–47

386. Sulcova, E., Mechoulam, R., and Fride, E. (1998) Biphasic Effects of Anandamide. *Pharmacol. Biochem. Behav.* **59**, 347–352

387. Ben-Shabat, S., Fride, E., Sheskin, T., Tamiri, T., Rhee, M. H., Vogel, Z., Bisogno, T., De Petrocellis, L., Di Marzo, V., and Mechoulam, R. (1998) An entourage effect: inactive endogenous fatty acid glycerol esters enhance 2-arachidonoyl-glycerol cannabinoid activity. *Eur. J. Pharmacol.* **353**, 23–31

388. Berdyshev, E., Boichot, E., Corbel, M., Germain, N., and Lagente, V. (1998) Effects of cannabinoid receptor ligands on LPS-induced pulmonary inflammation in mice. *Life Sci.* **63**, PL125–PL129

389. Sedeighzadeh, S. S., Galehdari, H., Tabandeh, M. R., Shamsara, M., and Roohbakhsh, A. (2021) The Endocannabinoid, Anandamide, Acts as a Novel Inhibitor of LPS-Induced Inflammasome Activation in Human Gastric Cancer AGS Cell Line: Involvement of CB1 and TRPV1 Receptors. *Mediators Inflamm.* **2021**, 6698049

390. Malfait, A. M., Gallily, R., Sumariwalla, P. F., Malik, A. S., Andreakos, E.,

Mechoulam, R., and Feldmann, M. (2000) The nonpsychoactive cannabis constituent cannabidiol is an oral anti-arthritic therapeutic in murine collagen-induced arthritis. *Proc. Natl. Acad. Sci. U. S. A.* **97**, 9561–9566

391. Zurier, R., Rossetti, R., … J. L.-… : O. J. of, and 1998, undefined. Dimethylheptyl-THC-11 oic acid: a nonpsychoactive antiinflammatory agent with a cannabinoid template structure. *Wiley Online Libr. Zurier, RG Rossetti, JH Lane, JM Goldberg, SA Hunter, SH BursteinArthritis Rheum. Off. J. Am. Coll. 1998•Wiley Online Libr.*

392. Burstein, S. (2000) Ajulemic acid (CT3): a potent analog of the acid metabolites of THC. *Curr. Pharm. Des.* **6**, 1339–1345

393. Burstein, S. H. and Sumner Burstein, C. H. (2018) Ajulemic acid: potential treatment for chronic inflammation. *Pharmacol. Res. Perspect.* **6**, e00394

394. Bidinger, B., Torres, R., Rossetti, R., Brown, L., … R. B.-C., and 2003, undefined. Ajulemic acid, a nonpsychoactive cannabinoid acid, induces apoptosis in human T lymphocytes. *Elsevier*

395. Zurier, R., Rossetti, R., pharmacology, S. B.-B., and 2003, undefined. Suppression of human monocyte interleukin-1β production by ajulemic acid, a nonpsychoactive cannabinoid. *ElsevierRB Zurier, RG Rossetti, SH Burstein, B BidingerBiochemical Pharmacol. 2003•Elsevier*

396. Sumariwalla, P. F., Gallily, R., Tchilibon, S., Fride, E., Mechoulam, R., and Feldmann, M. (2004) A Novel Synthetic, Nonpsychoactive Cannabinoid Acid (HU-320) with Antiinflammatory Properties in Murine Collagen-Induced Arthritis. *Arthritis Rheum.* **50**, 985–998

397. Wallace, J. L., Caliendo, G., Santagada, V., and Cirino, G. (2010) Markedly reduced toxicity of a hydrogen sulphide-releasing derivative of naproxen (ATB-346). *Br. J. Pharmacol.* **159**, 1236–1246

398. Tsuge, K., Inazumi, T., Shimamoto, A., and Sugimoto, Y. (2019) Molecular mechanisms underlying prostaglandin E2-exacerbated inflammation and immune diseases. *Int. Immunol.* **31**, 597–606

399. Reviews, R. C.-P. and 1994, undefined. Classification of prostanoid

receptors: properties, distribution, and structure of the receptors and their subtypes. *cir.nii.ac.jp*

400. Helliwell, R., Adams, L., Prostaglandins, M. M.-, and, L., and 2004, undefined. Prostaglandin synthases: recent developments and a novel hypothesis. *Elsevier*

401. Kurland, J. I. and Bockman, R. (1978) Prostaglandin E production by human blood monocytes and mouse peritoneal macrophages. *J. Exp. Med.* **147**, 952–957

402. Ham, E. A., Soderman, D. D., Zanetti, M. E., Dougherty, H. W., McCauley, E., and Kuehl, F. A. (1983) Inhibition by prostaglandins of leukotriene B4 release from activated neutrophils. *Proc. Natl. Acad. Sci.* **80**, 4349–4353

403. Talpain, E., Armstrong, R. A., Coleman, R. A., and Vardey, C. J. (1995) Characterization of the PGE receptor subtype mediating inhibition of superoxide production in human neutrophils. *Br. J. Pharmacol.* **114**, 1459–1465

404. Burelout, C., Thibault, N., Levasseur, S., Simard, S., Naccache, P. H., and Bourgoin, S. G. (2004) Prostaglandin E2 Inhibits the Phospholipase D Pathway Stimulated by Formyl-methionyl-leucyl-phenylalanine in Human Neutrophils. Involvement of EP2 Receptors and Phosphatidylinositol 3-kinase γ. *Mol. Pharmacol.* **66**, 293–301

405. Zasłona, Z., Serezani, C. H., Okunishi, K., Aronoff, D. M., and Peters-Golden, M. (2012) Prostaglandin E2 restrains macrophage maturation via E prostanoid receptor 2/protein kinase A signaling. *Blood* **119**, 2358–2367

406. Aronoff, D. M., Bergin, I. L., Lewis, C., Goel, D., O'Brien, E., Peters-Golden, M., and Mancuso, P. (2012) E-prostanoid 2 receptor signaling suppresses lung innate immunity against Streptococcus pneumoniae. *Prostaglandins Other Lipid Mediat.* **98**, 23–30

407. Aronoff, D. M., Canetti, C., and Peters-Golden, M. (2004) Prostaglandin E2 Inhibits Alveolar Macrophage Phagocytosis through an E-Prostanoid 2 Receptor-Mediated Increase in Intracellular Cyclic AMP. *J. Immunol.* **173**,

559–565

408. Agard, M., Asakrah, S., and Morici, L. A. (2013) PGE2 suppression of innate immunity during mucosal bacterial infection. *Front. Cell. Infect. Microbiol.* **4**, 55889

409. Kunkel, S. L., Wiggins, R. C., Chensue, S. W., and Larrick, J. (1986) Regulation of macrophage tumor necrosis factor production by prostaglandin E2. *Biochem. Biophys. Res. Commun.* **137**, 404–410

410. Stolina, M., Sharma, S., Lin, Y., Dohadwala, M., Gardner, B., Luo, J., Zhu, L., Kronenberg, M., Miller, P. W., Portanova, J., Lee, J. C., and Dubinett, S. M. (2000) Specific Inhibition of Cyclooxygenase 2 Restores Antitumor Reactivity by Altering the Balance of IL-10 and IL-12 Synthesis. *J. Immunol.* **164**, 361–370

411. Narumiya, S., journal, T. F.-F., and 2011, undefined. (2011) Fever, inflammation, pain and beyond: prostanoid receptor research during these 25 years. *Res. Narumiya, T FuruyashikiFASEB journal, 2011•researchgate.net*

412. Guo, R., Lin, J., Xu, W., Shen, N., Mo, L., Zhang, C., and Feng, J. (2013) Hydrogen sulfide attenuates doxorubicin-induced cardiotoxicity by inhibition of the p38 MAPK pathway in H9c2 cells. *Int. J. Mol. Med.* **31**, 644–650

413. Xu, W., Chen, J., Lin, J., Liu, D., Mo, L., Pan, W., Feng, J., Wu, W., and Zheng, D. (2015) Exogenous H2S protects H9c2 cardiac cells against high glucose-induced injury and inflammation by inhibiting the activation of the NF-κB and IL-1β pathways. *Int. J. Mol. Med.* **35**, 177–186

414. Chen, S., Saeed, A. F. U. H., Liu, Q., Jiang, Q., Xu, H., Xiao, G. G., Rao, L., and Duo, Y. (2023) Macrophages in immunoregulation and therapeutics. *Signal Transduct. Target. Ther. 2023 81* **8**, 1–35

415. Alquraini, A. and El Khoury, J. (2020) Scavenger receptors. *Curr. Biol.* **30**, R790

416. Taban, Q., Mumtaz, P. T., Masoodi, K. Z., Haq, E., and Ahmad, S. M. (2022) Scavenger receptors in host defense: from functional aspects to mode of action. *Cell Commun. Signal. 2021 201* **20**, 1–17

417. Whiteman, M., Armstrong, J. S., Chu, S. H., Jia-Ling, S., Wong, B.-S., Cheung, N. S., Halliwell, B., and Moore, P. K. (2004) The novel neuromodulator hydrogen sulfide: an endogenous peroxynitrite “scavenger”? *J. Neurochem.* **90**, 765–768

418. Stables, M. J., Newson, J., Ayoub, S. S., Brown, J., Hyams, C. J., and Gilroy, D. W. (2010) Priming innate immune responses to infection by cyclooxygenase inhibition kills antibiotic-susceptible and -resistant bacteria. *Blood* **116**, 2950–2959

419. Marsolais, D., Côté, C. H., and Frenette, J. (2003) Nonsteroidal Anti-Inflammatory Drug Reduces Neutrophil and Macrophage Accumulation but Does Not Improve Tendon Regeneration.

420. Díaz-González, F. and Sánchez-Madrid, F. NSAIDs: learning new tricks from old drugs.

421. Perna, A. F., Sepe, I., Lanza, D., Capasso, R., Zappavigna, S., Capasso, G., Caraglia, M., and Ingrosso, D. (2013) Hydrogen sulfide reduces cell adhesion and relevant inflammatory triggering by preventing ADAM17-dependent TNF-α activation. *J. Cell. Biochem.* **114**, 1536–1548

422. da Silva, M. C., dos Santos, V. M., da Silva, M. V. B., Prazeres, T. C. M. M., Cartágenes, M. do S. S., Calzerra, N. T. M., and de Queiroz, T. M. (2022) Involvement of shedding induced by ADAM17 on the nitric oxide pathway in hypertension. *Front. Mol. Biosci.* **9**, 1032177

423. Ball, C. J., Reiffel, A. J., Chintalapani, S., Kim, M., Spector, J. A., and King, M. R. (2013) Hydrogen sulfide reduces neutrophil recruitment in hind-limb ischemia-reperfusion injury in an L-selectin and ADAM-17 dependent manner. *Plast. Reconstr. Surg.* **131**, 487

424. Domínguez-Luis, M., Herrera-García, A., Arce-Franco, M., Armas-González, E., Rodríguez-Pardo, M., Lorenzo-Díaz, F., Feria, M., Cadenas, S., Sánchez-Madrid, F., and Díaz-González, F. (2013) Superoxide anion mediates the L-selectin down-regulation induced by non-steroidal anti-inflammatory drugs in human neutrophils. *Biochem. Pharmacol.* **85**, 245–256

425. Nauseef, W. M. and Borregaard, N. (2014) Neutrophils at work. *Nat. Immunol.* **15**, 602–611

426. Wright, H. L., Moots, R. J., Bucknall, R. C., and Edwards, S. W. (2010) Neutrophil function in inflammation and inflammatory diseases. *Rheumatology* **49**, 1618–1631

427. Kolaczkowska, E. and Kubes, P. (2013) Neutrophil recruitment and function in health and inflammation. *Nat. Rev. Immunol.* **13**, 159–175

428. Beauvillain, C., Cunin, P., Doni, A., Scotet, M., Jaillon, S., Loiry, M. L., Magistrelli, G., Masternak, K., Chevailler, A., Delneste, Y., and Jeannin, P. (2011) CCR7 is involved in the migration of neutrophils to lymph nodes. *Blood* **117**, 1196–1204

429. Iking-Konert, C., Csekö, C., Wagner, C., Stegmaier, S., Andrassy, K., and Hänsch, M. G. (2001) Transdifferentiation of polymorphonuclear neutrophils: Acquisition of CD83 and other functional characteristics of dendritic cells. *J. Mol. Med.* **79**, 464–474

430. Iking-Konert, C., Wagner, C., … B. D.-C. &, and 2002, undefined. Up-regulation of the dendritic cell marker CD83 on polymorphonuclear neutrophils (PMN): divergent expression in acute bacterial infections and chronic inflammatory. *Acad. Iking-Konert, C Wagner, B Denefleh, F Hug, M Schneider, K Andrassy, GM HänschClinical Exp. Immunol. 2002•academic.oup.com*

431. Förster, R., Davalos-Misslitz, A., Immunology, A. R.-N. R., and 2008, undefined. (2014) CCR7 and its ligands: balancing immunity and tolerance. *nature.comR Förster, AC Davalos-Misslitz, A RotNature Rev. Immunol. 2008•nature.com*

432. Hoyt, K., Anderson, E., Curran, M. L., Fuhlbrigge, R., Notarangelo, L., Pachman, L. M., Kim, S., and Henderson, L. (2017) The lymphocyte repertoire in juvenile dermatomyositis. *Arthritis Rheumatol.* **69(Supplem**, 29–31

433. Abramson, S., Edelson, H., Kaplan, H., Ludewig, R., and Weissmann, G.

(1984) Inhibition of Neutrophil Activation by Nonsteroidal Anti-Inflammatory Drugs. *Am. J. Med.* **77**, 3–6

434. Bannenberg, G. L. and Vieira, H. LA. (2009) Therapeutic applications of the gaseous mediators carbon monoxide and hydrogen sulfide. *Expert Opin. Ther. Pat.* **19**, 663–682

435. Wallace, J., Buret, A., Nagy, P., Muscara, M., and Nucci, G. de. (2019) THU0464 PHASE 2 CLINICAL TRIAL OF THE GI SAFETY OF A HYDROGEN SULFIDE-RELEASING ANTI-INFLAMMATORY DRUG (ATB-346).

436. Powell, C. R., Dillon, K. M., and Matson, J. B. (2018) A review of hydrogen sulfide (H2S) donors: Chemistry and potential therapeutic applications. *Biochem. Pharmacol.* **149**, 110–123

437. Powell, C. R., Foster, J. C., Okyere, B., Theus, M. H., and Matson, J. B. (2016) Therapeutic Delivery of H2S via COS: Small Molecule and Polymeric Donors with Benign Byproducts. *J. Am. Chem. Soc.* **138**, 13477–13480

438. Wright, S. D., Ramos, R. A., Tobias, P. S., Ulevitch, R. J., and Mathison, J. C. (1990) CD14, a receptor for complexes of lipopolysaccharide (LPS) and LPS binding protein. *Science* **249**, 1431–1433

439. Dobrovolskaia, M. A. and Vogel, S. N. (2002) Toll receptors, CD14, and macrophage activation and deactivation by LPS. *Microbes Infect.* **4**, 903–914

440. Iwahashi, H., Takeshita, A., and Hanazawa, S. (2000) Prostaglandin E2 Stimulates AP-1-Mediated CD14 Expression in Mouse Macrophages Via Cyclic AMP-Dependent Protein Kinase A. *J. Immunol.* **164**, 5403–5408

441. Heidenreich, S., Schmidt, M., August, C., Cullen, P., Rademaekers, A., and Pauels, H. G. (1997) Regulation of human monocyte apoptosis by the CD14 molecule. *J. Immunol.* **159**, 3178–3188

442. Lauener, R. P., Goyert, S. M., Geha, R. S., and Vercelli, D. (1990) Interleukin 4 down-regulates the expression of CD14 in normal human monocytes. *Eur. J. Immunol.* **20**, 2375–2381

443. Ricciotti, E. and Fitzgerald, G. A. (2011) Prostaglandins and Inflammation. *Arterioscler. Thromb. Vasc. Biol.* **31**, 986–1000

444. Liu, F., Liu, G., Liu, N., … G. Z.-E. and, and 2015, undefined. Effect of hydrogen sulfide on inflammatory cytokines in acute myocardial ischemia injury in rats. *spandidos-publications.comF Liu, GJ Liu, N Liu, G Zhang, JX Zhang, LF LiExperimental Ther. Med. 2015•spandidos-publications.com*

445. Song, Y., Wu, S., Zhang, R., Zhong, Q., Zhang, X., and Sun, X. (2024) Therapeutic potential of hydrogen sulfide in osteoarthritis development. *Front. Pharmacol.* **15**

446. Andruski, B., McCafferty, D. M., Ignacy, T., Millen, B., and McDougall, J. J. (2008) Leukocyte trafficking and pain behavioral responses to a hydrogen sulfide donor in acute monoarthritis. *Am. J. Physiol. - Regul. Integr. Comp. Physiol.* **295**

447. Batallé, G., Bai, X., Balboni, G., and Pol, O. (2023) The Impact of UFP-512 in Mice with Osteoarthritis Pain: The Role of Hydrogen Sulfide. *Antioxidants 2023, Vol. 12, Page 2085* **12**, 2085

448. Porta, A., Rodríguez, L., Bai, X., Batallé, G., Roch, G., Pouso-Vázquez, E., Balboni, G., and Pol, O. (2021) Hydrogen Sulfide Inhibits Inflammatory Pain and Enhances the Analgesic Properties of Delta Opioid Receptors. *Antioxidants 2021, Vol. 10, Page 1977* **10**, 1977

449. Blomqvist, A. and Engblom, D. (2018) Neural Mechanisms of Inflammation-Induced Fever. *Neurosci.* **24**, 381

450. Biosci, J. V.-A. and 2014, undefined. Inhibition of prostaglandin biosynthesis as the mechanism of action of aspirin-like drugs. *books.google.comJR VaneAdv Biosci, 2014•books.google.com*

451. Aronoff, D. M. and Neilson, E. G. (2001) Antipyretics: mechanisms of action and clinical use in fever suppression. *Am. J. Med.* **111**, 304–315

452. Christensen, A. D., Haase, C., Cook, A. D., and Hamilton, J. A. (2016) K/BxN serum-transfer arthritis as a model for human inflammatory arthritis. *Front. Immunol.* **7**, 192242

453. Rosu, A., Margaritescu, C., Stepan, A., Musetescu, A., P Pa Ap Pe Er R, A. L., Roşu, A., Mărgăritescu, C., Stepan, A., Muşetescu, A., and Ene, M. (2012) O OR RI IG GI IN NA IL-17 patterns in synovium, serum and synovial fluid from treatment-naïve, early rheumatoid arthritis patients. *Artic. Rom. J. Morphol. Embryol.* **2012**, 73–80

454. Alivernini, S., Tolusso, B., Gessi, M., Gigante, M. R., Mannocci, A., Petricca, L., Perniola, S., Di Mario, C., Bui, L., Fedele, A. L., Capacci, A., Bruno, D., Peluso, G., La Torre, G., Federico, F., Ferraccioli, G., and Gremese, E. (2021) Inclusion of Synovial Tissue–Derived Characteristics in a Nomogram for the Prediction of Treatment Response in Treatment-Naive Rheumatoid Arthritis Patients. *Arthritis Rheumatol.* **73**, 1601–1613

455. Cooles, F. A. H., Anderson, A. E., Lendrem, D. W., Norris, J., Pratt, A. G., Hilkens, C. M. U., and Isaacs, J. D. (2018) The interferon gene signature is increased in patients with early treatment-naive rheumatoid arthritis and predicts a poorer response to initial therapy. *J. Allergy Clin. Immunol.* **141**, 445-448.e4

456. Li, C., Zhang, J., Wang, W., Wang, H., Zhang, Y., and Zhang, Z. (2019) Arsenic trioxide improves Treg and Th17 balance by modulating STAT3 in treatment-naïve rheumatoid arthritis patients. *Int. Immunopharmacol.* **73**, 539–551

457. Dvergsten, J. A., Reed, A. M., Landerman, L., Pisetsky, D. S., Ilkayeva, O., and Huffman, K. M. (2021) Metabolomics Analysis Identifies a Lipidomic Profile in Treatment Naive Juvenile Dermatomyositis Patients versus Healthy Control Subjects. *Rheumatology* **29**, 29

458. Glossop, J. R., Emes, R. D., Nixon, N. B., Packham, J. C., Fryer, A. A., Mattey, D. L., and Farrell, W. E. (2016) Genome-wide profiling in treatment-naive early rheumatoid arthritis reveals DNA methylome changes in T and B lymphocytes. *Epigenomics* **8**, 209–224

459. Dixon, W. G., Suissa, S., and Hudson, M. (2011) The association between systemic glucocorticoid therapy and the risk of infection in patients with rheumatoid arthritis: systematic review and meta-analyses. *Arthritis Res. Ther.*

13, R139

460. Rutherford, A. I., Subesinghe, S., Hyrich, K. L., and Galloway, J. B. (2018) Serious infection across biologic-treated patients with rheumatoid arthritis: results from the British Society for Rheumatology Biologics Register for Rheumatoid Arthritis. *Ann. Rheum. Dis.* **77**, 905–910

461. Rees, P., Wohland, P., Norman, P., and Boden, P. (2012) Ethnic population projections for the UK, 2001–2051. *J. Popul. Res. 2012 291* **29**, 45–89

462. Corthay, A. (2009) How do Regulatory T Cells Work? *Scand. J. Immunol.* **70**, 326

463. Chen, Y., Kuchroo, V. K., Inobe, J., Hafler, D. A., and Weiner, H. L. (1994) Regulatory T Cell Clones Induced by Oral Tolerance: Suppression of Autoimmune Encephalomyelitis. *Science (80-.).* **265**, 1237–1240

464. Kawashiri, S. Y., Kawakami, A., Okada, A., Koga, T., Tamai, M., Yamasaki, S., Nakamura, H., Origuchi, T., Ida, H., and Eguchi, K. (2011) CD4+CD25highCD127low/- Treg Cell Frequency from Peripheral Blood Correlates with Disease Activity in Patients with Rheumatoid Arthritis. *J. Rheumatol.* **38**, 2517–2521

465. Kanjana, K., Chevaisrakul, P., Matangkasombut, P., Paisooksantivatana, K., and Lumjiaktase, P. (2020) Inhibitory activity of FOXP3+ regulatory T cells reveals high specificity for displaying immune tolerance in remission state rheumatoid arthritis. *Sci. Rep.* **10**

466. Lawson, C., Brown, A., Bejarano, V., … S. D.-, and 2006, undefined. Early rheumatoid arthritis is associated with a deficit in the CD4 + CD25 high regulatory T cell population in peripheral blood. *Acad. Lawson, AK Brown, V Bejar. SH Douglas, CH Burgoyne, AS GreensteinRheumatology, 2006•academic.oup.com*

467. Möttönen, M., Heikkinen, J., Mustonen, L., Isomäki, P., Luukkainen, R., and Lassila, O. (2005) CD4+ CD25+ T cells with the phenotypic and functional characteristics of regulatory T cells are enriched in the synovial fluid of patients with rheumatoid arthritis. *Clin. Exp. Immunol.* **140**, 360

468. Yan, S., Kotschenreuther, K., Deng, S., and Kofler, D. M. (2022) Regulatory T cells in rheumatoid arthritis: functions, development, regulation, and therapeutic potential. *Cell. Mol. Life Sci.* **79**, 533

469. Luo, P., Wang, P., Xu, J., Hou, W., Xu, P., Xu, K., and Liu, L. (2022) Immunomodulatory role of T helper cells in rheumatoid arthritis: A COMPREHENSIVE RESEARCH REVIEW. *Bone Jt. Res.* **11**, 426–438

470. Chen, Z., Bozec, A., Ramming, A., and Schett, G. (2018) Anti-inflammatory and immune-regulatory cytokines in rheumatoid arthritis. *Nat. Rev. Rheumatol. 2018 151* **15**, 9–17

471. McKinney, E. F., Lyons, P. A., Carr, E. J., Hollis, J. L., Jayne, D. R. W., Willcocks, L. C., Koukoulaki, M., Brazma, A., Jovanovic, V., Kemeny, D. M., Pollard, A. J., MacAry, P. A., Chaudhry, A. N., and Smith, K. G. C. (2010) A CD8+ T cell transcription signature predicts prognosis in autoimmune disease. *Nat. Med.* **16**, 586–591

472. Sawcer, S., Hellenthal, G., Pirinen, M., Spencer, C. C. A., Patsopoulos, N. A., Moutsianas, L., Dilthey, A., Su, Z., Freeman, C., Hunt, S. E., Edkins, S., Gray, E., Booth, D. R., Potter, S. C., Goris, A., Band, G., Oturai, A. B., Strange, A., Saarela, J., Bellenguez, C., Fontaine, B., Gillman, M., Hemmer, B., Gwilliam, R., Zipp, F., Jayakumar, A., Martin, R., Leslie, S., Hawkins, S., Giannoulatou, E., D'Alfonso, S., Blackburn, H., Boneschi, F. M., Liddle, J., Harbo, H. F., Perez, M. L., Spurkland, A., Waller, M. J., Mycko, M. P., Ricketts, M., Comabella, M., Hammond, N., Kockum, I., McCann, O. T., Ban, M., Whittaker, P., Kemppinen, A., Weston, P., Hawkins, C., Widaa, S., Zajicek, J., Dronov, S., Robertson, N., Bumpstead, S. J., Barcellos, L. F., Ravindrarajah, R., Abraham, R., Alfredsson, L., Ardlie, K., Aubin, C., Baker, A., Baker, K., Baranzini, S. E., Bergamaschi, L., Bergamaschi, R., Bernstein, A., Berthele, A., Boggild, M., Bradfield, J. P., Brassat, D., Broadley, S. A., Buck, D., Butzkueven, H., Capra, R., Carroll, W. M., Cavalla, P., Celius, E. G., Cepok, S., Chiavacci, R., Clerget-Darpoux, F., Clysters, K., Comi, G., Cossburn, M., Cournu-Rebeix, I., Cox, M. B., Cozen, W., Cree, B. A. C., Cross, A. H., Cusi, D., Daly, M. J., Davis, E., De Bakker, P. I. W., Debouverie, M., D'Hooghe, M. B., Dixon, K., Dobosi, R., Dubois, B.,

Ellinghaus, D., Elovaara, I., Esposito, F., Fontenille, C., Foote, S., Franke, A., Galimberti, D., Ghezzi, A., Glessner, J., Gomez, R., Gout, O., Graham, C., Grant, S. F. A., Guerini, F. R., Hakonarson, H., Hall, P., Hamsten, A., Hartung, H. P., Heard, R. N., Heath, S., Hobart, J., Hoshi, M., Infante-Duarte, C., Ingram, G., Ingram, W., Islam, T., Jagodic, M., Kabesch, M., Kermode, A. G., Kilpatrick, T. J., Kim, C., Klopp, N., Koivisto, K., Larsson, M., Lathrop, M., Lechner-Scott, J. S., Leone, M. A., Leppä, V., Liljedahl, U., Bomfim, I. L., Lincoln, R. R., Link, J., Liu, J., Lorentzen, A. R., Lupoli, S., MacCiardi, F., MacK, T., Marriott, M., Martinelli, V., Mason, D., McCauley, J. L., Mentch, F., Mero, I. L., Mihalova, T., Montalban, X., Mottershead, J., Myhr, K. M., Naldi, P., Ollier, W., Page, A., Palotie, A., Pelletier, J., Piccio, L., Pickersgill, T., Piehl, F., Pobywajlo, S., Quach, H. L., Ramsay, P. P., Reunanen, M., Reynolds, R., Rioux, J. D., Rodegher, M., Roesner, S., Rubio, J. P., Rückert, I. M., Salvetti, M., Salvi, E., Santaniello, A., Schaefer, C. A., Schreiber, S., Schulze, C., Scott, R. J., Sellebjerg, F., Selmaj, K. W., Sexton, D., Shen, L., Simms-Acuna, B., Skidmore, S., Sleiman, P. M. A., Smestad, C., Sørensen, P. S., Søndergaard, H. B., Stankovich, J., Strange, R. C., Sulonen, A. M., Sundqvist, E., Syvänen, A. C., Taddeo, F., Taylor, B., Blackwell, J. M., Tienari, P., Bramon, E., Tourbah, A., Brown, M. A., Tronczynska, E., Casas, J. P., Tubridy, N., Corvin, A., Vickery, J., Jankowski, J., Villoslada, P., Markus, H. S., Wang, K., Mathew, C. G., Wason, J., Palmer, C. N. A., Wichmann, E., Plomin, R., Willoughby, E., Rautanen, A., Winkelmann, J., Wittig, M., Trembath, R. C., Yaouanq, J., Viswanathan, A. C., Zhang, H., Wood, N. W., Zuvich, R., Deloukas, P., Langford, C., Duncanson, A., Oksenberg, J. R., Pericak-Vance, M. A., Haines, J. L., Olsson, T., Hillert, J., Ivinson, A. J., De Jager, P. L., Peltonen, L., Stewart, G. J., Hafler, D. A., Hauser, S. L., McVean, G., Donnelly, P., and Compston, A. (2011) Genetic risk and a primary role for cell-mediated immune mechanisms in multiple sclerosis. *Nature* **476**, 214–219

473. Nejentsev, S., Howson, J. M. M., Walker, N. M., Szeszko, J., Field, S. F., Stevens, H. E., Reynolds, P., Hardy, M., King, E., Masters, J., Hulme, J., Maier, L. M., Smyth, D., Bailey, R., Cooper, J. D., Ribas, G., Campbell, R. D., Clayton, D. G., Todd, J. A., Burton, P. R., Cardon, L. R., Craddock, N.,

Deloukas, P., Duncanson, A., Kwiatkowski, D. P., McCarthy, M. I., Ouwehand, W. H., Samani, N. J., Donnelly, P., Barrett, J. C., Davison, D., Easton, D., Evans, D., Leung, H. T., Marchini, J. L., Morris, A. P., Spencer, C. C. A., Tobin, M. D., Attwood, A. P., Boorman, J. P., Cant, B., Everson, U., Hussey, J. M., Jolley, J. D., Knight, A. S., Koch, K., Meech, E., Nutland, S., Prowse, C. V., Taylor, N. C., Walters, G. R., Watkins, N. A., Winzer, T., Jones, R. W., McArdle, W. L., Ring, S. M., Strachan, D. P., Pembrey, M., Breen, G., St Clair, D., Caesar, S., Gordon-Smith, K., Jones, L., Fraser, C., Green, E. K., Grozeva, D., Hamshere, M. L., Holmans, P. A., Jones, I. R., Kirov, G., Moskvina, V., Nikolov, I., O'Donovan, M. C., Owen, M. J., Collier, D. A., Elkin, A., Farmer, A., Williamson, R., McGuffin, P., Young, A. H., Ferrier, I. N., Ball, S. G., Balmforth, A. J., Barrett, J. H., Bishop, D. T., Iles, M. M., Maqbool, A., Yuldasheva, N., Hall, A. S., Braund, P. S., Dixon, R. J., Mangino, M., Stevens, S., Thompson, J. R., Bredin, F., Tremelling, M., Parkes, M., Drummond, H., Lees, C. W., Nimmo, E. R., Satsangi, J., Fisher, S. A., Forbes, A., Lewis, C. M., Onnie, C. M., Prescott, N. J., Sanderson, J., Mathew, C. G., Barbour, J., Mohiuddin, M. K., Todhunter, C. E., Mansfield, J. C., Tariq, A., Cummings, F. R., Jewell, D. P., Webster, J., Brown, M. J., Lathrop, G. M., Connell, J., Dominiczak, A., Braga Marcano, C. A., Burke, B., Dobson, R., Gungadoo, J., Lee, K. L., Munroe, P. B., Newhouse, S. J., Onipinla, A., Wallace, C., Xue, M., Caulfield, M., Farrall, M., Barton, A., Bruce, I. N., Donovan, H., Eyre, S., Gilbert, P. D., Hider, S. L., Hinks, A. M., John, S. L., Potter, C., Silman, A. J., Symmons, D. P. M., Thomson, W., Worthington, J., Dunger, D. B., Widmer, B., Frayling, T. M., Freathy, R. M., Lango, H., Perry, J. R. B., Shields, B. M., Weedon, M. N., Hattersley, A. T., Hitman, G. A., Walker, M., Elliott, K. S., Groves, C. J., Lindgren, C. M., Rayner, N. W., Timpson, N. J., Zeggini, E., Newport, M., Sirugo, G., Lyons, E., Vannberg, F., Hill, A. V. S., Bradbury, L. A., Farrar, C., Pointon, J. J., Wordsworth, P., Brown, M. A., Franklyn, J. A., Heward, J. M., Simmonds, M. J., Gough, S. C. L., Seal, S., Stratton, M. R., Rahman, N., Ban, M., Goris, A., Sawcer, S. J., Compston, A., Conway, D., Jallow, M., Rockett, K. A., Bryan, C., Bumpstead, S. J., Chaney, A., Downes, K., Ghori, J., Gwilliam, R., Hunt, S. E., Inouye, M., Keniry, A., King, E., McGinnis, R., Potter, S.,

Ravindrarajah, R., Whittaker, P., Withers, D., Cardin, N. J., Ferreira, T., Pereira-Gale, J., Hallgrimsdóttir, I. B., Howie, B. N., Su, Z., Yik, Y. T., Vukcevic, D., Bentley, D., and Compston, A. (2007) Localization of type 1 diabetes susceptibility to the MHC class I genes HLA-B and HLA-A. *Nature* **450**, 887–892

474. Raposo, B. R., Rodrigues-Santos, P., Carvalheiro, H., Água-Doce, A. M., Carvalho, L., Pereira Da Silva, J. A., Graça, L., and Souto-Carneiro, M. M. (2010) Monoclonal anti-CD8 therapy induces disease amelioration in the K/BxN mouse model of spontaneous chronic polyarthritis. *Arthritis Rheum.* **62**, 2953–2962

475. Laffón, A., García-Vicuña, R., Humbría, A., Postigo, A. A., Corbí, A. L., De Landázuri, M. O., and Sánchez-Madrid, F. (1991) Upregulated expression and function of VLA-4 fibronectin receptors on human activated T cells in rheumatoid arthritis. *J. Clin. Invest.* **88**, 546–552

476. Carvalheiro, H., Duarte, C., Silva-Cardoso, S., Da Silva, J. A. P., and Souto-Carneiro, M. M. (2015) CD8+ T cell profiles in patients with rheumatoid arthritis and their relationship to disease activity. *Arthritis Rheumatol.* **67**, 363–371

477. Cho, B. A., Sim, J. H., Park, J. A., Kim, H. W., Yoo, W. H., Lee, S. H., Lee, D. S., Kang, J. S., Hwang, Y. Il, Lee, W. J., Kang, I., Lee, E. B., and Kim, H. R. (2012) Characterization of effector memory CD8+ T cells in the synovial fluid of rheumatoid arthritis. *J. Clin. Immunol.* **32**, 709–720

478. Godfrey, D. I., Hammond, K. J. L., Poulton, L. D., Smyth, M. J., and Baxter, A. G. (2000) NKT cells: Facts, functions and fallacies. *Immunol. Today* **21**, 573–583

479. Elewaut, D. (2005) Natural killer T cells and rheumatoid arthritis: friend or foe? *Arthritis Res. Ther.* **7**, 88

480. Hammond, K. J. L. and Kronenberg, M. (2003) Natural killer T cells: Natural or unnatural regulators of autoimmunity? *Curr. Opin. Immunol.* **15**, 683–689

481. Mieza, M., Itoh, T., Cui, J., (Baltimore, Y. M.-…, 1950, M. ., and 1996,

undefined. Selective reduction of V alpha 14+ NK T cells associated with disease development in autoimmune-prone mice. *journals.aai.orgMA Mieza, T Itoh, JQ Cui, Y Makino, T Kawano, K Tsuchida, T Koike, T Shirai, H YagitaJournal Immunol. (Baltimore, Md. 1950), 1996•journals.aai.org*

482. Van Der Vliet, H. J. J., Von Blomberg, B. M. E., Nishi, N., Reijm, M., Voskuyl, A. E., Van Bodegraven, A. A., Polman, C. H., Rustemeyer, T., Lips, P., Van Den Eertwegh, A. J. M., Giaccone, G., Scheper, R. J., and Pinedo, H. M. (2001) Circulating V(alpha24+) Vbeta11+ NKT cell numbers are decreased in a wide variety of diseases that are characterized by autoreactive tissue damage. *Clin. Immunol.* **100**, 144–148

483. Kojo, S., Adachi, Y., Keino, H., Taniguchi, M., and Sumida, T. (2001) Dysfunction of T cell receptor AV24AJ18+, BV11+ double-negative regulatory natural killer T cells in autoimmune diseases. *Wiley Online Libr.* **44**, 1127–1138

484. He, H., Qiao, B., Guo, S., Cui, H., Zhang, Z., and Qin, J. (2022) Interleukin-7 regulates CD127 expression and promotes CD8+ T cell activity in patients with primary cutaneous melanoma. *BMC Immunol.* **23**, 1–12

485. Barata, J. T., Durum, S. K., and Seddon, B. (2019) Flip the coin: IL-7 and IL-7R in health and disease. *Nat. Immunol. 2019 2012* **20**, 1584–1593

486. Pallard, C., Stegmann, A. P. A., Van Kleffens, T., Smart, F., Venkitaraman, A., and Spits, H. (1999) Distinct roles of the phosphatidylinositol 3-kinase and STAT5 pathways in IL-7-mediated development of human thymocyte precursors. *Immunity* **10**, 525–535

487. Barata, J. T., Silva, A., Brandao, J. G., Nadler, L. M., Cardoso, A. A., and Boussiotis, V. A. (2004) Activation of PI3K is indispensable for interleukin 7-mediated viability, proliferation, glucose use, and growth of T cell acute lymphoblastic leukemia cells. *J. Exp. Med.* **200**, 659–669

488. Alves, N. L., van Leeuwen, E. M. M., Derks, I. A. M., and van Lier, R. A. W. (2008) Differential regulation of human IL-7 receptor alpha expression by IL-7 and TCR signaling. *J. Immunol.* **180**, 5201–5210

489. Churchman, S. M. and Ponchel, F. (2008) Interleukin-7 in rheumatoid arthritis. *Rheumatology (Oxford).* **47**, 753–759

490. Chen, D., Tang, T. X., Deng, H., Yang, X. P., and Tang, Z. H. (2021) Interleukin-7 Biology and Its Effects on Immune Cells: Mediator of Generation, Differentiation, Survival, and Homeostasis. *Front. Immunol.* **12**

491. Jian, M., Yunjia, Z., Zhiying, D., Yanduo, J., and Guocheng, J. (2019) Interleukin 7 receptor activates PI3K/Akt/mTOR signaling pathway via downregulation of Beclin-1 in lung cancer. *Mol. Carcinog.* **58**, 358–365

492. Corcoran, A., Riddell, A., Nature, D. K.-, and 1998, undefined. Impaired immunoglobulin gene rearrangement in mice lacking the IL-7 receptor. *nature.comAE Corcoran, A Riddell, D Krooshoop, AR VenkitaramanNature, 1998•nature.com*

493. Cui, G., Staron, M., Gray, S., Ho, P., Cell, R. A.-, and 2015, undefined. IL-7-induced glycerol transport and TAG synthesis promotes memory CD8+ T cell longevity. *cell.comG Cui, MM Staron, SM Gray, PC Ho, RA Amezquita, J Wu, SM KaechCell, 2015•cell.com*

494. Raeber, M. E., Zurbuchen, Y., Impellizzieri, D., Boyman, | Onur, and Boyman, O. (2018) The role of cytokines in T-cell memory in health and disease. *Wiley Online Libr. Raeber, Y Zurbuchen, D Impellizzieri, O BoymanImmunological Rev. 2018•Wiley Online Libr.* **283**, 176–193

495. Huang, J., Long, Z., Jia, R., Wang, M., Zhu, D., Liu, M., Chen, S., Zhao, X., Yang, Q., Wu, Y., Zhang, S., Tian, B., Mao, S., Ou, X., Sun, D., Gao, Q., and Cheng, A. (2021) The Broad Immunomodulatory Effects of IL-7 and Its Application In Vaccines. *Front. Immunol.* **12**, 680442

496. Meazza, R., Azzarone, B., Orengo, A. M., Ferrini, S., and Biassoni, R. (2011) Role of common-gamma chain cytokines in NK cell development and function: Perspectives for immunotherapy. *Wiley Online Libr. Meazza, B Azzarone, AM Orengo, S FerriniBioMed Res. Int. 2011•Wiley Online Libr.* **2011**, 16

497. Murray, R., Suda, T., Wrlghton, N., Lee, F., and Zlotnik, A. (1989) IL-7 is a

growth and maintenance factor for mature and immature thymocyte subsets. *Acad. Murray, T Suda, N Wrighton, F Lee, A ZiotnikInternational Immunol. 1989•academic.oup.com* **1**

498. Vogt, T., Link, A., Perrin, J., Blood, D. F.-, of, T. J., and 2009, undefined. Novel function for interleukin-7 in dendritic cell development. *ashpublications.orgTK Vogt, A Link, J Perrin, D Finke, SA LutherBlood, J. Am. Soc. Hematol. 2009•ashpublications.org*

499. Alderson, M., … H. S.-T. J. of, and 1990, undefined. (1990) Interleukin 7 enhances cytolytic T lymphocyte generation and induces lymphokine-activated killer cells from human peripheral blood. *rupress.orgMR Alderson, HM Sassenfeld, MB WidmerThe J. Exp. Med. 1990•rupress.org* **172**, 577–587

500. Sin, J. I., Kim, J., Patchuk, C., and Weiner, D. B. (2000) Interleukin 7 can enhance antigen-specific cytotoxic-T-lymphocyte and/or Th2-type immune responses in vivo. *Clin. Diagn. Lab. Immunol.* **7**, 751–758

501. Han, J. M., Patterson, S. J., and Levings, M. K. (2012) The Role of the PI3K Signaling Pathway in CD4+ T Cell Differentiation and Function. *Front. Immunol.* **3**

502. Leonard, W. J., Lin, J. X., and O'Shea, J. J. (2019) The γc Family of Cytokines: Basic Biology to Therapeutic Ramifications. *Immunity* **50**, 832–850

503. Martinez, F. O., Gordon, S., Locati, M., and Mantovani, A. (2006) Transcriptional Profiling of the Human Monocyte-to-Macrophage Differentiation and Polarization: New Molecules and Patterns of Gene Expression. *J. Immunol.* **177**, 7303–7311

504. Zhang, B., Zhang, Y., Xiong, L., Li, Y., Zhang, Y., Zhao, J., Jiang, H., Li, C., Liu, Y., Liu, X., Liu, H., Ping, Y. F., Zhang, Q. C., Zhang, Z., Bian, X. W., Zhao, Y., and Hu, X. (2022) CD127 imprints functional heterogeneity to diversify monocyte responses in inflammatory diseases. *J. Exp. Med.* **219**

505. Leung, G. A., Cool, T., Valencia, C. H., Worthington, A., Beaudin, A. E., and Camilla Forsberg, E. (2019) The lymphoid-associated interleukin 7 receptor

(IL7R) regulates tissue-resident macrophage development. *Dev.* **146**

506. Al-Mossawi, H., Yager, N., Taylor, C. A., Lau, E., Danielli, S., de Wit, J., Gilchrist, J., Nassiri, I., Mahe, E. A., Lee, W., Rizvi, L., Makino, S., Cheeseman, J., Neville, M., Knight, J. C., Bowness, P., and Fairfax, B. P. (2019) Context-specific regulation of surface and soluble IL7R expression by an autoimmune risk allele. *Nat. Commun. 2019 101* **10**, 1–11

507. Chen, Z., Kim, S., Chamberlain, N. D., Pickens, S. R., Volin, M. V., Volkov, S., Arami, S., Christman, J. W., Prabhakar, B. S., Swedler, W., Mehta, A., Sweiss, N., and Shahrara, S. (2013) The Novel Role of IL-7 Ligation to IL-7 Receptor in Myeloid Cells of Rheumatoid Arthritis and Collagen-Induced Arthritis. *J. Immunol.* **190**, 5256–5266

508. Kim, S. jae, Chang, H. J., Volin, M. V., Umar, S., Van Raemdonck, K., Chevalier, A., Palasiewicz, K., Christman, J. W., Volkov, S., Arami, S., Maz, M., Mehta, A., Zomorrodi, R. K., Fox, D. A., Sweiss, N., and Shahrara, S. (2019) Macrophages are the primary effector cells in IL-7-induced arthritis. *Cell. Mol. Immunol. 2019 177* **17**, 728–740

509. Pickens, S. R., Chamberlain, N. D., Volin, M. V., Pope, R. M., Talarico, N. E., Mandelin, A. M., and Shahrara, S. (2011) Characterization of interleukin-7 and interleukin-7 receptor in the pathogenesis of rheumatoid arthritis. *Arthritis Rheum.* **63**, 2884–2893

510. Cavanagh, L. L., Boyce, A., Smith, L., Padmanabha, J., Filgueira, L., Pietschmann, P., and Thomas, R. (2005) Rheumatoid arthritis synovium contains plasmacytoid dendritic cells. *Arthritis Res. Ther.* **7**, R230

511. Suwa, Y., Nagafuchi, Y., Yamada, S., and Fujio, K. (2023) The role of dendritic cells and their immunometabolism in rheumatoid arthritis. *Front. Immunol.* **14**

512. Ivashkiv, L. B. and Donlin, L. T. (2014) Regulation of type I interferon responses. *Nat. Rev. Immunol.* **14**, 36

513. Bonjardim, C. A. (2005) Interferons (IFNs) are key cytokines in both innate and adaptive antiviral immune responses—and viruses counteract IFN action.

Microbes Infect. **7**, 569–578

514. Tough, D. F. (2004) Type I interferon as a link between innate and adaptive immunity through dendritic cell stimulation. *Leuk. Lymphoma* **45**, 257–264

515. Serafini, N., Vosshenrich, C. A. J., and Di Santo, J. P. (2015) Transcriptional regulation of innate lymphoid cell fate. *Nat. Rev. Immunol.* **15**, 415–428

516. Sheikh, A. and Abraham, N. (2019) Interleukin-7 Receptor Alpha in Innate Lymphoid Cells: More Than a Marker. *Front. Immunol.* **10**, 2897

517. Dalbeth, N., Gundle, R., Davies, R. J. O., Lee, Y. C. G., McMichael, A. J., and Callan, M. F. C. (2004) CD56bright NK Cells Are Enriched at Inflammatory Sites and Can Engage with Monocytes in a Reciprocal Program of Activation. *J. Immunol.* **173**, 6418–6426

518. Takaki-Kuwahara, A., Arinobu, Y., Miyawaki, K., Yamada, H., Tsuzuki, H., Irino, K., Ayano, M., Kimoto, Y., Mitoma, H., Akahoshi, M., Tsukamoto, H., Horiuchi, T., Niiro, H., and Akashi, K. (2019) CCR6+ group 3 innate lymphoid cells accumulate in inflamed joints in rheumatoid arthritis and produce Th17 cytokines. *Arthritis Res. Ther.* **21**

519. Kurowska-Stolarska, M. and Alivernini, S. (2022) Synovial tissue macrophages in joint homeostasis, rheumatoid arthritis and disease remission. *Nat. Rev. Rheumatol. 2022 187* **18**, 384–397

520. Jung, H., Mithal, D. S., Park, J. E., and Miller, R. J. (2015) Localized CCR2 Activation in the Bone Marrow Niche Mobilizes Monocytes by Desensitizing CXCR4. *PLoS One* **10**, e0128387

521. Engelhardt, E., Toksoy, A., Goebeler, M., Debus, S., Bröcker, E. B., and Gillitzer, R. (1998) Chemokines IL-8, GROalpha, MCP-1, IP-10, and Mig are sequentially and differentially expressed during phase-specific infiltration of leukocyte subsets in human wound healing. *Am. J. Pathol.* **153**, 1849–1860

522. Meyer, A., Parmar, P. J., and Shahrara, S. (2022) Significance of IL-7 and IL-7R in RA and autoimmunity. *Autoimmun. Rev.* **21**, 103120

523. Steven, M. M., Lennie, S. E., Sturrock, R. D., and Gemmell, C. G. (1984)

Enhanced bacterial phagocytosis by peripheral blood monocytes in rheumatoid arthritis. *Ann. Rheum. Dis.* **43**, 435–439

524. Barczyk, K., Ehrchen, J., Blood, K. T.-, Journal, T., and 2010, undefined. Glucocorticoids promote survival of anti-inflammatory macrophages via stimulation of adenosine receptor A3. *ashpublications.orgK Barczyk, J Ehrchen, K Tenbrock, M Ahlmann, J Kneidl, D Viemann, J RothBlood, J. Am. Soc. Hematol. 2010•ashpublications.org*

525. Horta-Baas, G. (2022) Patient-Reported Outcomes in Rheumatoid Arthritis: A Key Consideration for Evaluating Biosimilar Uptake? *Patient Relat. Outcome Meas.* **13**, 79–95

526. DeWitt, E. M., Gross, H., Stucky, B. D., Liu, Y., Thissen, D., Lovell, D. J., and Wallace, C. A. (2011) Cross-sectional validation of the patient reported outcome measurement information system pediatric scales in juvenile idiopathic arthritis, childhood systemic lupus erythematosus, and juvenile dermatomyositis. *Arthritis Rheum. Conf. Annu. Sci. Meet. Am. Coll. Rheumatol. Assoc. Rheumatol. Heal. Prof.* **63**

527. Arayssi, T., Touma, Z., Nikpour, M., and Ghandour, L. (2013) The assessment of disease activity in rheumatic diseases. *Int. J. Rheumatol.* **2013 (no p**

528. Ossipov, M. H., Dussor, G. O., and Porreca, F. (2010) Central modulation of pain. *J. Clin. Invest.* **120**, 3779

529. Gerecz-Simon, E. M., Tunks, E. R., Heale, J. A., Kean, W. F., and Buchanan, W. W. (1989) Measurement of pain threshold in patients with rheumatoid arthritis, osteoarthritis, ankylosing spondylitis, and healthy controls. *Clin. Rheumatol.* **8**, 467–474

530. Hart, F. D. (1972) Pain Threshold and Arthritis. *Br. Med. J.* **4**, 193

531. Brady, S. M., Georgopoulos, V., Veldhuijzen van Zanten, J. J. C. S., Duda, J. L., Metsios, G. S., Kitas, G. D., Fenton, S. A. M., Walsh, D. A., and McWilliams, D. F. (2023) The interrater and test-retest reliability of 3 modalities of quantitative sensory testing in healthy adults and people with

chronic low back pain or rheumatoid arthritis. *Pain reports* **8**, e1102

532. Kılıçaslan, H. Ö., Genç, A., and Tuncer, S. (2023) Central sensitization in osteoarthritic knee pain: A cross-sectional study. *Turkish J. Phys. Med. Rehabil.* **69**, 89–96

533. Pollard, L. C., Ibrahim, F., Choy, E. H., and Scott, D. L. (2012) Pain thresholds in rheumatoid arthritis: the effect of tender point counts and disease duration. *J. Rheumatol.* **39**, 28–31

534. Cao, Y., Fan, D., and Yin, Y. (2020) Pain Mechanism in Rheumatoid Arthritis: From Cytokines to Central Sensitization. *Mediators Inflamm.* **2020**

535. Shubayev, V. I., Kato, K., and Myers, R. R. (2010) Cytokines in Pain. *Transl. Pain Res. From Mouse to Man* 187–214

536. Raza, K., Buckley, C. E., Salmon, M., and Buckley, C. D. (2006) Treating very early rheumatoid arthritis. *Best Pract. Res. Clin. Rheumatol.* **20**, 849

537. Kapellos, T. S., Bonaguro, L., Gemünd, I., Reusch, N., Saglam, A., Hinkley, E. R., and Schultze, J. L. (2019) Human monocyte subsets and phenotypes in major chronic inflammatory diseases. *Front. Immunol.* **10**, 482347

538. Yang, S., Lukey, P., Beerahee, M., and Hoke, F. (2013) Population pharmacokinetics of losmapimod in healthy subjects and patients with rheumatoid arthritis and chronic obstructive pulmonary diseases. *Clin. Pharmacokinet.* **52**, 187–198

539. Tawil, R., Wagner, K. R., Hamel, J. I., Leung, D. G., Statland, J. M., Wang, L. H., Genge, A., Sacconi, S., Lochmüller, H., Reyes-Leiva, D., Diaz-Manera, J., Alonso-Perez, J., Muelas, N., Vilchez, J. J., Pestronk, A., Gibson, S., Goyal, N. A., Hayward, L. J., Johnson, N., LoRusso, S., Freimer, M., Shieh, P. B., Subramony, S. H., van Engelen, B., Kools, J., Leinhard, O. D., Widholm, P., Morabito, C., Moxham, C. M., Cadavid, D., Mellion, M. L., Odueyungbo, A., Tracewell, W. G., Accorsi, A., Ronco, L., Gould, R. J., Shoskes, J., Rojas, L. A., and Jiang, J. G. (2024) Safety and efficacy of losmapimod in facioscapulohumeral muscular dystrophy (ReDUX4): a randomised, double-blind, placebo-controlled phase 2b trial. *Lancet Neurol.*

23, 477–486

540. Blair, T. A., Frelinger, A. L., and Michelson, A. D. (2019) Flow cytometry. *Platelets* 627–651

541. Behbehani, G. K. (2017) Applications of Mass Cytometry in Clinical Medicine: The Promise and Perils of Clinical CyTOF. *Clin. Lab. Med.* **37**, 945–964

9 Appendices

9.1 Appendix 1. RA study patient information sheet

LONDON'S GLOBAL UNIVERSITY

UCL

Patient Information Sheet

Resolution of acute inflammation in autoimmune rheumatic disease: Blister protocol

This study has been approved by West Midlands: Solihull Research Ethics Committee Ref: 15/WM/0368

Lead researcher name: Dr James Glanville
Contact details: Centre for Clinical Pharmacology, Rayne Building, 5 University Street, Tel: 020 7679 7615
Email: j.glanville@ucl.ac.uk

Introduction

We would like to invite you to take part in our research study. Before you decide we would like you to understand why the research is being done and what it would involve for you. One of our team will go through the information sheet with you and answer any questions you have. This should take about 15 minutes.

Part 1 tells you the purpose of this study and what will happen to you if you take part.

Part 2 gives you more detailed information about the conduct of the study.

Talk to others about the study if you wish and ask us if there is anything that is not clear.

PART 1

Why is this study being done?

When our body is confronted with an injury or an infection, we react with a process called 'inflammation'. This causes the redness, swelling, heat, and pain you may be familiar with. Inflammation can help the body to fight infection and repair the injury; however, in some rheumatic diseases the inflammation is prolonged, in so far as it begins to damage the tissues of the body rather than repair them.

In this project, we will induce a mild inflammation on the skin of the forearm. We will then examine the inflammatory cells and fluid at the site as it recovers. Our overall objective is to understand better the process of inflammation and repair in rheumatic disease, which we hope will lead to the identification of improved treatments. We also want to

understand how a novel drug, Lenabasum, works to reduce inflammation and whether it is able to do this in autoimmune rheumatic disease (such as rheumatoid arthritis), bringing about the resolution of inflammation and a possible new treatment strategy for these diseases.

What does it involve for me?

This study will involve a number of visits to the Gilroy Laboratory, Rayne Institute (University College London), or the Clinical Research Facility (University Hospital Birmingham) over a period of two weeks to see how your body behaves as inflammation goes away.

During your first visit, we cause a mild inflammation (but not infection) by injecting dead (inactive) bacteria into the skin of the forearm. The inflammation goes away by itself over a few days. We have chosen a strain of bacteria which is fully sensitive to antibiotics. But, before injecting the bacteria, we kill them, and check that they are all dead, in order to confirm that they cannot cause an infection in you. We have used this method in many previous studies in UCL.

We will then monitor your body's response, by taking measurements and samples (including skin blisters) at different times after the injection (see details below).

For 24 hours before, and during the study, we ask you not to drink alcohol and to avoid heavy exercise.

For one week before and during the study, we ask you not to take certain medications which can affect the immune system (non-steroidal anti-inflammatory medications or NSAIDs such as Ibuprofen). We will discuss this with you when we first meet.

Before any studies begin we will talk you through a consent form, which we will ask you to sign, indicating your understanding of what the study involves, and your willingness to participate. If you do choose to take part, you may be randomly allocated to a group of volunteers who will take a novel anti-inflammatory drug, Lenabasum, for four days prior to the first visit. These medications will be given to you to take twice daily before your first visit.

Time commitment:

You will need to spend approximately 45 minutes with us for your first visit (which includes the injection of bacteria).

You will then return for two further visits (between one and a half and two hours each), one for each blister (for about an hour of this time you will be free read or watch TV, but will need to sit still with one arm attached to the blister machine).

If any extra short (less than 1 hour e.g. blood test / Doppler) or long (e.g. blister) visits are required, we will discuss this with you at the start of the study.

We will discuss the sample collection times with you when we first meet, to ensure maximum convenience to you. You are asked to discuss with us if the proposed times do not suit your schedule, and we will endeavour to find mutually convenient times.

Compensation for your time and effort

We appreciate the time and effort involved in participating in this study. Please keep any receipts for travel expenses relating to the study, and we will reimburse you. If you need to travel long distance to participate, we will discuss this with you, and we can arrange and pay for any necessary overnight accommodation. You will be given £150 for completion of all visits. All payments / reimbursements will be paid by a BACS (or cheque if preferred) within 2-4 weeks of your final visit.

Details of procedures

1) Tests at start of study and to monitor response:

In order to accurately measure the swelling and redness at the site, we will take some measurements and scan the inflamed area using a laser Doppler scanner. The scanner does not touch your arm or cause any discomfort, but takes around 5 minutes to scan each forearm.

We will also collect a blood sample from you before the injection of killed bacteria and at various time-points after the injection. Over the whole study, a total of no more than 100 mL (7 tablespoons) of blood will be taken. This is to understand your body's overall response to the inflammation. You will be informed at the beginning of the study about which visits will involve a blood test.

2) Killed bacteria injection to cause localised inflammation:

At the first visit we will inject the upper layer of the skin (dermis), with dead bacteria in two places, one on each forearm (inner hairless side), (see picture 1).

3) Blister formation:

You will then be asked to return to have a blister formed on separate occasions.

A suction cup attached to negative pressure equipment will be placed over the injection site. This gradually separates the top layer of skin from the deeper layer over a period of about an hour, forming a blister (10mm in diameter, see picture 2). The fluid from the blister will be removed straight away using a sterile needle. The site will then be cleaned and a sterile dressing will be applied, which we advise you to keep on and dry for 2-3 days. On the second visit the same procedure will be performed but on the other arm at the other injection site.

4) Follow up:

For participants with rheumatic disease, we will request your permission to review your medical notes (those relating to your rheumatological condition only) both at the time of the study and for a period of 3 years afterwards. This is because your clinical condition or diagnosis may change in this time, and we would like to relate the results of this study both to your current clinical diagnosis as well as any future change in diagnosis. We may also contact you during this time to ask if you would be willing to provide an additional blood sample to investigate interesting findings. This would be optional. If you would prefer not to be contacted again following completion of the study, simply let us know.

Finally, we may contact you once your participation in this study is completed and ask you whether you would mind completing a short questionnaire regarding your experience. This is optional, but we would be very grateful for your feedback.

Side effects due to injection of killed bacteria:

- The injection itself can sting for a few seconds.
- After 2 hrs, the site will get red, warm and slightly tender, similar to a bee-sting. The tenderness will reach its worst at about 12-24 hours. Redness may continue to expand for up to 48hours, to a total area of around 10x5cm, but will then fade away.
- One in every three or four people who have these killed bacteria injected can get some 'general' symptoms such as ache or 'fullness' in the armpit, a headache, muscle aches or a slight rise in body temperature, but volunteers have described these as 'mild' and they should not affect your routine activities. In the unlikely event you feel very unwell or develop sustained symptoms (over 24hours) please contact the researchers, or if very concerned seek medical assistance.
- When this technique was first used, one individual suffered a severe skin reaction which required medical treatment to recover. However, we now inject a much smaller dose of bacteria (60 times less), and have not seen this side effect in more than 100 volunteers since, and so believe that this risk is very small.

Side effects associated with forming blister and taking samples:

- Taking a blood sample is the same as having a routine blood test at your doctor's surgery.
- Suction blister formation process can lead to mild discomfort as the superficial layer of skin is slowly separated from the deeper layers. The blister can sting for a few seconds after the fluid has been removed, whilst the dressing is applied.
- There is a minimal risk of infection at the blister site. In this case the site becomes red, painful and weepy. This risk is minimised by using an aseptic technique throughout and by applying a waterproof hypo allergic dressing over the blister site. However, if it did occur you might need treatment with antibiotics and should contact us on details below.
- Blister formation can lead to temporary skin marking that will usually fade after 6-12 weeks, but may persist for longer, particularly on darker skin.

Side effects due to Lenabasum:

- Lenabasum has been safely administered hundreds of human subjects in clinical trials.
- These studies suggest that Lenabasum at the dose being employed in this study (maximum total daily dose 40 mg) is both safe and well tolerated.
- A handful of mild adverse events have been reported in subjects exposed to the drug, but these were only present at doses higher than those that will be used in this study.
- These included fatigue, dizziness, reduced concentration, light-headedness, somnolence, nausea, and vomiting, slightly low blood pressure on standing and dry mouth.

- No severe adverse reactions have been reported to date.

PART 2: Further Information

Will this study help me?

This study will not benefit you directly. However, it will tell us about how inflammation recovers in people with certain rheumatic diseases, helping us to develop more focussed and individualised approach to treatment, and it could lead to the development and testing of new treatments in the future.

How will we use the samples we obtain from you?

We plan to use the cells/skin tissue obtained before and after the injection to understand changes in the types of cells present at the site of inflammation, and the gene expression (RNA). We will also look at the fluid obtained to understand changes in the soluble factors involved in inflammation.

Could I come to any harm if I take part in this study?

The potential side effects are listed in part 1. Your GP will be sent a letter informing them that you are participating in this study.

How will confidentiality be protected?

All the information obtained about you in the course of the study is confidential and will be kept in a locked room and on password-secured university computers. This information will include your unique study number (code) and we will label all your samples and records with this number. Only the researchers will be able to identify you from the samples or results, as they are the only ones that will have access to the code.

As the samples generated from your blood/tissue during the course of this study are extremely valuable, if there are cells, fluid or skin tissue left over after the completion of this study, we may use these samples for other studies underway in this laboratory if you consent to this. These samples will stay labelled, and be analysed, with your study number (code), and not your name.

Are there any factors that would exclude me from taking part in the study?

You will not be able to take part if you:

- Have moderately or severely active rheumatic disease
    - Pregnancy or breastfeeding
    - Smoker (nicotine containing products)
    - The use of recreational/party drugs.
    - Concurrent HIV infection or other immunodeficiency, leukopenia or neutropenia
    - Current infection or antibiotic treatment
    - Lack of ability to provide informed consent

- Use of systemic immunosuppressant medication within the last three months (including systemic corticosteroids)
- Inability to stop non-steroidal anti-inflammatory drugs (NSAIDs) for one week prior to the study, and until after their final sample collection
- Abnormal blood tests during screening
    - **Full Blood Count:** Haemoglobin, platelet count, total white cell count and differential
    - **Urea and Electrolytes:** Urea, creatinine, potassium, sodium, chloride
    - **Liver Function Tests:** Total protein, albumin, bilirubin, alkaline phosphatase, alanine aminotransferase
- Personal or family history of pyoderma gangrenosum
- Been vaccinated within the last three months
- Participants who are unable to communicate effectively with the research team in English
- Patients who are involved in current research or have recently been involved in research may be excluded if participation in multiple studies may cause risk to the participant, or if participation in multiple studies may impact on the results of either study.

What happens if something goes wrong?

This study has already been performed on many patients with inflammatory bowel disease and healthy individuals, and we believe that it is fundamentally safe. However, research can carry unforeseen risks and we want you to be informed of your rights in the unlikely event that any harm should occur as a result of taking part in this study. Every care will be taken to ensure that your wellbeing and safety are not compromised during the course of the study.

If you wish to complain or have any concerns about any aspect of the way you have been approached or treated by members of staff you may have experienced due to your participation in the research, National Health Service or UCL complaints mechanisms are available to you. Please ask your research doctor if you would like more information on this.

In the unlikely event that you are harmed by taking part in this study, compensation may be available. If you suspect that the harm is the result of the Sponsor's (University College London) or the hospital's negligence then you may be able to claim compensation. After discussing with your research doctor, please make the claim in writing to Professor Derek Gilroy who is the Chief Investigator for the research and is based at UCL. The Chief Investigator will then pass the claim to the Sponsor's Insurers, *via* the Sponsor's office. You may have to bear the costs of the legal action initially, and you should consult a lawyer about this.

You may contact the Patient Advice and Liaison Service (PALS) for independent advice:

UCLH: email pals@uclh.nhs.uk or telephone 0203 456 7890 ext 73002 / 73018

University Hospitals Birmingham: email PALS@uhb.nhs.uk or telephone 0121 371 3280

Who is organising and funding the research?

The research is organised by the Centre for Clinical Pharmacology, UCL. The study is being funded by the Wellcome Trust and Corbus Pharmaceuticals Ltd.

Do I have to take part in this study, and can I withdraw?

No, you do not have to take part in this study. If you do decide to take part, you may withdraw at any time without giving a reason and without any penalty. No further samples would be taken after this point. Any samples and data that have already been collected would be retained and used in the study unless you request that we dispose of them.

Details of how to contact the researchers

Centre for Clinical Pharmacology, The Rayne Building (UCL), 5 University Street, London WC1E 6JF

Dr James Glanville on 07719 642 875 (j.glanville@ucl.ac.uk)

Professor Derek Gilroy on 020 7679 6933 (d.gilroy@ucl.ac.uk)

Thank-you for taking your time to read this information leaflet. Please discuss the information above with others if you wish, and ask us if there is anything that is not clear or if you would like more information.

The decision is of course entirely yours whether you would like to take part or not.

Picture 1: Injection of killed bacteria

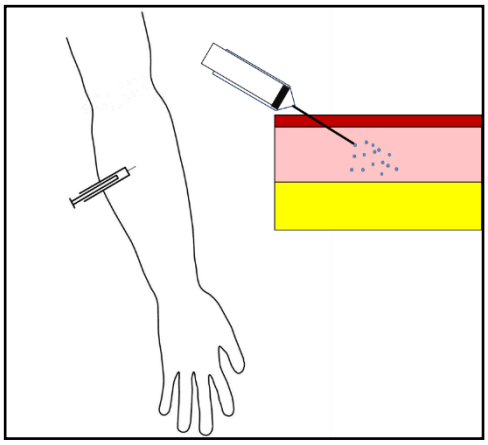

Picture 2: Creation of suction blister

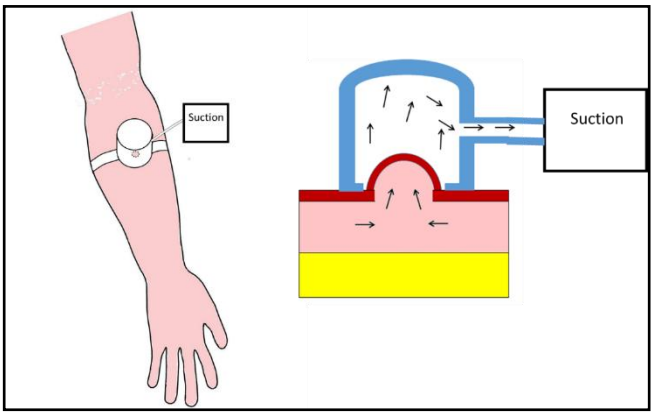

9.2 Appendix 2. RA study screening form

VOLUNTEER SCREENING FORM

Title of Project:

Resolution of acute inflammation in autoimmune rheumatic disease

This study has been approved by the Solihull NHS Research ethics committee (Reference number 15/WM/0368)

Please print details in block capitals (to be completed by the volunteer):

Full Name: _____

Date of Birth: _____

Home Address: _____

Home Telephone: _____

Mobile Telephone: _____

Email: _____

Ethnicity: _____

Next of kin emergency contact: _____

Name of GP: _____

Address of GP: _____

Exclusion Criteria:

1. Are you pregnant or breast feeding?
   YES ☐ NO ☐
2. Do you smoke?
   YES ☐ NO ☐
3. Do you take recreational / party drugs?
   YES ☐ NO ☐
4. Do you have HIV, immunodeficiency, leukopenia or neutropenia?
   YES ☐ NO ☐
5. Do you have a current illness or antibiotic treatment?
   YES ☐ NO ☐
6. Have you used any systemic immunosuppressant medication within the last three months?
   YES ☐ NO ☐
7. Do you have an inability to stop anti-inflammatory drugs for one week prior to the study?
   YES ☐ NO ☐
8. Have you been vaccinated in last three months?
   YES ☐ NO ☐
9. Are you unable to communicate effectively in English?
   YES ☐ NO ☐

10. Have you consumed alcohol in past 3 days?
    YES ☐ NO ☐

11. Are you currently enrolled in another study?
    YES ☐ NO ☐

Volunteer signature: _____

Date: _____

Study investigator name: _____

Study investigator signature: _____

Date: _____

9.3 Appendix 3. RA study consent form

CONSENT FORM FOR VOLUNTEERS IN RESEARCH STUDIES

Please complete this form after you have read the Information Sheet and/or listened to an explanation about the research.

Title of Study: ***Resolution of acute inflammation in autoimmune rheumatic disease***

Department: Metabolism and Experimental Therapeutics

Name and Contact Details of the Researcher(s):

Dr James Glanville

Centre for Clinical Pharmacology and Therapeutics, Rayne Building, 5 University Street, London, WC1E 6JF

j.glanville@ucl.ac.uk

07719 642 875

Name and Contact Details of the Principal Researcher:

Professor Derek Gilroy

Centre for Clinical Pharmacology and Therapeutics, Rayne Building, 5 University Street, London, WC1E 6JF

d.gilroy@ucl.ac.uk

020 7679 6933

Name and Contact Details of the UCL Data Protection Officer:

Lee Shailer

This study has been approved by Solihull NHS Research Committee (Reference No. 15/WM/0368)

Thank you for considering taking part in this research. The person organising the research must explain the project to you before you agree to take part. If you have any questions arising from the Information Sheet or explanation already given to you, please ask the researcher before you decide whether to join in. You will be given a copy of this Consent Form to keep and refer to at any time.

I confirm that I understand that by ticking/initialling each box below I am consenting to this element of the study. I understand that it will be assumed that unticked/initialled boxes means that I DO NOT consent to that part of the study. I understand that by not giving consent for any one element that I may be deemed ineligible for the study.

	Tick Box
*I confirm that I have read and understood the Information Sheet for the above study. I have had an opportunity to consider the information and what will be expected of me. I have also had the opportunity to ask questions which have been answered to my satisfaction	
*I consent to participate in the study. I understand that my personal information will be used for the purposes explained to me. I understand that according to data protection legislation, 'public task' will be the lawful basis for processing.	
Use of the information for this project only I understand that my data gathered in this study will be stored anonymously and securely. It will not be possible to identify me in any publications. All data collected will be anonymised. We will only use encrypted USB stick and data will not be taken off UCL property and will be stored on password-secured UCL computers	
I understand that my information may be subject to review by responsible individuals from the University (to include sponsors and funders) for monitoring and audit purposes.	
I understand that my participation is voluntary and that I am free to withdraw at any time without giving a reason. I understand that if I decide to withdraw, any personal data I have provided up to that point will be deleted unless I agree otherwise.	
I understand the potential risks of participating and the support that will be available to me should I become distressed during the course of the research.	
I understand the direct/indirect benefits of participating.	
I understand that the data will not be made available to any commercial organisations not affiliated to this study, but is solely the responsibility of the researcher(s) undertaking this study.	
I understand that I will not benefit financially from this study or from any possible outcome it may result in in the future.	
I understand that I will be compensated for the portion of time spent in the study (if applicable) or fully compensated if I choose to withdraw.	
I agree that my anonymised research data may be used by others for future research. And that no one will be able to identify you when this data is shared.	
I understand that the information I have submitted will be published as a report and I wish to receive a copy of it. Yes/No	
I hereby confirm that I understand the inclusion criteria as detailed in the Information Sheet and explained to me by the researcher.	
I hereby confirm that: (a) I understand the exclusion criteria as detailed in the Information Sheet and explained to me by the researcher; and (b) I do not fall under the exclusion criteria.	
I agree that my GP may be contacted if any unexpected results are found in relation to my health.	

I have informed the researcher of any other research in which I am currently involved or have been involved in during the past 12 months.	
I am aware of who I should contact if I wish to lodge a complaint.	
I voluntarily agree to take part in this study.	
Use of information for this project and beyond. I would be happy for the data I provide to be archived at Centre for Clinical Pharmacology and Therapeutics, Rayne Building, 5 University Street, London, WC1E 6JF. I understand that other authenticated researchers will have access to my anonymised data. It is expected that data generated from these studies be made available to the wider scientific community. The idea is that new understanding of how our immune system works should be shared with other scientific colleagues to maximise research opportunities, insight and highlight new targets for drug development. It's important that all data will be anonymised and in no way will the participant's personal details be identifiable.	

If you would like your contact details to be retained so that you can be contacted in the future by UCL researchers who would like to invite you to participate in follow up studies to this project, or in future studies of a similar nature, please tick the appropriate box below.

Yes, I would be happy to be contacted in this way	
No, I would not like to be contacted	

_____	_____	_____
Name of participant	Date	Signature
_____	_____	_____
Name of witness (If applicable)	Date	Signature
_____	_____	_____
Researcher	Date	Signature

9.4 Appendix 4. Healthy volunteer study information sheet

Information Sheet for Participants in Research Studies

You will be given a copy of this information sheet.

Title of Project: Characterisation of the anti-inflammatory role of ATB-346, using a UV-killed *E. coli* skin blister model of resolving inflammation in humans.

This study has been approved by the UCL Research Ethics Committee (Project ID Number): **10527/001**.

Name Professor Derek Gilroy.

Address Centre for Clinical Pharmacology,
Division of Medicine,
Rayne Building,
5 University Street,
London,
WC1E 6JF.

Contact Email: d.gilroy@ucl.ac.uk
Telephone: 020 7679 6933

We are recruiting healthy volunteers aged 18-50 for this research project and we would like to invite you to participate. You should only participate if you want to; choosing not to take part will not disadvantage you in any way. Before you decide whether you want to take part, it is important for you to read the following information carefully and discuss it with others if you wish. It is important for you to understand why it is being done and what it will involve, so please take the time to read the following information.

Why is this pilot study being done?

When our bodies are confronted with an insult, such as trauma or infection, they react with a process called 'inflammation'. This process involves dilatation of blood vessels locally and the recruitment of so-called inflammatory cells to the area. This causes the redness, swelling, heat, and pain you may be familiar with following a wound or an infection. Inflammation can help the body to fight infection and repair trauma; however, in some cases the inflammatory response is prolonged such that it begins to damage the tissues of the body rather than repair them.

Inflammation is commonly treated with non-steroidal anti-inflammatory drugs (NSAIDs). The safest of these in terms of

cardiovascular risk is naproxen, although you may be familiar with others such as ibuprofen or diclofenac. An emerging class of compounds with significant anti-inflammatory properties is the hydrogen sulfide-releasing non-steroidal anti-inflammatory drugs (H_2S-NSAIDs). They consist of a traditional NSAID to which an H_2S-releasing group is attached. One such novel drug, ATB-346, a derivative of naproxen, has been shown to have a reduced gastrointestinal side effect profile (namely in terms of ulceration and bleeding), compared to traditional naproxen. It has also been shown that levels of ATB-346 in the blood remained much higher than the equivalent dose of naproxen with comparable anti-inflammatory effect. In a first-in-human trial two participants (33% of those taking ATB-346) developed hepatitis (as seen demonstrated with elevated liver enzymes, but normal imaging). This was, however, at a dose of 1500 mg. both of these partipants had pre-existing hepatobiliary pathology (previous hepatitis A infection and gallstones, respectively). At a dose of 250 mg (the dose used in our study) 0% of subjects experienced adverse effect. Overall, no serious adverse effects or deaths occurred in the study (Antibe Inc. Therapeutics, 2015) Subsequent studies performed in humans where inflammation was treated with ATB-346 did not produce any serious adverse event, including significant gastrointestinal, cardiovascular, renal, and haematological. It was also safe at all doses which were administered (Wallace, 2015; Wallace and Wang, 2015). The details of these studies are available to potential participants on request (see contact details at the end of this information sheet). This suggests that there ATB-346 could represent an alternative to naproxen with the possibility of once daily dosing for chronic conditions, rather than twice daily as with naproxen, without the occurrence of significant gastrointestinal upset.

To further investigate the anti-inflammatory role of ATB-346 in humans, we intend to recruit a maximum of 30 healthy, male volunteers aged 18 to 50 years. Participants will be excluded if they have any medical problems, or take regular medication (prescription or over-the-counter). Each participant will be invited to take part in and be randomly allocated to one of three treatment arms: 1) control (no anti-inflammatory medication), 2) native naproxen or 3) ATB-346. The UV-killed *E. coli* blister model of inflammation will be employed and two treatment protocols will also be used with different dosing regimens.

We will induce mild inflammatory reactions on the skin of the forearm involving blister formation and then test the fluid from these to examine the inflammatory cells. Our overall objective is to work out how whether there is a difference in the resolution of inflammation, whether using naproxen, using ATB-346 or not using either.

What does it involve for me?

This study will involve between two and three visits to the Gilroy Laboratory, Rayne Institute (UCL) over one week. In total we anticipate the study will require 3-4 hours of your time.

You will be asked to participate in one of the three treatment arms using one of two protocols detailed below. The exact details of this will be indicated at the initial meeting so that you have time to consider your involvement. All participants will undergo the same technique, which involves the raising of blisters on the hairless part of both forearms and the triggering of localised inflammatory reactions. For 24 hours before and during both protocols you will be asked to refrain from alcohol containing beverages.

Before any studies begin you will be asked to sign a consent form indicating your understanding of what the study involves, and your willingness to participate. This acceptance and your understanding will also be confirmed verbally.

After re-confirming consent, we will inject the upper portion of the skin (dermis), with a number of dead bacteria at the two forearm sites. These bacteria have been prepared from a fully antibiotic sensitive strain of bacteria, killed with UV light with bacterial death verified by multiple tests: as such they cannot cause an infection. This method has been used in multiple previous studies in UCL.

The injections will cause a mild inflammatory reaction accompanied by redness, warmth and mild tenderness at the site which will be maximal at about 8-12 hours. The redness may continue to expand for up to 48 hours, to a total area of around 5 x 5 cm, but will recede afterwards. Intradermal injection may cause mild discomfort but is a very low-risk procedure. The local inflammatory reaction may be associated with mild 'general' symptoms such as a slight rise in body temperature but will not make you feel unwell or affect your routine activities.

Before the injection, depending on which treatment arm you are assigned to, you will be taking either no medication, naproxen or ATB-346. You will be informed throughout, as to which treatment arm you have been assigned. Two treatment protocols will be used with different dosing regimens of the respective treatments and corresponding timing of exudate aspiration. Protocol 1 will involve treatment arm 1 taking no anti-inflammatory prior to the *E. coli* injection. Treatment arm 2 will take a single dose of native naproxen twice daily for 48 hours prior to the *E coli* injection. Treatment arm 3 will take a single dose of ATB-346 once daily for 48 hours prior to the *E. coli* injection. The latter two treatment arms will take their last dose 30 minutes before the injection.

Protocol 2 will involve treatment arm 1 taking no anti-inflammatory prior to the *E. coli* injection. Treatment arm 2 will take a single dose of native naproxen 4 hours after the *E. coli* injection. Treatment arm 3 will take a single dose of ATB-346 4 hours after the *E. coli* injection.

For both protocols, at two time-points between 4 hours and 72 hours you will be asked to return to the laboratory for formation of a blister to evaluate local immune (defence) function. A suction cup attached to negative pressure equipment will be placed over the injection site and a blister raised. After the blister formation, the fluid will be removed by making a hole in the blister roof with a sterile needle and the fluid removed. The site will then be disinfected and a clean dressing will be applied. This process is associated with very mild discomfort. Over this 72 hour period we would ask you to refrain from alcohol and caffeine containing beverages and advise you to avoid intensive exercise.

You will be informed of the time-points that we would like you to return at before consent if taken. You are free to say no if they don't suit your schedule and we will endeavour to try and find mutually convenient times.

Will this study help me?

This study will not benefit you directly. However it will help provide a foundation for the development and testing of new treatments against inflammatory disorders.

Volunteers will be paid £100 to offer adequate reimbursement for your time, travel expenses and inconvenience.

Could I come to any harm if I take part in this study?

Injection of UV-killed bacteria under the skin (intradermal) can lead to mild discomfort initially. After 2 hours, the site will get red, warm and slightly tender, similar to a bee sting. Following 4-6 hours, you might feel slightly feverish and you may notice mild discomfort in the armpits on the side of the injection site, however this is rare and will quickly pass. Such a reaction indicates that the body is clearing the bacteria effectively. In the unlikely event you feel very unwell or develop sustained symptoms (longer than 12 hours) you are advised to contact the investigators, or if very concerned to seek medical assistance. The redness at the injection site will spread to around 5 cm diameter by 36-48 hours and reduce thereafter. Tenderness will peak around 8 hours and remain the same for 24-36 hours, reducing from this point.

From the experience of Professor Gilroy's laboratory, as described by Motwani et al. (2016), "The blister induction process in itself caused only mild discomfort. After blister aspiration, the site formed a scab which left a pigmented scar. This faded considerably within 4-6 weeks on Caucasian skin but took longer on darker skin types." Nonetheless, it will eventually fade from pigmented skin without scarring. Again, the details of this research paper are available on request to potential participants. There is minimal risk of infection from both having blood tests and blister formation, although we have had no cases of this during either procedure. As with any blood test there is a chance of bruising but this varies from patient to patient and is difficult to truly quantify. Aseptic technique will be used throughout to minimise this risk. The investigators are highly experienced and trained in performing all the stated techniques.

Are there any factors that would exclude me from taking part in the study?

You will not be able to take part in this study if you have any acute or chronic medical conditions, or take regular prescribed or over-the-counter medication. You will also not be able to take part if you have had a recent vaccination (within 3 months) or take recreational drugs. In particular, if you are known to suffer from any respiratory disease (breathing problems), such as asthma, or have any known allergies, please let the investigators know, as it is unlikely you will be able to partake in the study. You should not take part in this study if you are already involved in another study.

What are the arrangements for compensation?

Research can carry unforeseen risks and we want you to be informed of your rights in the unlikely event that any harm should occur as a result of taking part in this study. Every care will be taken to ensure that your wellbeing and safety are not compromised during the course of the study. UCL also has insurance arrangements in place in the unlikely event that something does go wrong and you are harmed as a result of taking part in the research study.

Do I have to take part in this study?

You do not have to take part in this study if you do not want to. If you decide to take part you may withdraw at any time without giving a reason and without any penalty. If you decide, now or at a later date that you do not wish to participate in this research project, it is entirely your right.

Whom do I speak to of a problem arises?

If you have any complaint about the way in which this research project has been, or is being conducted, please, in the first instance discuss them with the researcher, Doctor James Glanville, Centre for Clinical Pharmacology, The Rayne Institute, 5 University Street, London WC1E 6J. If the problems are not resolved or you wish to comment in any other way, please contact Professor Derek Gilroy, Centre for Clinical Pharmacology, The Rayne Institute, 5 University Street, London WC1E 6JJ. Details can be found on the first page of this leaflet.

Who is organising and funding the research?

The research is organised by the Centre for Clinical Pharmacology, UCL. The study is being funded in part by the Wellcome Trust and Departmental monies.

How will confidentiality be protected?

All the information obtained about you in the course of the study is confidential and will be kept in a locked room and on password-secured UCL computers. You will be assigned a study number and all samples and records labelled with this. Only the investigators will have access to this code and the data files.

What happens if anything goes wrong?

We believe that as a result of its design and exclusion criteria, this study is fundamentally safe. Each volunteer will be screened to determine his suitability and excluded if it is felt that he is not appropriate for this study. However, we carry insurance to make sure that if your health does suffer as a result of being in this study, then you will be compensated. In such a situation, you will not have to prove that the harm or injury which affects you is anyone's fault. If you are not happy with any proposed compensation, you may have to pursue your claim through legal action.

Finally: You do not have to join this study. You are free to decide not to be in this trial or to drop out at any time. If you decide not to be in the study, or drop out, there will be no penalty involved. This will not put at risk your ordinary medical care or benefits you are otherwise entitled.

Please discuss the information above with others if you wish or ask us if there is anything that is not clear or if you would like more information. It is up to you to decide whether to take part or not; choosing not to take part will not disadvantage you in any way. If you do decide to take part you are still free to withdraw at any time and without giving a reason. If you decide to take part, you will be given this information sheet to keep and be asked to sign a consent form. All data will be collected and stored in accordance with the Data Protection Act 1998.

References:

Antibe Therapeutics Inc. (2015). Investigator's Brochure: ATB-346 Oral Drug Product (Version Number: 151104-1).

Motwani, M. P., Flint, J. D., De Maeyer, R. P. H., Fullerton, J., Smith, A. M., Marks, D. J. B, Gilroy, D. W. (2016). Novel translational model of resolving inflammation triggered by UV-killed E. coli. J Pathol (Clin Res). 2(3): 154-165.

Wallace, J. (2015). THU0474: A Phase 1 clinical trial of ATB-346, a gastrointestinal-safe nonsteroidal anti-inflammatory drug. Ann Rheum Dis. 74:371-372.

Wallace, J. L., Wang, R. (2015). Hydrogen sulfide-based therapeutics: exploiting a unique but ubiquitous gasotransmitter. Nat Rev Drug Discov. 14(5): 329-345.

Details of how to contact the researchers

You can contact:

Professor Derek Gilroy on 020 7679 6933 (d.gilroy@ucl.ac.uk).

Doctor James Glanville on 07719 642875 (jamesglanville@nhs.net).

Thank you for taking your time to read this information leaflet and for considering taking part in this research. If you have any further questions please do not hesitate to contact the researchers using the above details.

Please discuss the information above with others if you wish or ask us if there is anything that is not clear or if you would like more information.

It is up to you to decide whether to take part or not; choosing not to take part will not disadvantage you in any way. If you do decide to take part you are still free to withdraw at any time and without giving a reason.

All data will be collected and stored in accordance with the Data Protection Act 1998.

9.5 Appendix 5. Healthy volunteer study screening form

VOLUNTEER SCREENING FORM

Title of Project:

Characterisation of the anti-inflammatory role of ATB-346, using a UV-killed *Escherichia coli* skin blister model of resolving inflammation in humans.

This study has been approved by the UCL Research Ethics Committee (Project ID Number): **5051/002**

Please print details in block capitals (to be completed by the volunteer):

Full Name: _____

Date of Birth: _____

Home Address: _____

Home Telephone: _____

Mobile Telephone: _____

Email: _____

Ethnicity: _____

Next of kin emergency contact: _____

Name of GP: _____

Address of GP: _____

Exclusion Criteria:

12. Do you have chronic inflammatory illness/allergies? YES ☐ NO ☐
13. Are you regularly taking any prescribed medication? YES ☐ NO ☐
14. Have you taken any over the counter medication in 7 days? YES ☐ NO ☐
15. Have you been vaccinated in last three months? YES ☐ NO ☐
16. Have you been ill in past 7 days? YES ☐ NO ☐
17. Do you smoke? YES ☐ NO ☐
18. Have you consumed alcohol in past 3 days? YES ☐ NO ☐
19. Do you take recreational drugs? YES ☐ NO ☐
20. Are you currently enrolled in another study? YES ☐ NO ☐

Volunteer signature: _____

Date: _____

Study investigator name: _____

Study investigator signature: _____

Date: _____

9.6 Appendix 6. Healthy volunteer consent form

Informed Consent Form for Participants in Research Studies

Please complete this form after you have read the Information Sheet and/or listened to an explanation about the research.

Title of Project: Characterisation of the anti-inflammatory role of ATB-346, using a UV-killed *E. coli* skin blister model of resolving inflammation in humans.

This study has been approved by the UCL Research Ethics Committee (Project ID Number): **10527/001.**

Thank you for your interest in taking part in this research. Before you agree to take part, the person organising the research must explain the project to you.

If you have any questions arising from the Information Sheet or explanation already given to you, please ask the researcher before you to decide whether to join in. You will be given a copy of this Consent Form to keep and refer to at any time.

Participant's Statement

I _____

agree that I

- have read the notes written above and the Information Sheet, and/or the project has been explained orally to me and understand what the study involves.
- had the opportunity to ask questions and discuss the study.
- Received satisfactory answers to all my questions, or have been advised of an individual to contact for answers to pertinent questions about the research and my rights as a participant, and whom to contact in the event of a research-related injury.
- understand that if I decide at any time that I no longer wish to take part in this project, I can notify the researchers involved and withdraw immediately without penalty.
- consent to the processing of my personal information for the purposes of this research study and understand that it will not be used for any other purpose.
- understand that such information will be treated as strictly confidential and handled in accordance with the provisions of the Data Protection Act 1998.
- agree that the research project named above has been explained to me to my satisfaction and I agree to take part in this study.

- understand that I am being pid fr my assistance in this research and that some of my personal details will be passed on UCL Finance for administration purposes.
- agree that my data, after it has been fully anonymised, can be shared with other researchers *[to satisfy Research Council funded projects as Research Councils have changed their guidance regarding data sharing].*

Signed: Date:

Investigators Statement

I _____

confirm that I have carefully explained the purpose of the study to the participant and outlined any reasonably foreseeable risks or benefits (where applicable).

Signed: Date: